THESIS SUBMISSION
Doctor of Philosophy in Engineering Science

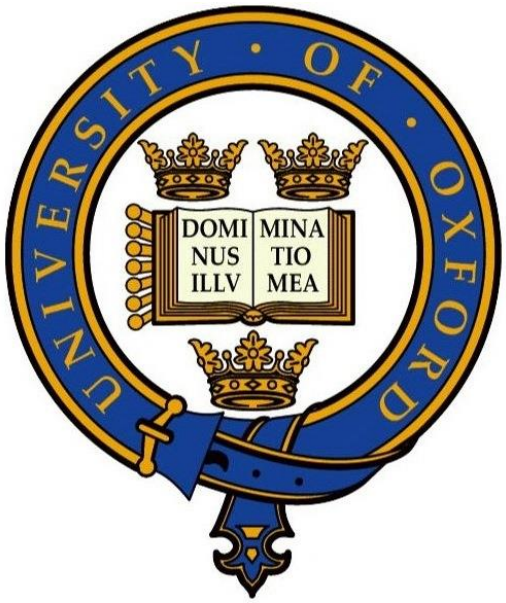

Membrane Filtration: Fouling and Cleaning in Forward Osmosis, Reverse Osmosis, and Ultrafiltration membranes

Farrukh Arsalan Siddiqui
Somerville College

A thesis submitted for the degree of *Doctor of Philosophy*

Department of Engineering Science
University of Oxford

Hilary Term 2017

Membrane Filtration: Fouling and Cleaning in Forward Osmosis, Reverse Osmosis, and Ultrafiltration membranes

Farrukh Arsalan Siddiqui, Somerville College, Hilary Term 2017
A thesis submitted for the degree of Doctor of Philosophy at the University of Oxford

Abstract

A comparison of fouling in osmotically driven processes with that in pressure driven processes is the main focus of the thesis. Forward osmosis (FO) and reverse osmosis (RO) have received considerable attention for water treatment and seawater desalination. This research compared the nature of fouling in FO mode with that in RO starting with the same initial flux in connection with cleaning effects and then comparing to those in ultrafiltration membranes. In all cases, with cleaning as an integral part, the extent of fouling reversibility, and the question whether a critical flux could be determined were examined.

The work during the first phase (undertaken at Oxford) quantified the removal of reversible fouling through rinsing by cold and hot water for a range of concentrations using the foulants dextran and carboxymethyl cellulose. The flux-TMP relationship was conventionally compared to that of the clean water flux.

The later phase (at Singapore) compared the fouling in FO and RO by alginate in terms of multiple parameters using cellulose tri acetate (CTA) and thin film composite (TFC) membranes. Silica and alginate were selected as model foulants. Whilst experimental water flux profiles in the present study did not exhibit significant differences in trend between FO and RO fouling, foulant resistance for FO was found to be increasingly greater than for RO with the progression of the fouling tests. This was further corroborated by membrane autopsies post fouling tests; both foulant mass deposition density and specific foulant resistance for FO were greater than for RO. The analysis clearly revealed that FO is essentially more prone to fouling than RO which was presumably due to less flux decline in

FO (or greater average flux) as compared to that in RO in result of ICP-self compensation effect which is opposite to the prevailing claim in the literature. Additionally, the present study did not find evidence that hydraulic pressure in RO has a role in foulant layer compaction.

FO membrane fouling by real waters was the focus of the final phase of the research at SMTC. Pilot scale FO experiments were conducted on spiral wound CTA membrane with treated waste water obtained from a NEWater factory (Singapore) as the feed. In the second stage, experiments were repeated at bench scale with membrane coupons taken from the spiral wound membranes used earlier. The key finding was that the mass transfer coefficients in the Spiral-Wound module were around 50% lower than the corresponding values in the flat sheet unit and this severely limited the fluxes. The reason could be attributed to strong internal concentration polarisation in the former, where tightly wound spacers act to increase the structural parameter.

I dedicate this piece of my work to:

My mother in heavens,

who taught me how to write by grabbing my hand.

I wish she were able to see the outcome of her teaching to an expected spoiled child;

My father,

a living legend,

I always have a wishful thinking to be like him some day.

Acknowledgements

If I look back at my D.Phil. life at Oxford, a number of names pop up in my mind who walked alongside me, guided me like stars, and showed me the doors that might be useful to open. The list of these people could surely take up the space of a whole lengthy chapter; however, I try my best to keep the list short, so that who are shortlisted may feel special.

First and the foremost, thanks to ALLAH for all blessings HE gave and the courage to handle all ups and downs during the roller coaster ride of D.Phil. and providing me an opportunity to meet wonderful people and the unforgettable moments I have spent in the city of spires.

The most important acknowledgement I wish to express is to my Supervisor, Professor Robert W. Field, who held my hand at times, when I was about to fall. My completion of this project could not have been accomplished without his constant motivation and encouragement, for which I will remain grateful throughout my entire life.

I extend my expression of gratitude to the Singapore Membrane Technology Centre (SMTC), NTU for hosting my year-long visit during which the major experimental data for this thesis was obtained under the kind supervision of world-wide renowned scientist Professor Anthony G. Fane (Tony Fane), whose guidance, imparting his knowledge, and expertise in this research during my stay at Singapore Membrane Technology Centre (SMTC), NTU, Singapore would always remain valuable. For my stay at SMTC, I am also grateful to Dr. Qianhong She for sharing his knowledge and technical know-how. A note of thanks for my College adviser Prof. Steve Roberts and the Senior Tutor of Somerville College, Oxford, Dr. Steve Rayner for their help in tough days and would never forget Prof. Richard Stone as well.

I am thankful to my parents; Prof. Dr. Hameed Raza Siddiqui for his continuous selfless inspiration and my mother who prayed for me while being in heavens. My heartfelt

appreciations are for Amna Zahidi, Sheharyar, and Aimen. The contributions of their sufferings and tolerance all along my D.Phil. journey have a special place. I am equally thankful to Aisha Khala and Farrukh uncle and my siblings Neelam, Erum, and Daniyal along with Tahir bhai, Khalid bhai and Mariam for their constant support and encouragement.

My appreciation extends to my friends and officemates for being there when I was bothered and annoyed. To name a dozen; Asad for long discussions and valuable advices; Abdullah Sethi for being with me like a brother; Smit for spending time under one roof; Himanshu for cheering up in odd times; Ansar for delicious cooked meals; Arif and Farhan for supporting me when I was upset, Shahnawaz for being friend at Oxford across the border; Shabi for long phone calls and remembering old UET days; Priya for sharing good moments; officemates including Jessie, Kim, Shivaskar, Xiafu, Pharima, Kat, Tamara, Elias, Tracy, Hans, Bo, Sihao, Tiger, Fozia, Ping, Linnet, Allamin, Wenchan, Ziming, Till, Shangyi, Chao, Wen, Chris, friends from Engine's group; Nathan, Kun, Mengchan, Felix, Joe, Ian, friends from London, Scotland, Singapore, and pals associated with Oxford University Pakistan Society, Oxford Islamic Society and Oxford town community. I am very much grateful to all of my friends in Pakistan and elsewhere who prayed for me and helped me when it was needed.

Finally, not forgetting to underscore the gratified acknowledgement I have for the financial support from the Higher Education Commission of Pakistan for this project without which the dream to graduate from the top ranked University of the world could not be fulfilled.

Table of Contents

List of abbreviations and symbols

AFM	atomic-force microscopy
AL–DS	active layer facing draw side
AL–FS	active layer facing feed side
CA	cellulose acetate
$CaCl_2$	calcium chloride
CEOP	cake-enhanced osmotic pressure
CMC	carboxymethyl cellulose
CP	concentration polarisation
CTA	cellulose triacetate
DCP	dilutive concentration polarisation
DECP	dilutive external concentration polarisation
DI	de-ionised
DOTM	direct observation through membrane (technique)
DS	draw solution
ECP	external concentration polarisation
FO	forward osmosis
FS	feed solution
HCl	hydrochloric (acid)
HTI	Hydration Technology Innovations
ICP	internal concentration polarisation
MBR	membrane bioreactor
MF	microfiltration
MWCO	molecular weight cut off
NaOCl	sodium hypochlorite
NaOH	sodium hydroxide
NF	nanofiltration
ODMPs	osmotically driven membrane processes
ORF	osmotic-resistance filtration
RO	reverse osmosis
RSD	reverse solute diffusion
SEM	scanning electron microscope
SMTC	Singapore membrane technology centre
S-W	spiral wound
TFC	thin film composite
TOC	total organic compound
UF	ultrafiltration
UV	ultraviolet

A	water permeability coefficient (m^3/m^2-Pa)
A_m	effective membrane area – spiral wound module (m^2)
B	solute permeability coefficient (m^3/m^2)
C	concentration (moles/m^3)
D	diffusion coefficient (m^2/s)
d_h	hydraulic diameter (m)
d_{in}	inner diameter of feed inlet in module – spiral wound module (m)
d_{out}	outer diameter of feed inlet in module – spiral wound module (m)
F_{cecp}	concentration polarization factor for CECP (dimensionless)
F_{dcp}	concentration polarization factor for DCP (dimensionless)
F_{ecp}	concentration polarization factor for ECP (dimensionless)
ΔH	enthalpy (J/kg)
J_{lim}	limiting flux (m^3/m^2 s)
J_s	solute flux (m^3/m^2 s)
J_w	water flux (m^3/m^2 s)
$J_{w,f}$	fouling water flux (m^3/m^2 s)
K	overall mass transfer coefficient (m/s)
k	mass transfer coefficient (m/s)
k_c	mass transfer coefficient for channel adjacent to active layer– S-W module (m/s)
k_{cecp}	mass transfer coefficient near the membrane surface (m/s)
k_D	mass transfer coefficient at draw side (m/s)
$k_{ecp,f}$	overall mass transfer coefficient across the foulant layer and external concentration polarization boundary layer (m/s)
$k_{ecp,f}^*$	mass transfer coefficient within the foulant layer on the membrane (m/s)
$k_{ecp,o}$	mass transfer coefficient to the ECP boundary layer above the foulant layer (m/s)
k_F	mass transfer coefficient at feed side (m/s)
k_{sup}	mass transfer coefficient for channel adjacent to support layer– S-W module (m/s)
M	molar (moles/m^3)
m_f	mass deposition density (g/m^2)
MW	molecular weight (Da)
P_s	porosity of spacer (dimensionless)
$Q_{d,\,in}$	draw (solution) inlet flow – spiral wound module (m^3/s)
$Q_{f,\,in}$	feed (solution) inlet flow – spiral wound module (m^3/s)
R_{ads}	additional foulant resistance (m^{-1})
R_{df}	difference in foulant resistance (m^{-1})
Re	Reynold's number (dimensionless)
R_f	foulant resistance (m^{-1})
R_f/m_f	specific foulant resistance (m/g)
R_g	universal gas constant (8.3145 m^3 Pa mol^{-1} K^{-1})
R_m	hydraulic resistance of the membrane (m^{-1})
S	structural parameter (m^{-1})
Sc	Schmidt number (dimensionless)

S_f	structural parameter of the foulant layer (m^{-1})
$\overline{S_f}$	overall effective thickness of the CP boundary layer (m)
Sh	Sherwood number (dimensionless)
T	temperature (K)
T_s	thickness of spacer (m)
TMP	transmembrane pressure (Pa)
TOC	total organic carbon (g/m^3)
U	velocity of the fluid (m/s)
w/w	weight by weight (dimensiuonless)
β	Van't Hoff coefficient
δ	boundary layer thickness (m)
ε	porosity of the membrane (dimensionless)
μ	fluid viscosity (Pa s)
η_{rej}	solute rejection
$\pi_{D,i}$	osmotic pressure of the draw solution in the porous support layer at the interface with active layer (Pa)
$\pi_{D,b}$	osmotic pressure at the bulk of the draw solution (Pa)
$\pi_{D,m}$	osmotic pressure at the membrane surface of the draw solution (Pa)
π_{ds}	osmotic pressure of the draw solution (Pa)
π_{fs}	osmotic pressure of the feed solution (Pa)
$\pi_{F,b}$	osmotic pressure at the bulk of the feed solution (Pa)
$\pi_{F,m}$	osmotic pressure at the membrane surface of the feed solution (Pa)
$\Delta\pi$	osmotic pressure difference across the membrane (Pa)
$\Delta\pi_{app}$	applied osmotic pressure difference across the membrane (Pa)
$\Delta\pi_{eff}$	effective osmotic pressure difference across the membrane (Pa)
$\pi_{F,i}$	osmotic pressure of the feed on the inside of active layer within porous support (Pa)
ΔP	applied hydraulic pressure (Pa)
τ	tortuosity of support layer (dimensionless)

The subscript '*f*' added with any symbol in the text represents the fouled condition.

List of Figures

List of Tables

1

Introduction and background

1.1 Background

This thesis presents a study on the analysis of mechanisms of fouling in different membrane filtration processes. Whilst this project is majorly oriented towards the experimental analysis, an emphasis is also rested on the modelling for demonstrating the fouling mechanism in pressure driven and osmotically driven membranes. The major part of research has been conducted in Singapore Membrane Technology Centre (SMTC), NTU Singapore after having an insightful study of fouling in ultrafiltration Ceramic Membrane module at Oxford. An outline and objectives of the thesis is given at the end of this chapter after a study of conventionally used membrane modules, processes and modern applications.

1.2 Conventional membrane modules and modes

1.2.1 Membrane modules

A module is the structural block of a membrane system. The type and shape of module is based on the configuration of the membrane. Different modules are in use for holding the membranes which are either of tubular or flat sheet configurations. Figure 1.1 demonstrates the configuration of membrane modules. The selection of type of module is

primarily related to their use in laboratory or at pilot or commercial scales (Thompson and Nicoll, 2011, Von Medeazza, 2005, Dreizin et al., 2008) along with the outcome efficiency of the filtration and the application. Crossflow filtration through membrane refers to the flow through a membrane module in which the fluid on the upstream side of the membrane moves parallel

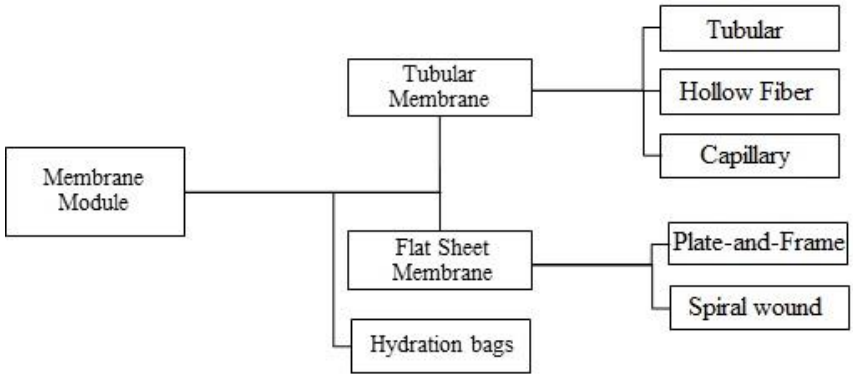

Figure 1.1: Configuration of membrane modules

to the membrane surface and the fluid on the downstream side of the membrane moves away from the membrane in the direction normal to the membrane surface (Koros et al., 1996). The simple structure of crossflow filtration is shown in Figure 1.2.

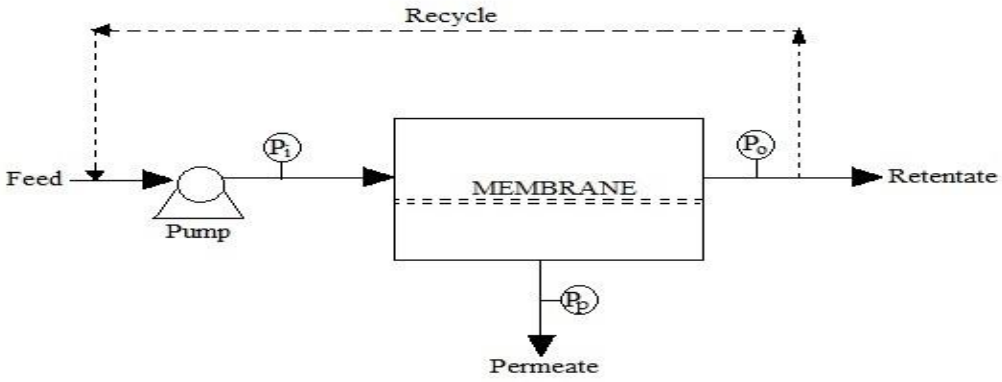

Figure 1.2: A simple crossflow membrane filtration module

Near to the membrane wall, the velocity is zero due to friction between the wall and the liquid. Solute is brought towards the membrane whereas some of the solvent is removed as

permeate. In connection with the structure of the module, the configurations in use are tubular and hollow fibre, plate-and-frame, spiral wound and bag configurations (Cath et al., 2006), the latter being exclusively for Forward Osmosis applications. Flat sheet membrane is configured in plate-and-frame module and spiral wound module. The configurations are briefly discussed below:

1.2.1.1 Tubular, hollow fibre and capillary membranes

In tubular, hollow fibre and capillary membranes, the internal diameter of the flow channel is of primary importance. In hollow fibre membranes, the internal diameter is less than 1 mm. Capillary membranes have the internal diameter of the range of 1 mm to 2 mm. However, for the tubular membranes, the internal diameter is greater than 2 mm (Frank et al., 2001). This results in some turbulence in flow and reduced concentration polarization in tubular membranes than the hollow fibre ones. Compared to hollow fibre membranes, tubular membranes have low packing density and fouling tendency with good cleaning capacity. However, tubular membranes unlike hollow fibres are not self-supporting. Hollow fibre membranes have an economic advantage; comparatively they require less investment.

In a module, the number of tubes may be different as according to requirement and module capacity. Figure 1.3 illustrates the schematic representation of a tubular membrane module. The feed flows across the respective membrane tube and exits from the other end as retentate. Permeation takes place through the membrane at the cost of driving force.

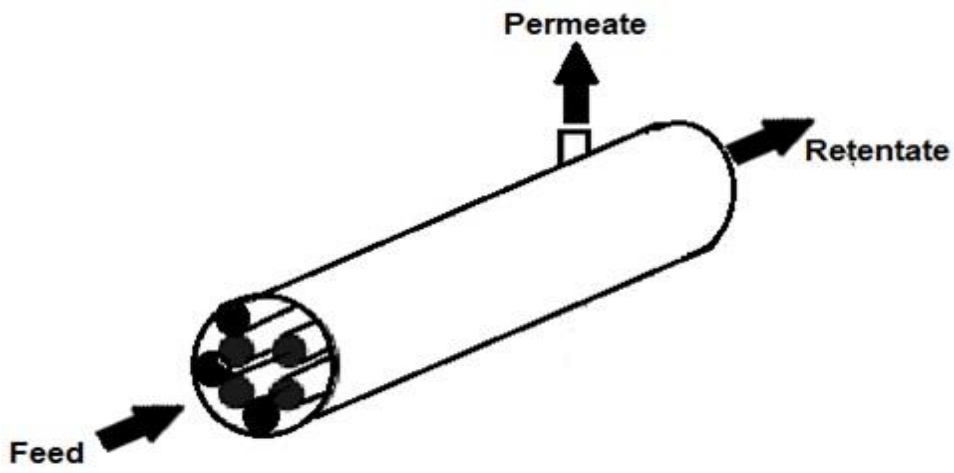

Figure 1.3: Schematic representation of a tubular membrane module

In hollow fibre membranes the pressure losses are moderately higher but there is increased area for permeation per unit volume of module. These modules are considered better when the feed stream is comparatively clean because of the smaller bore diameter. In this way, the pressure losses inside the fibres can be controlled or reduced.

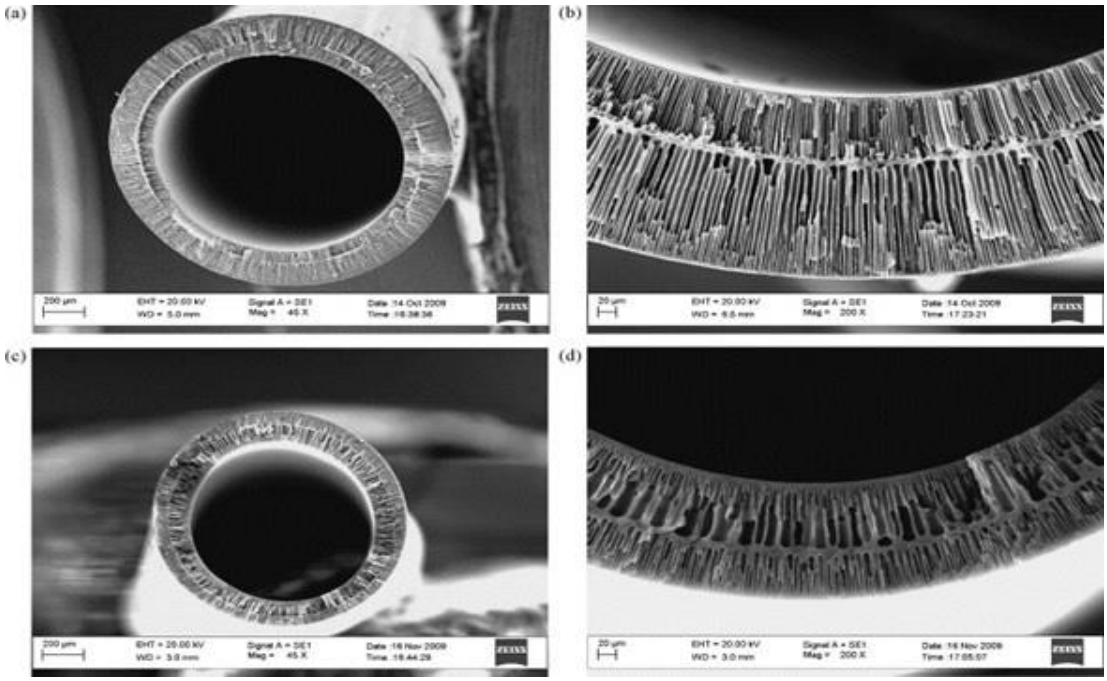

Figure 1.4: Morphology of hollow fibre substrates (a) cross-section at 45×, (b) enlarged at 200×, (c) cross-section at 45×, and (d) enlarged at 200× [Adapted from (Wang et al., 2010a)]

The hollow fibre membrane shown as sample A in Figure 1.4 has ultrafiltration like outer skin while sample B in the same Figure represents ultrafiltration like double skin layers. Both of the images almost have the same cross-section morphologies from inner and outer surface.

In Figure 1.4 (a) and (b), the hollow fibre substrate used tap water (as external coagulant) and an aqueous mixture of N-methyl-2-pyrrolidone as the bore fluid. While for Figure 1.4 (c) and (d), the hollow fibre substrate used water as external and internal coagulants. The application of external coagulant bath significantly increases the hydrophilicity and permeability of the membrane leading to noticeable improvement in antifouling along with better performance for normalized permeation (Xu et al., 2014).

The capillary modules can be divided into two categories namely inside-out module and outside-in module. In inside-out module, the feed solution flows through the bore of the capillaries and the permeate exits sideways. However, in outside-in module, the feed enters sideways from the shell side and the permeate exits from the bore of the capillary tube. Both types of capillary modules are diagrammatically illustrated in Figure 1.5.

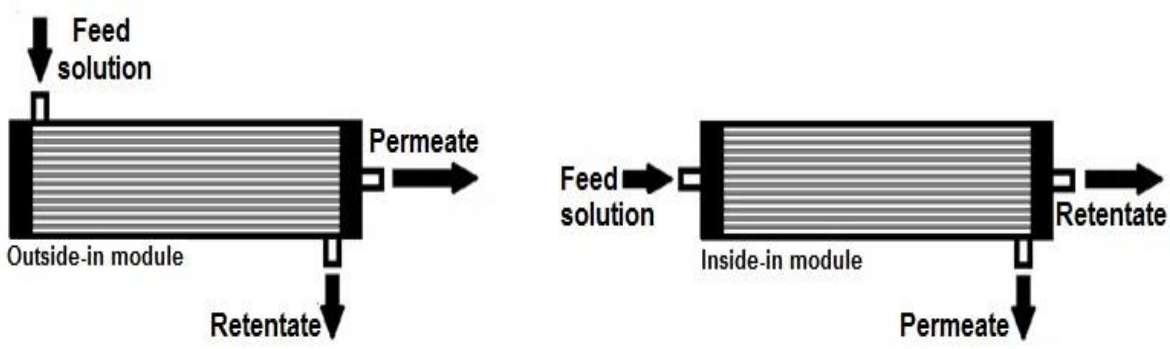

Figure 1.5: Two patterns of the capillary module

Capillaries have some advantages over tubular membranes that these are more durable with better support than tubular modules. Moreover, the packing density of capillaries is greater than tubular membrane elements but less than spiral wound and hollow fibre membrane modules.

1.2.1.2 Plate–and–frame membranes

Plate-and-frame modules are the simplest and most abundantly used membrane set-ups in a laboratory. With extendable flexibility, these modules can be built in a range of shapes and sizes ranging from holding a single small sized membrane coupon to multiple numbers of membranes. For this set-up, flat membranes are placed in parallel to each other typically with spacer plates in between on the feed side and on the permeate side. In some cases, a stop disc is also used which improves the design of the flow. It is a disc separating the series of aligned plate-and-frame membrane modules for redirecting the flow of feed across the channels. The schematic representation of plate-and-frame set-up is demonstrated in Figure 1.6.

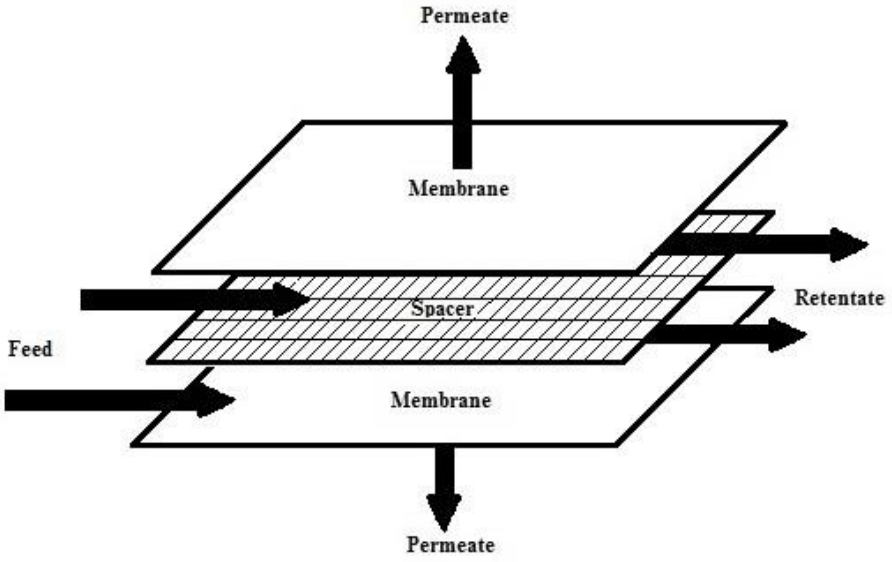

Figure 1.6: Plate-and-frame module set-up of a typical flat sheet membrane

A limitation of plate-and-frame modules is their low packing density in comparison to other modules. At plant scale, this results in a larger size of set-up leading to higher capital cost as well as higher operating costs because of difficulty in handling a large setup. Whilst low packing density is one of the major disadvantages of plate-and-frame membrane module, easy cleaning of the module along with easier control of hydrodynamics along with a greater degree of hydrodynamic control to combat ECP and reversible fouling are major advantages for this kind of membrane module.

1.2.1.3 Spiral wound membranes

A spiral-wound module is a modified form of plate-and-frame system with higher packing density. The membrane envelope is wrapped around an axial pipe which collects the permeate from the various leaves. The arrangement is demonstrated diagrammatically in Figure 1.7. The feed runs axially across the membrane; however, the permeate flows towards the axis of the cylinder in a spiral fashion. In these modules, the processing of the feed comprising of suspended particles is relatively difficult and hence, these modules work efficiently with comparatively clean streams, with little suspended substance. Generally for membrane modules, the size of the largest particle in the feed is required to be less than one-tenth of the channel height. However for spiral wound (and other systems with a feed side spacer) extra allowance has to be made for the spacer.

With reference to the power consumption, the spiral wound membranes are considered to be economical as the flow rates inside the membranes are quite low and need less energy compared to other modules (Cheryan and Kuo, 1984). However, in certain circumstances, the plate and frame module may consume less energy per permeate throughput than the spiral wound module particularly when spiral wound module is used in FO mode (Cath et

al., 2006). Despite the low flowrates in spiral wound module, the feed side pressure drop can be high and “telescoping” (the spiral pushing itself out in the flow direction) may damage the membrane.

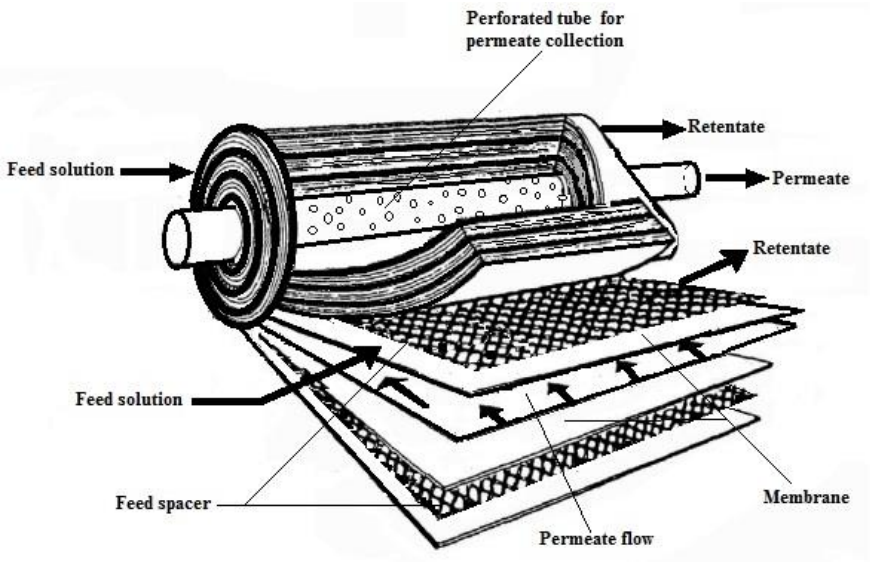

Figure 1.7: Schematic view of a spiral wound membrane module

1.2.1.4 Hydration bags membranes

One of the commercial use and practical application of the forward osmosis membrane is the hydration bags. FO membranes are structured as double-lined hydration bags and can be utilised to purify water. The internal bag is filled with draw solution and is made up of membrane. The draw solution could be a flavoured sucrose or glucose. However, the external bag is made up of plastic and is sealed. The external bag contains the draw solution (DS) bag inside and the feed water around the DS bag. As the hydration bag is submerged in the aqueous solution, the water from outer side diffuses into the bag due to the osmotic difference and gradually dilutes the draw solution. At the end, the diluted draw solution can be used as a nutrient drink. The hydration bags have high selectivity with low fouling propensity even with the use of muddy water as feed solution. A small scale personal device may take around 3 to 4 hours to hydrate a 12 ounce drink (Cath et al., 2006) for an average flux of around 3 LMH.

1.2.2 Pressurised and non-pressurised modes

In membrane filtration processes, there has been a continuous growing interest in analysing fouling behaviour and its mechanism for pressurised and non-pressurised processes. For pressurised processes, reverse osmosis (RO) is considered to be one of the most effective technologies for separation of water from the saline water and for waste water treatment (particularly as the second barrier in the NEWater process). In this process, through the application of pressure on feed side, water is forced to permeate through the membrane leaving behind the concentrated feed solution called retentate.

In non-pressurised processes, fluxes are agreed via other means e.g. in forward osmosis (FO) filtration takes place due to a difference in osmotic pressure. The water permeates from the feed side which is of lower osmotic pressure towards the other side diluting the draw solution of higher osmotic pressure. Both of the processes are discussed in detail in sections 2.2 and 2.3 respectively.

1.3 Applications of forward osmosis

The applications based on FO have been extended to a number of areas including waste water treatment, sea water desalination, food processing and in the pharmaceutical industry etc. (Cath et al., 2006, Wang et al., 2010b, Hoover et al., 2011, Thompson and Nicoll, 2011, Chung et al., 2012, Zhao et al., 2012, Field and Wu, 2013, Bell et al., 2016). Due to its low consumption of high grade energy during the whole process, FO has attracted great interest. A few applications of FO are discussed below:

1.3.1 Water purification

Water purification is the oldest application of forward osmosis applications. In a recent research, Luo et al. (2015) extracted water from mixed liquor of an aerobic bioreactor through forward osmosis and examined fouling and biomass characteristics. In another study, Minier-Matar et al. (2015) examined the application of forward osmosis for reducing the volume of produced/processed water using sea water as draw solution. However, in forward osmosis process, there is a limitation that water extracted from the feed solution is further mixed with the draw solution and in order to obtain fresh water from the draw solution, further separation is needed.

1.3.2 Seawater desalination

A number of researchers have considered and researched this technology for desalination of sea water from different oceans of the world. Kravath and Davis (1975) used this technology more than four decades ago using a cellulose membrane for desalinating Atlantic Ocean sea water using glucose as draw solution. The following year, Kessler and Moody (1976) demonstrated the use of the same technology for extracting potable water from sea water. In their experiments, they used concentrated solution of different nutrients on the draw solution side. In a recent study, the researchers from Yale used this technology and developed a process that used ammonium bicarbonate as draw (McGinnis et al., 2015). Choi et al. (2009) investigated the characteristics of forward and reverse osmosis processes for seawater desalination using simple film theory model. Work on FO desalination is still in progress by contemporary researchers e.g. Elimelech and Phillip (2011), Thompson and Nicoll (2011), Akther et al. (2015). Companies involved include Modern Water, OASYS Water and Hydration Technology Innovations (HTI).

1.3.3 Wastewater treatment

Waste water treatment is a notable potential application of forward osmosis. Early publications in this regard were those by Votta (1974) and Anderson (1977) although low key work on FO continued over the next 20 years (Shinjou and Shoji, 1988, Beaudry and Herron, 1997, York et al., 1999) with much more activity over the last 20 years. A number of recent developments are in progress for using forward osmosis technology in waste water treatment, landfill leachate, water recovery from wastewater and investigating concentration of liquids anaerobic sludge (Lutchmiah et al., 2014, York et al., 1999, Lutchmiah et al., 2011, Holloway et al., 2007).

1.3.4 Food processing

Some have considered that treatment of food products using the osmotic filtration technology might become an attractive application. Most of the studies have been on concentration of liquefied food items (Cath et al., 2006). Traditionally, fruit juices were concentrated using multistage vacuum evaporation technology but this often results in changes in flavours and colours. This has raised the importance of membrane processes in food processing and its research applications and ultrafiltration and reverse osmosis are employed (Jiao et al., 2004). In a recent study, Garcia-Castello et al. (2009) used flat sheet CA membrane to analyse performance of sucrose concentration in osmotically driven processes. Similarly, Zhao et al. (2011) examined the effects of membrane orientation in forward osmosis applications, including food processing. The contemporary studies (Hoover et al., 2011, Shaffer et al., 2015, Knoerzer et al., 2016) demonstrate the increasing interest of forward osmosis in food processes which is related to less irreversible fouling and easy cleaning compared to traditional pressure driven processes. However reverse salt flux is potentially a large problem.

1.4 Applications of reverse osmosis

1.4.1 Drinking water purification

The most common application of the reverse osmosis is purification of the drinking water. A number of successful applications demonstrate the removal of contaminants by using this technology. In a recent study, the applications of reverse osmosis can remove up to 88–96 % of arsenic which is one of the major contaminant in drinking water threatening lives of millions of people in the world (Ning, 2002). Radjenović et al. (2008) used thin film composite membranes for the removal of pharmaceutical residues detected in ground water. In a very recent study, removal of humic acid and chloroform from drinking water was investigated by RO using different commercial membranes and rejections of up to 98.5% were obtained (Abdel-Karim et al., 2017). However, the major concern for the installation and running of RO systems is cost in terms of module replacement and energy consumption. Normally, RO systems use electricity from the grid but in a comparative analysis, it was noted that RO systems driven by steam or gas turbines can be more cost effective (Darwish et al., 2009).

1.4.2 Desalination of seawater and brackish water

Desalination of sea water and brackish water is the important applications of reverse osmosis process. Sea water desalination is used on commercial scale for production of clean water from the sea water. Occasionally, this is alongside extraction of ocean salt as an alternate product (Vetter et al., 2007, Darwish et al., 2009, Monnot et al., 2017). Desalination of Brackish water refers to the treatment of the water which has lower salt contents than that in the sea water. This kind of water is generally obtained from saline wells or river creeks. As compared to the process applied on the sea water, reverse osmosis

for the brackish water needs less energy due to the requirement of low pressure on the feed side (Den and Wang, 2008, Qureshi and Zubair, 2015, Cay-Durgun et al., 2017).

As mentioned by Eisenberg and Middlebrooks (2013) regarding an inventory prepared by El-Ramly and Congdon (1981) for the desalination plants with treatment capacities of 95 cubic meter per day or more, it has been noted that there were 447 reverse osmosis plants in United States with a total treatment capacity of about 757,000 m^3/day.

1.4.3 Waste water treatment

The process of reverse osmosis is widely used for waste water treatment. Water is extracted from the waste water and is used for the useful purposes. In Singapore, the government practically implemented the process for waste water treatment named NEWater (Qin et al., 2006). Through this process, the domestic waste water is treated in membrane bioreactors before being polished with reverse osmosis technology and then the water is discharged back to the reservoirs.

The water used in certain industries becomes contaminated during its use and the contaminants need to be removed before discharging the water in connections with health and safety requirements. The contaminants may include heavy metals, oil, grease, and any other related compounds. These are generally removed by reverse osmosis processes (Kishino et al., 1996, Xiao-Jun et al., 1996, Gander et al., 2000, Lozier and Fernandez, 2001, Petrinic et al., 2015, Ochando-Pulido and Martinez-Ferez, 2017).

1.4.4 Food industry

Another important industrial application of the reverse osmosis processes is in the food industry. The fruit juices and other food liquids are concentrated using this technology (Gurak et al., 2010, Garcia-Castello et al., 2011, Al-Obaidi et al., 2017). As compared to other processes, reverse osmosis appears to be quite economical in this regard as it avoids any heat treatment processes. However, due to the limitation of high osmotic pressure, one of the disadvantages regarding application of RO processes is lower yield concentration as compared to the thermal process (Al-Obaidi et al., 2017).

Along with the juice industry, the technology is extensively used in the modern dairy industry for the treatment of milk and other dairy products. Dairy units are considered to have high consumption of water. This include washing, pasteurising, rinsing, cleaning, high temperature processes, cooling and chilling etc. in which, there is high consumption of water (Suárez et al., 2014, Suárez and Riera, 2015).

1.5 Research objectives

The main experimental part of this thesis concerns a comparative study of the fouling by alginate and silica in Forward Osmosis (FO) and Reverse Osmosis (RO) in terms of flux profiles, foulant resistance and effective driving force as well as foulant mass load (by autopsy). This was conducted in Singapore where the research was further extended with the use of real waters as feed on bench and pilot scales. Prior to that work, an experimental study of fouling in ultrafiltration ceramic tubular membrane for the foulants dextran and carboxymethyl cellulose was undertaken at Oxford.

In both phases, the question of whether a critical flux could be determined and the impact of rinsing after fouling were examined. A comparison has been made after an insightful analysis of the account of reversibility of the foulant layer in forward osmosis, reverse osmosis, and ultrafiltration membrane process along with post-fouling cleaning of the membranes in all setups. This links the two phases of the thesis research.

Hypothesis:

The major hypothesis of the thesis is that given the absence of the hydraulic pressure gradient, forward osmosis is more prone to fouling than reverse osmosis. It was further aimed to investigate that, in comparison to that in ultrafiltration membrane process; the reversibility of the fouling layer is greater in FO and RO than in UF.

Experimental design:

In the first phase, the experiments were designed to be performed on an ultrafiltration ceramic membrane at Oxford with dextran and carboxymethyl cellulose as foulants. For the second phase, the experiments were planned to be conducted, in SMTC Singapore, on a flat sheet bench scale set up that could be used for both FO and RO setups with polymeric membranes. Silica and dextran were used as potential foulants. This phase of the research was further extended to pilot scale spiral wound setup along with the bench scale one for studying the fouling behaviour. The details of the experimental setups are explained in Chapter 3. The experimental results and conclusions are reported in later chapters.

1.6 Thesis outline

This thesis includes 7 chapters, which are highlighted as below:

Chapter 1: Introduction and background

Introduction of the thesis, types of conventionally used membrane modules and membrane processes and applications of osmotically driven and pressure driven processes were discussed in this chapter. It also put light on conventionally used membrane modules and processes and related applications. The research objectives of this thesis and related links between the two phases of the research conducted at Oxford and Singapore have also been highlighted.

Chapter 2: Literature review

This chapter contains a brief literature survey which focusses on:

- Work of previous researchers
- Taxonomy and characterization of membrane processes
- Concentration polarization
- Fouling in forward osmosis
- Membrane cleaning; and
- Critical flux

Chapter 3: Materials and Methods

This chapter illustrates the techniques and methods used along with the description of the experimental setups and design and structure of the membrane modules used in the research. Based on three different phases of the research, the work in this chapter has been split into three main sections. One describes the experimental procedure and setup of flat sheet membrane used during comparative analyses of fouling experiments in forward and

reverse osmosis. The second part is related to a series of fouling and cleaning experiments using an ultrafiltration ceramic tubular membrane. The last section outlines the methods used in an assessment of spiral wound forward osmosis module used at pilot scale experiments.

Chapter 4: Tubular ultrafiltration ceramic membrane

Chapter 4 covers a series of experiments conducted on an ultrafiltration ceramic tubular membrane for the foulants dextran and carboxymethyl cellulose. The impact of foulant concentration on fouling resistance along with impact of cold and hot rinsing was recorded for both foulants. It was noted that in both cases, the reduction in resistance due to rinsing changed with C^n where C represents concentration and ‘n' is a suitable constant. A plausible semi-theoretical explanation for the determined value of n=0.3 is given. The effect of various cleaning chemicals on both foulants is also reported.

Chapter 5: Fouling mechanism in osmotically driven and pressure driven membranes

A systematic experimental study of fouling behaviour for osmotically driven and pressure driven processes in ALFS orientation was undertaken in order to have comparative fouling data. The importance of internal concentration polarisation in forward osmosis operation is highlighted. A notable finding was that the flux behaviour may not indicate the exact fouling behaviour as there are other factors such as the changing driving force across the active layer which governs the flux trend. It was also observed that critical flux is an important parameter for attaining the fouling condition.

Chapter 6: Performance of an osmotically driven module at pilot and bench scale

The performance of a spiral wound cellulose tri acetate pilot scale unit was evaluated using treated waste water obtained from Bedok NeWater factory in Singapore. In the second phase, the experiments were repeated on a bench scale using a flat sheet membrane setup with identical conditions. The effect of membrane orientation and its role in removing the reversible fouling after changing the direction in specified intervals was the part of the study. A comparison of experiments conducted at both scales is made.

Chapter 7: Concluding remarks and recommendations for future work

In this chapter, conclusions are extracted from the current research work and recommendations are made for future investigation.

2

Literature Review

This chapter presents a review on various aspects of fouling in osmotically driven and pressure driven membranes and cleaning applications. Fouling has always remained in the lime light of membrane study. For the research on fouling in both pressure driven and osmotically driven membranes, there are many factors which play key roles and these factors are discussed below. Background of membrane processes is part of section 2.1, whilst section 2.2 contains fouling in forward osmosis including in-depth discussion of concentration polarisation and other related mechanisms. Section 2.3 covers membrane cleaning whilst section 2.4 considers the concept of critical flux before conclusions are made in section 2.5.

2.1 Membrane processes for water production

2.1.1 Background

In 1950's, at the University of California (USA), it was shown that (Yuster et al., 1958) one can extract fresh water from brine solution. After a further decade, the development of improved reverse osmosis membranes through the Loeb–Sourirajan process emerged (Loeb and Sourirajan, 1962). The application of the process has been discussed elsewhere (Riley et al., 1966, Strathmann et al., 1971, Loeb, 1981). Along with the pressurised processes in membrane technology, osmotically driven membrane processes remained the

side story of the on-going research of the same decade. In the middle of the decade of 1950s, the idea of generating power due to osmotic pressure difference between sea water and river was proposed (Pattle, 1954). In later decades, the concept of osmotic power was further endorsed by other researchers (Norman, 1974, Levenspiel and de Nevers, 1974, Loeb et al., 1976, Loeb, 1976) and more findings were revealed.

At present, the interest in osmotically driven membrane processes, particularly forward osmosis, is still increasing steadily (Choi et al., 2005, Cath et al., 2006, Hoover et al., 2011, Chung et al., 2012, McGinnis and McGurgan, 2012, Zhao et al., 2012) along with the pressure driven ones (Vrijenhoek et al., 2001, Fritzmann et al., 2007, Greenlee et al., 2009, Lee et al., 2011, Kurth et al., 2012). In an osmotically driven membrane process, the concentrated draw solution on one side of the membrane generates the high osmotic pressure and pulls the water from the feed solution on the other side of the membrane, which is at considerably lower osmotic pressure. However, in a pressure driven membrane process (reverse osmosis), the driving force for water permeation through membrane is the application of hydraulic pressure from the feed side. Nevertheless, in both processes, fouling has always remained a point of interest for researchers because of its affect upon the membrane's filtration efficiency.

The difference in application of the driving force has an impact on fouling trend for both processes. A few of the researchers have analytically discussed the reasons for this difference in fouling behaviour for forward osmosis (FO) and reverse osmosis (RO), and it is claimed that FO is less prone to fouling than RO (Lee et al., 2010, Xie et al., 2012, Altaee et al., 2014). Previous studies have revealed that in FO, the flux decline with time is less with no compression of the foulant layer in FO as compared to that in RO. Higher

water flux recovery was found for FO than that for RO (Lee et al., 2010, Mi and Elimelech, 2010a, Mi and Elimelech, 2010b, Mi and Elimelech, 2013, Kim et al., 2014, Xie et al., 2015). In these studies, the comparison of results in FO and RO is somewhat unfair. In RO, pressure (or apparent driving force) was maintained constant. However, in FO, the concentration of draw solution was diluted with time and feed solution concentration was concentrated with time. So in FO osmotic pressure (or apparent osmotic driving force) was decreasing. To the best of the authors' knowledge, no study has been attempted yet to determine comparative foulant resistances in FO and in RO starting with the same initial flux. So, there is a lack of direct comparison of the extent of fouling in FO and RO and hence, insufficient evidence to prove that the pressure compresses the foulant layer. Whilst this claim is plausible, it seems equally valid to assert that the driving force for fouling is flux.

Tang and She (Tang et al., 2010, She et al., 2016) have systematically elaborated the ICP self-compensation effect which is inherent in FO and will moderate the flux decline. Previous studies did not explore this effect when comparing FO and RO fouling, which is a gap that will be filled by the present research.

At a commercial scale, there have been noteworthy developments in recent years which can be seen in installation of plants for sea water desalination in different countries. Dreizin et al. (2008) discussed the factors faced by planners for the installation of large scale desalination plants in Israel. Not only have the technical issues hindered the development, but the economic factors have slowed the progress. Nevertheless, continuing progress is further expected in coming decades for water purification (Shannon et al., 2008, Elimelech and Phillip, 2011, Chung et al., 2012).

2.1.2 Taxonomy and characterization

The membrane processes for water production are widely categorised into:

i. Pressure driven membrane processes and

ii. Osmotically driven membrane processes

In pressurised membrane processes, hydraulic pressure is applied on the feed water side which pushes the water through the membrane. However, in osmotically driven membranes, the permeation takes place due to osmotic pressure difference at both sides of feed and draw solutions (Tang et al., 2010). The membrane is a fundamental element in both applications. Typically used commercial membranes contain a porous support layer and a dense active layer. The orientation of the membrane in connection with the feed and draw side has a noteworthy effect on permeation behaviour. A number of studies have revealed this fact, and in chapter 5, the effect of membrane orientation has been studied experimentally for pilot as well as bench scale equipment.

It was discovered in a previous research conducted on thin film composite membranes (Lu et al., 2015) that fouling tendency of the active layer is affected notably by the support layer structure and hence when designing the support layer structure of the membranes, this impact should be taken in to account. Tang and his co-workers, with a comparative analysis for membrane orientation as active layer on feed side (ALFS) vs. active layer on draw side (ALDS), discussed the coupled effects of internal concentration polarisation and fouling for filtering humic acid solution through forward osmosis (Tang et al., 2010).

In recent years, for the membrane filtration processes, there has been a growing interest in analysing fouling behaviour and its mechanism for pressurised and non-pressurised processes. For pressurised processes, reverse osmosis (RO) is considered to be one of the

most effective technologies for separation of water from the saline water and waste water treatment.

2.2 Fouling in forward Osmosis

2.2.1 Introduction

Forward Osmosis (FO) appears to be one of the most promising technologies that are being used for water purification. It is a process by which water is separated from the dissolved solutes through use of a semi permeable membrane and is distinguished from reverse osmosis by the fact that the driving force for this separation is an osmotic pressure gradient caused by a highly concentrative draw solution on one side of the membrane while the feed solution is on the other side. This causes the water from the feed solution to pass through the membrane towards the draw solution. As in other membrane filtration processes', fouling has always remained a topic of interest for membrane researchers.

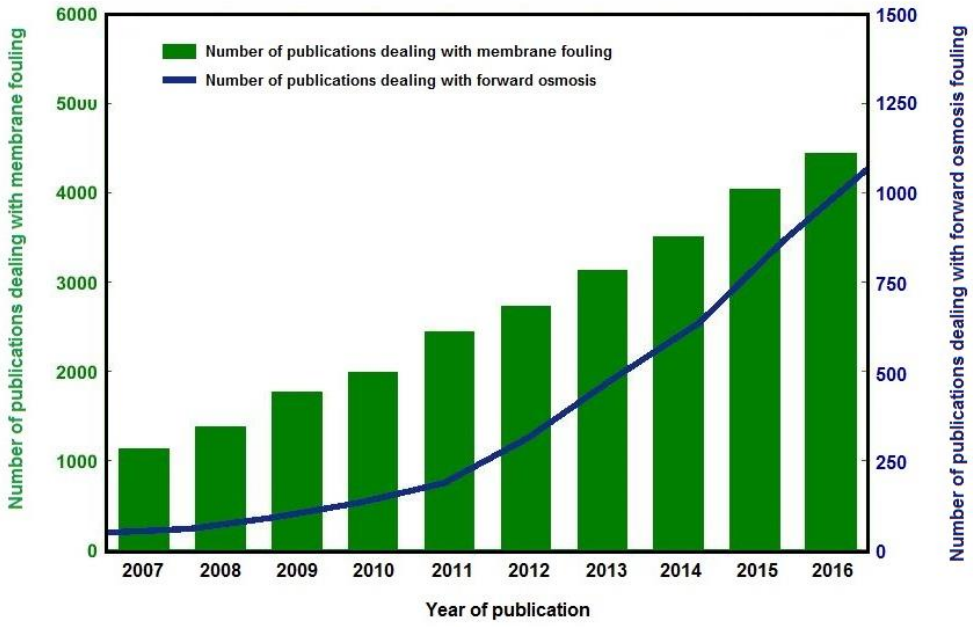

Figure 2.1 Growing evolution of the number of publications in journals related to fouling in *forward osmosis* and to *membrane fouling* for recent decade [source: https://www.scopus.com]

The publications on FO fouling have been increasing exponentially along with those on membrane fouling during the last decade (refer to Figure 2.1). However, FO faces some limitations as well which need to be tackled.

2.2.2 Concentration Polarisation

Concentration polarisation is a noteworthy problem in membrane processes and has thus attracted a number of researchers (Zydney and Colton, 1986, Elimelech and Bhattacharjee, 1998, Sablani et al., 2001, Nguyen et al., 2016). The polarisation has been quantitatively divided by its types as external and internal concentration polarisation. In the osmotically driven membrane processes, as the water permeates through the membrane from feed side to the draw side, the vicinity of the membrane surface at the feed side becomes more concentrated as compared to that of the bulk solution and conversely the concentration of the draw solute in the vicinity of the membrane is reduced.

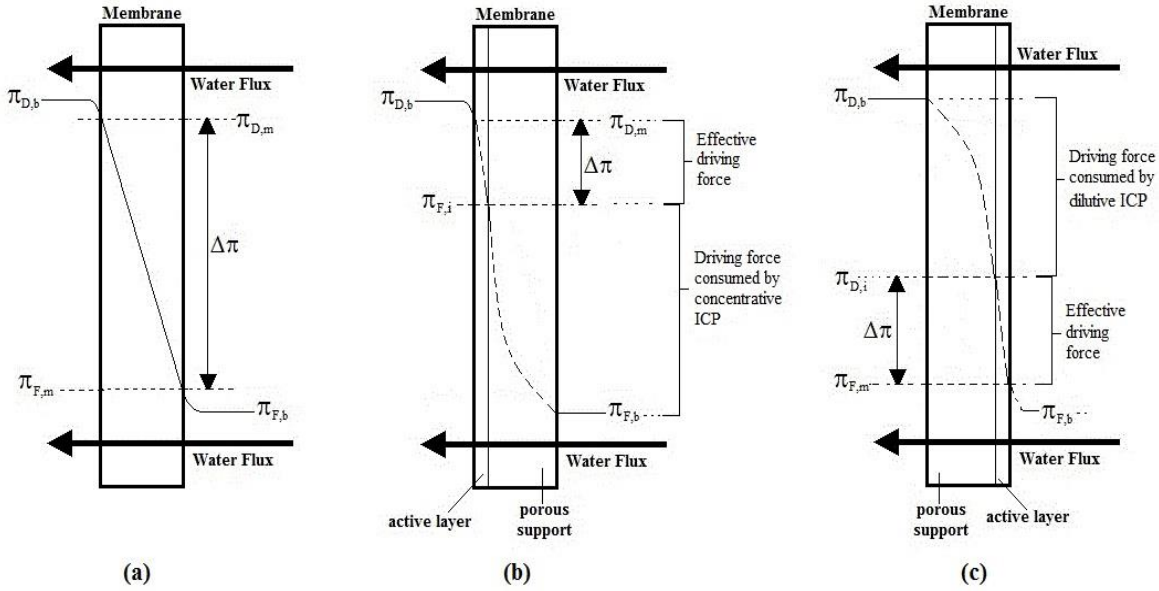

(a) external concentration polarisation in membrane **(b)** concentrative internal concentration polarisation in ALDS orientation of the membrane **(c)** dilutive internal concentration polarisation in ALFS orientation of the membrane

Figure 2.2 Illustration of concentration polarisation in different orientations

This reduces the concentration difference at both sides of the membrane and hence reduces the osmotic force which finally reduces the permeation. This phenomenon is called concentration polarisation and is diagrammatically discussed in Figure 2.2 for the feed and draw side. The polarisation within the support layer is referred to as internal concentration polarisation (ICP) (Porter, 1972, Sablani et al., 2001). External and internal concentration polarisation is further discussed below:

2.2.2.1 External concentration polarisation

In pressure driven membrane processes, the osmotic pressure at the active layer surface is affected due to the concentration polarisation at the surface and hence hinders the permeation through the membrane. Since the concentration polarisation occurs outside the membrane, this is regarded as external concentration polarisation (ECP). In case of osmotically driven membranes, external concentration polarisation occurs on both sides of the membrane for which the phenomenon concentrative and dilutive ECP are used (McCutcheon and Elimelech, 2006, Cath et al., 2006).

i. Concentrative external concentration polarisation

In osmotic as well as pressure driven membranes, the convective water flow at the feed side drags the solute to the membrane surface. As the water permeates from feed to the draw side, the concentration of the solute at the membrane surface is increased to more than that in the bulk solution due to the presence of the additional rejected solute. Therefore, the concentrative ECP takes place only on the feed side. In common with others the assumption that ratios of osmotic pressure at feed surface and bulk solution is equivalent to the corresponding ratio of solute concentrations has been made. As shown by the data tables made openly available by MIT, corrections for non-ideal behaviour would

be very minor (Nayar et al., 2016). There is a decrease in the effective driving force. For complete rejection (McCutcheon and Elimelech, 2006):

$$\frac{\pi_{\mathrm{F,m}}}{\pi_{\mathrm{F,b}}} = \exp\left(\frac{J_w}{k_F}\right) \tag{2.1}$$

where, J_w denotes the permeate water flux calculated experimentally while $\pi_{F,m}$ and $\pi_{F,b}$ represent the osmotic pressures at the membrane surface and in the bulk of the feed solution respectively. Now k_F the mass transfer coefficient (at feed side) is the ratio of the product of Sherwood number and the diffusion coefficient to that of the hydraulic diameter. The value of Sherwood number (*Sh*) for laminar and turbulent flow can be calculated (McCutcheon and Elimelech, 2006) as:

$$Sh = \frac{k\, d_h}{D} \tag{2.2}$$

where,
$$Sh = 1.85\ \left(Re\, Sc\ \frac{\mathrm{d_h}}{L}\right)^{0.33} \quad \text{(laminar flow)} \tag{2.3a}$$

$$Sh = 0.04\ Re^{0.75}\ Sc^{0.33} \quad \text{(turbulent flow)} \tag{2.3b}$$

where, k, d_h and D represent mass transfer coefficient, hydraulic diameter and solute diffusion coefficient respectively. *Re* and *Sc* are the Reynold's number and the Schmidt number respectively. In Equation 2.1, it is notable that the exponent is positive which indicates that $\pi_{F,m}$ is greater than $\pi_{F,b}$ in accord with concentrative external concentration polarisation.

ii. Dilutive external concentration polarisation

In osmotically driven membrane processes, as the water permeates from feed side and enters into the draw side, it dilutes the draw solution near the surface of the membrane on draw side. This reduces the effective driving force (i.e. osmotic difference) at the permeate side and hence the flux is reduced. This phenomenon is referred as the dilutive external concentration polarisation. The flux performance in forward osmosis in connection with the dilutive ECP is:

$$\frac{\pi_{D,m}}{\pi_{D,b}} = \exp\left(-\frac{J_w}{k_D}\right) \tag{2.4}$$

where $\pi_{D,m}$ and $\pi_{D,b}$ refers to the osmotic pressures of the draw solution at the membrane surface and in the bulk solution respectively. For osmotically driven processes, the general equation used for the water flux (J_w) is given by (Lee et al., 1981):

$$J_w = A\,(\Delta\pi_{eff} - \Delta P) \tag{2.5}$$

where A is the water permeability coefficient while $\Delta\pi_{eff}$ and ΔP represent the effective osmotic pressure difference and the net applied hydraulic pressure respectively. For the FO processes, the hydraulic pressure is zero. Therefore, the driving force across the membrane is the osmotic pressure difference across the membrane. McCutcheon and Elimelech modelled the flux performance of the FO process in the presence of ECP using the above equations (McCutcheon and Elimelech, 2006). In case of FO, the standard flux equation is given as:

$$J_w = A(\pi_{D,b} - \pi_{F,b}) \tag{2.6}$$

where, A is the water permeability coefficient. Assuming that there is no salt diffusion across the membrane in either direction, for higher flux rates including concentrative and dilutive ECP, Equation 2.6 becomes,

$$J_w = A\left[\pi_{D,b}\exp\left(-\frac{J_w}{k_D}\right) - \pi_{F,b}\exp\left(\frac{J_w}{k_F}\right)\right] \quad (2.7)$$

2.2.2.2 Internal concentration polarisation

The influence of a porous support layer of an asymmetric membrane is now taken into account. Concentration polarisation prevails inside the support layer and this phenomenon is regarded as the internal concentration polarisation (ICP). As with external concentration polarisation, there is dilutive and concentrative internal concentration polarisation for ALFS and ALDS orientations respectively.

i. Concentrative internal concentration polarisation

In the case of active layer facing the draw side (ALDS) of an asymmetric membrane; as the water permeates from feed side to the draw side, any salt in the feed enters freely in the porous support layer with the feed solution. But this salt does not diffuse across the membrane with the water and remains inside the porous support layer giving rise to concentrative internal concentration polarisation; a balance is achieved between convective inflow of solutes and diffusive outflow of solutes. Lee et al. (1981) derived the flux expression in connection with pressure retarded osmosis. It is applicable to Forward Osmosis and links internal concentration polarisation with other membrane parameters.

The expression demonstrates the link of solute resistivity with the other parameters as follows:

$$K = \left(\frac{1}{J_w}\right) \ln \frac{B + A\,\pi_{D,m} - J_w}{B + A\,\pi_{F,b}} \tag{2.8}$$

where, A and B are the pure water permeability and the salt permeability coefficient respectively. Solute resistivity is further defined as:

$$K = \frac{\iota\tau}{D\varepsilon} \tag{2.9}$$

where D represents the diffusion coefficient of the solute while, ε, τ and ι denote porosity, tortuosity and thickness of the support layer respectively. With higher solute rejection, salt permeability is negligible and B factor in Eq (2.8) can be ignored. So:

$$J_w = A\,[\pi_{D,m} - \pi_{F,b} \exp(J_w K)] \tag{2.10}$$

McCutcheon and Elimelech (2006) regarded the exponential term in Equation (2.10) as a correction factor that can be taken as the concentrative ICP modulus. Hence they defined the modulus as:

$$\frac{\pi_{F,i}}{\pi_{F,b}} = \exp(J_w K) \tag{2.11}$$

where, $\pi_{F,i}$ represents the osmotic pressure of the feed on the inside of the active layer within porous support. The positive exponent reveals that $\pi_{F,i}$ is greater than $\pi_{F,b}$ indicating

concentrative internal concentration polarisation. Figure 2.2 (b) illustrates the phenomenon of the concentrative internal concentration polarisation.

For computing the flux, Equation (2.10) needs the link with membrane surface concentration at the permeate side. However, switching Equation (2.4) into Equation (2.10) gives the calculable analytical model which illustrates the relationship of internal and external concentration polarisation with the permeate flux. In Figure 2.2(b) and 2.2(c) unlike Figure 2.2(a), only one external mass transfer boundary layer is shown. Whilst not true theoretically this has been justified on the basis that the measured *K* incorporates one external boundary layer. This is illustrated in Equation (2.12).

$$J_w = \mathrm{A}\,[\pi_{D,b}\, exp\left(-\frac{J_w}{k_D}\right) - \pi_{\mathrm{F,b}} \exp\left(J_w K\right)] \qquad (2.12)$$

ii. Dilutive internal concentration polarisation

In case of active layer facing the feed side (ALFS) of an asymmetric membrane, as the water permeates from feed side into the draw side in the porous support layer, the solute is locally diluted. The salt diffuses back to the interior surface and a steady state is quickly attained. However, the concentration of the solute inside the porous support layer is lower than that in the bulk draw solution which results in reduction in permeation. This phenomenon is dilutive internal concentration polarisation. For dilutive ICP, the flux equation is given by Gray et al. (2006) as:

$$K = \left(\frac{1}{J_w}\right) \ln \frac{B + A\,\pi_{\mathrm{D,b}}}{B + J_w + A\,\pi_{\mathrm{F,m}}} \qquad (2.13)$$

For higher solute rejection, as illustrated by McCutcheon and Elimelech (2006), the salt permeability is negligible. Re-arranging Equation (2.13):

$$J_w = \mathrm{A}\,[\,\pi_{D,b}\,exp\,(-J_w\,K) - \pi_{\mathrm{F,m}}\,] \tag{2.14}$$

The dilutive ICP model was further illustrated by using the exponential term as its correction factor which is given by:

$$\frac{\pi_{D,i}}{\pi_{D,b}} = \exp\,(-J_w\,K) \tag{2.15}$$

where, $\pi_{\mathrm{D,i}}$ represents the osmotic pressure of the draw solution in the porous support layer at the interface with an active layer. It is less than the osmotic pressure of the draw solution in the bulk solution ($\pi_{\mathrm{D,b}}$) as indicated by the negative exponent showing dilutive internal concentration polarisation. Combining Equation (2.1) with Equation (2.14) a model with water flux for an asymmetric membrane is derived where the feed solution is placed against the active layer and the draw solution against the porous support layer. The resulting equation is:

$$J_w = \mathrm{A}\,[\,\pi_{D,b}\,\exp\,(-J_w\,K) - \pi_{\mathrm{F,b}}\,\exp\left(\frac{J_w}{k_F}\right)\,] \tag{2.16}$$

In Equation 2.12 and Equation 2.16, ‘K’ is the inverse of the overall mass transfer coefficient at the support layer side. In the former mode, the support layer faces the feed solution while in latter, it faces the draw side. So, in both cases, the coefficient ‘K’ is used accordingly. However, the smaller ‘k’ is used in the traditional manner and represents the

mass transfer coefficients on the active layer sides as described by the respective subscripts for feed side or draw side. The flux, in general is directly affected by the concentration polarisation, particularly ICP. Internal concentration polarisation, in both forms, affects the overall driving force and this effect increases with flux.

2.2.2.3 Mathematical illustration of internal and external concentration polarisation

Mathematically, the impact of concentration polarisation on membrane filtration has been calculated by many researchers (Zydney and Colton, 1986, Elimelech and Bhattacharjee, 1998, She et al., 2016). Apart from its severe effects in reducing the driving force, it is also associated with membrane fouling. Discussing specifically forward osmosis, two forms of concentration polarisation i.e. internal and external concentration polarisation are applicable.

Along with a few other factors, the impact of internal and external concentration polarisation is widely dependent on membrane orientation. Tang et al. (2010) observed that severe internal concentration polarisation was identified when the membrane active layer was set to face the feed water i.e. ALFS orientation as compared to that in ALDS orientation. They referred it to the reason of dilutive internal concentration polarisation (ICP) in the membrane support layer. They also observed that for ALFS orientation, diluting the draw solution had a negligible effect on flux reduction due to compensation by a proportional decrease in ICP; hence this orientation enjoyed comparatively stable flux. Therefore, it is necessary to discuss both cases separately. She et al. (2016) discussed the said impact through the model depicted in Figure 2.3.

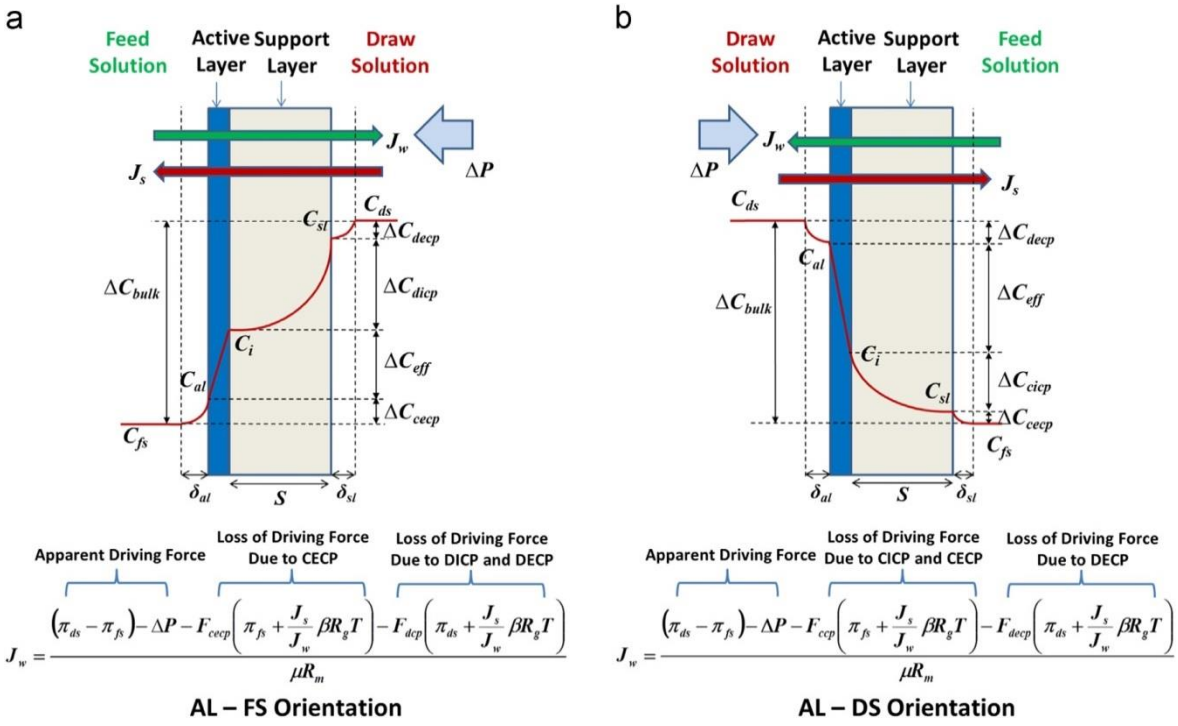

Figure 2.3 Schematic demonstration of osmotic-resistance filtration model in ODMPs in (a) active-layer-facing-feed-solution (AL-FS) orientation with Equation (2.21) and (b) active-layer-facing-draw-solution (AL-DS) orientation with Equation (2.23) [adapted - (She et al., 2016)]

It was claimed by the authors that in osmotically driven membrane processes, the concentration driving force is majorly affected by four factors:

(a) Dilutive external concentration polarisation (DECP).

(b) Internal concentration polarisation (dilutive or concentrative as per orientation)

(c) Effective concentration driving force across active layer.

(d) Concentrative external concentration polarisation (CECP).

Taking the above mentioned factors into account, She et al. (2016) successfully developed the model equations for demonstrating the difference in imposed driving force and the effective driving force. The support layer side of the membrane possesses internal concentration polarisation within the support layer along with external concentration polarisation. Based on the osmotic resistance filtration model, the expressions for the membrane resistance (R_m) and foulant resistance (R_f) are given by:

For AL-FS orientation:

$$R_m = \frac{(\pi_D - \pi_F) - \Delta P - F_{dcp}\left(\pi_D + \frac{J_s}{J_w}\beta R_g T\right) - F_{cecp}\left(\pi_F + \frac{J_s}{J_w}\beta R_g T\right)}{\mu J_w} \quad (2.17)$$

$$R_f = \frac{(\pi_D - \pi_F) - \Delta P - F_{dcp,f}\left(\pi_D + \frac{J_{s,f}}{J_{w,f}}\beta R_g T\right) - F_{cecp,f}\left(\pi_F + \frac{J_{s,f}}{J_{w,f}}\beta R_g T\right)}{\mu J_{w,f}} - R_m \quad (2.18)$$

where, F_{dcp} denotes concentration polarisation factor for dilutive concentration polarisation (internal and external) at the support layer side while F_{cecp} represents the same factor for concentrative external concentration polarisation at the active layer side in AL-FS orientation. In Chapter 5, expressions for R_m and R_f will be required and these will be calculated from the above equations.

For AL-DS orientation:

$$R_m = \frac{(\pi_D - \pi_F) - \Delta P - F_{ccp}\left(\pi_F + \frac{J_s}{J_w}\beta R_g T\right) - F_{decp}\left(\pi_D + \frac{J_s}{J_w}\beta R_g T\right)}{\mu J_w} \quad (2.19)$$

$$R_f = \frac{(\pi_D - \pi_F) - \Delta P - F_{ccp,f}\left(\pi_F + \frac{J_{s,f}}{J_{w,f}}\beta R_g T\right) - F_{decp,f}\left(\pi_D + \frac{J_{s,f}}{J_{w,f}}\beta R_g T\right)}{\mu J_{w,f}} - R_m \quad (2.20)$$

where, F_{ccp} denotes concentration polarisation factor for concentrative concentration polarisation (internal and external) at the support layer side while F_{decp} represents the same factor for dilutive external concentration polarisation at the active layer side in AL-DS orientation. The factors were mathematically derived by She et al. (2016) as:

$$F_{dcp} = 1 - \exp\left(-\frac{J_w}{k_{dcp}}\right) \quad (2.21)$$

$$F_{cecp} = \exp\left(\frac{J_w}{k_{cecp}}\right) - 1 \quad (2.22)$$

$$F_{ccp} = \exp\left(\frac{J_w}{k_{ccp}}\right) - 1 \quad (2.23)$$

$$F_{decp} = 1 - \exp\left(-\frac{J_w}{k_{decp}}\right) \quad (2.24)$$

In equations 2.19 – 2.24, ΔP, J_s, β, R_g and T represent hydraulic pressure, solute flux, van't Hoff coefficient, universal gas constant and absolute temperature respectively. The corresponding mass transfer coefficients are the various *k* values.

It is notable that there is a considerable decrease in the imposed driving force due to imposition of all modes of concentration polarisation. In forward osmosis, the difference in hydraulic pressure is zero, therefore, in eqs. (2.17) – (2.20), the value of ΔP becomes zero. The detailed derivation of these equations is provided in **APPENDIX–I**.

2.2.2.4 ICP self–compensation effect

In osmotically driven membrane processes, internal concentration polarisation can affect the permeation process to a notable extent. In a recent study (Tang et al., 2010), it was observed that in FO, a stability in flux trend was noted which was independent of any attempt to increase or decrease flux. It was further realised that the flux stability is exhibited more in AL-FS orientation than that in AL-DS orientation. It was also realised that this stability was not exclusively due to membrane orientation and ICP-self compensation effect played a significant role in this regard, according to which any attempt to reduce or increase the flux is compensated by increase or decrease in ICP.

In a membrane fouling process, the submission of the foulant particles to the membrane surface contributes to an increase of the fouling resistance. This subsequently reduces the flux. The decrease in flux exponentially decreases the impact of internal concentration polarisation, as less water is permeated from the feed to the draw side. As a result the osmotic gradient across the fouled active layer of the membrane is increased and this increases the driving force. This increase in driving force partially compensates for the increase in hydraulic resistance due to the deposition of particles at the membrane surface.

ICP-self compensation effect demonstrates that any attempt at increasing or decreasing the driving force may not have a considerable effect on flux as ICP self-compensation effect would moderate the flux increase or flux decline by increase or decrease in internal concentration polarisation effect respectively. Equations (2.17) – (2.20) mathematically demonstrate the mechanism of foulant resistance as a function of applied driving force (osmotic pressure difference) and effective driving force (with further incorporation of ECP and ICP effects) illustrating that any change in applied driving force would be compensated by a subsequent change in effective driving force.

Tang et al. (2010) in a series of baseline tests noted that the ICP self-compensation effect is stronger in AL-FS configuration. Along with a general reason of more severe ICP in AL-FS orientation, ALDS configuration is compounded by a severe tendency of additional fouling mechanisms like internal clogging and cake enhanced concentration polarisation. In comparison to ALFS configuration, these additional effects in ALDS configuration contribute to flux instability and comparatively higher flux decline (and ultimately affect the mechanism of ICP self-compensation effect). During the membrane fouling process, the flux decreases and since, ICP is flux dependent (exponentially so) ICP also decreases.

This results in an increase in effective driving force. In this way, reduced water permeability is compensated. A comparative analysis of flux behaviour in connection with ICP self-compensation effect in AL-FS and AL-DS orientation is illustrated in Figure 2.4.

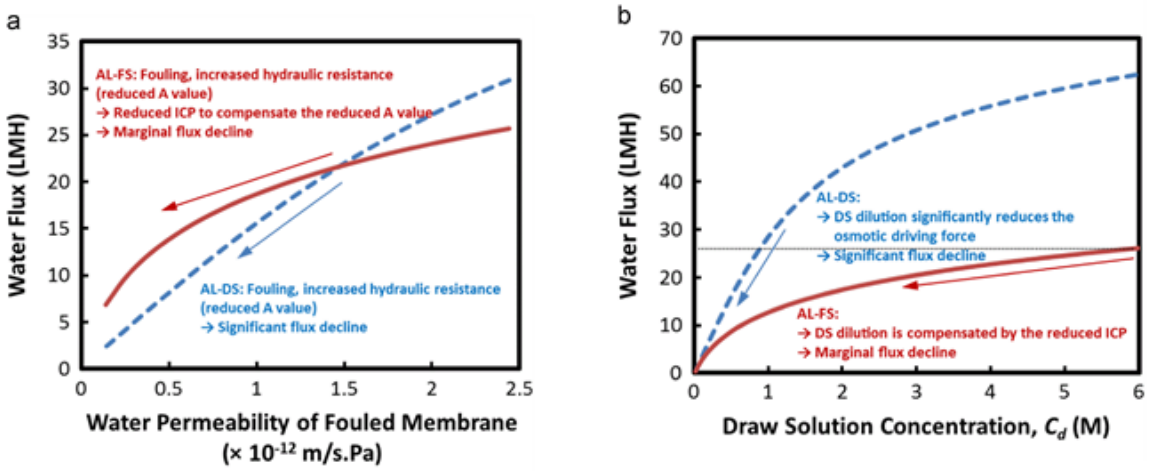

Figure 2.4 ICP self-compensation effect for the AL-facing-FS configuration in different scenarios [adapted from (Tang et al., 2010)]

Extending the observation, it was found that the change in draw concentration had a milder effect in AL-FS orientation than that in AL-DS because increased concentration in the former is compensated by the ICP self-compensation effect (Figure 2.4 b). The preferred mode of operation for FO is AL-FS and in summary the impact of ICP-self compensation effect is significant in AL-FS orientation which results in greater flux stability and less decline. On the other hand, by reversing the membrane orientation to ALDS mode, the degree of ICP is diminished but severe flux declines can occur as the solute in the feed solution may induce severe internal clogging of the support layer resulting in intense concentrative ICP.

2.2.3 Reverse solute diffusion

In osmotically driven membranes, there is reverse solute diffusion of draw solute from the draw solution to the feed solution, known as reverse flux (J_s). Not only does this decrease the osmotic pressure difference, these solutes can also act as fouling promoters (e.g. monovalent and divalent cations) and intensify the organic fouling (She et al., 2012) and may result in development of a biofilm. The reverse solute flux is commonly described by:

$$J_s = B\,\Delta C_{eff} \tag{2.25}$$

where, B is regarded as the solute permeability coefficient of the membrane while ΔC_{eff} represents the effective solute concentration difference across the membrane.

Generally, quantification relative to the water flux is used for the measurement of reverse solute diffusion (She et al., 2016). The integrated form of van't Hoff equation is given as (John and Weeks, 2000):

$$\frac{d\ln K}{d(\frac{1}{T})} = -\frac{\Delta H}{R_g} \tag{2.26}$$

where, ΔH, T and R_g represent enthalpy, temperature and universal gas constant respectively. Dividing Equation (2.25) by (2.5) and relating $\Delta\pi_{eff}$ to ΔC_{eff} with the Van't Hoff equation:

$$\frac{J_s}{J_w} = \frac{B}{A\beta R_g T}\left(1 + \frac{A\,\Delta P}{J_w}\right) \tag{2.27}$$

where, β, R_g and T represents the Van't Hoff coefficient, universal gas constant and absolute temperature respectively. Van't Hoff coefficient remains constant subject to the linear relationship of concentration and the osmotic pressure of the solution. While discussing the relationship between theoretical $\frac{J_S}{J_w}$ and ΔP, She et al. (2016) claimed that in FO processes, the value of $\frac{J_S}{J_w}$ is constant for a given membrane as net applied hydraulic pressure (ΔP) is zero. As shown, in Equation (2.27), theoretical $\frac{J_S}{J_w}$ is independent of the operating conditions like membrane orientation; hydrodynamic conditions and concentrations of feed and draw solutions. However, its value is dependent on the working temperature and the membrane's intrinsic separation properties.

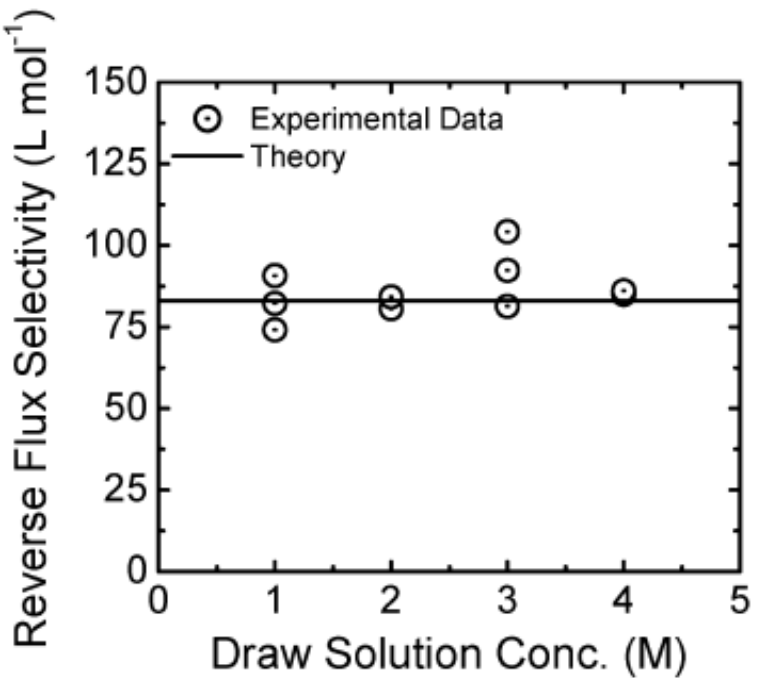

Figure 2.5 Reverse flux selectivity as a function of draw solution concentration in forward osmosis analysis [adapted – (Phillip et al., 2010)]

Phillip et al. (2010) had previously attained the above result and confirmed it experimentally namely that the reverse flux selectivity, i.e. the ratio of forward water flux to the reverse solute flux ($\frac{J_w}{J_s}$) is given as:

$$\frac{J_w}{J_s} = \frac{A}{B}\beta R_g T \tag{2.28}$$

Figure 2.5 reveals the accurate prediction of the reverse flux selectivity using the measured values of *A* and *B* with its independent behaviour with respect to the draw solution concentration and the support layer structural parameter *S*. The experimental and the predicted values were found to be having strong agreement with each other.

2.2.4 Cake-enhanced osmotic pressure

In membrane filtration, cake-enhanced osmotic pressure (CEOP) has been found as one of the major key mechanisms for flux decline (Hoek and Elimelech, 2003, Chong et al., 2008, Boo et al., 2012). According to this phenomenon, the cake layer hinders the back diffusion of salt into the bulk solution. As a result, the osmotic pressure of near the membrane surface is increased. This increased osmotic pressure leads to considerable drop in overall driving force and results in flux decline. Boo et al. (2012) during the investigation of fouling behaviour in forward osmosis, using colloidal silica as foulant, found that the salts diffused to the feed side from the draw side and accumulated within the foulant layer. This accelerated cake-enhanced osmotic pressure (CEOP) which reduced the osmotic driving force for permeate water flux. The concept of CEOP is illustrated conceptually in Figure 2.6 in connection with variations in concentration polarisation and pH values.

In reverse osmosis, CEOP is due to the rejected salt and the effect is generally considered to be less pronounced as compared to that in forward osmosis because in the latter process, it directly affects the driving force i.e. osmotic pressure difference. However, in both processes, the extent depends upon the amount of cake accumulation and the overall effect can be subtle.

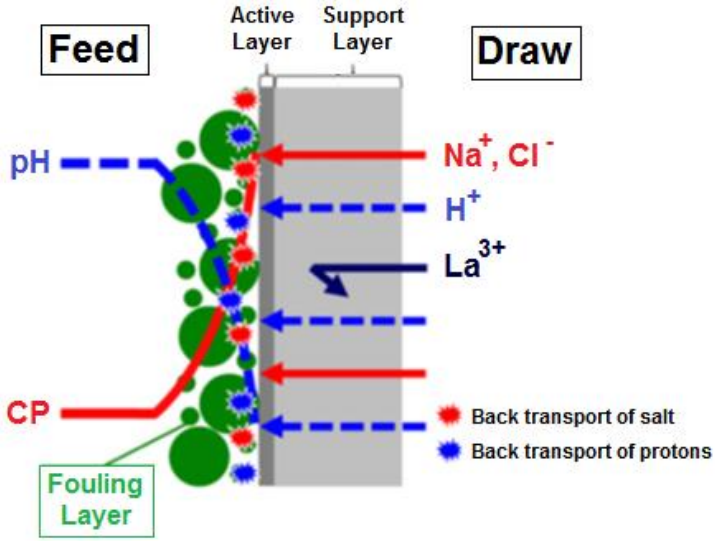

Figure 2.6 A conceptual illustration for the effect of reverse diffusion of draw solution on the concentration polarisation (CP) within the fouling layer resulting in cake enhanced osmotic pressure- adapted from (Boo et al., 2012)

2.3 Membrane cleaning

Membrane cleaning is an important part of the overall filtration operation. It can be defined as the process in which material is relieved from a substance which is not the integral part of that material (Trägårdh, 1989). In membrane technology, the cleaning of the membrane is related to the cleaning by physical, chemical and biological cleaning. The physical affects the hydrodynamics or applies turbulence or variation in temperature and eventually force the foulants to leave the membrane surface. Chemical cleaning aims to eliminate all impurities through the application of chemicals. Biological cleaning aims to remove all microorganisms. Selection of processes and the cleaning solution depends upon nature of fouling, membrane material, cleaning solution and hydrodynamic conditions.

2.3.1 Physical cleaning

Physical cleaning usually involves the application of electrical, mechanical or hydraulic forces. A number of methods have been proposed to alleviate membrane fouling. Electrical cleaning includes application of voltage across the membrane which results in formation of micro bubbles at the surface of the membrane (Shorrock and Bird, 1998). This drives the foulants free from the membrane surface. Special designing of the module is needed in this regard and the membrane must be conductive. Other applications involve alternating the shear forces on the membrane surface or the lessening of foulant deposits through hydraulic flushing, using air or sponge balls or by increasing turbulence through rotating disks which have been used industrially (Shorrock and Bird, 1998).

Hydraulic flushing is the most commonly used method for alleviating reversible fouling. It includes forward flushing and back flushing. Forward flushing is the turbulent crossflow across the membrane which reduces the deposits on the membrane surface (Verberk and Van Dijk, 2003). The flow of the forward flush is usually with enhanced crossflow velocity and could be in either direction. Li et al. (2012), during the forward osmosis experiments with commercial cellulose tri-acetate membrane, using natural sea water as feed and 2 M NaCl as draw solution, found that most natural organic matters in the fouling matrix could be removed by water flushing while silica scaling was difficult to remove by hydraulic flushing. Siddiqui and Field (2016), in an experimental study with an ultrafiltration ceramic membrane using dextran and carboxymethyl cellulose as foulants, found that intermittent rinsing during the fouling experiment improved the filtration efficiency and that it was further improved when the membrane was intermittently rinsed with cold water followed by hot water (40°C).

Back washing is a process in which flow is pushed from the permeate side to the feed side. In microfiltration and ultrafiltration membranes, back washing is applied to flush the pores inside out by applying pressure from the permeate side to the feed side (Arnal et al., 2011). During back wash in osmotically driven membranes, the concentrated draw solution is replaced with pure water so that there is no movement of water from the feed side to the draw side. The crossflow velocities on both sides are kept same. In this way, the water permeates in the backward direction towards the fouled membrane surface and loosens the fouled layer (Motsa et al., 2014). In general, back washing requires a flux value to be two times higher than the normal filtration flux. This helps in dislocating the clogged foulant particles and eventually getting them free from the membrane, but this is difficult to achieve in FO systems due to limitation in increasing the driving force for flux increase. However, it can be done if backflow is pressurised. Also, the application of higher flux requires careful execution in order to avoid membrane damage (Baker, 2004).

During their experiments on microfiltration membrane using commercial yeast as test suspension, it was found that in comparison to techniques of air bubbling and enhanced crossflow velocity, back washing technique appeared to be comparatively more efficient in reducing cake layer foulant deposition on the membrane surface (Qaisrani and Samhaber, 2011). In another study, while observing various back wash parameters including pressure, duration and frequency of back wash and the effects of these parameters on flux, Laitinen et al. (2001) found that the highest value of flux was attained with frequent back wash i.e. of one second in every 2 minutes. Liang et al. (2008), during their study on cleaning ultrafiltration membranes, found that backwashing followed by forward flushing was more effective for flux recovery than flushing separately at different intervals.

2.3.2 Chemical cleaning

Chemical cleaning is done by using chemical agents, normally oxidants. It is usually applied for those foulants which are unable to be removed by mere physical cleaning and are hydraulically irreversible. Chemical cleaning can be carried out in a number of ways including directly immersing the fouled membrane in chemicals, soaking with cleaning agents with higher concentration in a separate chamber, adding chemicals on the feed side or backwashing with chemical solutions (Lin et al., 2010). Porcelli and Judd (2010) explained the process of the chemical cleaning which could be summarised as:

- transporting the cleaning agent to the fouled membrane surface by transition through the fouled layers
- cleaning reactions with the foulants, resulting in detachment from the membrane surface;
- transportation of cleaning agent with foulants back to the interface; and
- transportation of waste matter back to the bulk solution on the retentate side

Previous studies have revealed that hydrophobic natural organic matter (NOM) fouling favours the application of alkaline solution followed by acid treatment, whilst inorganic fouling favours the application in reversed sequence. The time of cleaning also has a significant importance and application at optimum time for cleaning of membranes can further reduce the operational cost (Mohammadi et al., 2003). Cleaning agents that are widely used can be divided into six categories (Trägårdh, 1989, Mohammadi et al., 2003) as:

1. Acids, 2. Alkalis, 3. Oxidants, 4. Surfactants, 5. Chelants and 6. Enzymes

Application of acids as cleaning agents helps in dissolving inorganic salt precipitates along with hydroxides and metal oxides (Trägårdh, 1989). Acids also work as chelating agents as

they remove metal cations quite effectively. However, the negative impact of pH of the solutions appears to be the main drawback of using strong acids as cleaning agents. Too low a pH can affect the membrane surface and decreases a membrane's life. This effect is much more pronounced for polymeric membranes as compared to that for ceramic membrane.

Alkaline solutions help in weakening the bonds between foulants and the membrane surface. They also play a role in promoting quick hydrolysis of proteins into small amides and sugars along with neutralisation of acidic organics and expansion of molecules of hyaluronic acid. Alkali also assists in regulation of pH to suitable working condition in connection with other chemicals (Lee et al., 2001, D'souza and Mawson, 2005, Porcelli and Judd, 2010). The major drawback in using alkaline solutions as the cleaning agents is their lack of buffering capacity. Therefore, in order to adequately neutralize all the acidic components, cleaning with a solution of a high pH levels (i.e. 11–12) is generally recommended.

The oxidants are strong cleaners with strong tendency of disinfection and elimination all of pathogenic microorganisms. Disinfection is frequently applied in waste water treatment, pharmaceutical and dairy industry. Commonly used oxidants are sodium hypochlorite (NaOCl) and hydrogen peroxide (H_2O_2). The former is the most frequently used one and it hydrolyses quickly in water to form hypochlorous acid (HOCl). In the cleaning of ceramic membranes, the application of a combination of alkaline solutions with oxidizing agent (generally sodium hypochlorite) followed by acid application is found to be appropriate for cleaning (Siddiqui and Field, 2016). Similarly, Field et al. (2008) categorized the cleaning solutions of microfiltration membranes into three categories namely strong acids, strong

bases and strong oxidants like sodium hypochlorite (NaOCl) which is a source of free chlorine.

Surfactants are the amphiphilic compounds which may act as emulsifiers, wetting agents dispersants, detergents and biocides and help in lowering the interfacial tension between liquid with solids or between two liquids. Due to their amphiphilic properties with molecules possessing hydrophilic and hydrophobic nature, they diffuse in water and adsorb at interfaces. They also help to improve rinse-ability and wettability of the surface of the membrane by solubilising and dispersing proteins resulting in reduced rinsing times (Trägårdh, 1989, Marriott and Gravani, 2006). Surfactants are categorised into four major subgroups, namely anionic, cationic, non-ionic, and zwitter-ionic (Trägårdh, 1989). They possess stability in both acidic and alkaline solutions. In membrane filtration processes, anionic and non-ionic surfactants are frequently used. The major drawback of surfactants is that their adsorption may be unfavourable as they can cause severe irreversible re-fouling on the surface of the membrane.

A chelant is a specialized molecule designed to bind positively charged metal ions (typically calcium and magnesium) in the solution and hence prevent these ions forming precipitates that foul. The most common example of chelant is ethylenediamine tetra-acetic acid (EDTA) which is very effective in destroying the cross-linked fouling layer by taking the cations away (Li and Elimelech, 2004). However, the cleaning efficiency of a chelant is a function of pH value.

Enzymes are selective catalysts which are designed for targeted and highly efficient reactions. They degrade organic fouling such as protein deposits by cutting the molecular

chain at certain points. Argüello et al. (2002) studied the cleaning of inorganic (ceramic) membranes fouled with whey solution. They observed the cleaning efficiency as a function of operating conditions and used a commercial proteolytic enzyme as a cleaning agent. Enzymatic cleaning has a number of advantages as compared to cleaning with other cleaning agents which includes prolonging the membrane life, low operating temperature, less rinsing requirement and being environmental friendly (D'souza and Mawson, 2005).

2.3.3 Traditional membrane cleaning processes

A number of cleaning methods are applied for the removal of the layer of retained material on the membrane surface. For the maintenance and the good performance of the microfiltration and ultrafiltration membranes, consistent cleaning is required. In general, the appropriate cleaning solution needs to be circulated for a couple of hours. However, the period of the cleaning cycle varies depending on the type of foulant and the membrane material. Layers of gelatinous materials and organic polymer colloids are commonly treated with hot detergent solutions after treating with alkaline solutions. Similarly, for protein gel layer, enzymatic detergents are considered to be most suitable while for treating ferrous iron salt which is accumulated on the membrane surface in the form of insoluble iron oxide, acidic wash is recommended. Typical steps for the cleaning cycle are as follows:

1. Flushing the system several times with increased rate of circulation with hot water.
2. Washing the system with suitable acid or alkali, according to the nature of the foulant.
3. Treating/washing the system with a hot detergent solution for a given period of time.
4. Thoroughly flushing the system with water in order to remove all traces of detergent used in the previous step.
5. Measuring the pure water flux and repeating the procedure if standards are not met.

Generally, the cleaning efficiency is checked by measuring the water flux after the cleaning procedure at defined experimental conditions and comparing that with the flux measured with the virgin membrane.

2.3.4 Cleaning of ceramic membranes

Ceramic membranes are cleaned through the cleaning chemicals which have been widely divided into five categories, namely caustic, oxidants/disinfectants, acids, chelating agents, and surfactants (Liu et al., 2001). However, the hypochlorite normally remains a preferred choice for multiple reasons including availability, price and efficient cleaning of bio-fouling. Many researchers have found this chemical suitable for the successful cleaning operations for membranes. Tomaszewska and Białończyk (2012) working with a similar membrane type and fouling category found an effective cleaning action by using a combination of sodium hydroxide, phosphoric acid and sodium hypochlorite as a disinfectant to achieve an optimum recovery of the membrane properties. Ogunbiyi et al. (2008) discovered an effective impact on the microfiltration process in ceramic membranes through cleaning by using a combination of alkaline, hypochlorite and acid cleaning. They used solutions of caustic soda, sodium hypochlorite and nitric acid in different proportions and achieved a considerable increase in flux in the tubular membrane. Vanysacker et al. (2014) through a comparative analysis against citric acid, showed that sodium hypochlorite has a significantly higher cleaning efficiency. Whilst recognizing the cleaning efficiency of hypochlorite solutions, it is also noted that carefully controlled cleaning conditions and precision in chlorine concentration is most important because frequent use of these solutions weakens the membrane material and results in weakening of its mechanical strength. Over use may cause a much earlier loss in membrane integrity than that stated by the manufacturer (Arkhangelsky et al., 2007).

Along with selecting a suitable chemical solution for cleaning the membrane fouling, adopting the appropriate cleaning method is also imperative. In addition to straight forward crossflow, the popular methods are back-flushing, back-washing and back-pulsing. Gabrus and Szaniawska (2009) during their experiments on microfiltration observed a significant increase in permeation flux value upon using the back-flushing technique. Research made by Sondhi and Bhave (2001) indicated the impact of different back pulse parameters during the membrane cleaning including the cleaning time. It was found that in the back-pulsing technique, cleaning time increased with the increase in permeate viscosity, membrane resistance or thickness of the membrane and decreased with increase in transmembrane pressure.

2.3.4.1. Back-flushing in Ceramic membranes

The back-flushing process appears to be an important application in cleaning the cross-flow filtration modules particularly the ceramic membranes; such systems are robust and amenable to hydraulic stresses. It is a cyclic operation in which a reversed flow is pushed from the permeate side to the feed side. The reversed run displaces the foulant deposits on the membrane pores and loosening the cake. In a typical backwashing process in crossflow membranes, a differential pressure is established across the length of the membrane. Keeping the permeate valve closed, the feed water (or solution) flows from the higher pressure end to the lower. At the higher pressure end, the feed water flows across the membrane producing permeate as the backwashing solution. This backwashing solution is pushed to flow back to the feed side at the lower pressure end and is referred as back-flushing. If the flow is reversed, the order of back-flushing would be reversed as well and the membrane would be fully cleaned (Shi et al., 2014, Baker, 2004). Figure 2.7 demonstrates a typical back-flushing mechanism in a crossflow module.

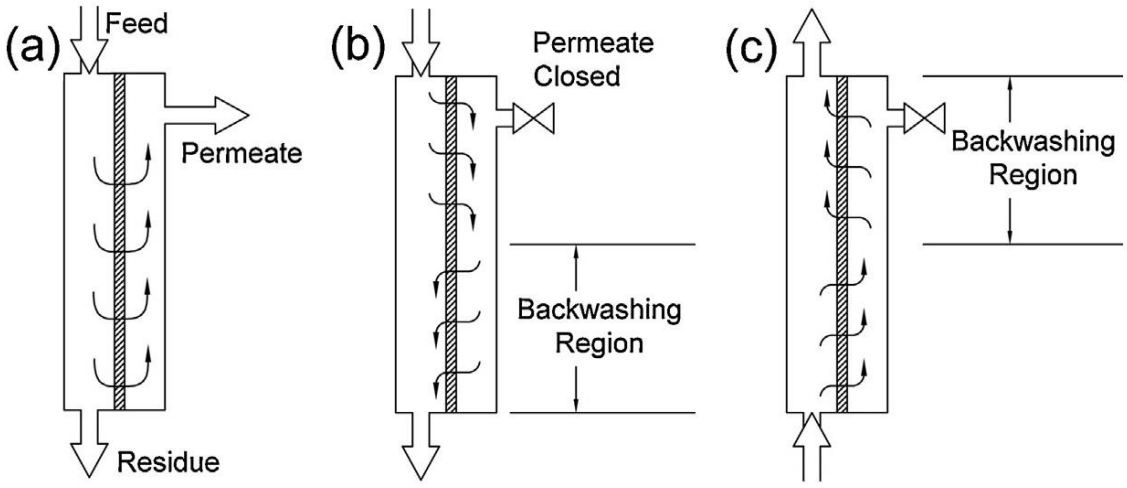

Figure 2.7 Illustration of back-flushing mechanism for a crossflow module: (a) normal filtration technique; (b) forward flow backwashing technique; (c) reverse flow backwashing technique–adapted from (Shi et al., 2014)

A number of previous applications of back-flushing have proved this application as a successful tool for cleaning the surface fouling and pore clogging for microfiltration (MF) and ultrafiltration (UF) membranes. While working on separation of yeast from yeast suspension by microporous ceramic membrane, Matsumoto et al. (1988) realised that higher flux values were noted when membrane was back washed by forcing the filtrate into the membrane by compressed air of 0.1 MPa on regular intervals. Along with that, they realised internal suction technique i.e. suction of the filtrate with a pump periodically also resulted in improving membrane's filtration efficiency. In another study on crossflow microfiltration of oil emulsion feeds through zirconia ceramic membranes at bench scale, it was observed that with the application of back-flushing technique, the permeate flux was increased at a level of three times than the flux in the absence of back-flushing for a longer run (Cakl et al., 2000). Not only for the prepared feeds at bench scale, the application of back-flushing technique has been found efficient with real waters as well. Salladini et al. (2007) performed ultrafiltration experiments with and without back-flushing with mono-tubular ceramic membranes of pore size 20 and 50 nm and used biologically treated municipal wastewater as feed. They realised that flux was improved up to 17% with the

periodic application of back-flushing for 0.5 seconds in every minute. However, for these membranes, a clear understanding of nature of fouling is of primary importance to that of cleaning protocols (Porcelli and Judd, 2010). A study on back-flushing application with ceramic membrane (Alumina) of pore size 0.8 μm by (Gabrus and Szaniawska, 2009) using yeast suspensions revealed that deposited cake on membrane surface was successfully removed by back-flushing, while, this application was found to be less beneficial for internal pore blocking. In a very recent research on municipal waste water fouling, Chang et al. (2017) concluded that in comparison to polymeric membranes, inorganic membranes are more suitable for this cleaning technique albeit the use of the former is very common for the production of drinking water.

2.4 Critical flux

Criticality is a flux-based hypothesis of membrane fouling, suggesting that a flux exists on start-up such that operation at a lower flux results in no flux decline with time. This flux was named as critical flux by Field et al. (1995). This concept has gained importance in membrane operations since the mid-nineties when it was first introduced. For constant rate filtration mode operation, Figure 2.8 indicates that for the crossflow velocity of 0.76 ms^{-1}, the constant-flux behaviour was maintained at about 40 LMH; the corresponding TMP was always at the level of about 0.1 bar except for the first four minutes, when it was 0.075 bar. When an initial TMP of 0.16 bar was used together with a higher cross-flow velocity of 0.84 m s^{-1} it was only possible to maintain constant flux by gradually increasing TMP to over 0.60 bar. Thus the earlier flux of 40 LMH (corresponding to the TMP of about 0.1 bar) is critical.

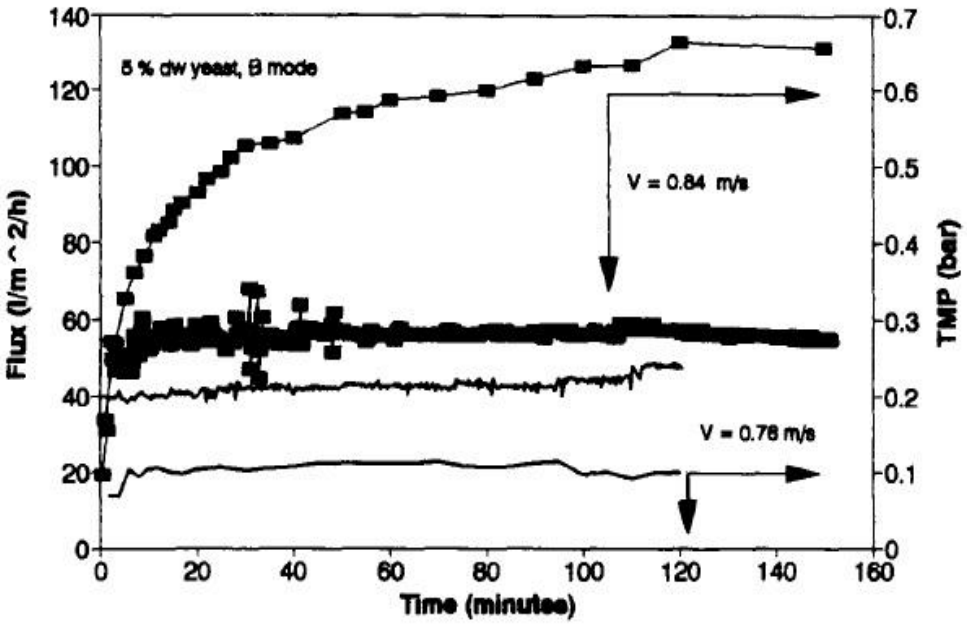

Figure 2.8 Comparison of two constant-flux filtrations for 5% dry weight yeast cell suspension and a Carbosep 0.14 μm tubular membrane–adapted from (Field et al., 1995)

2.4.1 Methods for detecting critical flux

Different methods for detecting the critical flux have been discovered and the frequently used methods for the critical flux detection are discussed below.

2.4.1.1. Flux step method

The widely used method of flux stepping increments of the flux at intervals and examines the filtration behaviour at constant flux mode. A constant behaviour of TMP with the flux indicates sub-critical conditions but beyond criticality the flux declines with time. Figure 2.9 illustrates a method for critical flux determination for synthetic sewage for the experiments performed by Le Clech et al. (2003). They detected the critical flux value through the flux stepping method for the synthetic and real sewage respectively, with a step-height of 2 LMH and 15 minutes duration for each run.

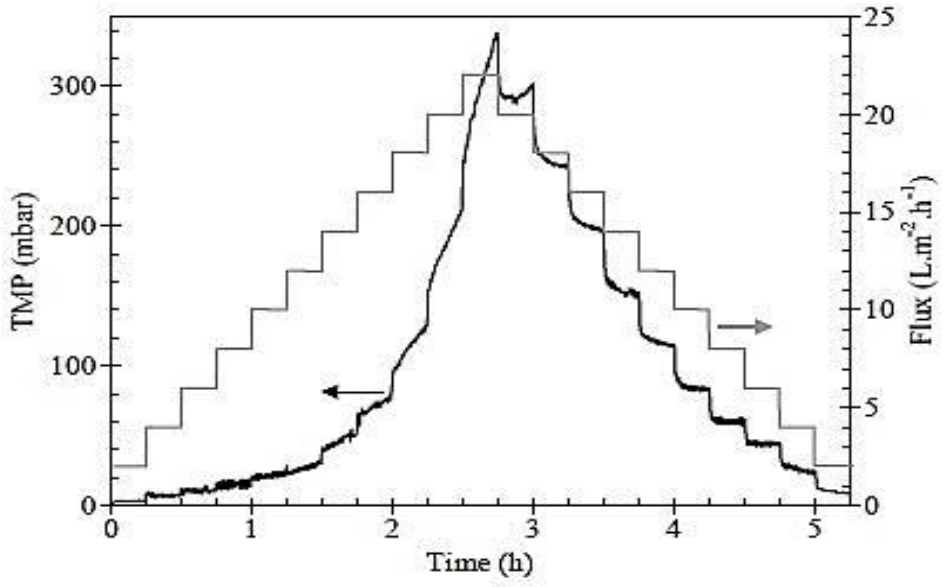

Figure 2.9 Critical flux determination by flux stepping method for synthetic sewage–adapted from (Le Clech et al., 2003)

2.4.1.2. Improved flux step method

An improved flux-step method was introduced by van der Marel et al. (2009), incorporating cleaning steps by relaxation. Membrane relaxation is a simple yet effective method for removing reversible fouling, allowing filtration to be maintained for longer periods before the need for further cleaning if reversible fouling predominates over irreversible fouling. However, its efficiency can be further increased when air scouring is applied during relaxation (Shi et al., 2014). By the comparative analysis of traditional common flux-step method and new improved flux-step method, the critical flux can be determined. It is found to be lower in the latter case because the rate of fouling and fouling history is altered by the intermittent relaxation after each successive flux. This results in removal of reversible fouling. Figure 2.10 illustrates Flux-TMP profile for this method along with its schematic illustration.

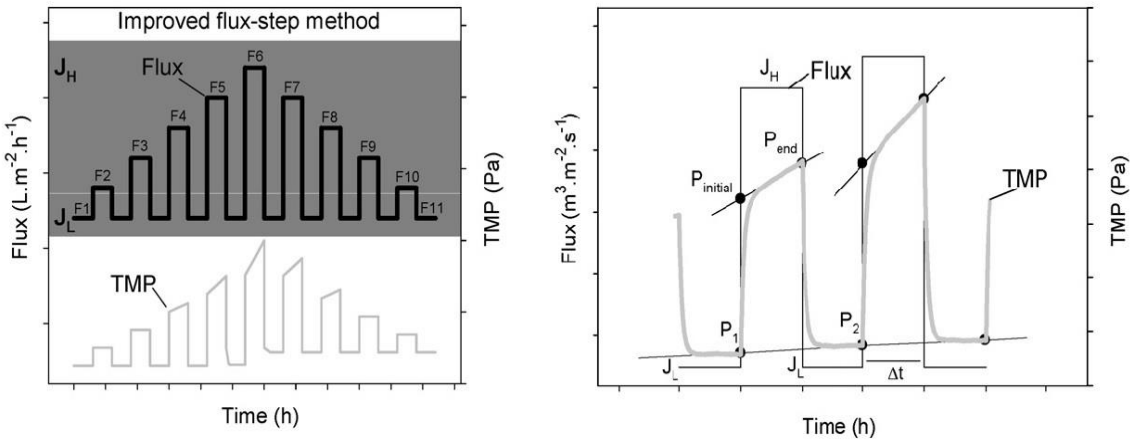

Figure 2.10 (a) Example of a flux–TMP profile of the improved flux-step method and (b) Schematic representation of the improved flux-step protocol – adapted from (van der Marel et al., 2009)

Although the experiment (Ref. Figure 2.10) was done under sub-critical conditions, still some irreversible fouling was detected because of pore blocking, adsorption of macromolecules or/and gel formation. Due to such reasons, the value of critical flux in improved flux-step method is less than the value determined by other methods. Such fouling is unable to be removed by mere relaxation.

2.4.1.3. Direct observation through membrane

The direct observation through membrane (DOTM) technique is a useful technique, although it incurs higher initial costs for visual detection membrane fouling and is only applicable to transparent membranes and relatively large particles. The objective lens of a microscope is positioned on the permeate side of the module and adjusted to focus through the membrane surface. The image observed by the microscope is recorded and viewed via a video camera attached to a video recorder and a monitor. The experimental set-up of the DOTM facility is illustrated in adapted Figure 2.11. Li et al. (2000) used this technique in crossflow microfiltration to monitor the deposition of super micron particles to find the critical flux for cake formation in crossflow microfiltration membranes.

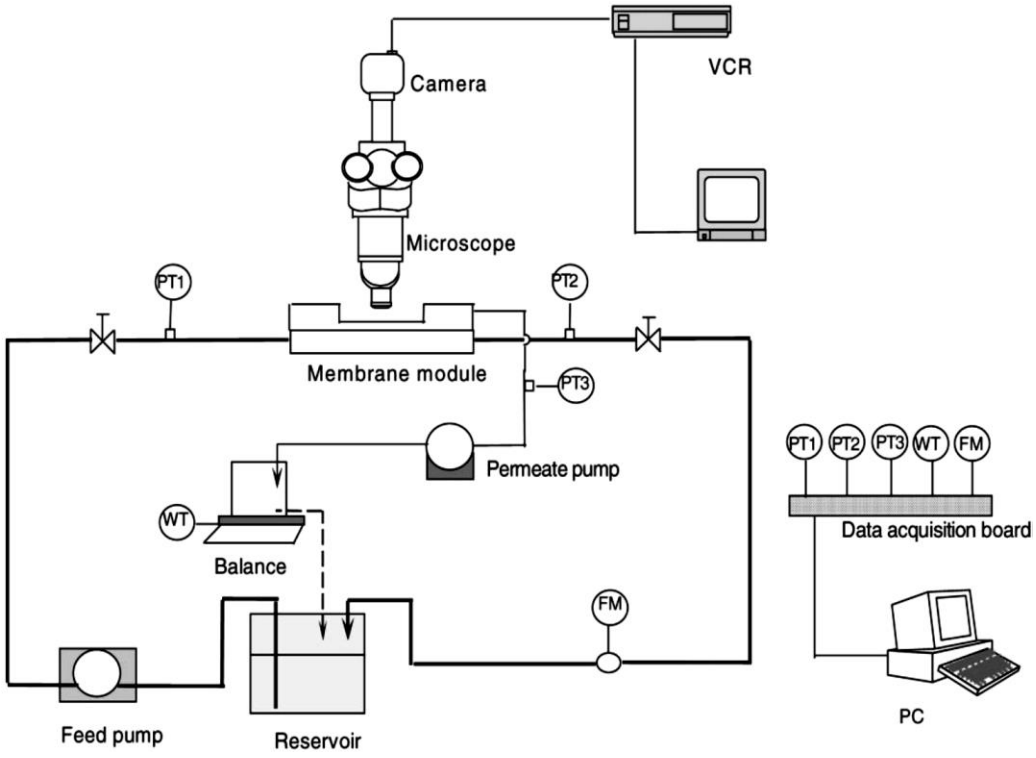

Figure 2.11 Crossflow microfiltration rig with direct observation through the membrane (DOTM) facility – adapted from (Li et al., 2000)

The results were used to assess the shear induced diffusivity model and inertial lift model for the identifying the critical flux value. Through DOTM, the fouling can be observed visually, however, Pongpairoj et al. (2011) concluded that one should not solely depend upon this method and increase in TMP should also be observed.

2.5 Parameters for membrane module design and cost estimation

Selection and cost estimation is an important task to be covered for membrane designers. For this, the cost is generally dictated by membrane replacement, chemicals consumed, cleaning of the membrane, and energy consumption but it fluctuates from one system to another. For example, a major drawback of RO systems is that its cost is affected by energy consumption and replacement of membrane (Malaeb and Ayoub, 2011). In comparison, FO can be quite cost-effective in its operation.

Sometimes information can be confusing. For example in a comparative analysis, it was noted that average module cost of ultrafiltration cellulose acetate membrane was noticeably higher than that of polyamide RO membranes but the costs for both membranes were almost in the same order (Schäfer et al., 2001). In the selection of the membranes and modules one has to primarily find an optimal balance. An excellent guide (see Table 2.1) on module manufacturing cost along with other major factors determining module selection was given by Baker (2004).

Table 2.1: Parameters for membrane module design [adapted – (Baker, 2004)]

Parameter	Hollow fibre membranes	Capillary fibres	Spiral wound	Plate-and-frame	Tubular
Manufacturing cost (US$/m^2)	5 – 20	10 – 50	5 – 100	50 – 200	50 – 200
Concentration polarization fouling control	Poor	Good	Moderate	Good	Very good
Permeate – side pressure drop	High	Moderate	Moderate	Low	Low
Sustainability for high-pressure operation	Yes	No	Yes	Yes	Marginal
Limited to specific types of membrane materials	Yes	Yes	No	No	No

2.6 Concluding remarks

Based on the review of literature, the following observations can be made.

- Fouling is the major factor affecting the membrane filtration performance. An insightful understanding of fouling mechanism and its underlying scientific principles is essential for an optimised operation.

- Concentration polarisation (CP) plays a significant role in membrane permeation in all membrane processes in general and osmotically driven membrane processes in particular. In order to deal with this, the mechanisms related to CP need insightful understanding in order to have an efficient performance.

- The contribution of reverse solute diffusion and cake enhanced osmotic pressure affects the permeation process and the effect could be reduced through system design.

- As revealed by previous findings, application of critical flux concept is helpful for optimised filtration process and fouling control.

- Membrane cleaning is an essential and continuous part of the process. A successful application of cleaning protocols is vital for optimised filtration processes.

3

Materials and Methods

3.1 Introduction

The work in this chapter has been split into two main sections, according to three different phases of the research. One part relates to the comparative analysis of the fouling experiments done with reference to forward and reverse osmosis using a flat sheet membrane setup at Singapore Membrane Technology Centre (SMTC), Singapore. The second part concerns a series of fouling experiments using an ultrafiltration ceramic tubular membrane. The chapter will outline the design and structure of the membrane modules used for both setups along with methodology, materials and chemicals used. Thirdly, an assessment of spiral wound forward osmosis modules at pilot scale is also made.

3.2 Flat sheet membrane setup

3.2.1 Chemicals and membranes

Unless otherwise stated, all of the chemicals were used as received. The chemicals had purity over 99% and were of analytical grade. Ultrapure deionised water, which had a resistivity of 18.2 MΩ cm, was supplied by a Milli-Q Ultrapure water system (Millipore Singapore Pte Ltd). The feed solution in both FO and RO experiments was composed of 45 mM NaCl and 5 mM $CaCl_2$ while for the draw solution, 3 M and 2 M of NaCl solution was used for thin film composite and cellulose-tri-acetate membranes respectively. The initial

volume of the draw solution was fixed at 5 L. The alginate foulant used during all the experiments was the sodium salt of alginic acid obtained from brown algae provided by Sigma-Aldrich Company Ltd. U.K. The concentration of the alginate in the feed solution was 200 mg/L.

The membranes used during the experiments were provided by Hydration Technologies (Albany, OR). One was Cellulose-tri-acetate (CTA) while the other was a polyamide thin film composite (TFC). Being proprietary, the detailed membrane chemistry is unknown. The CTA membranes were supported by a woven fabric whilst the thin film composite (TFC) polyamide membranes were supported by non-woven fabric.

3.2.2 Experimental setup and fouling tests

The membrane set up used during the experiments was able to be used for both forward and reverse osmosis experiments. It was equipped with self-recording data loggers. The membrane cell had an active membrane area of 34 square centimetres approximately. The crossflow velocity at the feed side of both FO and RO experiments was 7.4 cm/s while the crossflow velocity on the draw side of FO was fixed to be 11.1 cm/s.

3.2.2.1 Forward osmosis setup and test procedure

The schematic representation of the forward osmosis system is given in Figure 3.1. The membrane was sealed inside the membrane cell. A thin spacer was placed on the draw side for increasing the membrane support. The spacer also reduced the dilutive external concentration polarization by creating turbulence in the flow of draw solution. However, at the feed side, no spacer was placed in order to have the complete and undisturbed fouling layer. A gear pump (Cole-Palmer, Vernon Hills, Illinois) was used to re-circulate the feed

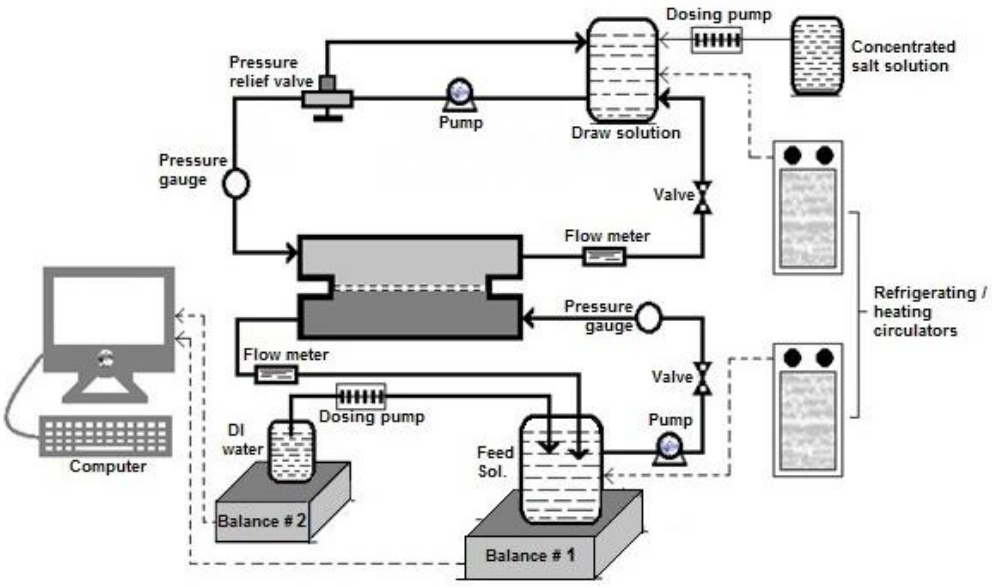

Figure 3.1 Schematic diagram of FO experimental setup at bench scale

solution, while for the draw solution, a high pressure Hydra-Cell pump (D/G-03, Minneapolis, MN) was used because the rig in use was initially designed and had been used for pressure retarded osmosis process. The system was also equipped with a back pressure regulator located downstream to the cell with a pressure reader with pressure being monitored via a digital transmitter. In FO experiments, the pressure on both feed and draw side were kept essentially at zero gauge pressure. Two refrigerating and heating circulators were installed for both feed and draw buffer tanks to keep the temperature constant throughout the test.

Before starting any permeation test, the crossflow rates at the feed and draw sides were fixed to the stated values i.e. 7.4 cm/s and 11.1 cm/s respectively. The membrane coupons were soaked in deionised water for at least 24 hours in order to remove any protecting chemicals. The membrane coupon was then stabilized through baseline test. The duration of the baseline test was at least half an hour or more and was until achieving a stable flux. Once stability had been achieved, a calculated amount of foulant was added to the feed

tank placed on balance 1 (Figure 3.1). The feed solution was mixed by an internal stirrer. With water permeating across the membrane from feed side to the draw side, the feed solution becomes concentrated while on the other side the draw solution became diluted. As a result, the driving force would decrease and foulant concentration would increase if no action were taken. To achieve time invariant conditions, both feed and draw solutions were continuously dosed. For the feed side, the concentration was maintained by replenishing deionised water to the feed tank based on mass measurements from balance 1. As the mass of solution in feed tank decreased due to permeation, the required amount was added through an automatic system from the DI water tank which was placed on balance 2 (Figure 3.1). The automatic system works in a way that at the start of the experiment the mass of the feed solution tank was noted and feed into the system along with setting a software command that any decrease in mass of the feed solution (due to water permeation to the draw side) may be compensated by supplying the same amount of DI water from the DI water tank. Both of the balances (balance 1 and balance 2) were precisely calibrated before each test to ensure the reliability. The amount of DI water supplied per minute was noted by a data logger which ultimately resulted in a calculated flux. For the draw solution, the concentration was maintained by dosing a more concentrated salt solution into the draw solution tank. This was done by fixing the conductivity of the draw solution at the beginning of the test and then continuously recording that conductivity. Due to the permeated water decreasing concentration and conductivity dosing of a more concentrated salt solution restored the initial conditions. Pressure gauge valves were set in order to ensure that hydraulic pressure was set at zero on both feed and draw side. In order to determine the reverse solute flux, samples from the feed tank were taken out at predetermined time for conductivity analysis. For these conductivity measurements a calibrated hand conductivity meter (ULTRAMETER II^{TM} 4P) was used.

3.2.2.2 Reverse osmosis setup and test procedure

The schematic demonstration of the reverse osmosis system at bench scale is depicted in Figure 3.2. The rig used during RO tests was essentially the same as was used in the FO

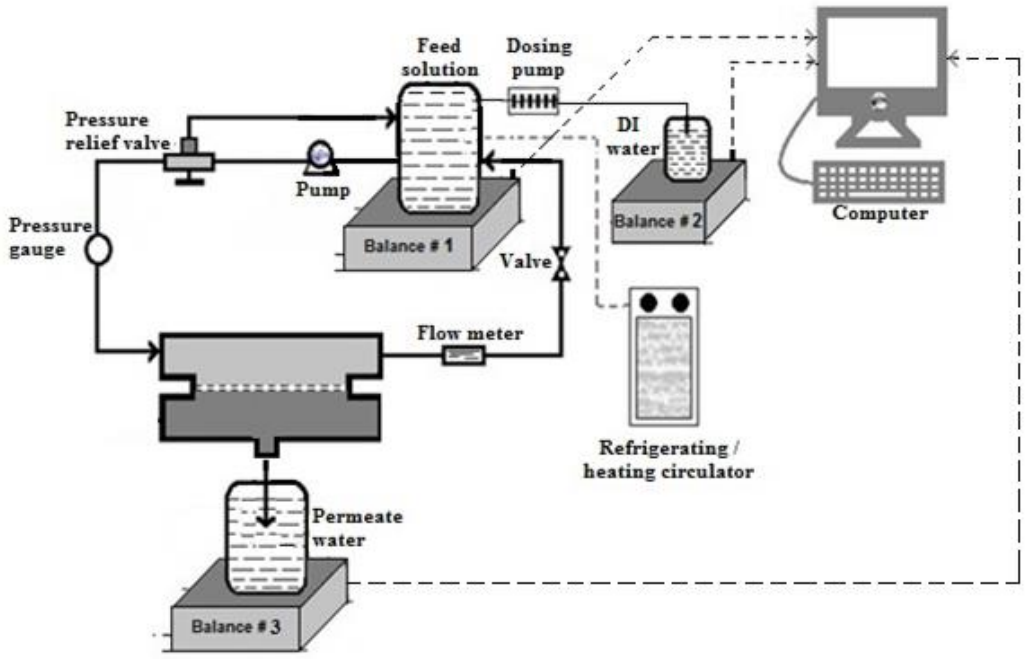

Figure 3.2 Schematic diagram of RO experimental setup at bench scale

tests but the permeate side plate of the cell in FO setup was replaced with a commercial stainless steel RO cell (GE SEPA II, Osmonics, with same active membrane area as that of FO setup). This plate was well supported by porous flat stainless support to bear the applied hydraulic pressure. For circulating the feed, the high pressure Hydra-Cell pump (D/G-03, Minneapolis, MN) was used. Before starting the permeation test, the crossflow rate at the feed side was fixed to the stated value. At least half an hour was allowed in order to obtain stable baseline conditions with no fluctuations in hydraulic pressure. For the RO experiments, the hydraulic pressure at the feed side was set during the baseline test in order for the starting flux to be the same as that in the FO tests. Once stability had been achieved, the calculated amount of foulant stock was added to the feed solution in the feed tank placed on balance 1 (Figure 3.2) and mixed by stirrer.

As the permeated water is collected, the feed water becomes concentrated and, for the ongoing experiment at bench scale, the experimental conditions would be changed. In order to overcome this problem, a system of continuous dosing the feed tank was implemented. This dosing was based on calculating the loss of mass of water due to permeation. The details of the continuous dosing system have been elaborated in section 3.2.2.1. The permeate accumulated in the permeate tank which was placed on balance 3 through which the mass of permeated water was calculated (Figure 3.2). The amount of water collected as permeate per unit time was noted by data logger which ultimately resulted in a calculated flux. The conductivity of the permeate samples along with the feed sample after regular intervals was measured using a calibrated hand conductivity meter (ULTRAMETER II^{TM} 4P). These measurements enabled the calculation of rejection.

3.2.3 Protocols for performing FO and RO fouling experiments

For both the FO and RO modes of operation, the normal duration of each run was about 1000 minutes. During this time the driving force was essentially invariant. The driving forces (osmotic difference in FO and hydraulic pressure in the case of RO) were adjusted in order to have the same initial flux in each case. A value of 17.5 LMH was chosen because it was suitable for both modes of operations.

3.2.3.1 Measurement of mass of deposited foulant

After FO and RO fouling experiments, the mass of foulant deposition on the membrane was measured. It was measured with reference to the measurement of total organic compound (TOC) present in the deposited foulant (alginate) on the membrane samples and expressed as an amount per unit area. The first step after carefully taking out the fouled

membrane coupon was rinsing with Milli-Q water on the draw side to remove salt, particularly that on the draw side (FO mode).

Three small fouled membrane samples (each has an area of 4 cm^2) were cut from multiple locations of the fouled membrane coupon. The samples were transferred into three sample tubes each containing 40 ml of basic solution with pH 11. In order to avoid the interference from the membrane dissolution during foulant extraction, blank solutions were also prepared for both clean CTA and clean TFC membranes. Again, three samples were prepared for the TOC measurement. All of the sample tubes were put on a shaking table to extract the deposited foulant on the membrane for a time duration of 12 hours.

The TOC of the extracted foulant solutions and the blank solution were measured subsequently by a TOC analyser. The actual TOC of the deposited foulant was determined by the difference of the TOC in the extracted foulant solution and in the blank solution. The concentration of the deposited foulant in the extracted solution was determined by comparing its TOC with the TOC of standard solutions with concentrations of 0–50 mg of foulant per litre. Finally, in comparison to the measurements from the standard solutions, the mass of foulant deposition on the membrane surface was calculated.

3.2.3.2 Images of membrane samples through scanning electron microscope

Membrane images were taken through Scanning electron microscope (SEM) and atomic-force microscopy (AFM). Samples of each fouled membrane and the respective cleaned membrane were selected for evaluation.

3.2.4 Determination of membrane and foulant resistances

The membrane separation properties were measured during the FO process and also during the RO process. For FO mode the membrane resistance (R_m) was calculated by using the model derived by She et al. (2016) for osmotically driven membranes (in ALFS orientation) as shown in Equation 3.1:

$$R_m = \frac{(\pi_D - \pi_F) - \Delta P - F_{cecp}\left(\pi_F + \frac{J_S}{J_W}\beta R_g T\right) - F_{dcp}\left(\pi_D + \frac{J_S}{J_W}\beta R_g T\right)}{\mu J_W} \quad (3.1)$$

where π_{Ds} and π_{Fs} represent the osmotic pressures at draw and feed side respectively. The osmotic pressure (π) for a solution with concentration "C" was calculated by Van't Hoff's equation (Nobel, 1969) as stated below:

$$\pi = \beta\ R_g\ T\ C \quad (3.2)$$

F_{cecp} in Equation (3.1) represents the factor for concentrative external concentration polarization at the active layer side which is a function of exp ($\frac{J_w}{k_F}$) while F_{dcp} is the factor for dilutive concentration polarization (for both internal and external) when active layer is on feed side. F_{dcp} is a function of –exp ($-\frac{J_w}{K}$) where K relates to both internal and external concentration polarization; K is essentially $\frac{D}{S}$ where D and S are diffusion coefficient and structural parameter respectively. The terms J_s, J_w, β, R_g, k, T and μ denote solute flux, water flux, Van't Hoff coefficient, universal gas coefficient, mass transfer coefficient, absolute temperature and fluid viscosity respectively. The deposition of the foulant particles on the surface of the membrane leads to changes in F_{cecp} and F_{dcp} because of changes in flux. Thus for the fouled membrane, the following modified form of Equation (3.1) was used to calculate the membrane resistance (R_f):

$$R_f = \frac{(\pi_D - \pi_F) - \Delta P - F_{cecpf}\left(\pi_F + \frac{J_{sf}}{J_{wf}}\beta R_g T\right) - F_{dcpf}\left(\pi_D + \frac{J_{sf}}{J_{wf}}\beta R_g T\right)}{\mu\ J_{wf}} - R_m \quad (3.3)$$

where, "*f*" symbol with respective parameters indicate their association with the "fouled" membrane.

3.2.5 Separation and structural properties of membrane

3.2.5.1 Membrane separation properties

The membrane separation properties (A and B values) were evaluated experimentally. The membrane water permeability (A value in L/bar) was evaluated in relation to fluid viscosity (μ) and the membrane resistance (R_m in m^{-1}) as:

$$A = \frac{1}{\mu\ R_m} \quad (3.4)$$

The solute permeability coefficient (B value) was calculated by using classical diffusion theory (Lee et al., 1981) as:

$$B = \frac{(1-R)\ A\ (\Delta P - \Delta\pi)}{R} \quad (3.5)$$

where, R is the salt rejection and ΔP represents the difference in hydraulic pressure across the membrane.

3.3 Tubular ultrafiltration ceramic membrane setup

The tubular ultrafiltration membrane at Oxford was previously used by researchers for filtration experiments with dextran as a potential foulant. As the membrane was not properly cleaned after these filtration tests, the protocols were made physical and chemical clean before applying filtration techniques further.

3.3.1 Membrane structure

The membrane had a hexagonal cross section that contains 19 parallel cylindrical channels, each 4 mm in diameter and 1020 mm long resulting in a total surface area of 0.24 m^2. The membrane element is made from ultrapure aluminium oxide (Al_2O_3) with zirconium oxide (zirconia) and titanium oxide (titania) in the filtering layers. Its multi-layered structure has a thin filtering layer on the surface, which will only let through particles below a certain molecular weight cut off (MWCO). The general definition of MWCO is the molar mass of a globular protein which is 90 % retained by the membrane. Below the filtering layer, there is an intermediate layer with larger pore size and finally a supporting structure that makes up the majority of the membrane element. It is enclosed in a cylindrical stainless steel module with a feed input at the base, an outlet of the retentate at the top and a permeate outlet on the side, just above the base. The ceramic membrane is hydrophilic in nature having a contact angle around 30° (Cheryan, 1998). Figure 3.3 shows the cross-section of a typical membrane element; this type was used in the current work.

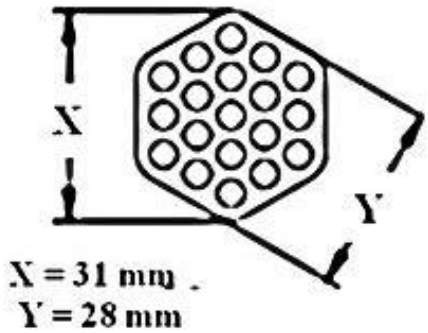

Figure 3.3 Cross-sectional view of hexagonal channel of the ultra- filtration membrane element

3.3.2 Experimental setup

Figure 3.4 shows the schematic view of the apparatus used including the peristaltic pump, pressure gauges and flow meters. The membrane element and casing, collectively called the module, is mounted vertically. There is a 6 litre cylindrical feed tank with a removable

lid to which both permeate and retentate lines are attached. The lines can be detached in order to separate the two streams. There is a valve in the retentate line that allows the outlet pressure, and thus the transmembrane pressure (TMP) to be controlled. The peristaltic pump (Watson-Marlow 520S) has a range of 20 to 220 rpm in 0.1 rpm intervals and produces a pulsed flow. Flow meters (CT Platon glass tube and float) on the feed line and permeate give an indication of the feed flow rate but because of the pulsed flow, they give fluctuating readings, as do the pressure gauges.

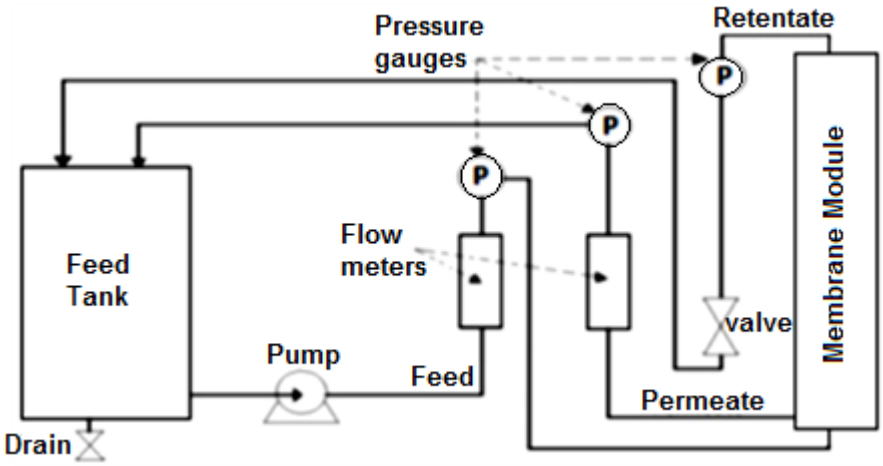

Figure 3.4 Schematic view of ultrafiltration rig

3.3.3 Feed and cleaning chemicals

All of the chemicals were used as received, and had purity over 99% and were of analytical grade. Dextran (average MW 19,500 Da) and carboxymethyl cellulose (average MW of 90,000 Da) were the model foulants. Solutions of both foulants of selected concentration (w/w) of 0.03, 0.05, 0.1, 0.15 and 0.2 were prepared. Each solution was prepared in a quantity of 5L and thoroughly stirred using a magnetic stirrer.

For the chemical cleaning of the membrane, sodium hydroxide (NaOH) of concentration 2% w/w, sodium hypochlorite (NaOCl) with 0.1% free chlorine and hydrochloric acid (HCl) of concentration 1% w/w were used either individually or in suitable combination.

3.3.4 Filtration process

The filtration process was either operated without intermittent rinsing or with intermittent rinsing. The exact definition of rinsing was not found in literature though during this research, the rinsing was the process of circulating the DI water over the surface of the fouled membrane with specified crossflow velocity and temperature. The rinseable fouling is the fouling which can be removed by mere rinsing. The conditions of the rinsing fouling summarised below:

Table 3.1: Conditions of rinsing of fouling

Process	Rinsing liquid	Temperature	Crossflow velocity	Time (min)	Hydraulic pressure
Ultrafiltration	DI water	Room temp. / 40°C	11 cm/s	30-40	Nil

3.3.4.1 Without intermittent rinsing

The solutions were filtered through the tubular ultrafiltration membrane at a crossflow velocity of 0.11 m/s at room temperature with intermittent stepping of transmembrane pressure. Permeate collected per minute was used to determine flux. The membrane was rinsed thoroughly after each complete test with strong alkaline solution of NaOH (2% w/w), a solution of NaOCl with 0.1% free chlorine and 1% w/w HCl. Before each chemical rinse, the membrane was washed with de-ionized water to clear any impact of the previously used chemical. It was observed that raised temperature (up to 40°C) resulted in better cleaning than that at room temperature. To avoid pore blocking by fragmented foulant particles that are freed from the membrane surface, each cleaning was done mainly with the permeate valve closed; it was gently opened for the cleaning inside the pores towards the end of each cleaning period. The clean water flux was considered as the yard stick and if necessary, cleaning procedures were repeated.

3.3.4.2 With intermittent rinsing

For the analysis of the reversible fouling, the prepared solutions for the foulants of dextran and carboxymethyl cellulose with concentrations (w/w) of 0.03%, 0.05%, 0.1%, 0.15%

and 0.2% respectively were filtered with intermittent water rinsing being undertaken after each TMP rise. During the rinsing phase, the membrane was rinsed with cold and then hot water each for 30 minutes. The flux was checked after each rinse. The change in foulant resistance was noted. The membrane was carefully cleaned with chemicals after each test.

3.3.5 Cleaning procedure

3.3.5.1 Restoration of membrane permeability

Previous to the current investigation, there had been some historical longstanding dextran fouling of the membrane. In this part of the work, fluxes at different values of transmembrane pressure were recorded before and after various cleans which sought to restore the original permeability. The membrane was initially treated with a strong alkaline solution of NaOH (2% w/w) for 60 min keeping the crossflow velocity constant at 0.11 m/sec. The permeate valve was kept closed in order to have zero TMP between two ends of the module. After the prescribed time, the alkaline solution was drained and membrane was rinsed with deionised water twice. Next, the membrane was treated with solution of sodium hypochlorite (NaOCl) with 0.1% free chlorine. This operation was undertaken for 60 minutes with the permeate valve closed. The crossflow velocity was 0.11 m/sec. After cleaning with NaOCl solution, the membrane was again rinsed twice with DI water to remove the chlorine effects. In the similar way as before, the flux was recorded and membrane resistance calculated. The membrane was given a second run with NaOCl solution at the same parametrical conditions.

Then the membrane was cleaned with a solution consisting of a mixture of 2% w/w alkaline solution of NaOH and NaOCl with 0.1% free chlorine. Equal amounts of both

solutions were mixed thoroughly with a magnetic stirrer. The membrane was run with this solution at 0.11 m/s for 1 hour again with permeate valve closed.

The solution was drained and the flux recorded after rinsing twice. After the application of alkaline solution and oxidizing agent, the membrane was cleaned with HCl (1% w/w) at 0.11 m/sec for 60 minutes. The membrane was then washed twice with DI water. The flux was then recorded using clean water. In order to achieve the targeted clean water flux, the membrane was re-treated with the same cleaning chemicals heated up to 40°C. For each application, the permeate valve was kept closed until near the end when it was gently opened. In between each run, the membrane was washed with pre-heated DI water (up to 40°C) to remove any effect of the previously used chemical.

3.3.5.2 General cleaning procedure

During the second part of the work, reversible fouling was removed intermittently by use of water rinsing. The fouled membrane was rinsed first with cold and then hot water. The removal of fouling (regarded as the reversible fouling) was observed by noting the change in foulant resistance.

3.4 Assessment of spiral wound forward osmosis module at pilot scale

This work related to that reported in Chapter 6. After working at pilot scale in an industrial location, bench scale experiments were undertaken using membrane material cut from the spiral wound module. The bench scale setup was essentially the same as that described above in section 3.2.2.1. Further details are given in chapter 6, which is concerned mainly with the pilot scale experiments at Bedok NEWater Plant in Singapore.

4

Tubular ultrafiltration ceramic membrane

4.1 Introduction

A series of experiments with an ultrafiltration ceramic tubular membrane were carried out for the foulants dextran and carboxymethyl cellulose. Dextran is complex chained glucan available in variable lengths. It is easily accessible and commercially available with an average molecular size range of 2.68 to 21.36 nm. In a number of studies on ceramic membranes, dextran has remained a good choice for researchers. Similarly, carboxymethyl cellulose (CMC) is a sodium salt derivative of carboxymethyl groups with good solubility and chemically reactive, it is often used as potential foulant for membrane filtration. (Kokugan et al., 1995, Cortalezzi et al., 2002, Zuriaga-Agustí et al., 2014). For these reasons and because they were readily available, dextran and carboxymethyl cellulose were the foulants chosen. Firstly, the impact on fouling of concentration changes was investigated with the increase in resistance being used as the key parameter. In the second phase, removal of reversible fouling was investigated by employing intermittent rinsing consisting of a cold water rinse followed by a hot one. A comparative analysis for both foulants is included. Across a range of concentrations and for both foulants, the reduction in resistance due to rinsing was found to depend upon concentration (C); it changed as C^n, where n was found to be 0.3. A plausible semi-theoretical explanation is given. Thirdly, for both foulants, the application of a combination of strong alkaline solutions with oxidizing agent (mainly sodium hypochlorite) followed by acid was found to be appropriate for cleaning of the ceramic

membrane. The effect of increased temperature for cleaning agents followed by a warm water rinse contributed positively to cleaning.

4.2 Cleaning of tubular ultrafiltration ceramic membrane

Table 4.1 shows the comparative results of the chemical cleanings with NaOH, NaOCl, HCl and their respective solutions to restore membrane permeability. The membrane had been pre-fouled by previous users and left uncleaned for a long time (> 3 years). After the treatment with the NaOH solution (2% w/w) for an hour at 0.2 bar and 0.11 m/sec, the permeate flux was observed to have recovered slightly (10.3%). The repeated treatment of membrane with sodium hydroxide failed to show increasing improvement in flux, indicating that the capacity of cleaning with NaOH solution had reached its limit. Application of sodium hypochlorite (0.1% chlorine w/w) resulted in a further small improvement of flux i.e., 4.9%. The repeated treatment of the membrane with the oxidizing agent NaOCl (0.1% free chlorine w/w) with the same parametrical conditions did not show any improvement in the flux recovery, indicating that the NaOCl solution too had exhausted its capacity for further cleaning. Then the 50:50 mixture of NaOH (2% w/w) and NaOCl solution (0.1% of free chlorine) was used. This resulted in a further recovery of 6.0%. The membrane was further treated with the same chemicals with the temperature raised to 40°C. A notable flux recovery was experienced, namely 34.5%. The combination of strong alkaline solution, oxidant and acid has remained a preferred choice for experimentalists for cleaning ceramic membrane fouling (Cabero et al., 1999, Shi et al., 2014, Wang et al., 2014). Therefore, in the current study, the same combination of cleaning agents was used.

It is widely accepted that the cleaning agents are unable to achieve 100% flux recovery. According to Field et al. (2008), this can be related to two reasons i.e., relatively low

concentration of cleaning solutions and the cleaning was undertaken at low temperature. Ceramic membranes have a capacity to bear high pressure as well as having a good ability to deal with strong cleaning agents. The cleaning is as important as the filtration through the membrane. Therefore, it is necessary to use a combination of strong cleaning agents to recover flux and remove the historic fouling that had been inherited. **Table 4.1** also shows the decrease in resistance for the filtration after cleaning tests. The application of hydrochloric acid in the cleaning resulted in a notable flux recovery of 22.9%. The reason behind this good recovery is that the acids can weaken and then break the bonds between the foulants and the membrane surface (Lim and Bai, 2003). However, it is very important to select the appropriate concentration of the acid, as excessive amounts may damage the membrane surface. The technique of using the preheated chemicals had a very positive impact and was further applied during the filtration experiments.

Table 4.1: Decrease in resistance of fouled membrane after various chemical cleans

Sr. No.	Application	Foulant resistance (m^{-1})	Percentage decrease in foulant resistance
1.	Before cleaning	13.6×10^{12}	-
2.	After cleaning with NaOH solution (2% w/w)	12.2×10^{12}	10.3
3.	After cleaning with NaOCl solution (0.1% chlorine w/w)	11.6×10^{12}	4.9
4.	After cleaning with NaOH solution (2% w/w) and NaOCl (0.1% Chlorine w/w)	10.9×10^{12}	6.0
5.	After cleaning with HCl (1% w/w)	8.4×10^{12}	22.9
6.	After cleaning with heated chemical mixtures	5.5×10^{12}	34.5

4.3 Experiments with constant transmembrane pressure

4.3.1 Without intermittent rinsing

After the thorough cleaning detailed above the rig was used for the fouling experiments, starting with a solution of Dextran (with concentration of 0.03% w/w) for which some of the rheological properties of the solution were analysed using a rheometer (Physica MCR 301).

The permeate pressure was set to zero and the TMP was raised step wise while recording the flux at each step. A series of solutions of carboxymethyl cellulose (Fisher Chemicals) were applied at identical conditions. The experiments were repeated for the concentrations (w/w) of 0.03, 0.05%, 0.1%, 0.15% and 0.2% respectively. A plateau in the flux-TMP relationship was found beyond 0.3 bar for Dextran and 0.2 bar for carboxymethyl cellulose (CMC).

4.3.2 With intermittent rinsing

In the second phase of experiments, the membrane was intermittently rinsed with cold and hot water. Again, the concentrations (w/w) of both solutions were 0.03%, 0.05%, 0.1%, 0.15% and 0.2% respectively.

Carboxymethyl cellulose **Dextran**

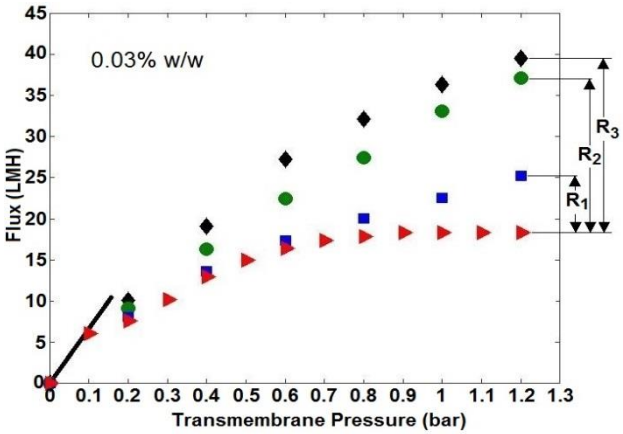

4.1 (a)

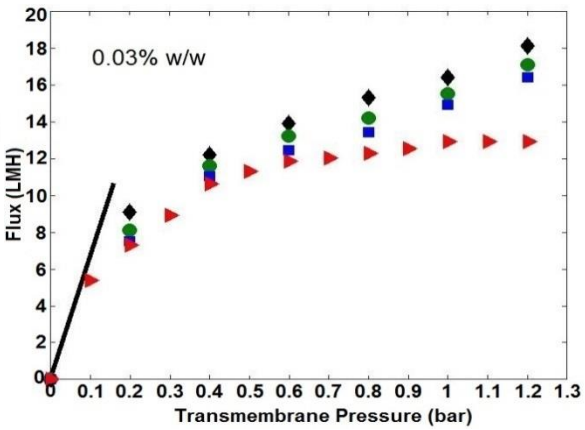

4.1 (f)

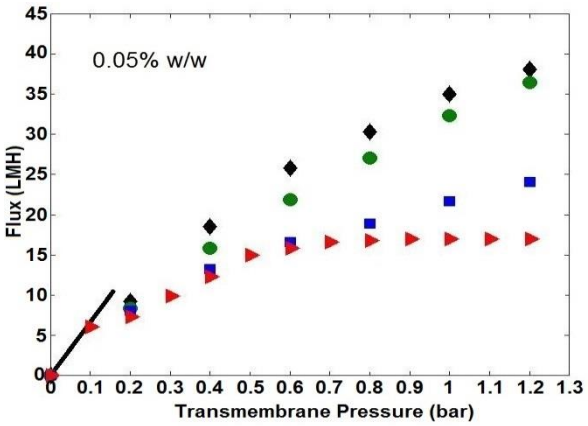

4.1 (b)

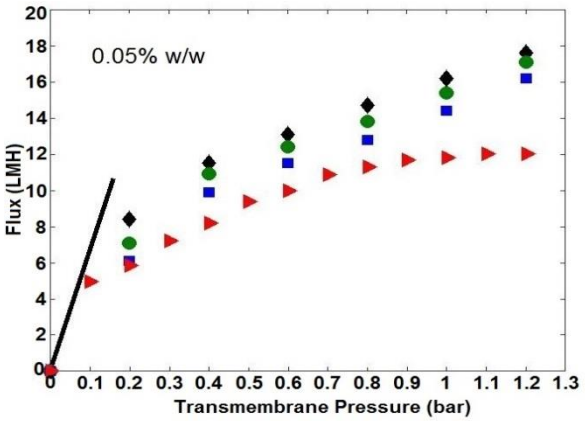

4.1 (g)

Figures 4.1 Continued…

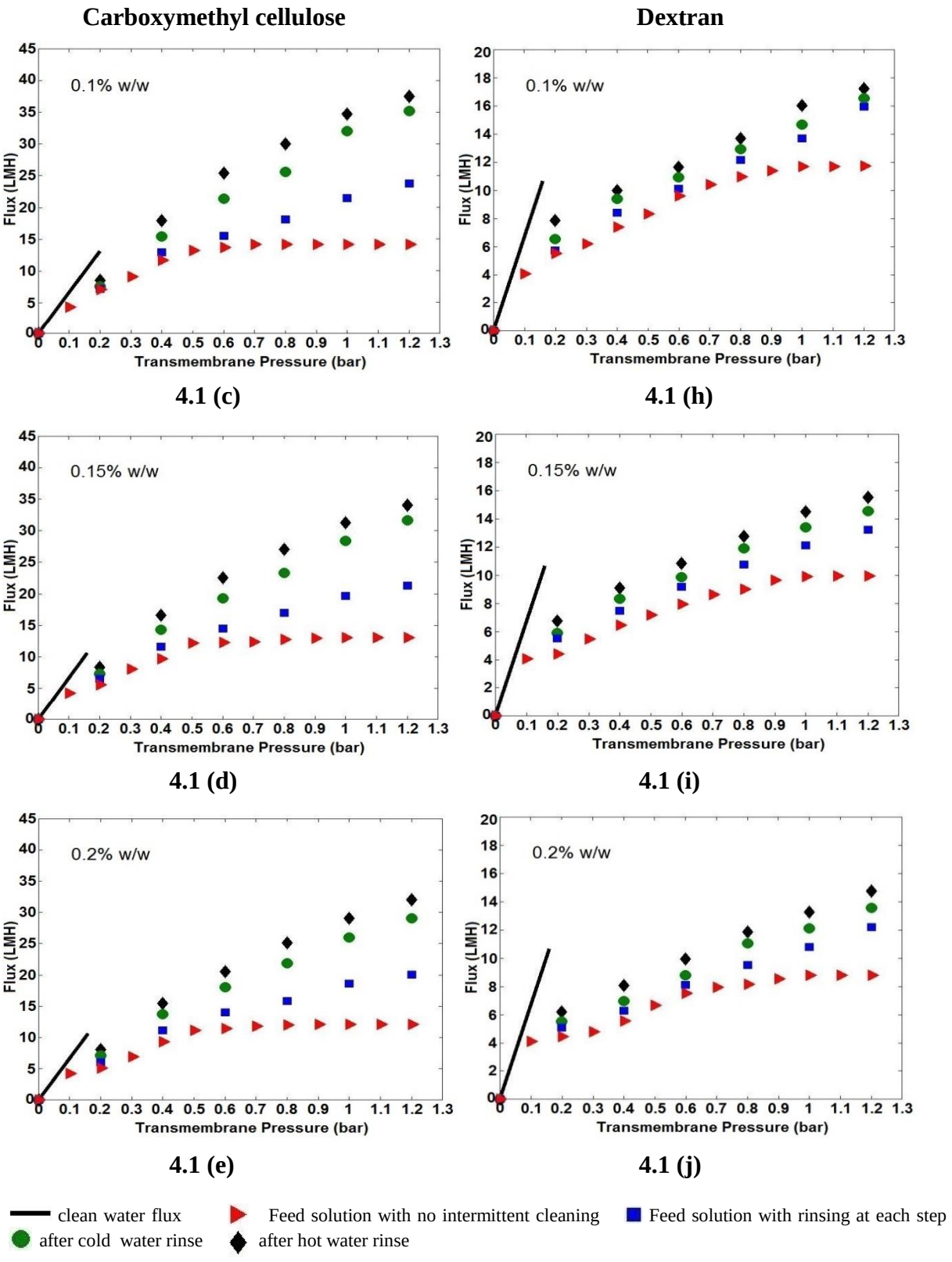

Figures 4.1 (a)-(j) : Flux-TMP diagrams for foulants of CMC and Dextran for 0.03%, 0.05%, 0.1%, 0.15% and 0.2% solutions (w/w) with and without water rinsing. Figures 4.1 (a)-(e) are for increasing concentration of CMC whilst Figures. 4.1 (f)-(j) refers the same for the dextran. Figure 4.1 (a) shows R1, R2 and R3. These represent the changes in fouling that are referenced in Section 4.4.

A notable increase in flux was observed after each intermittent rinse. The corresponding decrease in foulant resistance was noted. Flux-TMP graphs in Figures 4.1 (a)–(e) are for increasing concentration of CMC. These illustrate the improvement in flux due to intermittent rinsing with cold water followed by the hot one. Figures 4.1 (f)–(j) refer to the same for the dextran. It is evident from the graphs that water rinsing has more impact with CMC solutions than with the dextran solutions. This suggests that CMC molecules are more loosely attached to the membrane walls and are more easily removed by rinsing than dextran molecules. This is probably due to the loose intermolecular and intramolecular hydrogen bonding in CMC as detected by Hishikawa et al. (2005) in comparison with strong multiple intermolecular hydrogen bonding in dextran (Guizard et al., 1984). However, in both cases some foulant particles are unable to be removed by mere rinsing and these contribute to the irreversible fouling. Analysis indicates that, as a percentage of overall resistance, reversible fouling decreases as the concentration increases. The reason behind this could be that during filtration of a more concentrated solution, dense cake layers are formed. For the plants running at commercial scale, the application of intermittent rinsing may have a vital role. It can be queried as to whether this makes economic sense and for each application; a case study would be required. One area where it might well make sense is in agro-food. Typically, these plants are run in production for two shifts per day and cleaned during part of the night shift. Thus, time is available and attention to extensive rinsing might well enable the use of NaOH and acid to be reduced. The strength of ceramic membranes lend themselves to the application of short sharp backwashes and, as noted by Wu et al. (2008a) for fouling mitigation, the effect of backwashing strength can be more significant than the duration or interval of backwashing.

4.3.3 Foulant resistance

Based upon Darcy's law and neglecting the osmotic pressure effects, the clean water flux (i.e., the flux before any fouling) is given by:

$$J = \frac{\text{TMP}}{\mu R_m} \tag{4.1}$$

where, TMP (transmembrane pressure) is defined as the pressure gradient across the membrane that drives the water across the membrane from feed side to the permeate side. As the fouling occurs, the foulant resistance, which is shown as $R_f(t)$, needs to be added

$$J = \frac{\text{TMP}}{\mu\,[R_m + R_f(t)\,]} \tag{4.2}$$

Where, J is the flux at any instance, μ is the dynamic viscosity, R_m represents the resistance of the membrane while R_f (t) is the resistance of the foulants at a time 't'. When some of the particles adhere before the start of actual filtration, due to electrostatic interaction or van der Waals forces etc. and resulting in additional resistance (R_{ads}), one may distinguish between this initial amount of fouling and that which occurs later. So, after the membrane has equilibrated with the feed but before filtration:

$$J = \frac{\text{TMP}}{\mu\,(R_m + R_{ads})} \tag{4.3}$$

If, but only if, there is no additional increase in resistance up to a certain flux, then the filtration is said to be operating below a weak form of critical flux (Field et al., 1995, Bacchin et al., 2006). From the point on, as more fouling occurs due to flux, the general equation becomes:

$$J = \frac{\text{TMP}}{\mu\,[R_m + R_{ads} + R_f(t)]} \tag{4.4}$$

In this work, R_{ads} was not separated from a general fouling resistance. The following Figures 4.2 and 4.3 depict the relationship between transmembrane pressure and fouling resistance

which has been obtained by Darcy's law using Equation 4.2. The change in foulant resistance with time has been divided into four regions which have been explained later.

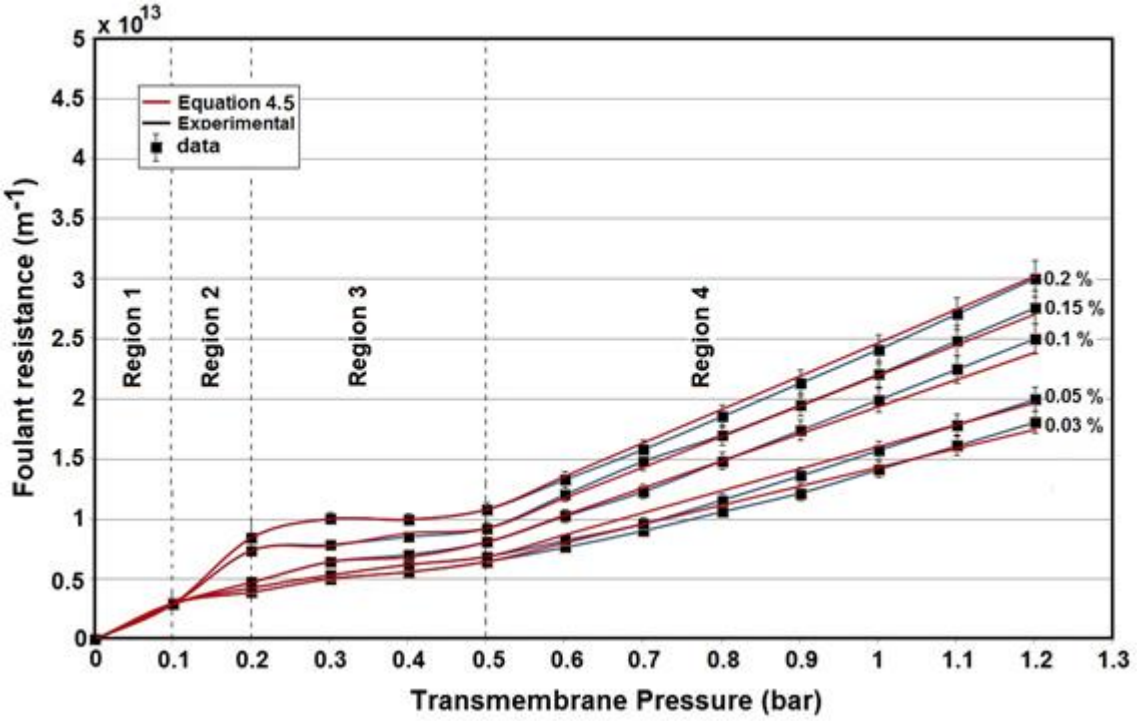

Figure 4.2: Fouling resistance vs transmembrane pressure for solutions of carboxymethyl cellulose for concentrations (w/w) of 0.03%, 0.05%, 0.1%, 0.15% and 0.2%. In addition to Equation 4.5, lines through data added for visualization.

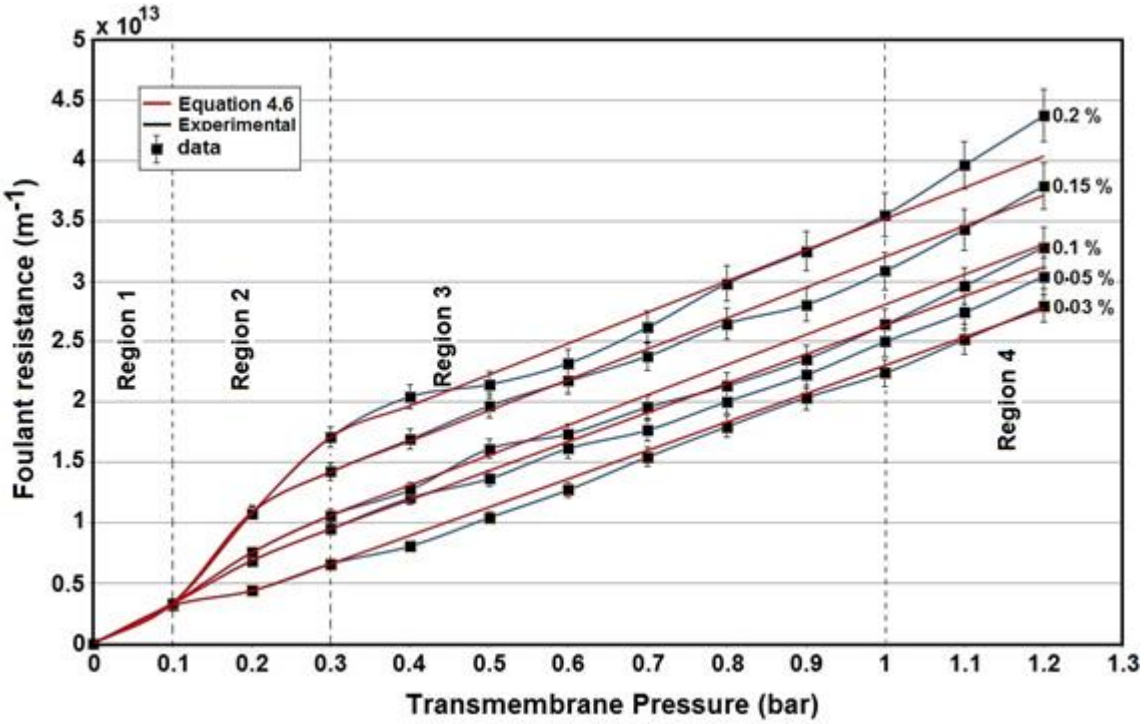

Figure 4.3: Fouling resistance vs Transmembrane pressure for solutions of dextran for concentrations (w/w) of 0.03%, 0.05%, 0.1%, 0.15% and 0.2%. In addition to Equation 4.6, lines through data added for visualization.

The graphs in Figure 4.2 and Figure 4.3 indicate that the relationship between fouling resistance, concentration and TMP is complex. Whilst the fouling resistance vs. TMP relationship for dextran is quite linear, that for CMC shows a sharp change in gradient at 0.5 bar TMP. In general the gradients are greater for dextran than CMC. With regard to CMC, up to 0.5 bar, the gradient of resistance with respect to TMP is around 1.5×10^{13} m^{-1} per bar. These values are for 0.1 w/w % CMC. The curve for dextran is almost straight; for 0.1% w/w, the value is around 3×10^{13} m^{-1} per bar. In both figures, the solid lines were added for visualisation and the dotted lines indicate boundaries between different regions. For a specific concentration of CMC, a linear relationship between the foulant resistance and TMP exists for a TMP greater than 0.5 bar. The data can be represented by:

$$R_f = R_{f-0.5} + b\,(\mathrm{TMP} - 0.5) \qquad (4.5)$$

where, $b = 4.5\,C^{0.3}$ with C being the percentage concentration. The fit to the data is excellent (Figure 4.2).

For dextran, the gradient was found to be essentially independent of concentration. The gradient of the concentration data set shows a very moderate dependency upon feed concentration as shown in Figure 4.3 and modelled through Equation (4.6)

$$R_f = R_{f-0.3} + b\,(\mathrm{TMP} - 0.3) \qquad (4.6)$$

Here, $b = 2.8\,C^{0.05}$ with C being the percentage concentration. Given the weak dependency upon concentration, it is reasonable to say that in region 1, the gradient is essentially independent of *C*. The fit is reasonable in region 3.

In Figure 4.2, region 1 is the one where the foulant resistance is independent of the concentration of CMC. Region 2 is a transition region from region 1 to region 3, in which concentration has an influence. In region 3, the resistance is roughly constant for a given concentration, whilst in region 4, Equation (4.5) applies and the fouling resistance increases with TMP. Equation (4.5) is not independent of concentration, as the gradient has a modest dependency upon C. The change in gradient between region 3 and 4 suggests that at these points, there are threshold conditions as described by Field and Pearce (2011). An increase in transmembrane pressure increases the flux bringing more foulants towards the membrane resulting in increase in foulant accumulation and foulant resistance, however, the nature of fouling is different from region to region.

Figure 4.3 shows that the fouling caused by dextran is broadly similar to that caused by CMC. Similar to CMC, region 1 represents the point where concentration does not have any influence on foulant resistance. Also region 2 is similar in that it is a transition region where both concentration and TMP influence the value of R_f. However, with regard to the other two regions, the fouling phenomenon is somewhat different. For both regions 3 and 4, Equation (4.6) is applicable and dextran solutions do not display the threshold displayed by CMC solutions.

4.4 Reversible fouling

It was observed that the difference in resistance after each rinse was related to the concentration of the solution. Much of the reversible fouling was removed through cold water rinsing and then more by hot water rinsing. If the influence of the concentration of the feed solution is of the form C^n, with n being a suitable exponent, then the difference in foulant resistance (R_{df}) is given by Equation (4.7):

$$R_{df} = K_{av}\, C^{n} \qquad (4.7)$$

where, C represents the feed concentration and K_{av} is the modulus. K_{av} is called modulus as it relates two given quantities i.e. R_{df} and C^n linearly to obtain a unique remainder value at specified conditions. The value of the latter depends solely upon the transmembrane pressure. The value of n was found to be 0.3 for both foulants. This value of 'n' being 0.3 for both foulants is related to the expression for linking the difference in foulant resistance (R_{df}) after rinsing i.e. how much reversible fouling was present unlike an expression of 'n' used earlier (where the value of 'n' was 0.05 for dextran) was related to overall resistance of the foulants at specified conditions. For dextran as well as CMC, K_{av} was found to be a function of transmembrane pressure and not concentration. K_{av} was calculated for each transmembrane pressure for the following three cases:

(i) The change in resistance without and with intermittent rinsing between each TMP step, represented as R_1 in Figure 4.1 (a).

(ii) The change in resistance measurements between without rinsing and after cold water rinsing (where rinsing is done at each step), represented as R_2 in Figure 4.1 (a).

(iii) The change in resistance between without rinsing measurements and after hot water rinsing represented as R_3 in Figure 4.1 (a).

A plausible semi-theoretical explanation for the 0.3 dependency in Equation (4.7) can be represented by the following equations, where in 'spacing' refers to the average distance between foulant molecules.

$$R_{df} \propto \text{Spacing}^{-1} \qquad (4.8a)$$

$$\text{Spacing} \propto \left(\frac{1}{C}\right)^{0.33} \qquad (4.8b)$$

$$R_{df} \propto C^{0.33} \qquad (4.8c)$$

To illustrate further, the pressure gradient in the direction of mean flow as given by Carmen – Kozney equation (Carrier III, 2003):

$$\frac{dp}{dx} = -\frac{180\,\mu U\,(1-\varepsilon)^2}{{d_s}^2\ \varepsilon^3} \qquad (4.9)$$

where μ is the viscosity, U and ε are the mean velocity and porosity respectively. The above equation can be represented in terms of resistance per unit depth and is:

$$\frac{dR}{dx} \propto \frac{(1-\varepsilon)^2}{{d_s}^2\ \varepsilon^3} \qquad (4.10)$$

{ Considering mean velocity (U) and the viscosity constant

where, ds is the mean diameter of the foulant particles. For dextran, taking the mean diameter as d_s = 15nm. To illustrate further, the R.H.S term in Equation (4.10) has been simulated at different values of porosity (ε) as is illustrated diagrammatically in Figure 4.4.

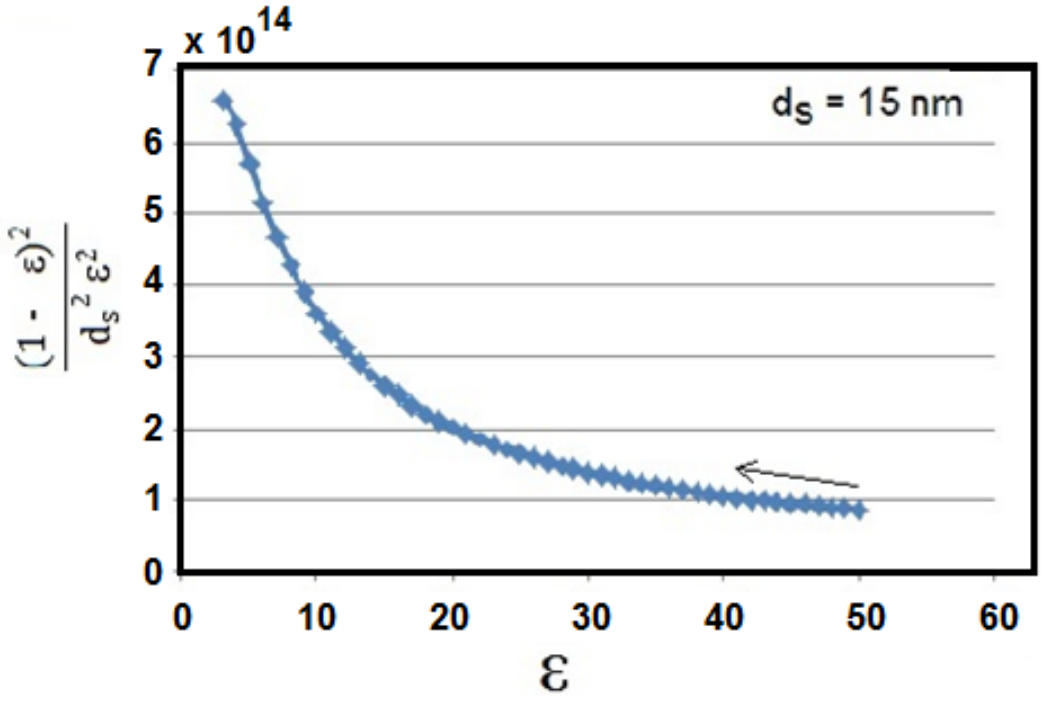

Figure 4.4: Simulation for the effect of porosity on Carmen-Kozney equation

In Figure 4.4, the curve shows that with the decrease in porosity of the membrane, the fractional change in resistance is increased. The above relation (4.10) links the fractional

change in resistance with the porosity and there is no direct expression which links resistance directly with the concentration. However, as the concentration of the foulant particles is increased, it is seen that the porosity/voidage of the cake is decreased which is consistent with a greater feed concentration giving a cake with tighter feed spacing as found empirically – expression (4.8c).

The calculated values of K_{av} are tabulated in **Table 4.2** and trends with TMP shown in Figure 4.5. These values of K_{av} reveal that it increases with the increase in transmembrane pressure. However, through rinsing, the reversible fouling is removed as these are loosely attached particles and can be easily freed by just rinsing.

Table 4.2: Modulus (K_{av}) at different values of transmembrane pressure for dextran and carboxymethyl cellulose solutions

	Trans-membrane pressure (bar)	For change in resistance (R_1) for the feed solutions without and with intermittent rinsing (m^{-1} for % concentration of solute) × 10^{13}	For change in resistance (R_2) for the feed solution without rinsing and after cold water rinsing (m^{-1} for % concentration of solute) × 10^{13}	For change in resistance (R_3) for the feed solution without rinsing and after hot water rinsing (m^{-1} for % concentration of solute) × 10^{13}
Carboxymethyl Cellulose	0.2	0.28	0.44	0.66
	0.4	0.30	0.71	0.99
	0.6	0.39	1.09	1.43
	0.8	0.76	1.72	2.04
	1	1.43	2.58	2.80
	1.2	2.10	3.40	3.57
Dextran	0.2	0.17	0.42	0.73
	0.4	0.28	0.60	0.85
	0.6	0.36	0.67	0.98
	0.8	0.69	1.11	1.43
	1	1.19	1.61	1.98
	1.2	2.17	2.56	2.87

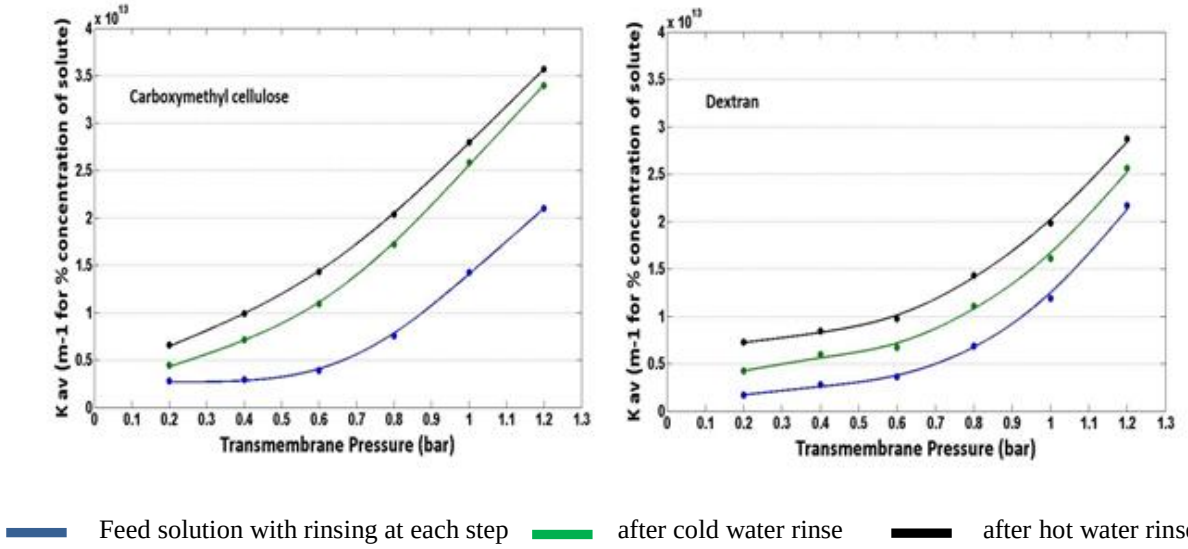

Figure 4.5: Concentration modulus (K_{av}) Vs. transmembrane pressure for carboxymethyl cellulose and dextran

The particle deposition on the membrane can be divided into 3 zones, based on the packing of the foulant particles. As the water permeates from the feed side to the permeate side, particles are convective on the membrane surface giving rise to a foulant layer the thickness of which generally increases with the passage of time and the average spacing between the particles is

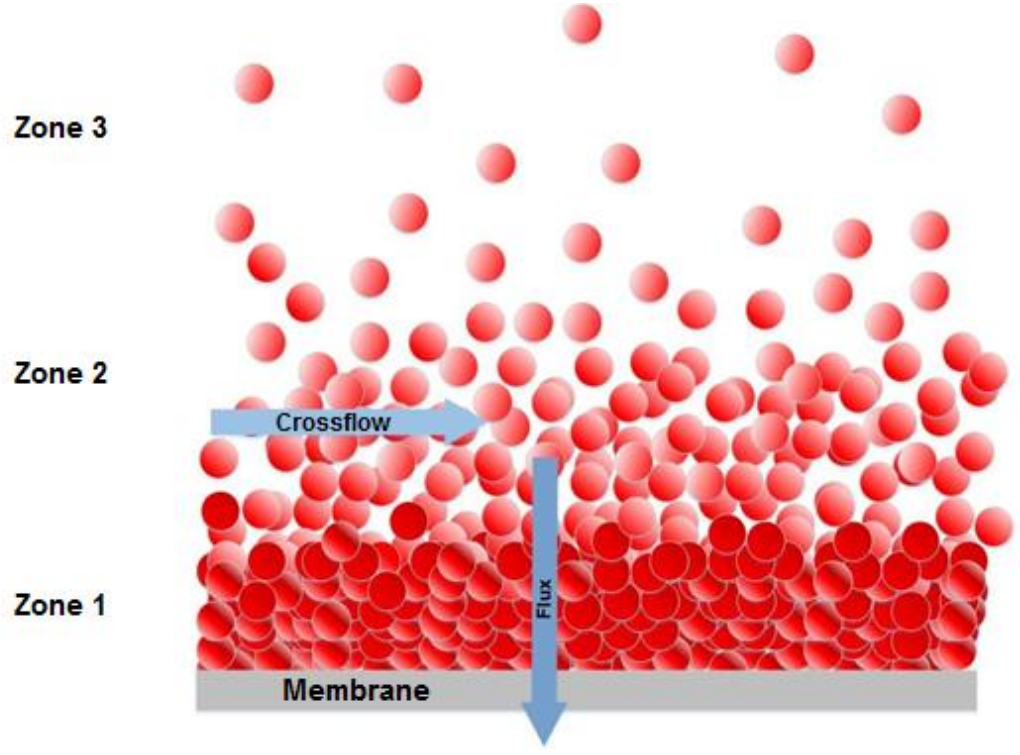

Figure 4.6: Three-zoned illustration of the foulant particle deposition on the membrane surface

reduced. In passing, it is noted that in addition in FO there is hindered diffusion of salt coming from the draw side due to the reverse solute diffusion. Thus, the effects of cake formation extend beyond the creation of a hydraulic resistance.

With the passage of time the submitted foulant particles nearest to the membrane surface constitute a closely packed irreversible foulant layer. This is depicted as Zone 1 in Figure 4.6. Above 'Zone 1' is an accumulation of foulants with the intermediate value of spacing between the particles. This is represented as 'Zone 2' in Figure 4.6. In Zone 2, the particles are loosely packed and the fouling is reversible in nature which can be removed by mere rinsing. Just above the two zones of foulants (reversible and irreversible), there is the concentration polarisation layer zone (*Zone 3*). The spacing between the foulant particles is larger than that in Zone 1 and Zone 2. The foulant resistance for particles is minimal. This phenomenon is demonstrated in terms of pressure gradient in the Carmen-Kozeny equation (Carrier III, 2003) i.e. the pressure gradient increases with the decrease in porosity (i.e. decrease in spacing between the foulant particles) which can be further co-related with the concentration. It is notable that the relationship between resistance and the concentration differs from case to case, depending upon many factors. The resistance of the loosely attached foulants that is removed by rinsing is assumed to have a resistance that is related to the spacing between molecules in the immediate vicinity of the foulant layer i.e. the molecules are closer together immediately before attachment will form a denser layer. The foulant resistance (R_f) decreased in the order by intermittent rinsing (R_1), rinsing with cold water (R_2) and rinsing with hot water (R_3). The fouling tendency might well be inversely proportional to the spacing and as shown in Equations (4.8a) – (4.8c), this suggests that the dependency upon concentration will be $C^{0.33}$ which is close to the dependency found experimentally.

4.5 Trends in reversible fouling

Based on the matrix of K_{av} values, the difference in foulant resistance was calculated using Equation (4.7) and compared graphically with the experimental values. For both carboxymethyl cellulose and dextran this was done in three ways:

(i) for the change in resistance for feed solutions without and with intermittent rinsing,

(ii) for the change in resistance for feed solution without rinsing and after cold water rinsing and

(iii) for the change in resistance for feed solution without rinsing and after hot water rinsing.

It is recalled that three categories of respective foulant resistance are represented as R_1, R_2 and R_3 in Figure 4.1 (a). It has already been noted that both the value of '*n'* in Equation (4.7) is 0.3 and, as shown in **Table 4.2**, K_{av} values increase with TMP so one can summarise that the average reversible fouling per unit area reflected by the R_{df} in Equation (4.7) is increasing with concentration and TMP. From the TMP values of 0.2 bar to 0.5 bar, the difference of the foulant resistance was independent of the TMP increase. However, as the TMP was further increased above 0.5 bar, the gradient of the difference in foulant resistance was found to be increasing notably. This would be probably due to the reason that at higher TMP, the foulant cake is compressed and the fouling is difficult to be removed by mere rinsing and giving rise to irreversible fouling. The experimental and modelled values for R_{df} vs TMP are illustrated graphically in Figures 4.7 (a) – (f).

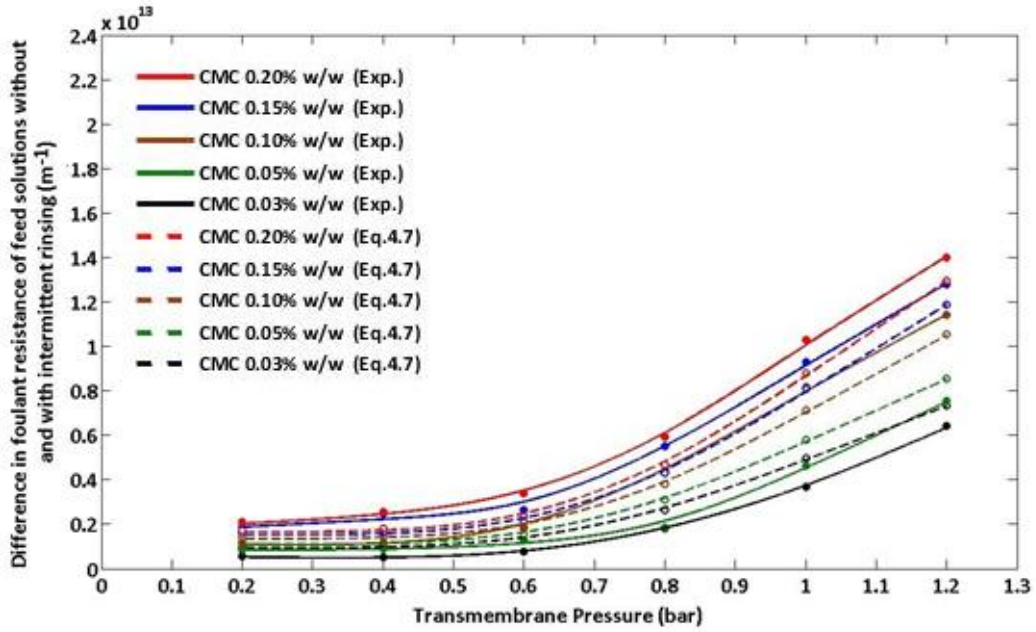

Figure 4.7 (a): Difference in fouling for the feed solutions without and with intermittent rinsing for carboxymethyl cellulose for concentrations (w/w) of 0.03%, 0.05%, 0.1%, 0.15% and 0.2% at different values of transmembrane pressure (stage represented as 'R_1' in Figure 4.1a)

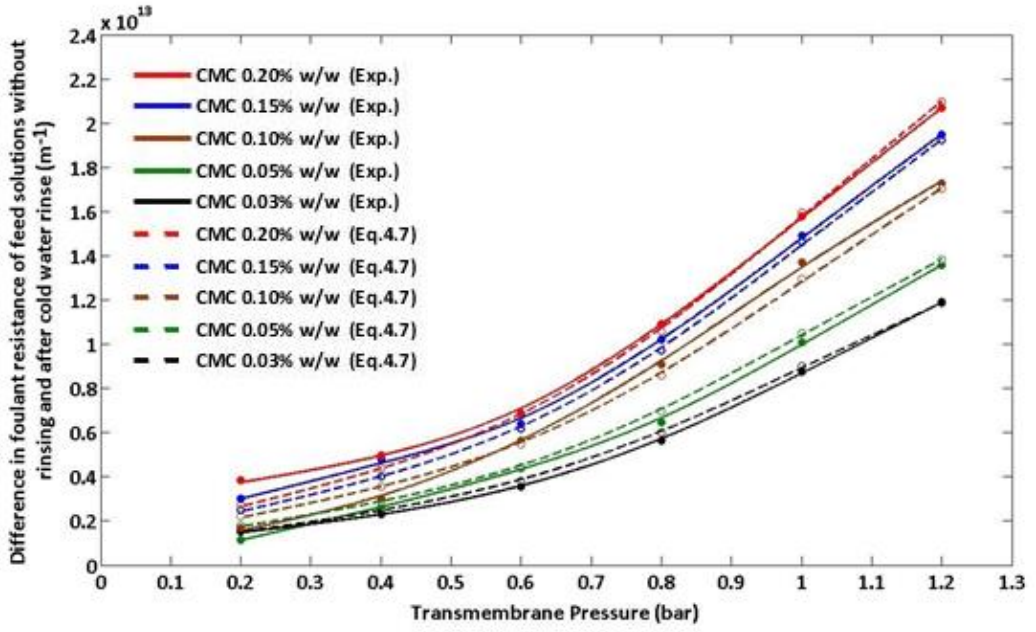

Figure 4.7 (b): Difference in fouling for the feed solution without intermittent rinsing and after cold water rinse for carboxymethyl cellulose for concentrations (w/w) of 0.03%, 0.05%, 0.1%, 0.15% and 0.2% at different values of transmembrane pressure (stage represented as 'R_2' in Figure 4.1a)

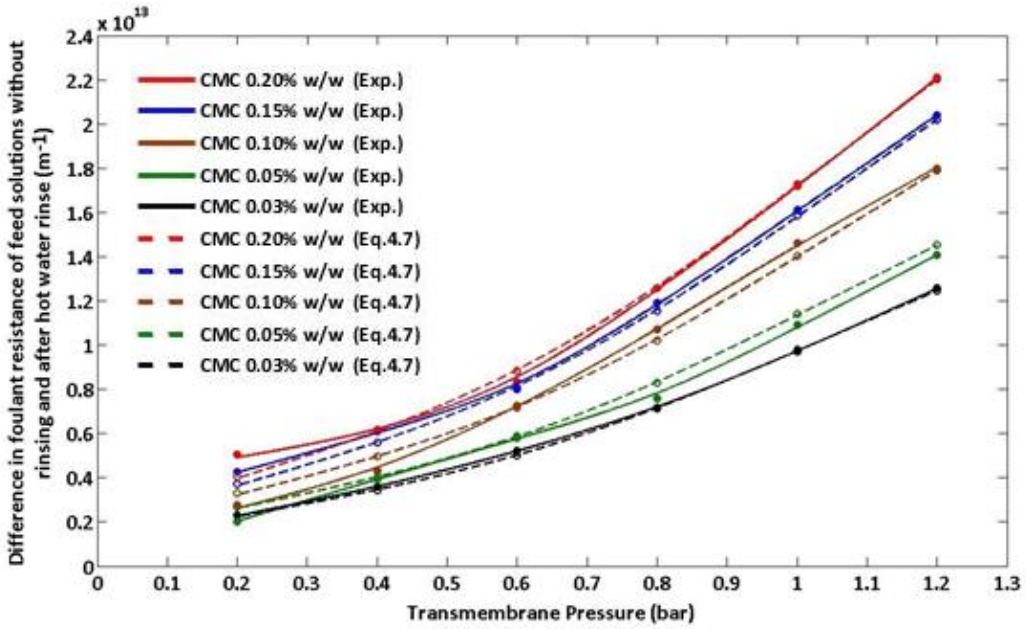

Figure 4.7 (c): Difference in fouling for the feed solution without intermittent rinsing and after hot water rinse for carboxymethyl cellulose for concentrations (w/w) of 0.03%, 0.05%, 0.1%, 0.15% and 0.2% at different values of transmembrane pressure (stage represented as 'R_3' in Figure 4.1a)

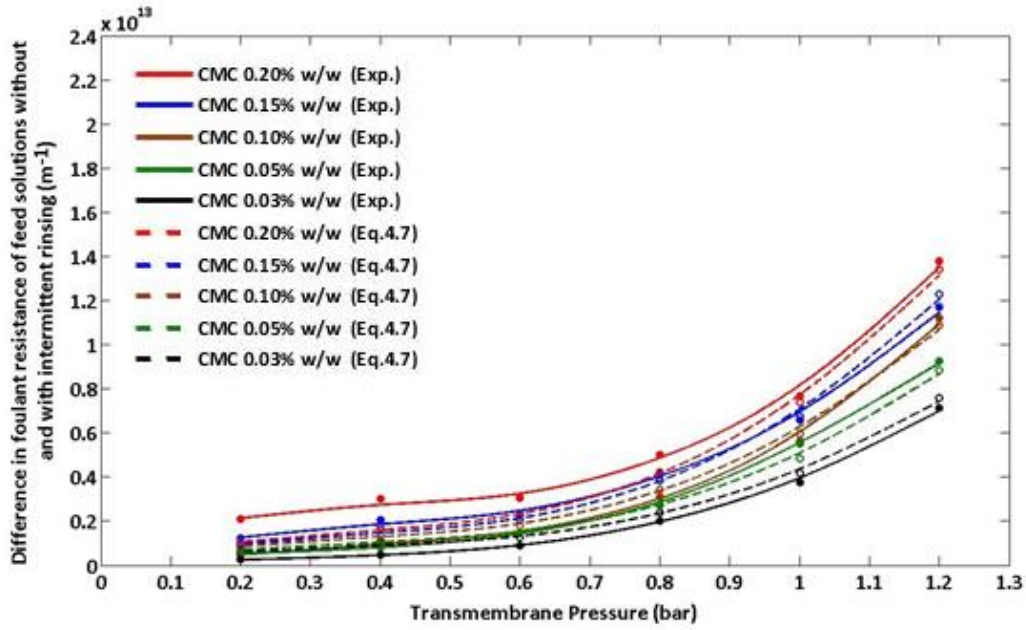

Figure 4.7 (d): Difference in fouling for the feed solutions without and with intermittent rinsing for dextran for concentrations (w/w) of 0.03%, 0.05%, 0.1%, 0.15% and 0.2% at different values of transmembrane pressure (stage represented as 'R_1' in Figure 4.1a)

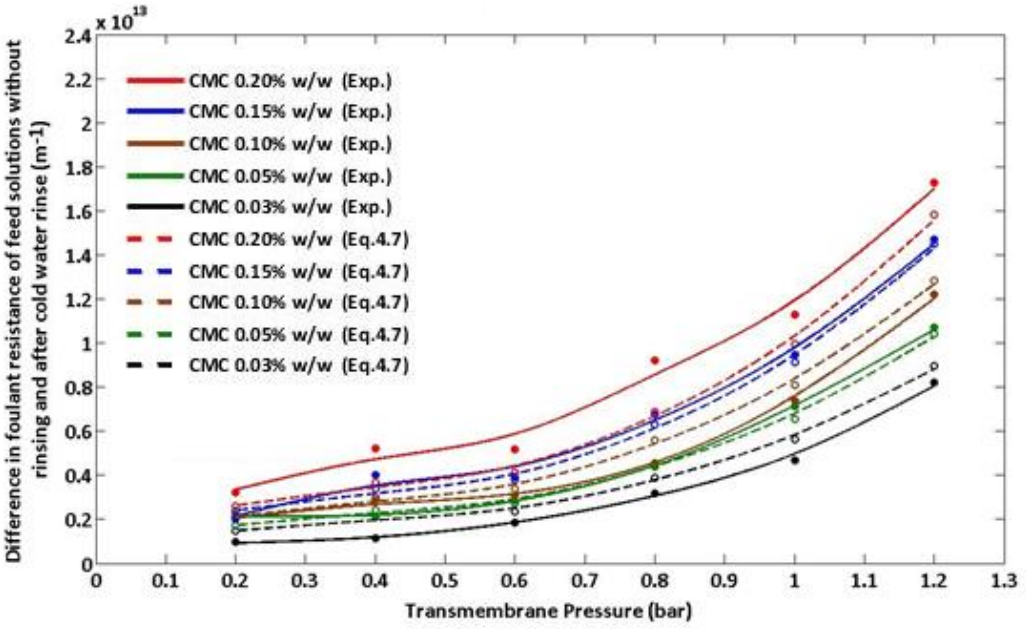

Figure 4.7 (e): Difference in fouling for the feed solution without intermittent rinsing and after cold water rinse for dextran for concentrations (w/w) of 0.03%, 0.05%, 0.1%, 0.15% and 0.2% at different values of transmembrane pressure (stage represented as 'R_2' in Figure 4.1a)

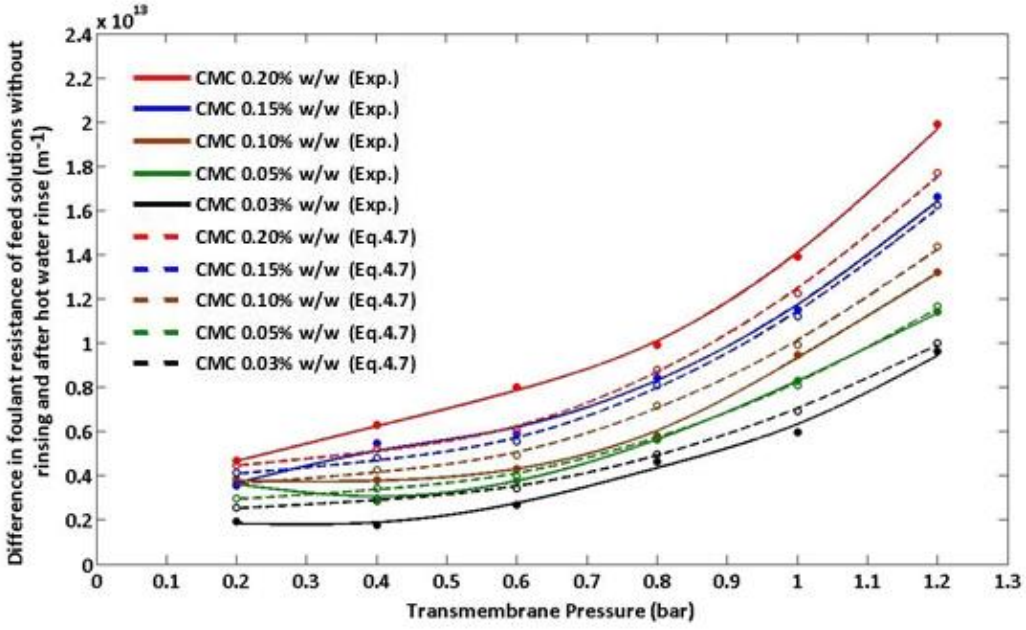

Figure 4.7 (f): Difference in fouling for the feed solution without intermittent rinsing and after hot water rinse for dextran for concentrations (w/w) of 0.03%, 0.05%, 0.1%, 0.15% and 0.2% at different values of transmembrane pressure (stage represented as 'R_3' in Figure 4.1a)

Figures 4.7 (a) – 4.7 (f): Change in foulant resistance on account of rinsing with cold and hot water for different concentrations of carboxymethyl cellulose and dextran

An implication of the graphical demonstration in Figures 4.7 (a)–(f) is that there is a considerable increase in flux after each step of rinsing i.e., reversible fouling is a significant component of the overall fouling. This trend was observed for the solutions of both carboxymethyl cellulose as well as the dextran. For 0.03% solutions of CMC, at TMP of 1.2 bar, the reversible fouling removed by intermittent rinsing, rinsing with cold water and rinsing with hot water was around 36%, 66% and 70% respectively. The same for dextran was 26 %, 29% and 34% approximately. Similarly, for 0.2% of CMC solution, the reversible fouling removed by intermittent rinsing, rinsing with cold water and rinsing with hot water was around 47%, 69% and 73% respectively and likewise for dextran, it was 32%, 40%, 46% in the same order.

As a final observation, there might be a link between optimising intermittent rinsing and optimising intermittent backwash as practised in direct-flow filtration, which is the technology of choice for surface water treatment by membranes (Pearce, 2011). Relaxation and/or backwashing have been incorporated in many membrane bioreactor (MBR) designs as standard operating strategies to limit fouling and it is therefore no surprise that rinsing under conditions of zero TMP had a beneficial effect. Following Wu et al. (2008b), we will in future work give consideration to having an initial short duration period (circa 100s) of elevated high flux followed by a longer filtration for the rest of the filtration cycle. This approach is said (at least for Wu's application) to limit irreversible fouling by having an initial fouling layer that prevents more highly fouling material from attaching onto the membrane surface. The initial layer acts as a filter aid. Whether one can achieve a filter aid situation as opposed to an over-clogging situation will depend upon the feed-membrane combination (Hughes and Field, 2006).

4.6 Conclusions

- The application of a combination of strong alkaline solutions containing oxidizing agent (mainly sodium hypochlorite) followed by acid was found to be appropriate for cleaning of the ceramic membrane previously fouled extensively by dextran.

- The rate of change of foulant resistance with TMP is greater for dextran solutions than CMC solutions indicating that the foulant layer of dextran is more compressible and becomes irreversible allowing less permeate to pass through. For dextran, a typical gradient is 2.5×10^{13} m^{-1} per bar and does not change with TMP. For CMC, the gradient increases above 0.5 bar but never exceeds 2.0×10^{13} m^{-1} per bar. Below 0.5 bar, it is 1.0×10^{13} m^{-1} per bar.

- The intermittent rinsing improved filtration efficiency at each step for both solutions of CMC and dextran (up to 47.3 % and 34.2 % in CMC and dextran solutions respectively). Rinsing intermittently with cold water followed by the hot one (40°C) removed the reversible fouling quite effectively (up to 71.8 % and 74.9 % respectively for CMC while for dextran, it was up to 39.7 % and 45.7 % likewise).

- A modulus (K_{av}) was introduced; this factor relates reversible fouling resistance with concentration. Although the value of the K_{av} itself depends upon transmembrane pressure, it is interesting to note that at each value of TMP, five of the six dependencies of the effect of concentration were of the form $C^{0.3}$. However, at the TMP of 0.2 bar (in comparison with the other five TMPs of 0.4, 0.6, 0.8, 1.0 and 1.2 bar), the effect of the concentration change was not of the same form. A semi-theoretical justification for this dependency was given.

5

Fouling in osmotically driven and in pressure driven membranes

5.1 Introduction

The main objective of this experimental study is to have a systematic insightful and comparative analysis of fouling behaviour and of fouling reversibility in osmotically and pressure driven membrane processes, focussing on the factors which affect the fouling behaviour and their extent. The structuring of the fouling cake is of primary importance. How closely the foulant molecules are fitted together on the membrane surface constitutes the fouling arrangement. The role of internal and external concentration polarisation (CP) is very vital in fouling. Unlike in reverse osmosis, internal CP is a unique characteristic of forward osmosis operations (Porter, 1972, Sablani et al., 2001, McCutcheon and Elimelech, 2006, Gray et al., 2006).

For a fair comparison, the experiments were operated on a rig which could operate both FO and RO processes. Along with the application of similar hydrodynamic conditions and feed water chemistries, the membrane cell used during the experiments and the size of the membrane coupon was also the same. This test gives a clear path for the analysis of underlying mechanisms of fouling behaviour and the factors promoting its severity. For each experiment in this chapter, the membrane orientation was set to ALFS.

Section 5.3 covers the main experiments that used alginate as a foulant. This is proceeded by a record of the experiments with silica as foulant. Cleaning is the integral part of the study with a continuation from the previous chapter particularly in connection with removal of reversible fouling. Two types of foulants, incompressible and compressible, were selected for the tests as silica and alginate respectively. A number of researchers used these foulants previously for membrane filtration experiments (Den and Wang, 2008, Mi and Elimelech, 2008, Mi and Elimelech, 2013, Tow and Lienhard V, 2017).

5.2 Experiments with silica as the foulant

In the starting phase, experiments were performed using colloidal silica (Sigma-Aldrich), formula weight 60.08 g/mol, particle size of 50 nm to 200 nm and surface area of 140 m^2/g (information by supplier), as the foulant in the quantity of 2 g per litre of deionised water. The purpose of the tests was to analyse the fouling behaviour with an incompressible foulant. The variation of flux with time was analysed for different modes and experimental conditions.

5.2.1 Forward osmosis experiments with thin film composite membrane

Flux variation was noted for experiments with silica, using thin film composite membrane for analysing the fouling behaviour. Feed solution (comprising of 45 mM NaCl + 5 mM $CaCl_2$) in a quantity of 5 L with 2g/L with silica as foulant (provided by Sigma-Aldrich) was used. On the draw side, there was a solution of 3 M NaCl. The crossflow velocity of the feed solution was set at 7.4 cm/s, while at the draw side it was 20.4 cm/s. At the draw side, identical diamond spacers were fixed in the channel. The presence of spacers was to reduce the effect of external concentration polarisation and to improve the membrane support. However, at the feed side, no spacer was placed, in order to have fair analysis of

fouling layers. At both feed and draw sides, dosing pumps were installed to keep the concentrations at both sides constant. The function and working of both dosing pumps was

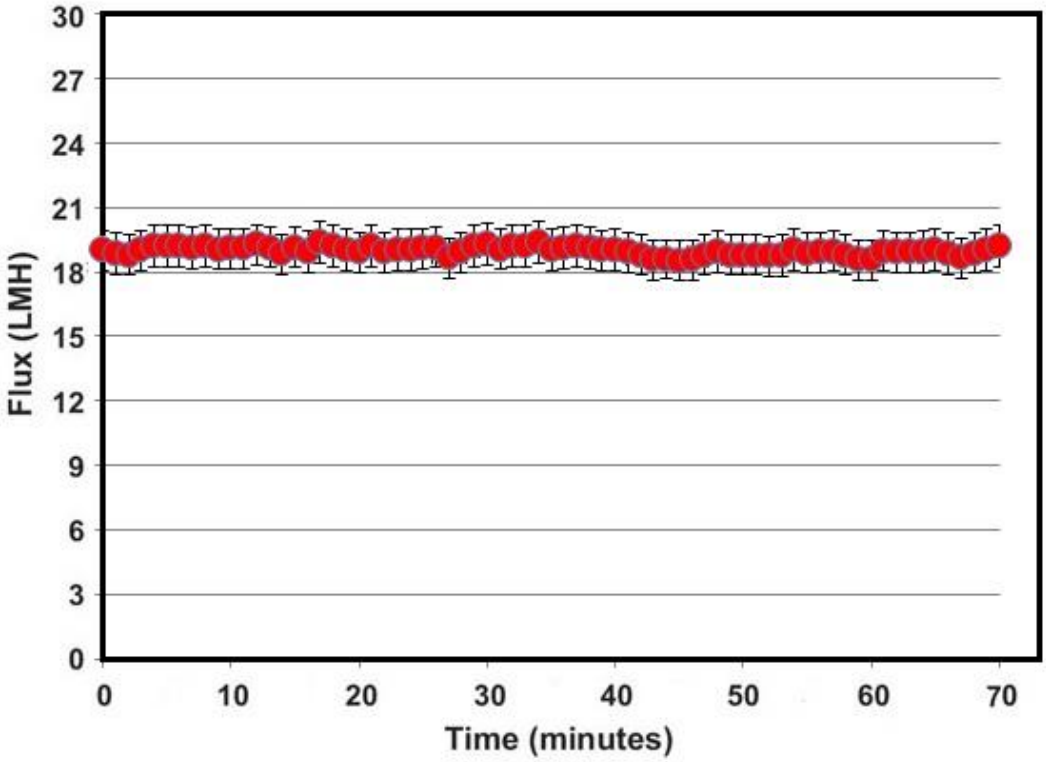

Figure 5.1: Variation in flux with time using TFC membrane for forward osmosis baseline experiment (ALFS orientation) with feed solution (45 mM NaCl solution + 5 mM $CaCl_2$) and draw solution of 3 M NaCl. Crossflow velocity of draw solution: 14.9 cm/s. Crossflow velocity of feed solution: 7.4 cm/s.

explained in section 3.2.2.2 in detail. After a baseline test for about 70 minutes (as shown in Figure 5.1), colloidal silica was added to the feed solution in estimated amounts. After adding silica as foulant (2g/L), variation in flux was noted (illustrated in Figure 5.2). It was noted that even after adding silica and running the experiment for about 100 minutes, no fouling was detected, which could be associated with not exceeding the critical flux (Field et al., 1995) of any form. There was no decline in flux and average flux was around 18.3 LMH. Due to the limitations in increasing the concentration of the draw solution from 3 M, the driving force could not be exceeded.

From experiments with cellulose tri acetate and thin film composite membranes, it was noted that in order to attain the fouling condition, an increase in flux up to the point of

criticality was necessary which seemed to be impossible under the set conditions with both membranes; in particular the limitation was with FO mode.

5.2.2 Forward osmosis experiments with Cellulose tri-acetate membrane

The experiments were repeated with standard experimental conditions for 5 L of feed solution with 2 g/L of colloidal silica in a solution of 45 mM NaCl and 5 mM $CaCl_2$. At the draw side, 5 litres of 3 M NaCl solution were used. The crossflow velocity, dosing pump and spacers' description was the same as described in section 5.2.1. After the baseline test of 40 minutes, colloidal silica in calculated amounts was added into the feed solution and mixed gently by the stirrer. The variation in flux with time at the set experimental conditions for a period of one hour is depicted in Figure 5.2.

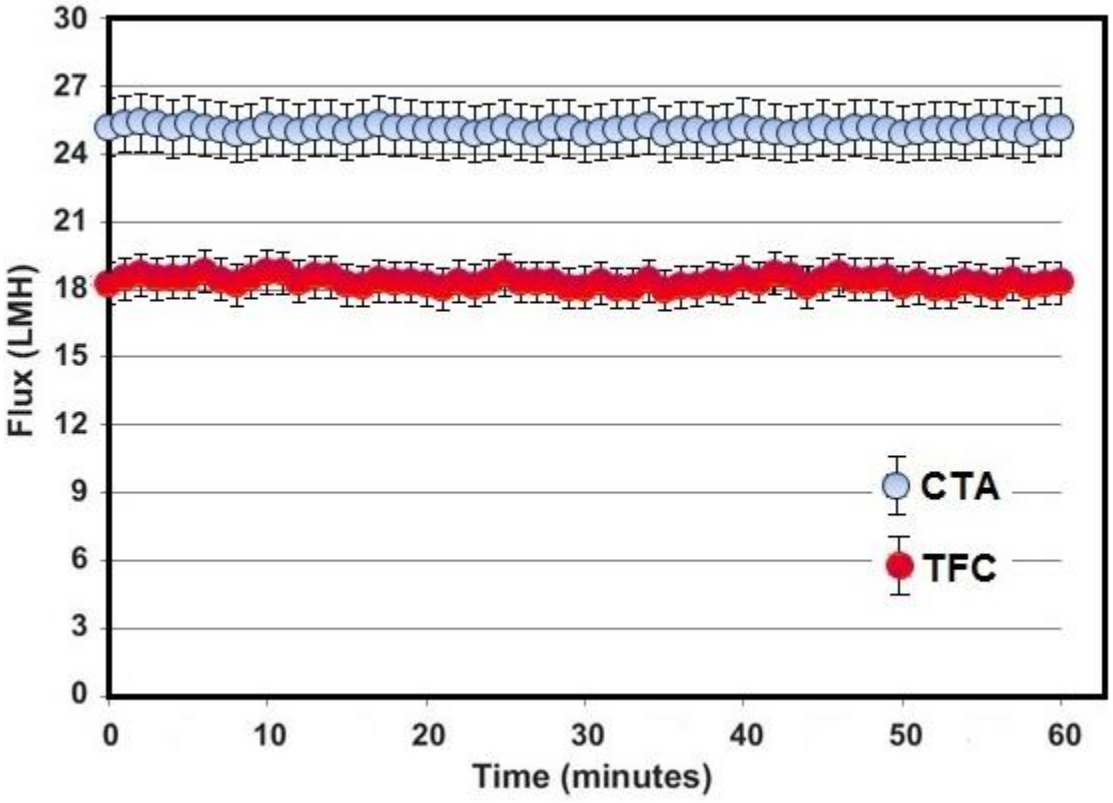

Figure 5.2: Variation in flux with time using CTA and TFC membranes for forward osmosis experiment (ALFS orientation) with feed solution (45 mM NaCl solution + 5 mM $CaCl_2$) with colloidal silica (2g/L) as foulant and draw solution 3 M NaCl. Crossflow velocity of draw solution: 14.9 cm/s. Crossflow velocity of feed solution: 7.4 cm/s.

Figure 5.2 reveals that colloidal silica did not foul the CTA membrane at 25 LMH; there was no decrease in flux, indicating no fouling even after running the experiment for about one hour. This could be related to several explanations. Boo et al. (2012) performed a series of experiments and experienced no fouling with 24 nm commercial silica particles, and attributed this to be associated with the size of the foulant particles. However, the major reason in this regard is failure to attain critical flux; the concept given by Field et al. (1995). The critical flux is that value of flux at given conditions below which decline in flux does not occur, or in other words it is that flux at which fouling starts. The concentration of NaCl in the draw solution could not exceed 3 molar and was kept constant. Moreover, for higher concentrations of draw solution in ALFS orientation, the performance of the permeation is affected badly due to higher internal concentration polarisation.

5.2.3 Forward osmosis experiments at different feed crossflow velocities

The crossflow velocity can have a notable effect in membrane permeation processes. Reversible fouling can be effectively prevented if the feed solution is circulated at a sufficiently high crossflow velocity (Choi et al., 2005). The filtration experiments used silica (2g/L) as a foulant with crossflow velocities on the feed side of 7.4 cm/s or 3.7 cm/s for the layer facing the feed side. Feed solution of quantity 5 L containing 45 mM NaCl + 5 mM $CaCl_2$ 2g/L was used. Draw solution comprising of 3 M NaCl was used, as detailed in Chapter 3, with a crossflow velocity of 14.8 cm/s. The variation in flux with variation in crossflow velocity of the feed solution is depicted in Figure 5.3, which reveals that with increase in crossflow velocity of the feed solution, the flux also increases and vice versa. The same effect was also revealed by Choi et al. (2005) for a series of experiments during ultrafiltration and microfiltration of biological suspension with mixed liquor suspended

solids. They concluded that the higher crossflow velocities result in preventing the reversible fouling.

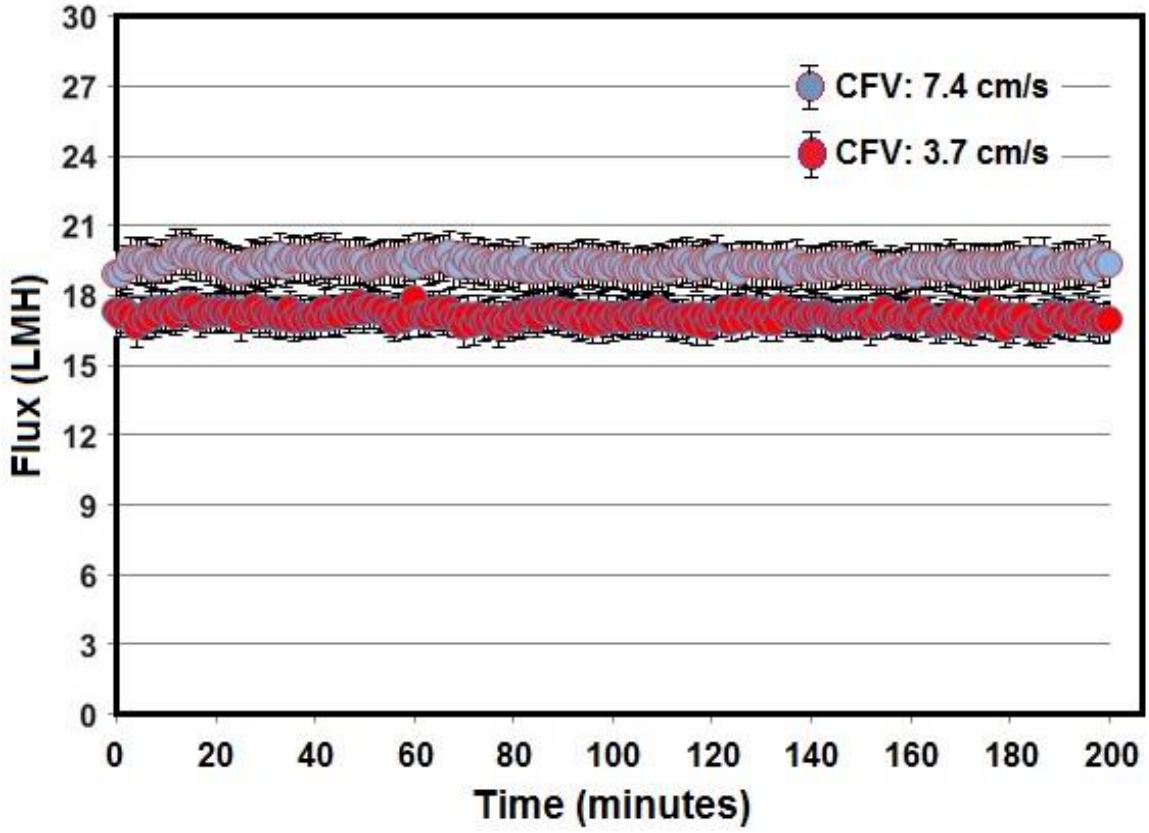

Figure 5.3: Variation in flux with time using TFC membrane for forward osmosis experiment (ALFS orientation) with feed solution (45 mM NaCl solution + 5 mM $CaCl_2$) and draw solution of 3 M NaCl at different feed crossflow velocities with colloidal silica as foulant (2g/L). Crossflow velocity of draw solution: 14.9 cm/s.

The degree of concentration polarisation and the amount of cake formation can be reduced by higher surface shear forces induced by higher crossflow velocities (Tardieu et al., 1999). In the present case of ALFS orientation, the concentrative external concentration polarisation is reduced by higher crossflow velocity and the driving force is increased which results in increase in permeate flux. However, the purpose of change in crossflow velocity of feed was to target the stage of fouling. The stability in flux in Figure 5.3 even after changing the crossflow velocity implies that no fouling occurs such as that due to the build-up of a cake layer. The flux with a feed-side cross flow velocity of 7.4 cm/s is, within experimental error, identical to that of the baseline in Figure 5.1. The reduction in

flux with a reduction in feed-side cross flow velocity to 3.7 cm/s suggests that there might be a flowing cake at this velocity that possesses a modest hydraulic resistance equating to around 10% of the membrane resistance. However, there is no evolution of fouling with time and the investigation of the effect of crossflow velocity was thus not continued. The lower feed side velocity of 3.7 cm/s was used in the experiments on the effect of pH. The purpose of change in pH value of the feed solution was to target change in zeta potential and its effect on magnitude of the electrostatic attraction or repulsion between the foulant particles which could result in targeted fouling. The results are discussed below in section 5.2.4.

5.2.4 Forward osmosis experiments at different pH values of the feed

In seeking to attain fouling with colloidal silica, the membrane was tested with solutions at various pH values with the otherwise identical feed solution as used in section 5.2.1 and 5.2.2. In this regard, the pH value of the feed solution was set at 7.0 in the first instance. In the second phase, the pH value of the solution was increased to 8.5, and finally the pH value of the feed solution was decreased to 4.5. The target was to bring the flux up to the level of criticality in order to attain fouling. In each of the three cases, the orientation of the membrane was set as active layer facing the feed side. The flux variation in each case (being the indication of fouling) was analysed carefully and is explained individually.

5.2.4.1 With pH value of 7.0

The flux was found to be constant throughout the test with an average value around 17.2 LMH, as depicted in Figure 5.4, indicating no fouling build-up and essentially the same as that in Figure 5.3 at the identical flowrates.

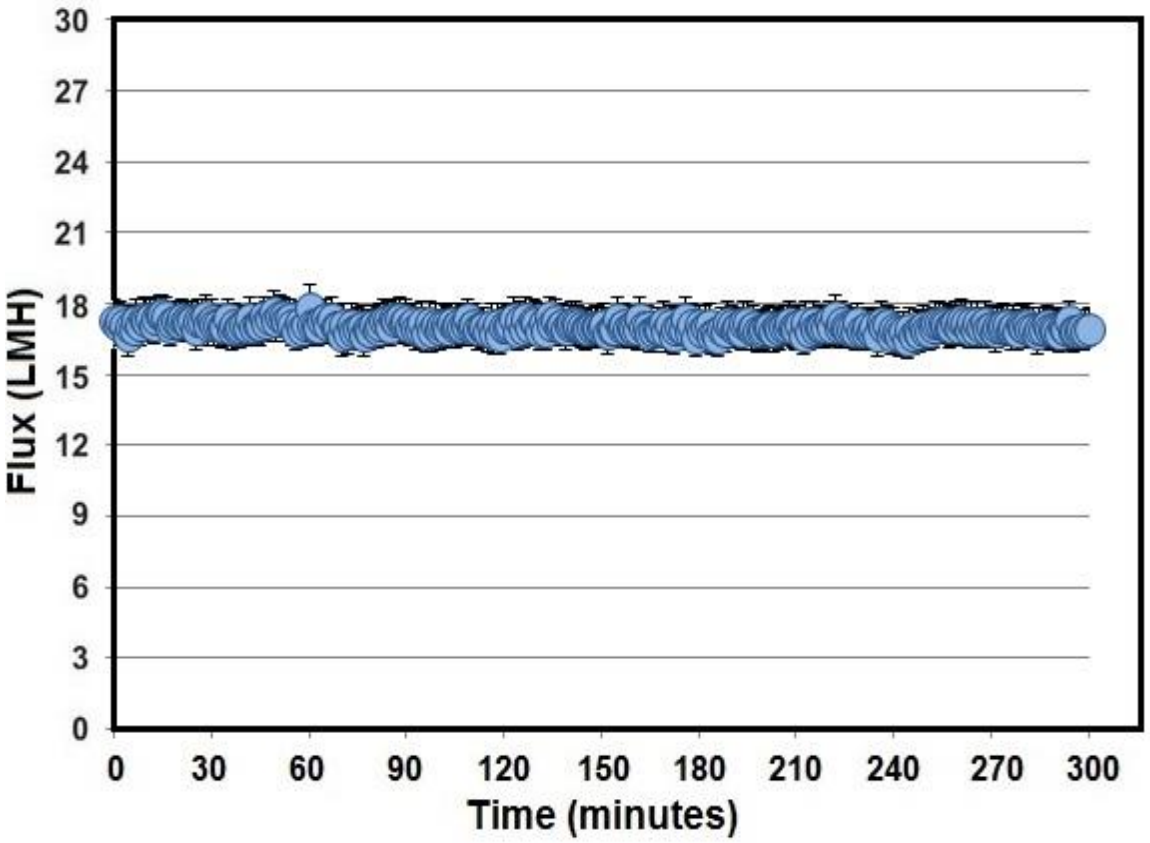

Figure 5.4: Variation in flux with time using TFC membrane for forward osmosis (ALFS orientation) with feed solution (45 mM NaCl + 5 mM $CaCl_2$) with colloidal silica (2g/L) as foulant and draw solution of 3 M NaCl. Crossflow velocity of feed and draw solution set at 3.7 cm/s and 14.9 cm/s respectively. pH value was set at 7.0

5.2.4.2 With pH value of 8.5

The pH value of the feed solution was increased to a value of 8.5 to see if this increase in pH would induce fouling. For increasing the pH value, sodium hydroxide (NaOH) solution was added to the feed solution in a very minute amount. The experiment was run for about 300 minutes under such condition. The variation in flux is given in Figure 5.5. The average flux in this case appears to be around 15.8 LMH, which reveals that upon increasing the pH value of the feed solution the average flux value has decreased, however the flux was still constant which demonstrates that the fouling stage was still not attained.

5.2.4.3 With pH value of 4.5

The pH value of the feed solution was decreased to 4.5 by adding dilute hydrochloric acid (HCl) and the flux trend was analysed. Results are depicted in Figure 5.5. The average flux was noted to be around 14.5 LMH which is about 16 % less than the flux attained with the same feed solution at a pH of 7. The experiments showed that variation of pH value of the feed solution affects the flux at a minor level, and that the flux is almost invariant from the first measurement point. The results are consistent with the hypothesis of a flowing cake whose hydraulic resistance is pH dependent.

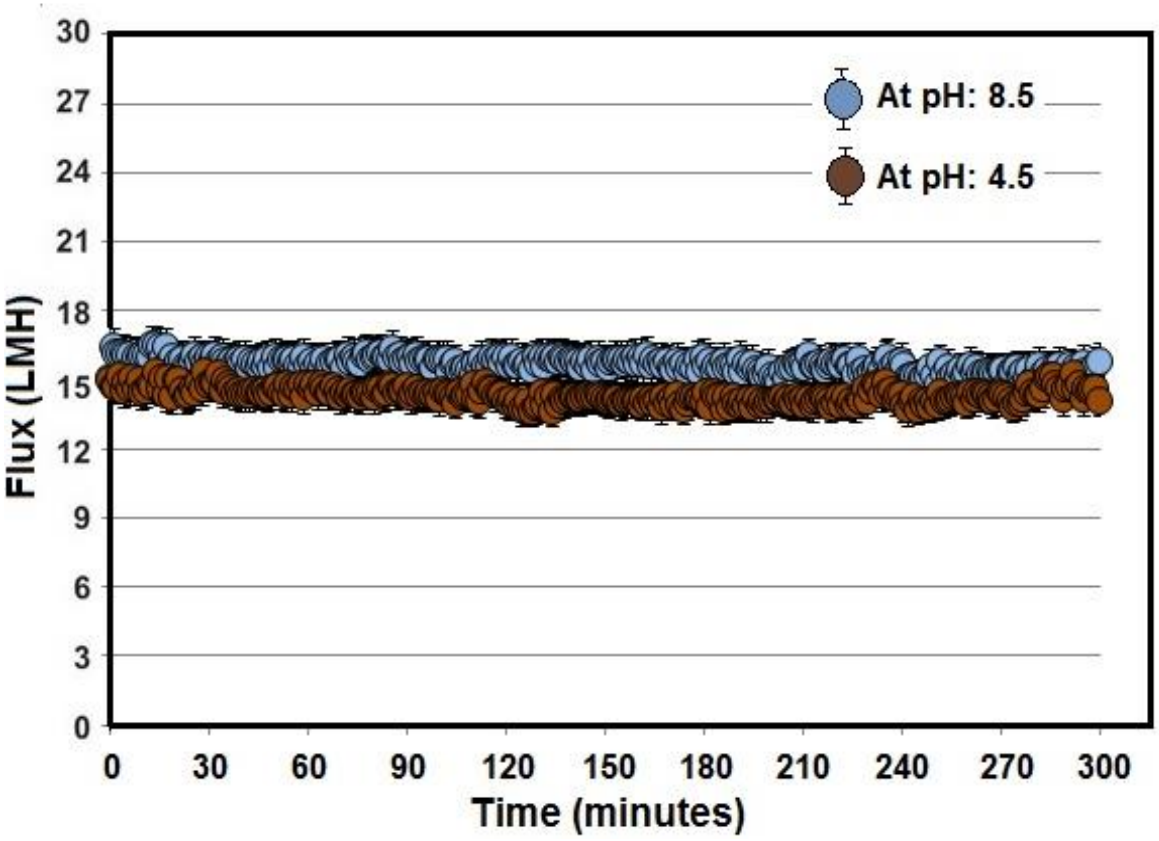

Figure 5.5: Variation in flux with time using TFC membrane for forward osmosis (ALFS orientation) experiment with feed solution (45 mM NaCl + 5 mM $CaCl_2$) with colloidal silica (2g/L) as foulant and draw solution of 3 M NaCl. Crossflow velocity of feed and draw solution set at 3.7 cm/s and 14.9 cm/s respectively. pH value was set at 8.5 and 4.5.

5.2.5 Reverse osmosis experiments with Cellulose tri-acetate membrane

During this phase, filtration experiments were carried out with cellulose tri-acetate membrane in reverse osmosis mode. Experimental conditions were set for 5 L of feed solution with 2 g/L of colloidal silica in a solution of 45 mM NaCl and 5 mM $CaCl_2$. The pressure at the feed side was set at 27.5 bar. After the baseline test of 40 minutes, colloidal silica was added into the feed solution and mixed gently by the stirrer to give (2g/L). The flux variation with time was analysed at the set experimental conditions for 300 minutes, and is illustrated graphically in Figure 5.6. It is notable that at a feed pressure of 27.5 bar, the initial flux was 37.2 LMH. A gradual decrease was noted for the first 30 minutes, after which the flux became smooth reflecting the attainment of pseudo steady-state flux around a value of 30.5 LMH.

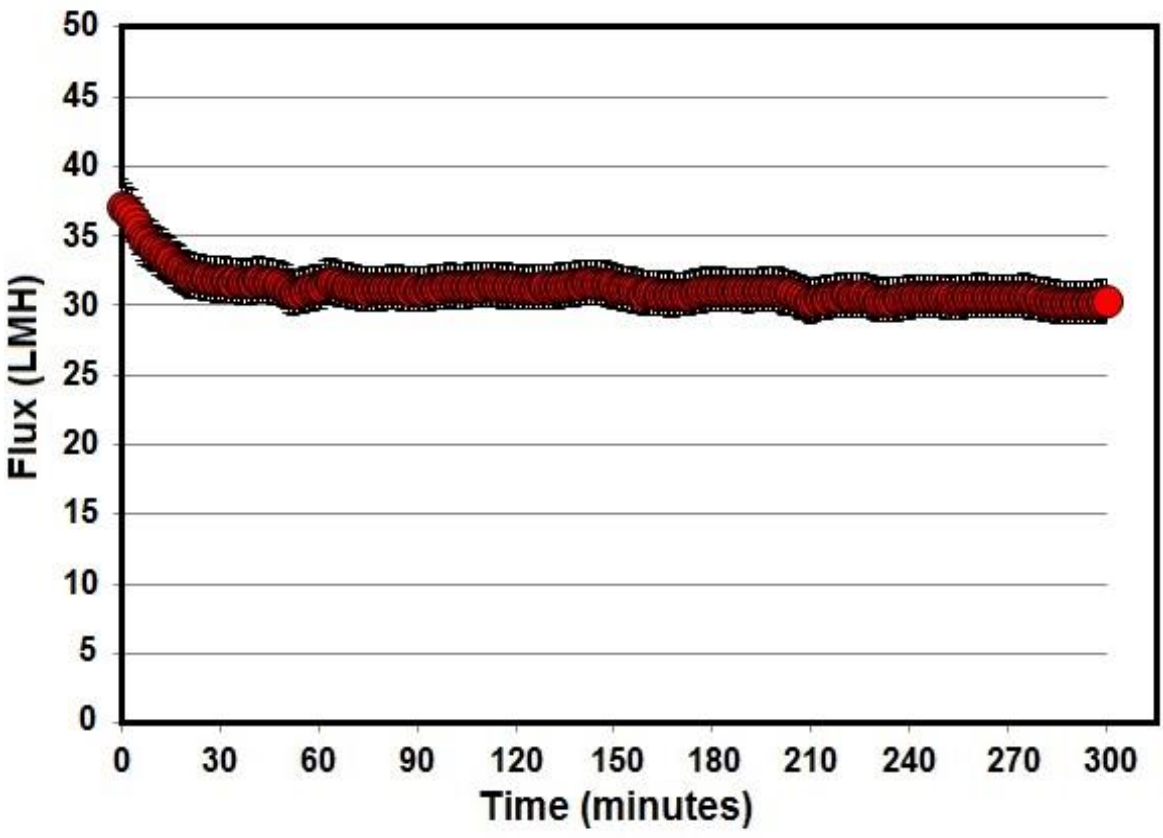

Figure 5.6: Variation in flux with time using CTA membrane for reverse osmosis experiment (ALFS orientation) with feed solution (45 mM NaCl + 5 mM $CaCl_2$) with colloidal silica (2g/L) as foulant and 27.5 bar hydraulic pressure at feed side. Crossflow velocity of feed was set at 7.4 cm/s.

The steady decrease in flux in the first 30 minutes clearly indicates fouling by the colloidal silica on the membrane surface; this could not be attained through forward osmosis experiments even after using techniques for altering the crossflow velocity and changing the pH value of the feed solution. This could be related to not attaining the critical flux (Field et al., 1995) in the FO experiment but exceeding it in the RO experiment.

The maximum flux attained in forward osmosis tests was 25.1 LMH, which did not result in fouling. However, in the reverse osmosis experiment, by increasing the driving force i.e. hydraulic pressure at the feed side, the flux was raised up to 37.2 LMH at which one was able to observe fouling. Consideration was given to selection of a solution other than NaCl which could be used as a stronger draw solution and could bring the flux up to a level of criticality. However, the dosing mechanism was based on conductivity and this excludes glucose. Colloidal silica was replaced with alginate for the later experiments and this foulant was found to have an appropriately lower value of critical flux.

5.3 Experiments with alginate as foulant

After the work with colloidal silica, fouling experiments were performed using the foulant as alginic acid sodium salt from powdered brown algae (alginate), straight-chain with density 1.6 g/cm^3 and molecular weight of 216.12 g/mol by the supplier SIGMA-ALDRICH. The quantity of the foulant used in each test was 200 mg per litre of deionised water. The main purpose of the study was to analyse fouling behaviour in osmotically driven (FO) and pressure driven (RO) membranes, and to have an insightful comparison of both fouling and fouling reversibility. The variation of flux as well as the measurement of foulant resistance as an indication of fouling with time was examined under standard conditions (see section 3.2). The test conditions of the experiments are listed in **Table 5.1**.

Table 5.1: Test conditions for baseline and fouling tests with membrane orientation of active layer facing the feed side. All feed solutions contained 45 mM NaCl+5mM $CaCl_2$ with alginate (200 mg/L) as foulant in fouling tests.

Test No.	Process	Membrane	Driving force	Baseline Test duration	Fouling Test duration	Crossflow velocity of feed solution (cm/s)	Crossflow velocity of draw solution (cm/s)
1	FO	CTA	Draw solution of 2 M NaCl	50 min	1100 min	7.4	11.1
2	FO	CTA	Draw solution of 2 M NaCl	40 min	1000 min	7.4	11.1
3	FO	TFC	Draw solution of 3 M NaCl	50 min	1200 min	7.4	11.1
4	FO	TFC	Draw solution of 3 M NaCl	85 min	1200 min	7.4	11.1
5	FO	TFC	Draw solution of 3 M NaCl	30 min	1450 min	7.4	11.1
6	RO	CTA	19.4 bar hydraulic pressure on feed	70 min	1200 min	7.4	--
7	RO	CTA	18.8 bar hydraulic pressure on feed	30 min	270 min	7.4	--
8	RO	CTA	18.5 bar hydraulic pressure on feed	30 min	270 min	7.4	--
9	RO	CTA	16.5 bar hydraulic pressure on feed	50 min	1050 min	7.4	--
10	RO	TFC	7.0 bar hydraulic pressure on feed	50 min	270 min	7.4	--
11	RO	TFC	7.1 bar hydraulic pressure on feed	30 min	270 min	7.4	--
12	RO	TFC	7.3 bar hydraulic pressure on feed	50 min	1200 min	7.4	--

5.3.1 Comparison of FO and RO separation performance

Separation performance for forward and reverse osmosis in terms of water flux is compared in this section. For both FO and RO tests, the apparent driving force (i.e., the applied hydraulic pressure 'ΔP' in RO and the osmotic pressure difference between the bulk DS and the bulk FS '$\Delta\pi$' in FO) was maintained constant.

5.3.1.1 Baseline Tests

The baseline tests, as shown in Figure 5.7 (a) and Figure 5.7 (b), without adding foulant in the feed solution, were performed before fouling tests. The results show that baseline fluxes for both FO and RO were almost constant. Therefore, the flux decline during the fouling tests was solely due to the addition of foulant on the feed side.

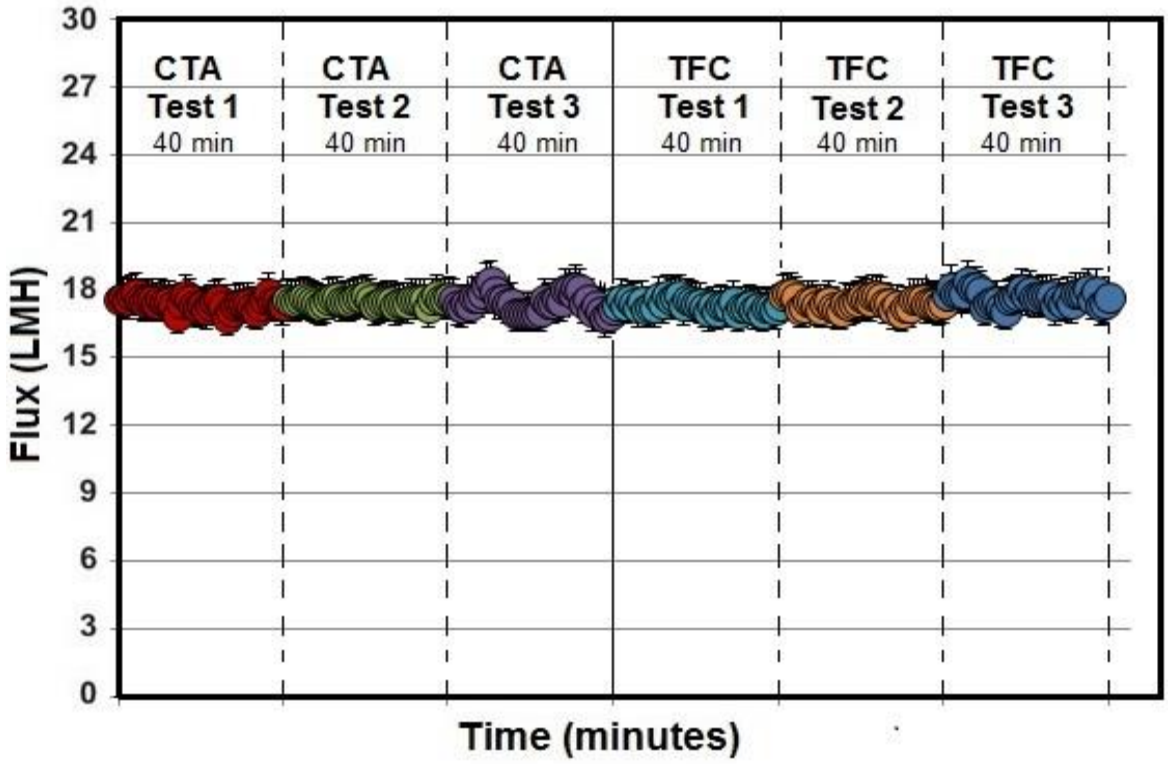

Figure 5.7: **(a)** Flux variation with time in **baseline experiments for forward osmosis** with CTA and TFC membranes (ALFS orientation) with feed solution (45 mM NaCl + 5 mM $CaCl_2$). Crossflow velocity of feed solution 7.4 cm/s of draw solution 11.1 cm/s. Draw solution concentration for CTA and TFC membranes was NaCl solution with concentrations of 2 M and 3 M respectively.

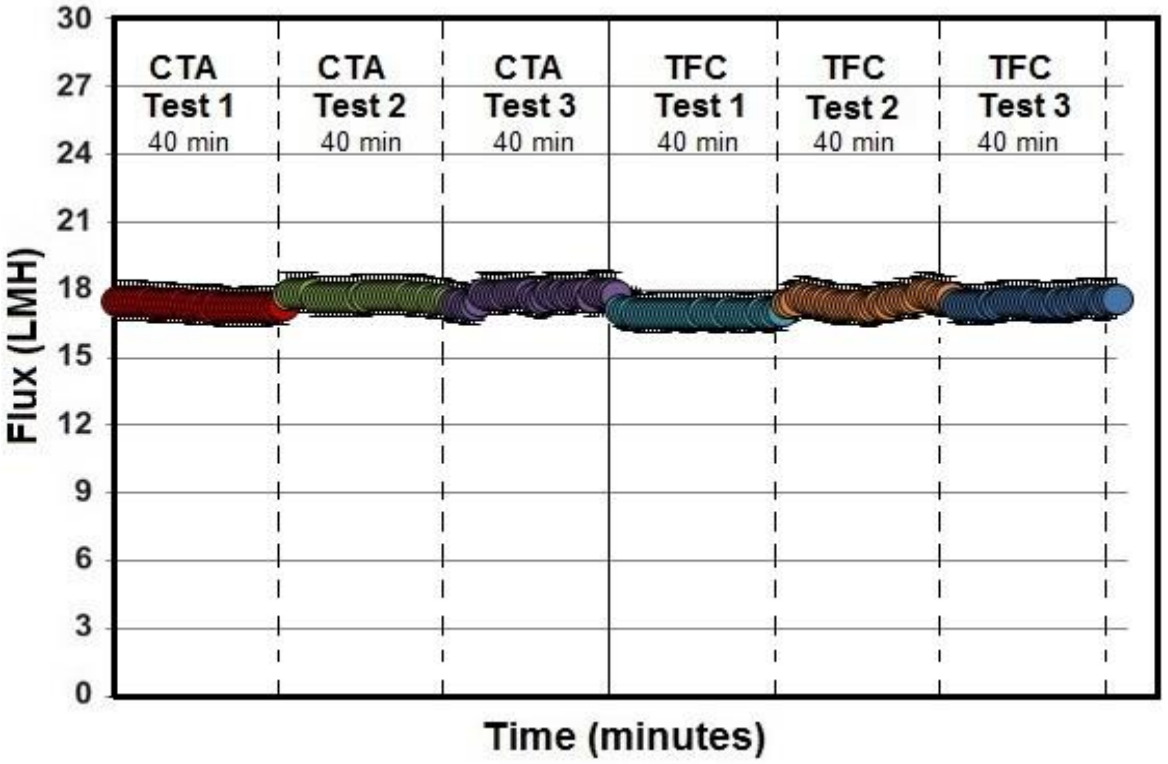

Figure 5.7: **(b)** Flux variation with time in **baseline experiments for** r**everse osmosis** with CTA and TFC membranes (ALFS orientation) with feed solution (45 mM NaCl + 5 mM $CaCl_2$). Crossflow velocity of feed solution 7.4 cm/s. Hydraulic pressure on feed for CTA and TFC membranes was 17.6 bar and 7.5 bar respectively.

5.3.1.2 Fouling Tests

Figures 5.8 (a – d) show the water flux behaviour during FO and RO fouling tests and flux restoration after membrane cleaning using CTA and TFC membranes. A few more repeated experimental results are shown in Appendix-II. Both FO and RO were operated at the same initial flux of ~18 LMH. As shown in Figure 5.8 a (with CTA membrane), the water flux decline due to membrane fouling in both FO and RO followed a similar trend. The flux decline was more pronounced in the first 8 hours and tended to be much milder later. At the end of 16 hours, the water flux had declined by ~50% for RO and around 30% for FO. Similar observations were also reported previously (Xie et al., 2015, Mi and Elimelech, 2013, Mi and Elimelech, 2010b). This indicates that FO does not always have superior separation performance (i.e. separation of foulants) or filtration efficiency in terms of flux during alginate filtration compared to RO. However, in Figure 5.8 b (with TFC membrane), RO experiment shows more flux decline from the beginning. After the physical cleaning, water fluxes for both FO and RO were recovered significantly (Figure 5.8 (c – d). The recovery was almost 100 % for both CTA and TFC membranes. Repeated results are revealed in **Appendix-II**. In RO, the flux recovery with CTA membrane is greater (95.2%) than that with TFC (83.8%). This observation is not different from that reported in previous studies (Xie et al., 2015, Mi and Elimelech, 2010a, Mi and Elimelech, 2010b, Kim et al., 2014b). The results indicate that FO and RO could have nearly similar water flux behaviour during fouling test and water flux reversibility after physical cleaning. However, only comparing water flux performance could not essentially demonstrate which process is more prone to membrane fouling. On the other hand, the foulant resistance (R_f) is a typical indicator to quantify the extent of membrane fouling. A greater R_f indicates a great degree of membrane fouling (whether it is more severe depends upon the degree of reversibility.) The subsequent sections will provide an in-depth analysis

of membrane fouling in both FO and RO modes of operation via the comparison of R_f in both membrane processes.

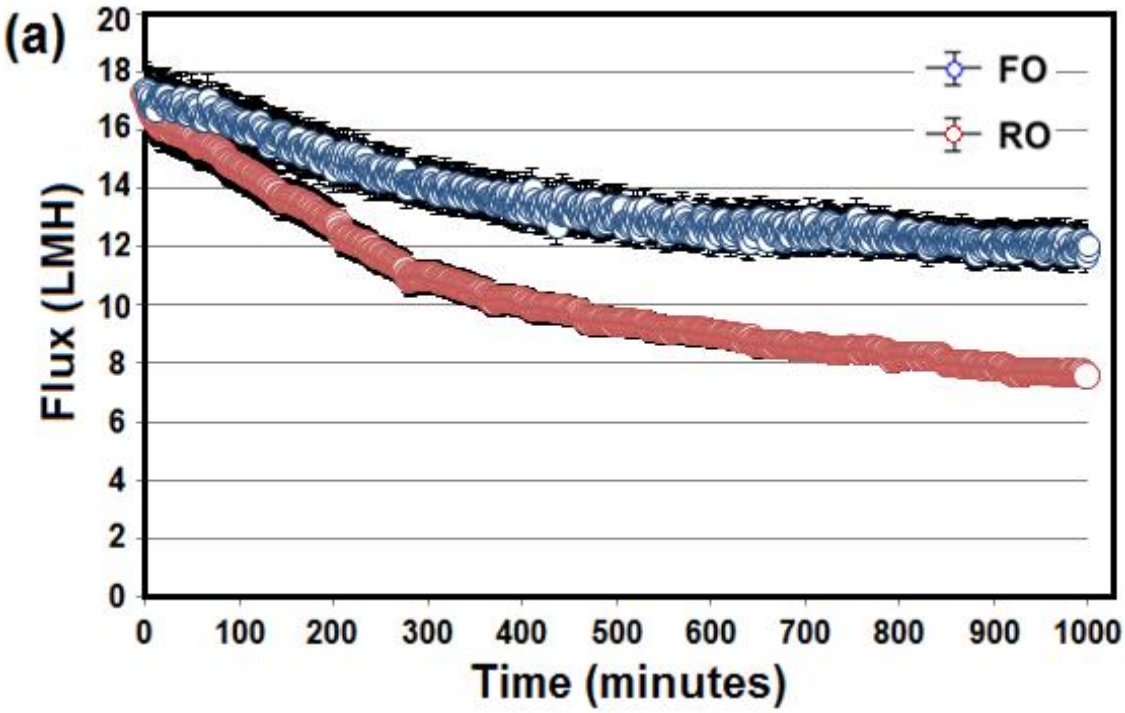

Figure 5.8: (a) Comparison of FO and RO performance during membrane fouling using **CTA membrane** for forward and reverse osmosis experiments (ALFS orientation) with feed solution (45 mM NaCl + 5 mM $CaCl_2$) with alginate (200 mg/L) as foulant for variation in water flux with time

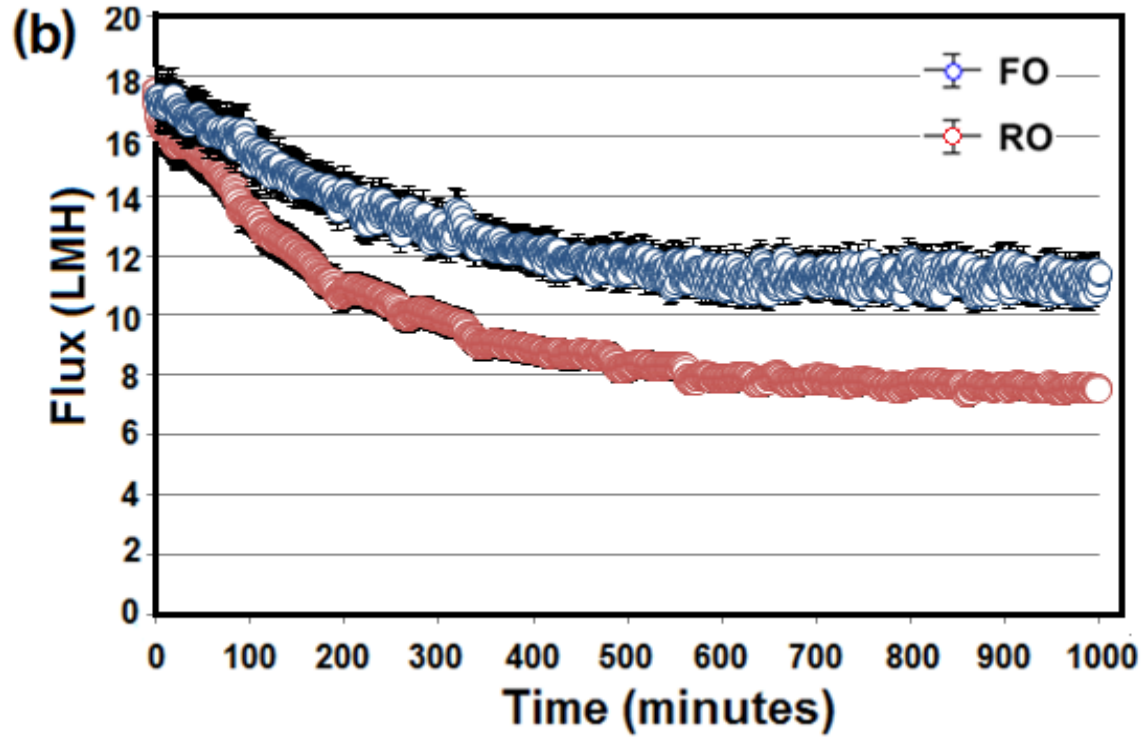

Figure 5.8: (b) Comparison of FO and RO performance during membrane fouling using **TFC membrane** for forward and reverse osmosis experiments (ALFS orientation) with feed solution (45 mM NaCl + 5 mM $CaCl_2$) with alginate (200 mg/L) as foulant for variation in water flux with time

Figure 5.8: continued…

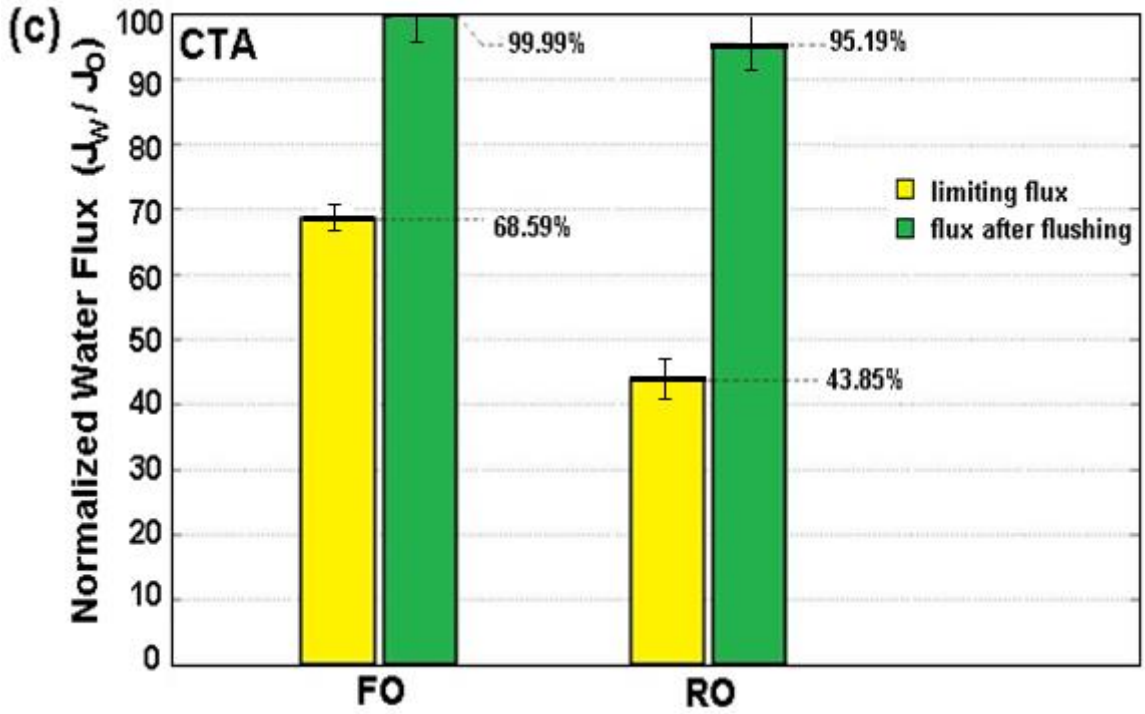

Figure 5.8: (c) Comparison of FO and RO performance during membrane fouling using **CTA membrane** for forward and reverse osmosis experiments (ALFS orientation) with feed solution (45 mM NaCl + 5 mM $CaCl_2$) with alginate (200 mg/L) as foulant for water flux recovery after membrane cleaning

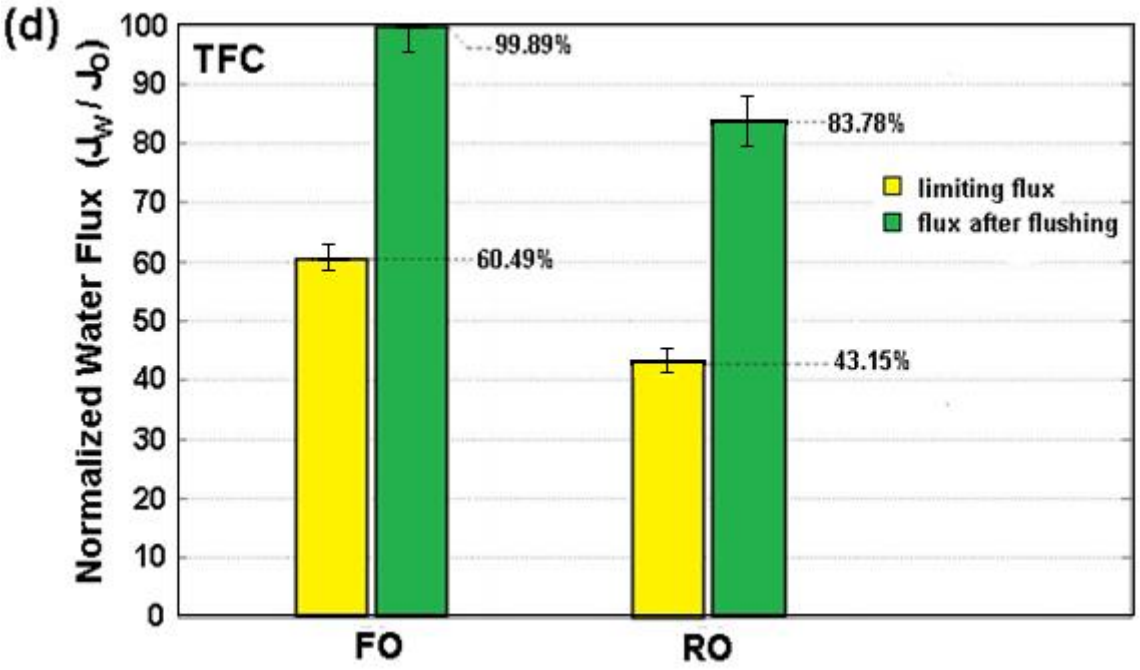

Figure 5.8: (d) Comparison of FO and RO performance during membrane fouling using **TFC membrane** for forward and reverse osmosis experiments (ALFS orientation) with feed solution (45 mM NaCl + 5 mM $CaCl_2$) with alginate (200 mg/L) as foulant for water flux recovery after membrane cleaning

In the FO test with CTA membrane, the draw solution (DS) was 2 M NaCl i.e. equivalent to 99.1 bar by Van't Hoff's equation (Nobel, 1969); in RO test applied hydraulic pressure on feed solution was 17.7 bar. For TFC membrane tests, the draw solution (DS) was 3 M (equivalent to 148.6 bar) and applied hydraulic pressure in RO was 7.6 bar. Other fouling experimental conditions: feed solution (FS) contained 200 mg/L alginate, 45 mM NaCl and 5 mM $CaCl_2$; no spacer was placed in FS flow channel, and a diamond spacer was placed in DS flow channel; cross-flow velocity in FS flow channel was 7.4 cm/s and that in DS flow channel was 11.1 cm/s. During membrane cleaning, feed solution was replaced with deionised water and cross-flow velocity was increased to 29.6 cm/s. The cleaning session was run for 30 minutes. Further details are given in Chapter 3.

5.3.1.3 Membrane separation properties and structural parameters

The separation and structural properties of CTA and TFC membranes are discussed in **Table 5.2 (a)** and **Table 5.2 (b)**. The values calculated from the experiments include J_{lim} / J_w where J_{lim} is the flux at the end of an experiment and J_w is the flux at the beginning.

Table 5.2 (a): Summary of performance of CTA and TFC membranes

Membrane	Process	Initial Flux	Limiting Flux	%age reference to initial Flux	Flux recovered after flushing	%age reference to initial Flux
		J_w (LMH)	J_{lim} (LMH)	$J_{lim} / J_w * 100$	$J_{recovered}$ (LMH)	$J_{recovered} / J_w * 100$
CTA	FO	17.5	10.2	58.3 %	17.48	99.9 %
CTA	RO	17.4	7.6	43.7 %	16.56	95.19 %
TFC	FO	17.6	11.4	64.8 %	17.58	99.89 %
TFC	RO	17.5	7.5	42.8 %	14.66	83.78 %

Table 5.2 (b): Structural properties of CTA and TFC membranes

List of Rm, S and A value for CTA and TFC membranes by FO and RO						
Membrane	Membrane resistance (R_m)	Structural parameter (S)	Water permeability (A value)			
			By RO	By FO	By RO	By FO
	m^{-1}	mm	m/s Pa	m/s Pa	LMH/bar	LMH/bar
CTA	3.93×10^{14}	0.498	2.83×10^{-12}	2.62×10^{-12}	1.02	0.943
TFC	1.14×10^{14}	0.937	9.75×10^{-12}	3.65×10^{-12}	3.51	1.316

5.3.2 Analysis of membrane fouling in FO and RO

5.3.2.1 Comparison of water flux behaviour between FO and RO at the same extent of fouling

Many fouling studies on the comparison of FO and RO are based on the evaluation of water flux decline. However, assessing the extent of membrane fouling only based on water flux decline may be misleading, since water flux is related to both driving force and membrane hydraulic resistance (the sum of clean membrane resistance and foulant resistance). In this section, the water flux in forward osmosis and reverse osmosis are compared with respect to the change of foulant resistance.

Figure 5.9 shows the simulated water flux as a function of foulant resistance (R_f) in FO and RO based on the osmotic resistance model (Equation 2.18). It is assumed that membrane fouling only leads to an increase of R_f (or the decrease in $A_{fouling}$ value) while other membrane parameters (i.e. S value) are unchanged. The values are mentioned in Table 5.2(b).

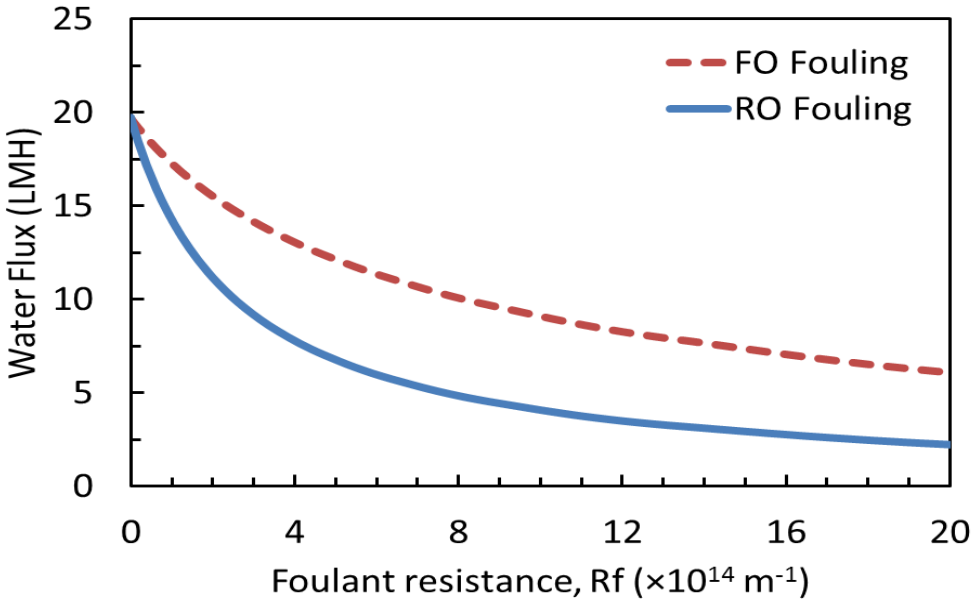

Figure 5.9: Simulated water flux in FO and RO as a function of foulant resistance based on the osmotic-resistance filtration model for CTA membrane

The initial water flux is maintained the same when there is no fouling (i.e. $R_f = 0$). With the progress of membrane fouling (i.e., increase of R_f or decrease of A), water flux in both FO and RO decreases. However, water flux in FO is always greater than that in RO after the membrane has suffered the same extent of fouling (i.e., at a fixed R_f when $R_f > 0$). This indicates that FO has superior water flux performance compared to RO during membrane fouling. This can be attributed to the ICP self-compensation effect that is uniquely found in FO. A decrease of water flux due to fouling leads to a reduction in ICP and thus an increase in effective osmotic driving force. Therefore, water fluxes in FO were found to be higher than those in RO. Figure 5.9 also shows that, at a fixed water flux, R_f for FO is always greater than that for RO. Combining Figure 5.8, the results in Figure 5.9 imply that membrane fouling in FO should be much greater than that in RO. This has been further demonstrated in Figure 5.10 which gives a comparison of foulant resistance for forward and reverse osmosis experiments for both CTA and TFC membranes and a comparison of their respective resistances after membrane physical cleaning via water flushing.

5.3.2.2 Comparison of foulant resistance between forward and reverse osmosis

The R_m for the clean membrane was estimated using the following osmotic-resistance filtration (ORF) model for RO that was reported elsewhere (She et al., 2013) and can be simplified from the universal ORF model for osmotically driven membrane processes (ODMPs) (She et al., 2016) and in APENDIX-III.

$$J_w = \frac{\Delta P - \eta_{rej}\pi_{fs} exp\left(\frac{J_w}{k_{ecp}}\right)}{\mu R_m} \quad (5.1)$$

where ΔP is the effective applied hydraulic pressure, η_{rej} is the solute rejection that was determined based on conductivity measurement of permeate and feed water, π_{fs} is the osmotic pressure of the feed solution (that can be correlated by the van't Hoff equation

$\pi = C\beta R_g T$ where C is concentration, β is vant Hoff coefficient, R_g is gas constant and T is temperature), J_w is the water flux, k_{cecp} is the mass transfer coefficient near the membrane surface, and μ is the viscosity of the feed solution. Note that external concentration polarisation (ECP) has been incorporated in Equation (5.1). In an open flow channel k_{cecp} can be estimated following the approach reported elsewhere (Hoek et al., 2002). In Equation (5.1) the membrane resistance R_m is correlated with the water permeability coefficient (*A*) by $A = 1/\mu R_m$. The structural parameter (*S*) of the FO membrane was determined by inputting π_{ds} and π_{fs}, and the experimentally obtained parameters (i.e. J_w, J_s/J_w, R_m) into the following equation that is rearranged from the ORF model (She et al., 2016).

$$S = \frac{D}{J_w} \ln \left[\frac{\pi_{ds} + \frac{J_s}{J_w} \beta R_g T}{\left(\pi_{fs} + \frac{J_s}{J_w} \beta R_g T\right) exp\left(\frac{J_w}{k_{ecp}}\right) + \mu R_m J_w} \right] \quad (5.2)$$

The value of k_{ecp} was the same value as that estimated for RO because the membrane cell for the FO tests and RO tests had the same feed-side flow channel.

The foulant resistance (R_f) on the RO fouled membrane was determined by inputtingπ_{fs}, ΔP, and the experimentally obtained $J_{w,f}$, $\eta_{rej,f}$ into Equation (5.3). Allowance was made for the cake-enhanced concentration polarisation (CECP)

$$J_{w,f} = \frac{\Delta P - \eta_{rej} \pi_{fs} exp\left(\frac{J_{w,f}}{k_{ecp,f}}\right)}{\mu (R_m + R_f)} \quad (5.3)$$

where $J_{w,f}$ is the fouling water flux, $\eta_{rej,f}$ is the membrane rejection during the RO fouling test, and $k_{ecp,f}$ is the overall mass transfer coefficient across the foulant layer and external concentration polarisation boundary layer. As shown by Equation (5.4) the overall coefficient is dependent on both the external concentration polarisation (ECP) and cake-

enhanced concentration polarisation at the feed side. Thus $k_{ecp,f}$ consists of two terms, one is related to the mass transfer within the foulant layer on the membrane (k_{ecp,f^*}) and the other to the ECP boundary layer above the foulant layer ($k_{ecp,0}$).

$$\frac{1}{k_{ecp,f}} = \frac{1}{k_{ecp,o}} + \frac{1}{k_{ecp,f*}} = \frac{\delta}{D} + \frac{S_f}{D} = \frac{\overline{S_f}}{D} \tag{5.4}$$

where δ is the boundary layer thickness adjacent to the foulant layer and it can be estimated from k_{ecp} for an empty channel (Hoek et al., 2002); S_f is the structural parameter of the foulant layer that has an analogous definition to the membrane structural parameter (Tow and Lienhard V, 2016); $\overline{S_f}$ is the sum of δ and S_f and is defined as the overall effective thickness of the CP boundary layer that incorporates both CECP within the foulant cake layer and the external CP adjacent to the foulant layer. A reasonable range of $\overline{S_f}$ was assumed and sensitivity analysis was performed for the calculation of R_f. Numerator of Equation (5.3) represents the effective driving force for RO during fouling test and was recorded during calculation. The R_f on the FO fouled membrane was calculated (Equation 2.18) using π_{ds}, π_{fs}, and the experimentally obtained parameters ($J_{w,f}$, $J_{s,f}/J_{w,f}$, R_m and S) based on the ORF model given below (She et al., 2016):

$$J_{w,f} = \frac{(\pi_D - \pi_F) - \Delta P - F_{dcp,f}\left(\pi_D + \frac{J_{s,f}}{J_{w,f}} \beta R_g T\right) - F_{ecp,f}\left(\pi_F + \frac{J_{s,f}}{J_{w,f}} \beta R_g T\right)}{\mu (R_m + R_f)} \tag{5.5}$$

where, the external concentration polarisation (ECP) factor, $F_{ecp,f}$, at the feed side and dilutive concentration polarisation (DCP) factor, F_{dcp}, at the draw side are expressed by Equation (5.6) and Equation (5.7), respectively.

$$F_{ecp,f} = exp\left(\frac{J_{w,f}}{k_{ecp,f}}\right) - 1 \tag{5.6}$$

$$F_{dcp} = 1 - exp\left(-\frac{J_{w,f}}{k_{dcp}}\right) = 1 - exp\left(-\frac{J_{w,f}}{D/S}\right) \tag{5.7}$$

Equation (5.5) incorporates the effect of reverse solute diffusion (i.e., J_s/J_w), internal concentration polarisation (included in F_{dcp}), and cake-enhanced concentration polarisation (included in $F_{ecp,f}$). $k_{ecp,f}$ in Equation (5.5) was determined by Equation (5.4) following similar approaches for RO. The numerator of Equation (5.5) represents the effective driving force for FO during the fouling test. The effect of different scenarios of $k_{ecp,f}$ on the calculated R_f and effective driving forces for FO and RO fouled membranes will be evaluated and compared. ORF models show that the mass transfer limitation for RO (Equation (5.3)) only lies on the feed side but for FO (Equation (5.5)) it lies on both the feed and draw sides which concurs with an earlier analysis (Field and Wu, 2013). As shown later ICP (or k_{dcp}) at the draw side plays a significant role in determining the differences between FO and RO fouling behaviours.

Figures 5.10 (a)–(d) show the foulant resistance (R_f) during FO and RO fouling for CTA and TFC membranes. Foulant resistance (R_f) is calculated via the osmotic-resistance filtration model using the experimental water flux from Figure 5.8, the specific reverse solute flux (J_s/J_w) from Figure 5.16 for FO, and rejection from Figure 5.17 for RO.

Interestingly, although water fluxes in both FO and RO followed almost the same trend, the foulant resistance (R_f) for FO was increasingly greater than that for RO with the progress of fouling. At the end of 1000 mins tests, R_f for FO was remarkably greater than that for RO indicating that FO is much more prone to fouling than RO. This is also consistent with the theoretical analysis of the water flux in Figure 5.9. That the fouling in FO is more reversible in comparison to that in RO is consistent with the findings of previous studies (Xie et al., 2015, Mi and Elimelech, 2013, Mi and Elimelech, 2010b, Kim et al., 2014b).

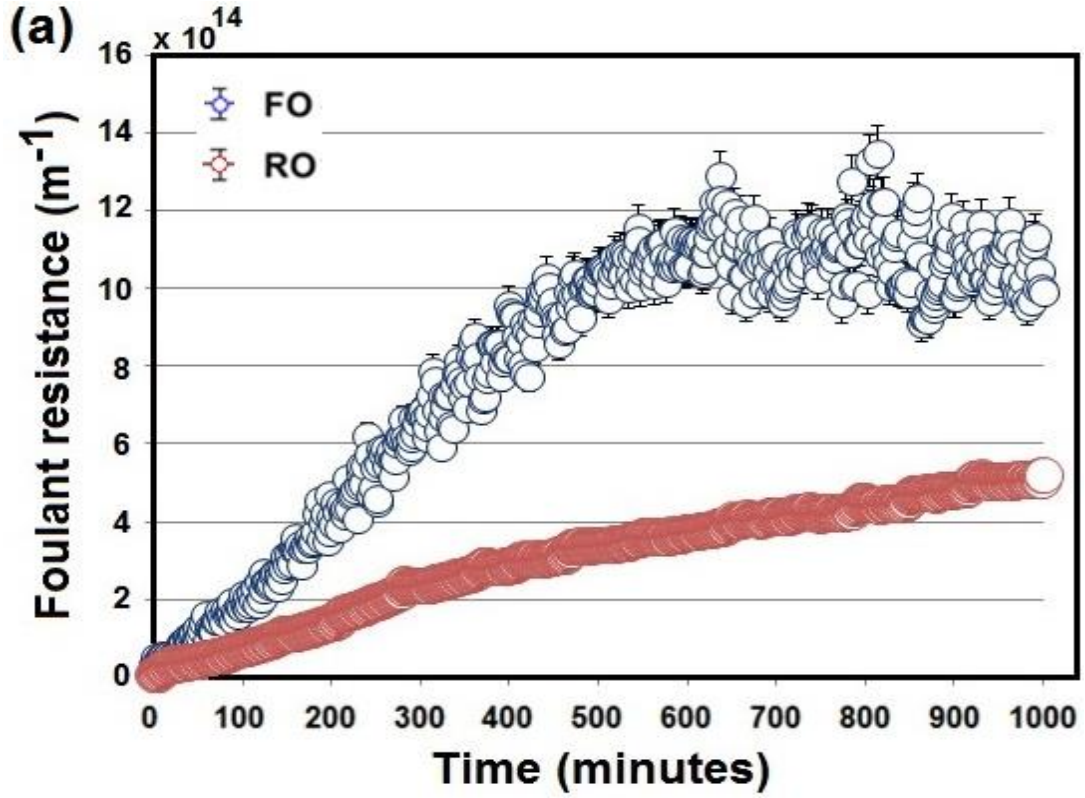

Figure 5.10: **(a)** Comparison of foulant resistance for FO and RO experiments using CTA membrane (ALFS orientation) with feed solution (45 mM NaCl + 5 mM $CaCl_2$) with alginate (200 mg/L) as foulant. Driving force as 2 M NaCl draw solution in FO and a hydraulic pressure of 19.4 bar on feed solution in RO

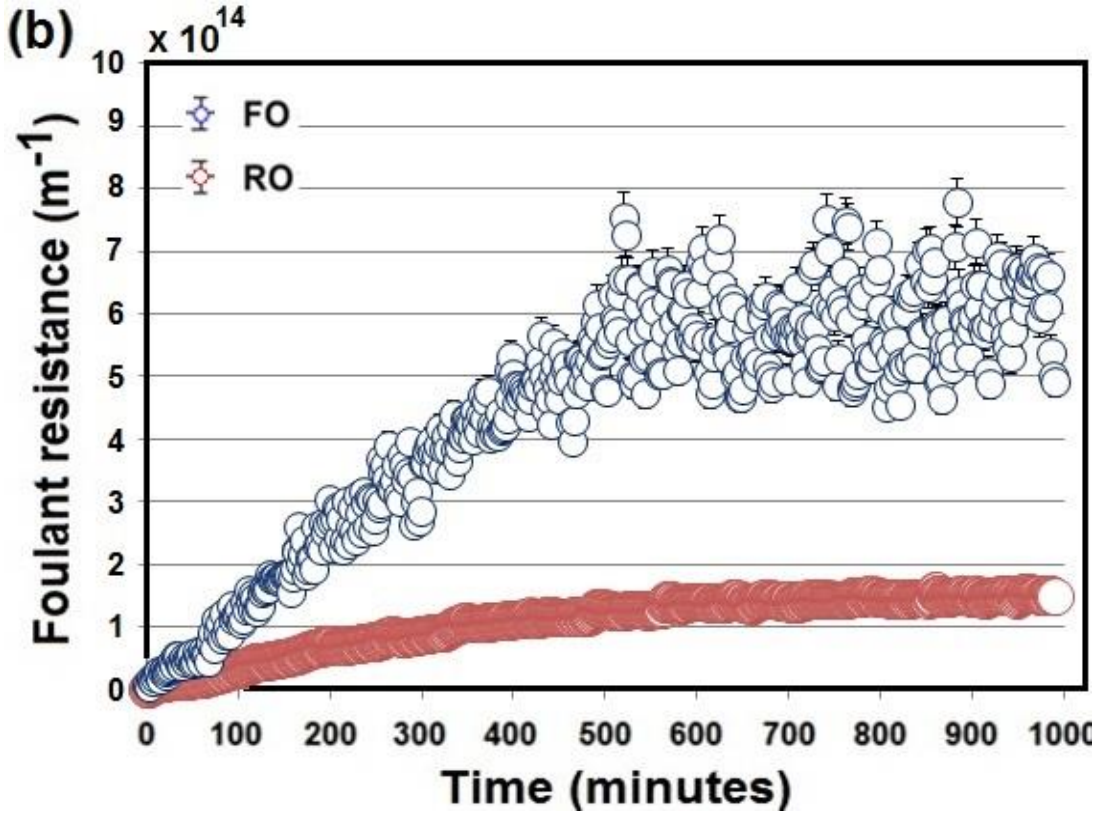

Figure 5.10: **(b)** Comparison of foulant resistance for FO and RO experiments using TFC membrane (ALFS orientation) with feed solution (45 mM NaCl + 5 mM $CaCl_2$) with alginate (200 mg/L) as foulant. Driving force as 3 M NaCl draw solution in FO and a hydraulic pressure of 7.3 bar on feed solution in RO

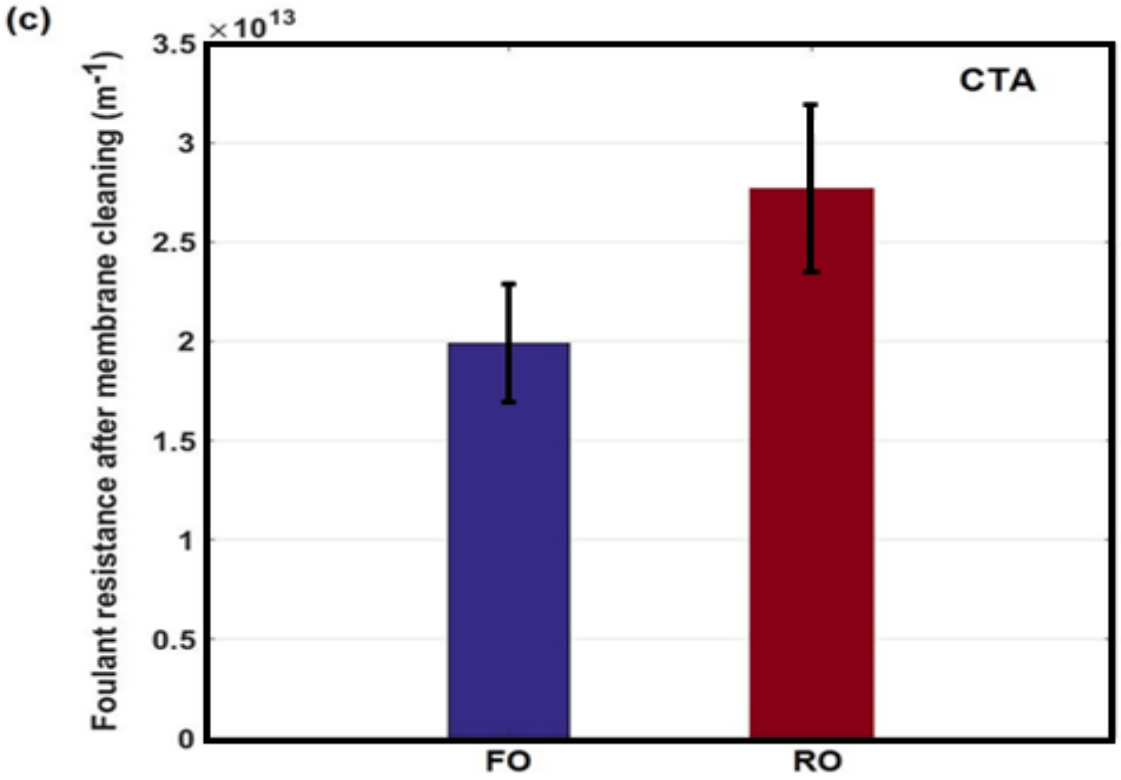

Figure 5.10: **(c)** Comparison of foulant resistance R_f after membrane cleaning in forward and reverse osmosis experiments (ALFS orientation) using CTA membrane as demonstrated in Figure 5.10 (a).

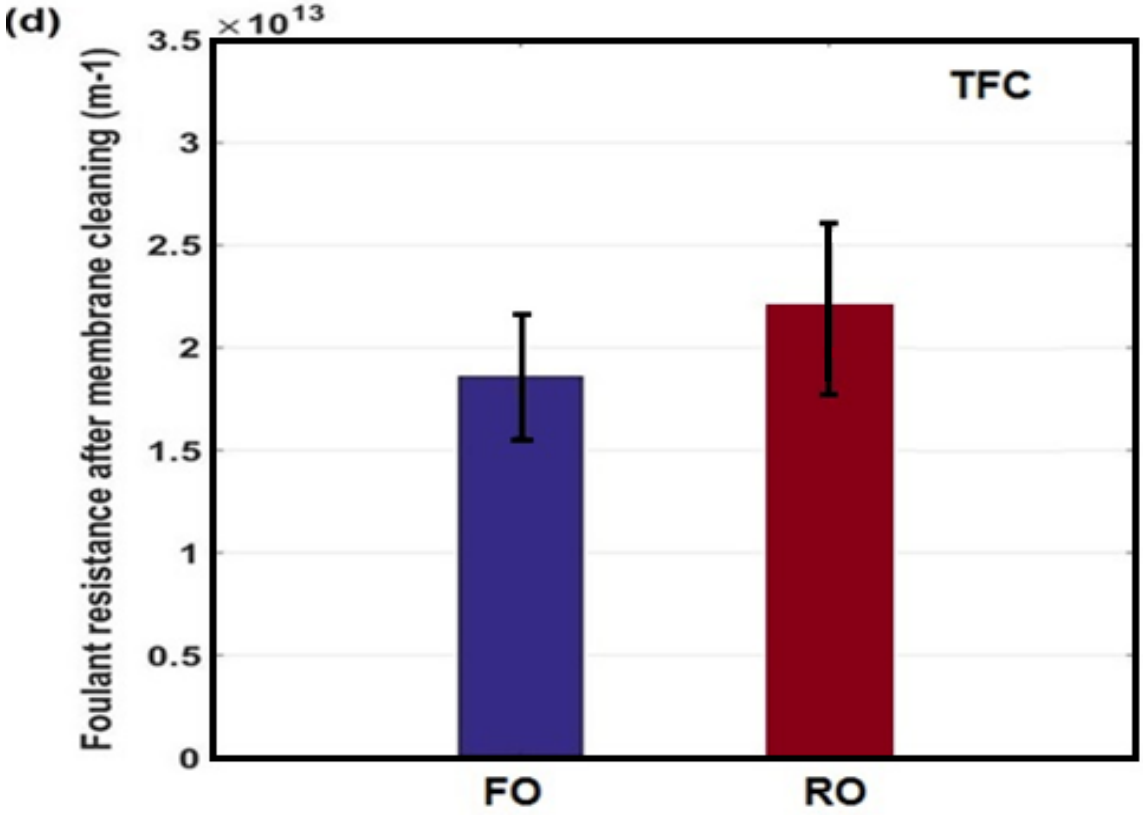

Figure 5.10: **(d)** Comparison of foulant resistance R_f after membrane cleaning in forward and reverse osmosis experiments (ALFS orientation) using TFC membrane as demonstrated in Figure 5.10 (b)

After membrane cleaning, it was noted that the foulant resistance R_f for RO was greater than that for FO as depicted in Figure 5.10(c) and Figure 5.10(d) with unidentical flux recoveries as well. However, assuming the flux recovery to be identical in both cases, more interestingly, the foulant resistance in FO could be greater than that in RO. This analogy has been explained through a simulated analysis later in section 5.3.2.8.

The foulant deposition density (m_f) was determined via a measurement of total organic carbon (TOC) as explained later in section 5.3.4. The findings are shown in Figure 5.11 (a) which depicts that at the end of fouling tests the amount of alginate depositing on the CTA and TFC membrane surface for FO was more than one and a half times greater than that for RO. Moreover, the specific foulant resistance (R_f/m_f) as shown in Figure 5.11 (b) indicates that the unit amount of alginate depositing on the membrane for FO caused greater hydraulic resistance than that for RO.

That greater values of both m_f and R_f/m_f were observed for FO is contradictory to previous studies in which fouling is associated with the compaction of the layer and hydraulic pressure (Xie et al., 2015, Mi and Elimelech, 2013, Mi and Elimelech, 2010b, Kim et al., 2014b). Whilst there is, for the FO mode, a greater resistance (see Figure 5.10) which, in addition, also arising from a greater amount of deposition on the foulant layer. Thus experiments specifically designed to investigate the effect of hydraulic pressure on the compaction of the foulant layer were undertaken which has been discussed in detail in section 5.3.2.4.

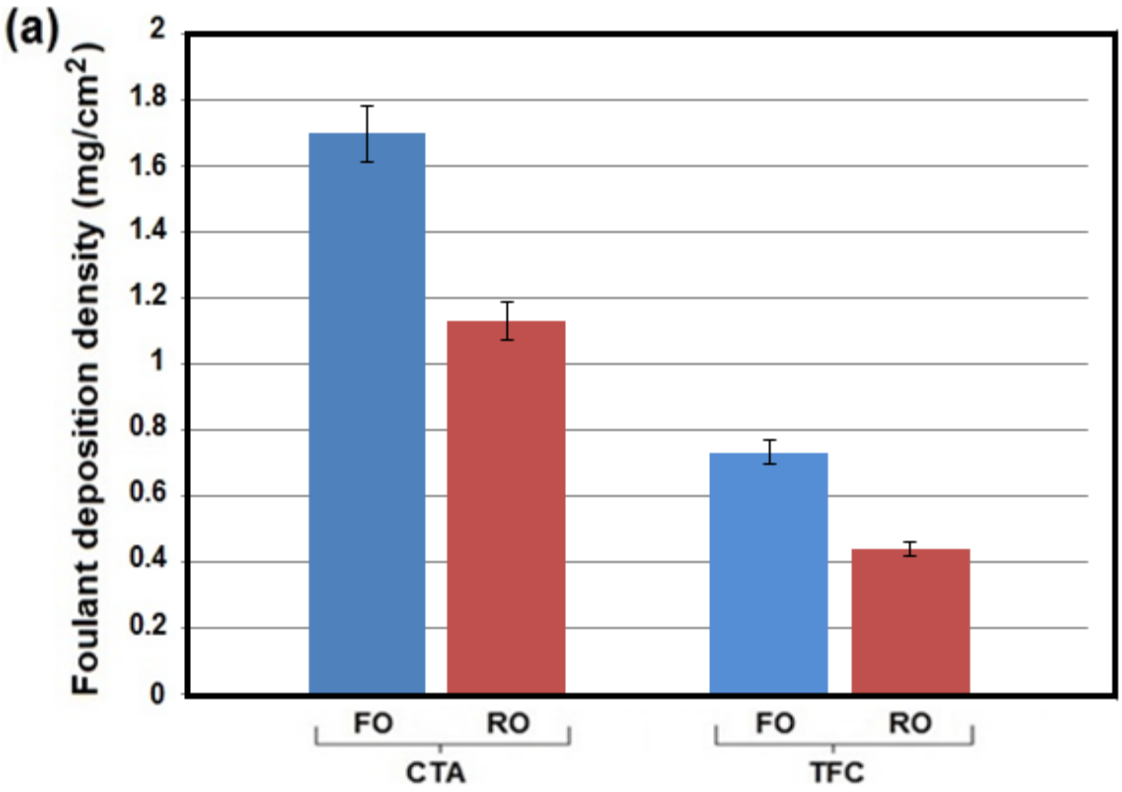

Figure 5.11: **(a)** Comparative analysis of **Foulant deposition density, m_f** for forward and reverse osmosis experiments (ALFS orientation) for CTA and TFC membrane using alginate (200mg/L) as foulant in feed solution of 45 mM Nacl+5mM of $CaCl_2$ with application of suitable driving force in each case.

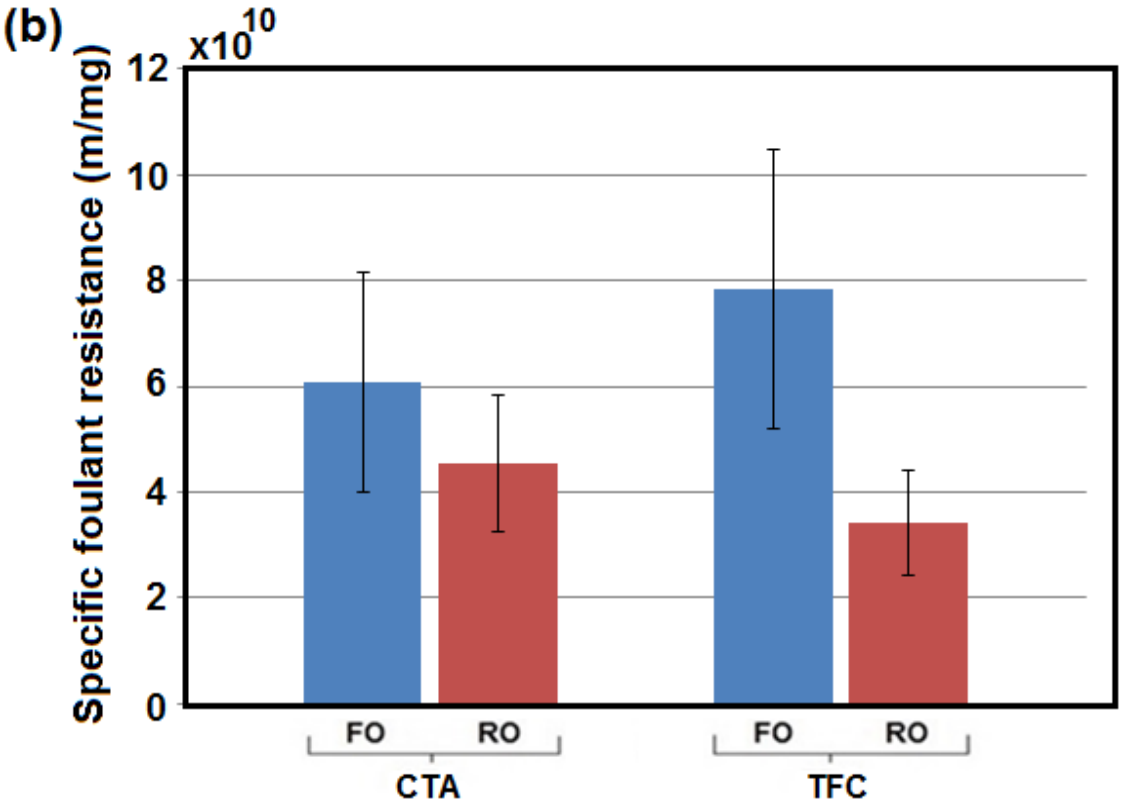

Figure 5.11: (b) Comparative analysis of **Specific foulant resistance** for forward and reverse osmosis experiments (ALFS orientation) for CTA and TFC membrane using alginate (200mg/L) as foulant in feed solution of 45 mM Nacl+5mM of $CaCl_2$ with application of suitable driving force in each case.

5.3.2.3 Comparison of water permeability during fouling tests in FO and RO

From knowledge of the permeation rate and the calculated driving force across the membrane, which increased for FO mode by itself, the water permeability through the fouled CTA and TFC membranes was calculated (Figure 5.12 (a) and 5.12 (b)). It is notable that the water permeability of TFC membranes during the fouling test is higher than that in CTA membranes due to structural properties of the membranes. Analysing CTA membrane, the variation in permeability with time for FO and RO remained closer; that the permeability of RO remains higher than that of FO reflects the fact that FO is fouled to a greater extent. For TFC membrane, the permeability during RO tests was higher than in FO tests by a large amount, reflecting the greater foulant resistance (R_f) in FO than that in RO.

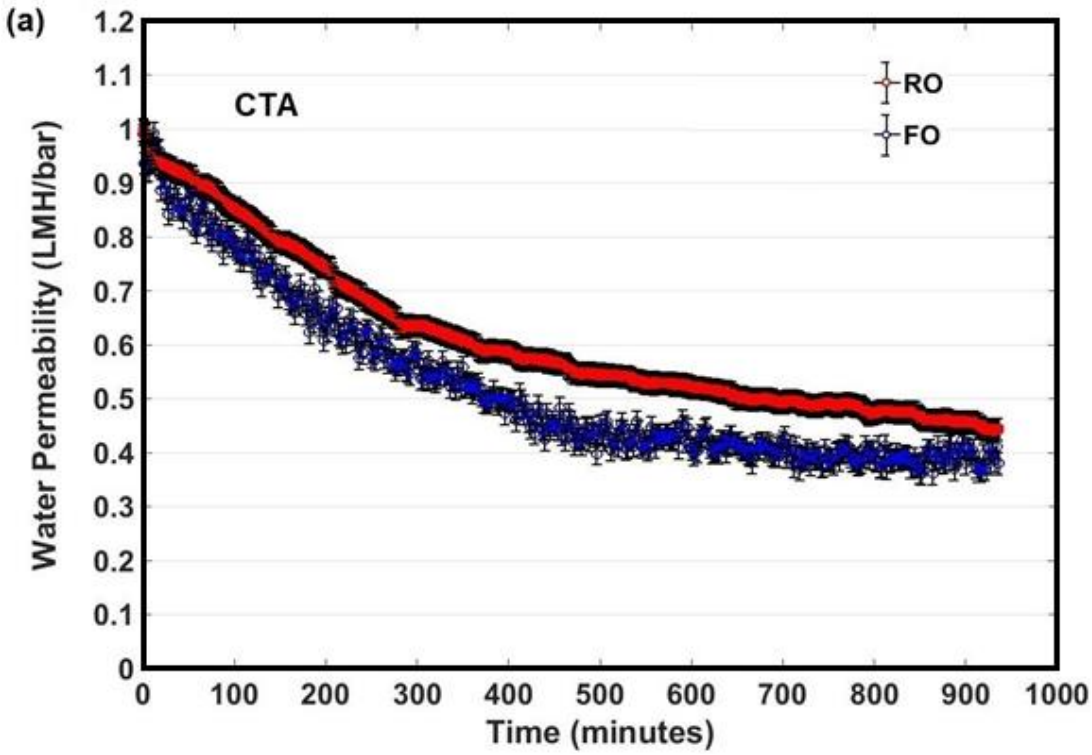

Figure 5.12: **(a)** Water permeability with time during the fouling test for forward osmosis and reverse osmosis experiments (ALFS orientation) using **CTA membrane**. The feed solution (45 mM NaCl + 5 mM $CaCl_2$) with crossflow velocity 7.4 cm/s and alginate (200 mg/L) as foulant was used. The draw solutions for CTA and TFC FO tests were NaCl solution of concentration 2 M and 3 M respectively. The hydraulic pressure for CTA and TFC RO tests was 19.4 bar and 7.3 bar respectively.

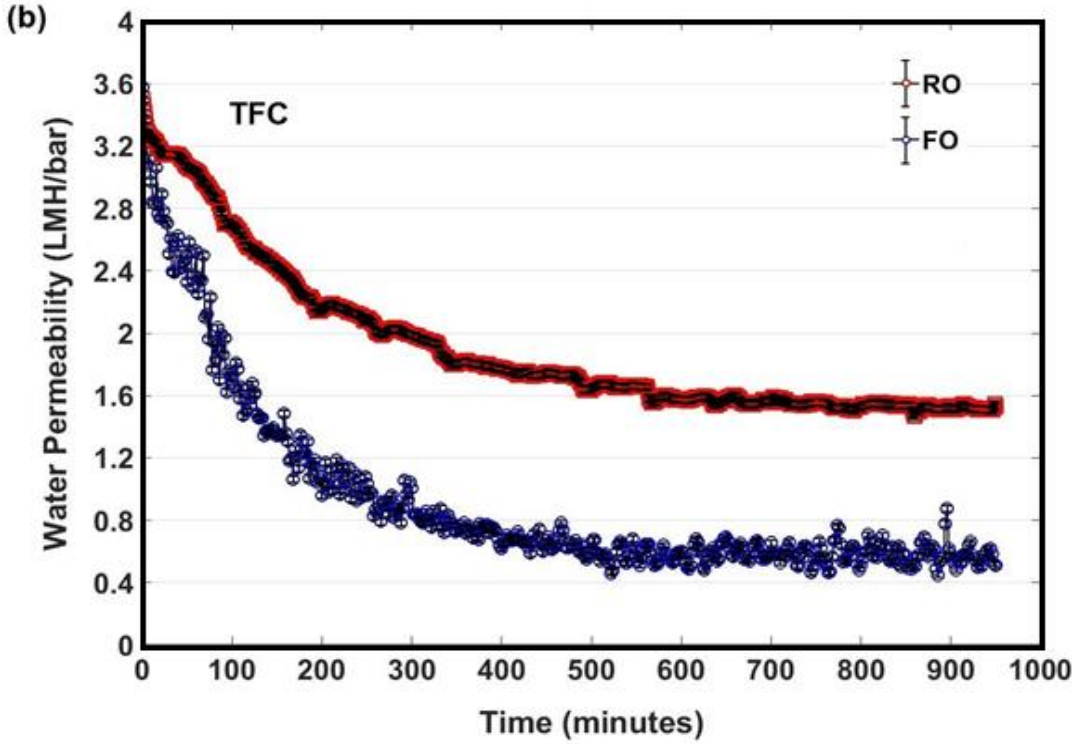

Figure 5.12: **(b)** Water permeability with time during the fouling test for forward osmosis and reverse osmosis experiments (ALFS orientation) using **TFC membrane**. The feed solution (45 mM NaCl + 5 mM $CaCl_2$) with crossflow velocity 7.4 cm/s and alginate (200 mg/L) as foulant was used. The draw solutions for CTA and TFC FO tests were NaCl solution of concentration 2 M and 3 M respectively. The hydraulic pressure for CTA and TFC RO tests was 19.4 bar and 7.3 bar respectively.

5.3.2.4 Effect of hydraulic pressure on the compression of foulant layer

In the forward osmosis process, the compression of the foulant layer on the membrane surface is solely caused by the hydrodynamic drag force due to water permeation. In the pressure-driven RO process, many studies reported that not only the hydrodynamic drag force but also the hydraulic pressure compresses the foulant layer (Xie et al., 2015, Mi and Elimelech, 2013, Mi and Elimelech, 2010b, Kim et al., 2014b, Lee et al., 2010b). Xie et al. (2015) suggested that the hydraulic pressure may play a critical role in foulant compaction, and eventually leads to an irreversible fouling layer with operation in RO mode.

In order to demonstrate whether the hydraulic pressure is important in the compression of the foulant layer, a number of RO fouling experiments (indicated in Figure 5.13 (a) as stage 1) were further performed with the CTA membrane. The permeate valve was closed

once the foulant layer was formed on the membrane (indicated in Figure 5.13 (a) as stage 2). This created a situation of no permeation in which only the hydraulic pressure was "compressing" the foulant layer. As shown in Figure 5.13 (b), the water flux had declined over 30% in the initial 4-hour fouling test during which a foulant layer had formed on the membrane. Then the permeate valve was closed for 4 hours whilst maintaining the feed hydraulic pressure (~17.6 bar) and crossflow. No data is shown for stage 2 in Figure 5.13 (b) for this period because there was no permeate collection. After the 4-hour hydraulic compaction, the permeate valve was opened again and the permeate water flux was re-measured (indicated in Figure 5.13 (a) as stage 3). Unexpectedly, the results show that the water flux increased significantly rather than maintaining the same or decreasing. A similar experiment was performed under the same conditions except that the hydraulic pressure was elevated to ~27.6 bar in order to see if a greater 'elevated pressure' could play a role in "compressing" the foulant layer. After 4 hours, when the permeate valve was re-opened, it was noted that the water flux still went up to a similar level as previously with the 17.6 bar experiment and was independent of the pressure used to solely "compact" the foulant layer. If there had been compaction during the period of elevated pressure, then the elastic relaxation was rapid. The increased water flux may be due to the removal of the foulant layer by the cross-flow shear force i.e. during the period of no permeation, there is net removal. Such removal would, to a first approximation, be the same but the higher pressure should have led to great compaction if compaction was indeed a factor. The experiments were repeated with the TFC membrane as well with the same pressure application during the closing of valves and the same results were found. The bar chart in Figure 5.13 (c) depicts the percent increase in flux after reopening of permeate valve. Overall, it was concluded that for alginate fouling, there is no evidence of a compaction effect. The findings from the constant-pressure RO operation are in agreement with those recently

reported by Tow and Lienhard V (2017) and earlier by Fane et al. (2009). The former demonstrated that alginate gel compaction by high feed hydraulic pressure does not occur and suggested that other explanations should be sought for FO's fouling resistance relative to RO.

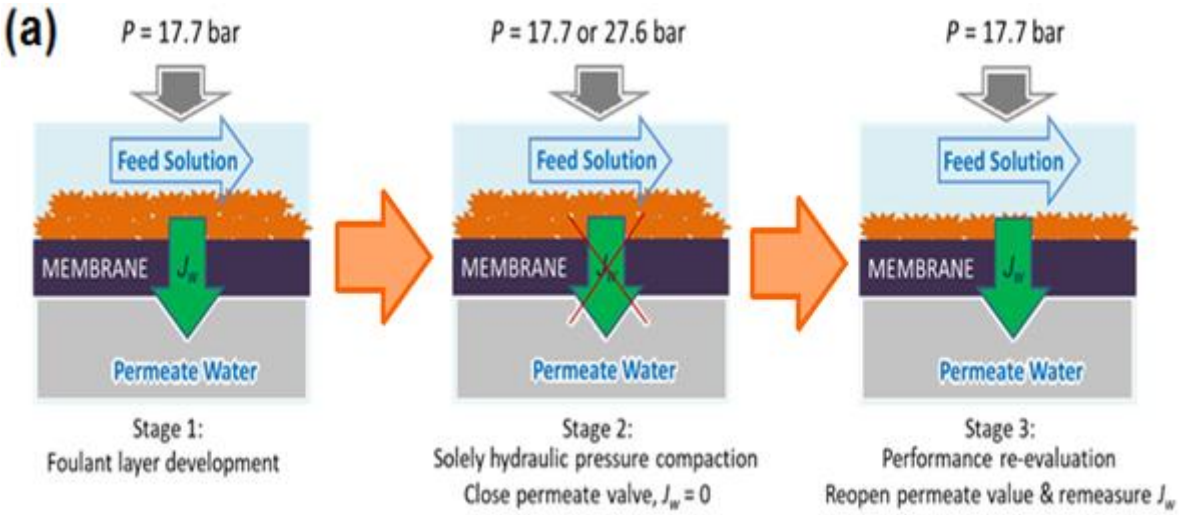

Figure 5.13: **(a)** Schematic illustration of the experimental protocols for solely hydraulic pressure compaction of foulant layer

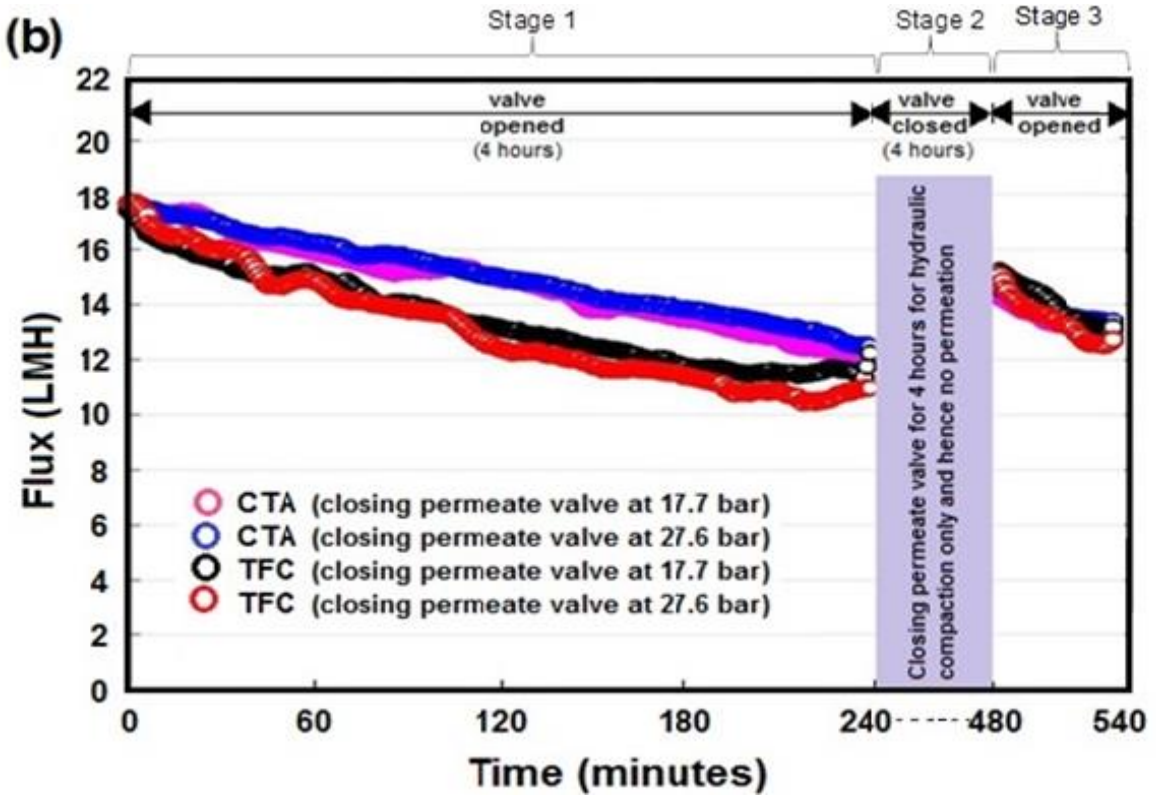

Figure 5.13: **(b)** Effect of of hydraulic pressure on the compaction of foulant layer by stopping the permeation (by closing the permeation valve) after substantial fouling of 4 hours (ALFS orientation). In this way there was hydraulic pressure only and no permeation. The valve was reopened after further 4 hours to analyse the **variation in flux**

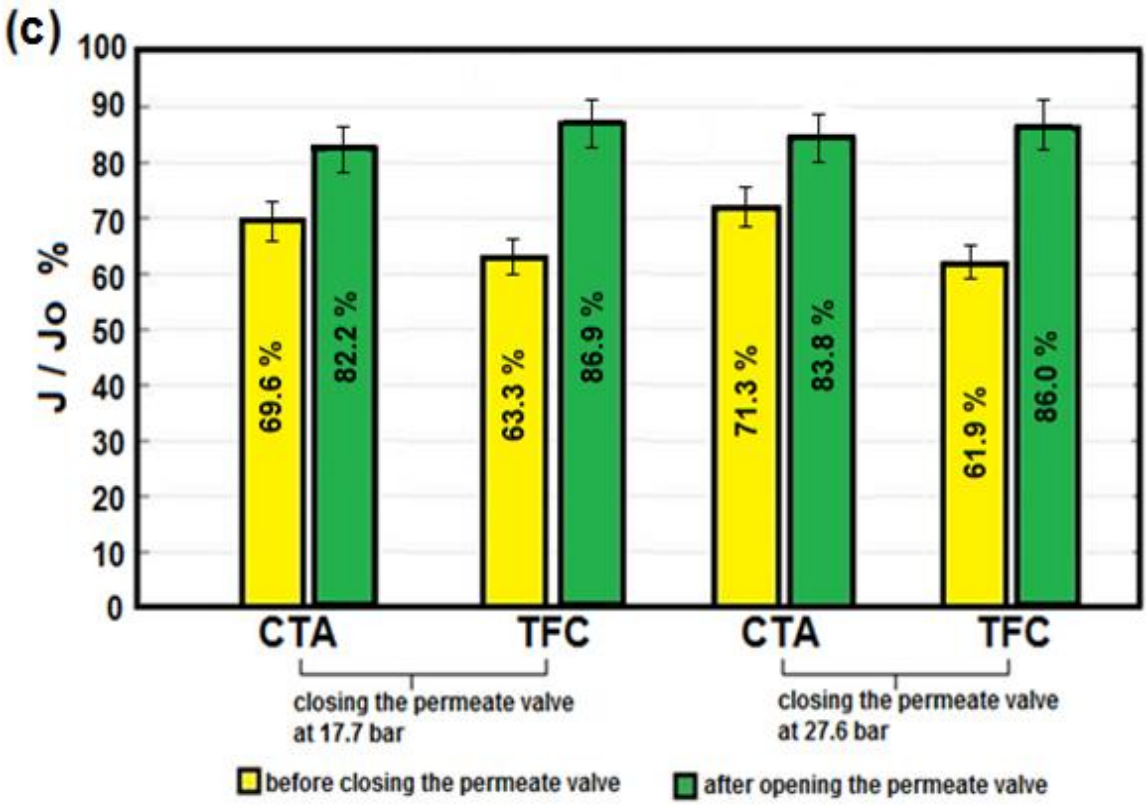

Figure 5.13: **(c)** Effect of of hydraulic pressure on the compaction of foulant layer by stopping the permeation (by closing the permeation valve) after substantial fouling of 4 hours (ALFS orientation). In this way there was hydraulic pressure only and no permeation. The valve was reopened after further 4 hours to analyse the **percent increase in flux after opening the permeate valve**

5.3.2.5 Mechanisms of different fouling behaviour in FO and RO

Although the observed decline in water flux (and also flux recovery) is similar for both FO and RO, the extent of fouling for FO is greater than that for RO. This conclusion is based on both the analysis of foulant layer resistance and foulant accumulation density.

In forward osmosis, the effective osmotic driving force is significantly limited by the effect of internal concentration polarisation (ICP) that is exponentially proportional to the water flux. As shown in Figure 5.14, the effective driving force in FO increased significantly with the water flux decline, while the effective driving force for RO was almost unchanged. Despite having the same effective driving force for both FO and RO at the beginning of fouling tests, the effective driving force for FO at the end of the fouling test, which lasted 1000 minutes, was nearly three times of that for RO.

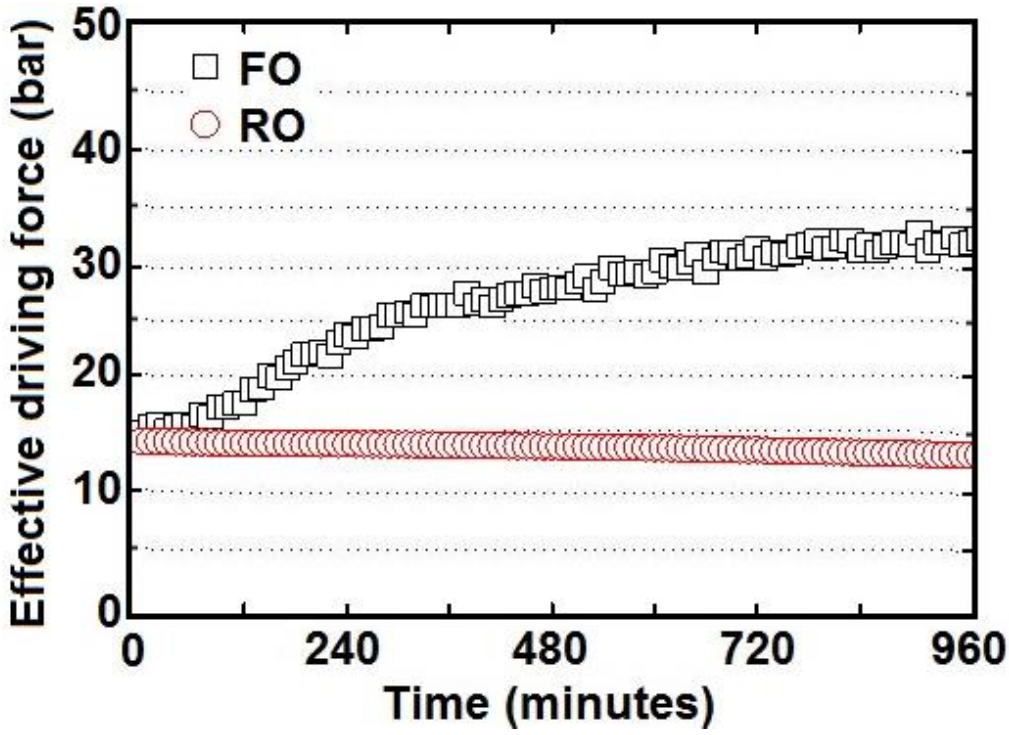

Figure 5.14: Comparison of effective driving force in the forward osmosis and the reverse osmosis

The progressively increased effective driving force in FO is attributed to the ICP self-compensation effect. The decreased water flux due to fouling results in a decrease of ICP, which in turn leads to an increase of the effective driving force. On the other hand, the increased effective driving force would have the tendency of attenuating the decline of the water flux. A schematic illustration is given in Figure 5.15.

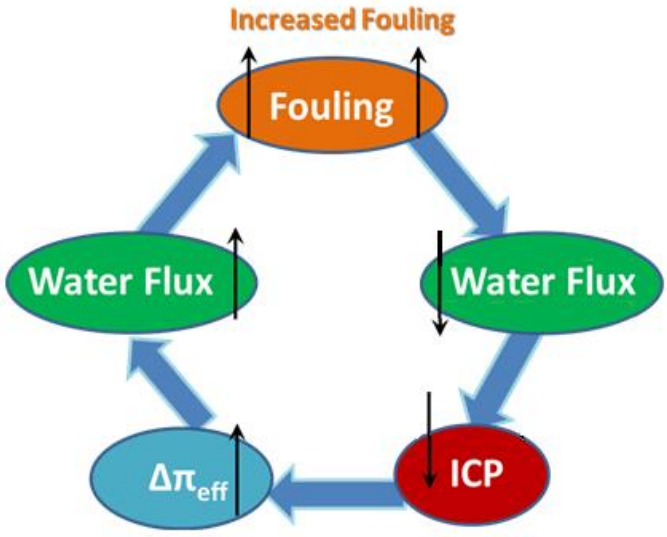

Figure 5.15: Schematic illustration of the relationship between fouling, water flux, ICP and effective osmotic pressure (π_{eff}) in FO process

5.3.2.6 Reverse solute diffusion and specific cake resistance

It can be observed that the S_f value of Equation (5.4) will probably be higher for the thicker foulant layers found in FO and therefore that for a given flux, the Ca^{2+} concentrations near the active layer surface will be higher for FO compared to RO. However the concentration of Na^{+} ions are also elevated and at higher ionic strengths charges on macromolecules are shielded which tends to create tighter pores. This would promote a tendency towards a higher specific cake resistance for FO.

Firstly, it is noted that the reverse diffusion of draw solute into the FS can influence the fouling behaviour (either increasing or decreasing fouling) due to the change of local feed solution chemistry near the FO membrane surface, which has been identified to be a unique fouling mechanism for osmotically driven membrane processes (She et al., 2016, She et al., 2012). In the current study the reverse diffusion of NaCl from draw solution into feed solution would elevate the ionic strength of FS. As shown in Figure 5.16, it was estimated, based on the approach reported previously (Zhang et al., 2014, Zhang et al., 2017), that the local ionic strength near the active layer surface was elevated from ~98 mM at the beginning to ~167 mM at the end of the fouling test due to both cake-enhanced concentration polarisation and reverse solute diffusion (RSD). In comparison, during the RO fouling test the bulk FS ionic strength is constant (~60 mM) and the local ionic strength near the active layer surface was elevated from ~86 mM to ~117 mM due to cake-enhanced concentration polarisation.

Secondly, the ratio of Na^{+} to Ca^{2+} will be larger in FO than in RO due to the reverse salt diffusion of NaCl. However, for the ratios in the present work which vary from around 10:1 to 20:1. Tow and Lienhard V (2016) (see their Figure A1) have shown (albeit for a

feed with 1 mM $CaCl_2$) that the pores in the cake layer will be unchanged. Though this suggests that an unchanged specific cake resistance might be anticipated, a change of just 20% in pore diameter would lead to a doubling of the specific cake resistance if the number of pores was unchanged. Clearly the influence of local ionic strength (influences the balance one way) and the changing Na^+ to Ca^{2+} ratio (influencing the balance in the opposite direction) is on balance altering the pore size of the cake by around 1nm assuming the pore sizes to be similar to those found by Tow and Lienhard V (2016). This shows the subtlety of the water chemistry.

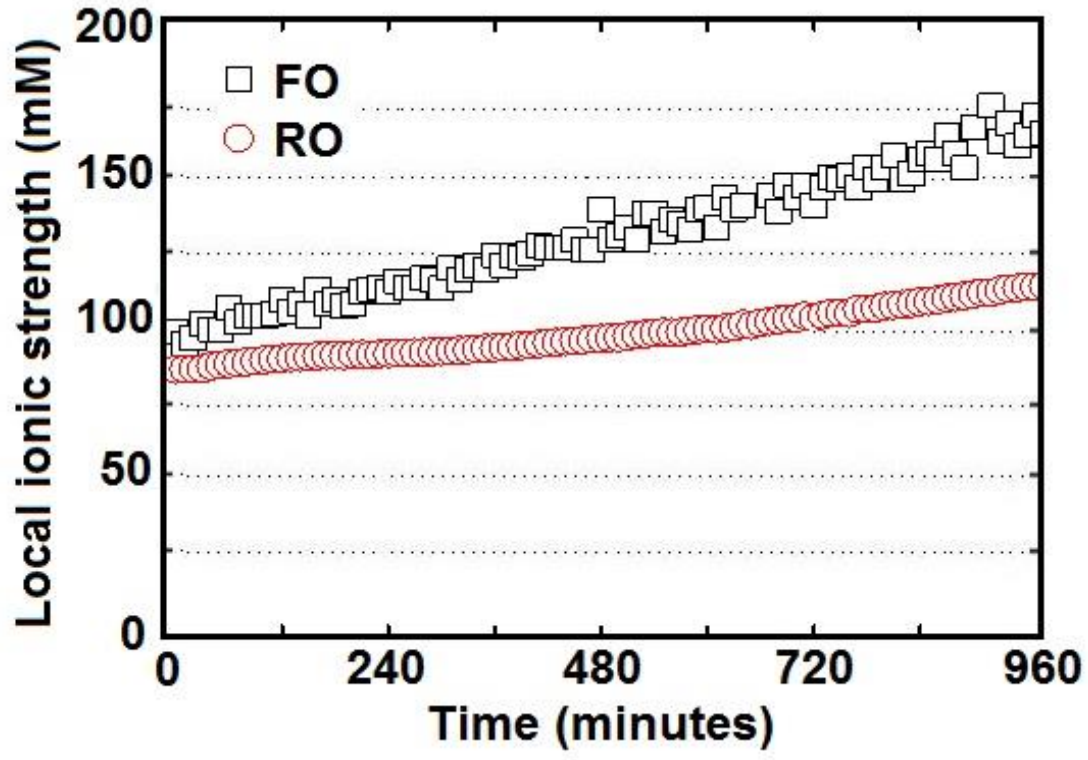

Figure 5.16: Estimated local ionic strength near the membrane active layer surface for FO and RO during the fouling test. The calculation of local ionic strength followed the method reported (Zhang et al., 2014, Zhang et al., 2017) incorporating cake-enhanced concentration polarization.

Figure 5.17 (a) demonstrates the specific reverse solute flux through the membrane. This is a useful quantification which describes the amount of draw solute diffusing into the feed side per unit volume of water permeating into the draw solution. For the 1000 minutes of

the experiments, it was noted that the specific reverse solute flux in forward osmosis increased with time. This could be related to the decrease in internal concentration polarisation in ICP-self compensation effect which is explained in detail in section 2.2.3 (Chapter 2). A decrease in internal concentration polarisation naturally increases the draw solution concentration next to the skin layer of the membrane.

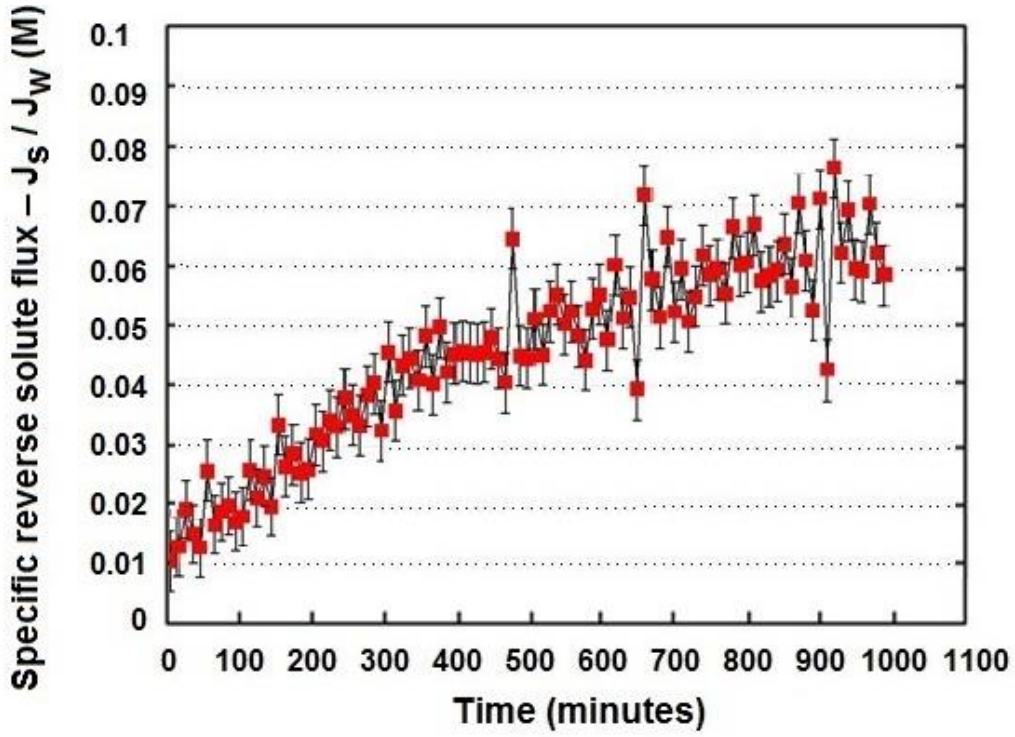

Figure 5.17: **(a)** Specific reverse solute flux with time for CTA membrane for forward osmosis experiment (ALFS orientation) with feed solution (45 mM NaCl + 5 mM $CaCl_2$) with alginate (200 mg/L) as foulant. Crossflow velocity of feed was set at 7.4 cm/s and DS crossflow velocity at 14.8 cm/s

This diffusion of salt into the feed side passes through any foulant layers. As there is poor mass transfer within these layers, the concentration of salt of the feed side becomes elevated at the foulant-membrane interface and results in an increase in osmotic pressure at the feed surface. This phenomenon is commonly referred as *cake enhanced osmotic pressure* (Hoek and Elimelech, 2003). This suggests that it is ICP which plays the major role for more fouling and comparatively less flux decline in FO than in RO. Salt rejection in the reverse osmosis process was calculated for 1000 minutes (Figure 5.17(b)), and it is notable that in 1000 minutes the salt rejection was decreased by just 5%.

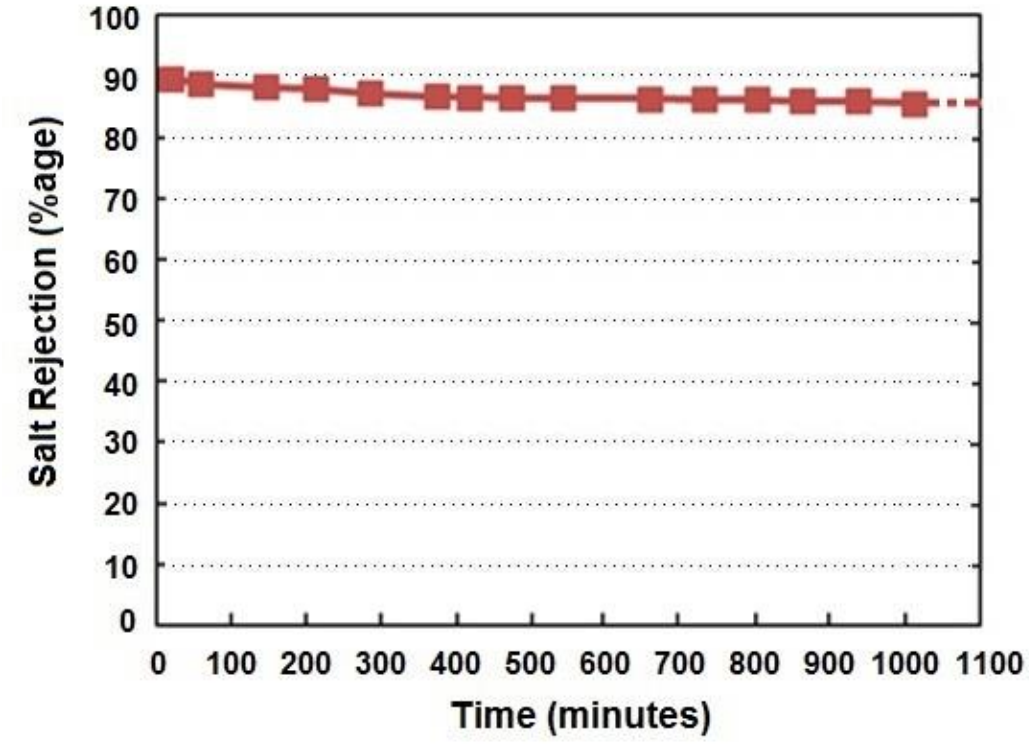

Figure 5.17: **(b)** Salt rejection with time for CTA membrane for reverse osmosis experiments (ALFS orientation) with feed solution (45 mM NaCl + 5 mM $CaCl_2$) with alginate (200 mg/L) as foulant and 27.5 bar hydraulic pressure at feed side. Crossflow velocity of feed was set at 7.4 cm/s

5.3.2.7 Effect of cake enhanced osmotic pressure on the foulant resistance

The modeling of the cake layer resistance and its mechanism has been widely discussed by a number of researchers (Belfort et al., 1994, Tang et al., 2011) but fewer have reported on this in osmotically driven processes. However, realising the importance, there is an increasing interest in osmotically driven membrane processes regarding this important phenomenon and its impact on membrane permeation processes (Tang et al., 2010, Gu et al., 2013, Yip and Elimelech, 2013, Aydiner, 2015).

Figure 5.18 reveals the calculated effect of cake enhanced osmotic pressure in osmotically driven membrane processes in comparison with the external concentration polarisation. In osmotically driven as well as in pressure driven membranes, the unstirred foulant layer on

the surface of the membrane may hinder the back diffusion of salt ions back to the bulk solution. In addition, the reverse solute flux from the draw solution to the feed side may cause the salt ions to be trapped in the foulant layer on the surface of the membrane on the feed side. This increases the osmotic pressure on the foulant cake layer at the surface of the feed side of the membrane in comparison to the overall osmotic pressure of the bulk solution. This reduces osmotic gradient across the membrane and hence reducing the effective driving force. This phenomenon of a cake enhanced osmotic pressure has been widely discussed (Hoek and Elimelech, 2003, Chong et al., 2008b, Chong et al., 2008a, Sim et al., 2011). Figure 5.18 shows that for FO, CEOP effect does influence the results whereas the effect of external concentration polarisation is negligible. Both effects are negligible for RO. Allowance for the effect of CEOP does not change the earlier conclusion that the foulant resistance in FO is greater than that in RO.

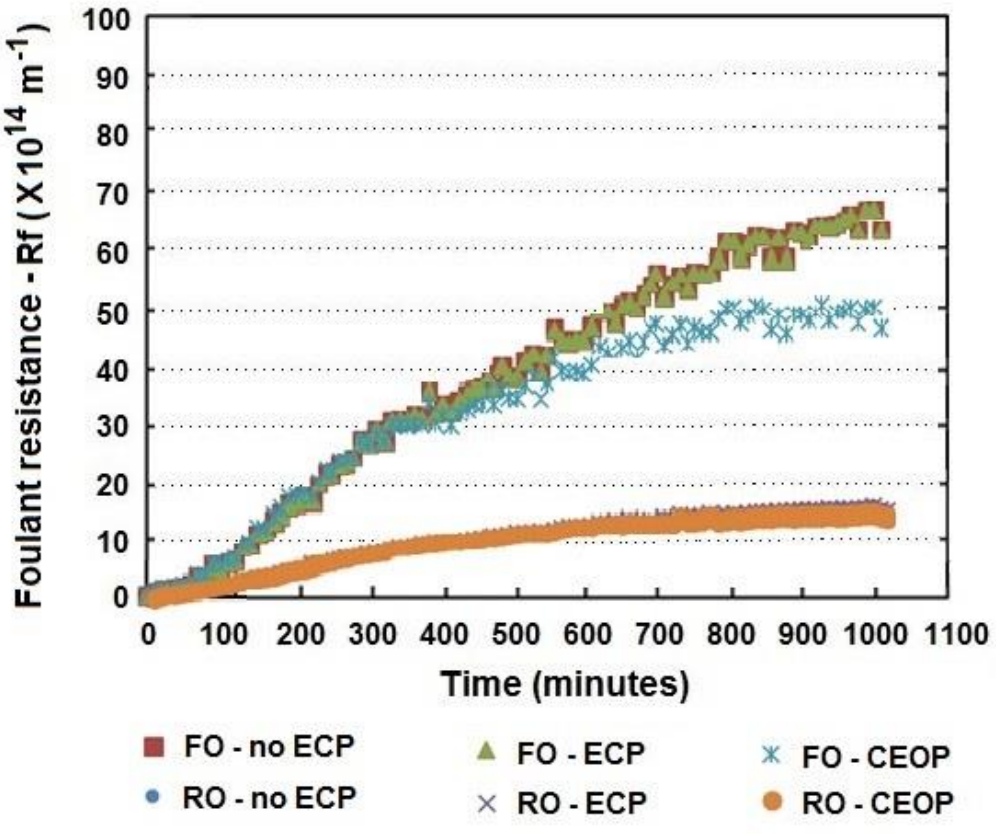

Figure 5.18: Variation in foulant resistance with time for cake enhanced osmotic pressure and external concentration polarisation

The results in Figure 5.14 on the analysis of effective driving force also suggest that cake-enhanced concentration polarization (CECP) might play a less important role in FO in the AL-FS orientation compared to that in RO. The reasoning again relates to the ICP self-compensation effect – the decreased ICP at the draw side due to the decrease of water flux by fouling was much more significant than the cake-enhanced CP at the feed side in this study. This result was demonstrated through sensitivity analysis for a wide range of scenarios - see Figure A3 in **APPENDIX–III**. This shows that the increase of effective driving force for FO could be moderately slowed down at an increased CECP, but the overall trend (effective driving force for FO significantly > RO) remains unchanged as long as the fouling continues to lead to an increase of foulant resistance (R_f). This finding supports an earlier study on the modelling of the effect of feed concentration on FO water flux, where She et al. (2016) suggested that CECP might not be important for FO in the AL-FS membrane orientation due to the strong ICP self-compensation effect.

5.3.2.8 Fouling reversibility

Fouling reversibility was examined through simulation to resolve the apparent contradiction between flux recovery and the extent of membrane cleaning. Figure 5.19 shows the simulated water flux in FO and RO as a function of foulant resistance based on ORF models (Equation (5.3) and Equation (5.5)) for the same initial flux. For the same extent of fouling (i.e., at the same R_f when $Rf > 0$) it is apparent that the water flux for FO is intrinsically higher than that for RO. Furthermore, during membrane cleaning, the water flux for FO can be recovered to a higher level than RO even though the fouled FO membrane is not cleaned to the same extent as the fouled RO membrane. To illustrate this point consider that the foulant resistance for FO is reduced from $R_{f,3}$ to $R_{f,2}$ after membrane cleaning (Figure 5.19). The water flux for FO will still be greater than that for RO when

the foulant resistance reduced from $R_{f,2}$ to $R_{f,1}$ in Figure 5.19. Again this indicates that the change of water flux in FO in response to the change of foulant resistance (i.e. fouling) is much less than that in RO. This also explains why fouling reversibility, based on measured water fluxes, appears to be more effective for FO than RO as found by others (Mi and Elimelech, 2010c, Lee et al., 2010a, Mi and Elimelech, 2013, Kim et al., 2014a, Kwan et al., 2015, Xie et al., 2015, Lotfi et al., 2017, Lee et al., 2017).

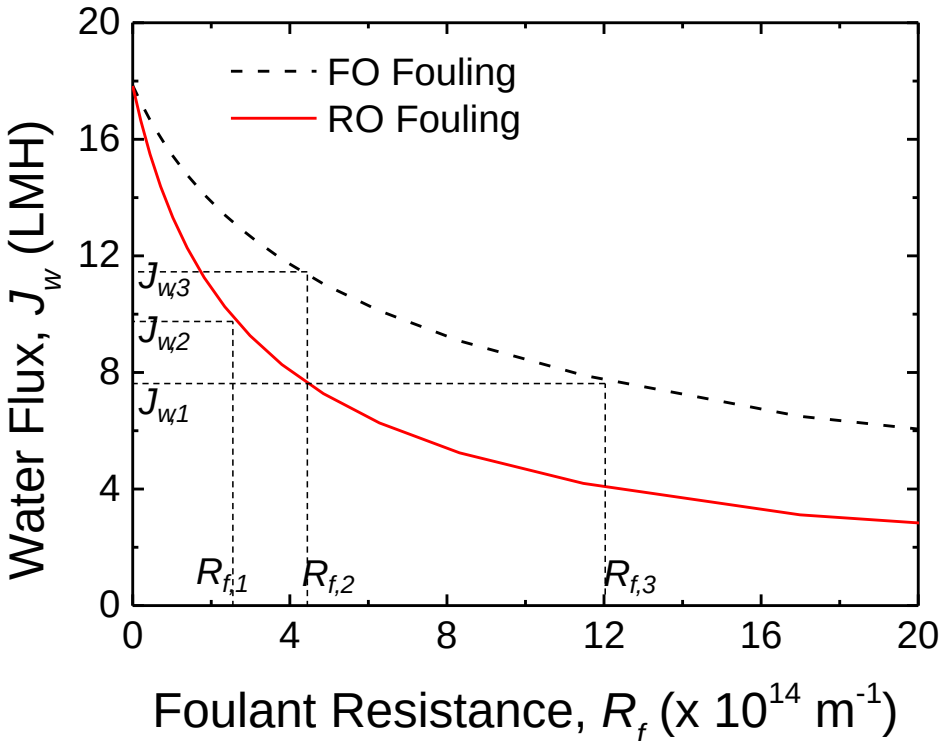

Figure 5.19: Simulation of water flux of FO and RO as a function of foulant resistance. The simulation is based on the osmotic-resistance filtration models (Equation (5.3) and Equation (5.5)) assuming that membrane fouling only leads to the increase of R_f while other membrane parameters (solute permeability coefficient B value and structural parameter S value etc.) are unchanged.

While ICP is generally regarded as a detrimental effect for FO, the current study reveals that ICP can also have an upside in that it helps to maintain water flux stability. An interesting corollary to this is that the quest for FO membranes with smaller and smaller S values to reduce ICP needs to consider whether there is an optimal S value that balances the magnitude of flux and the resilience that the ICP compensation imparts upon the system.

5.3.2.9 Investigation on the effect of pre-compaction of membranes before fouling tests

The above tests had subjected those operated in RO mode to elevated pressure but not those operated in FO mode. So in order to analyse the impact of compactness on fouling due to possible change (if any) in membrane structure, membrane coupons were initially compacted under a pressure of 28 bar for 24 hours before fouling experiments for the set conditions with ALFS orientation. The method adopted for both forward and reverse osmosis tests is described below:

FORWARD OSMOSIS

Feed solution: 45mM NaCl+5mM $CaCl_2$ (5L)

Foulant: 200mg/L Alginate

Draw solution: varies

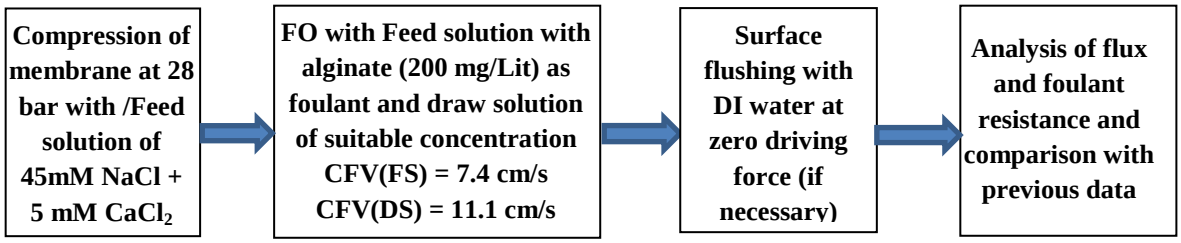

REVERSE OSMOSIS

Feed solution: 45mM NaCl+5mM $CaCl_2$ (5L)

Foulant: 200 mg/L alginate

Hydraulic Pressure: varies

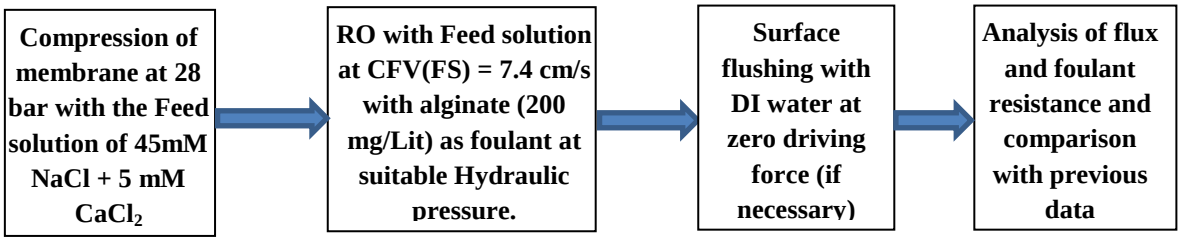

The test conditions of the forward and reverse osmosis experiments for pre-compacted CTA and TFC membranes are given in **Table 5.3** below:

Table 5.3: Test conditions for the baseline and fouling tests of Pre-compacted CTA and TFC membranes. The feed solution used was of 45 mM NaCl+5mM $CaCl_2$ with alginate (200 mg/L) as foulant and membrane orientation of active layer facing the feed side.

Test No.	Process	Membrane	Driving force	Baseline Test duration	Fouling Test duration	Crossflow velocity of feed solution (cm/s)	Crossflow velocity of draw solution (cm/s)
P1	FO	CTA	Draw solution of 2 M NaCl	60 min	1200 min	7.4	11.1
P2	FO	TFC	Draw solution of 3 M NaCl	60 min	1400 min	7.4	11.1
P3	RO	CTA	15.6 bar hydraulic pressure on feed	50 min	500 min	7.4	--
P4	RO	TFC	12.3 bar hydraulic pressure on feed	40 min	500 min	7.4	--
P5	RO	CTA	15.1 bar hydraulic pressure on feed	60 min	500 min	7.4	--
P6	FO	CTA	Draw solution of 2 M NaCl	30 min	950 min	7.4	11.1

5.3.2.9.1 Baseline Experiments with pre-compacted membranes

After the compaction of CTA and TFC membranes, baseline experiments were performed, on FO and RO modes, before moving measured through the test of total organic ards the fouling tests. The graphical demonstration of the said baseline results is given in Figure 5.20.

The results show that baseline fluxes for both FO and RO with pre-compacted membranes were almost constant and at the same level to the results of baseline tests with un-compacted membranes (Figure 5.7). Therefore, pre-compaction did not play any discernible role in determining water permeability. Although one might conclude from the baseline tests alone that flux decline during the fouling tests was solely due to the addition

of foulant on the feed side, fouling experiments with pre-compacted membranes was undertaken.

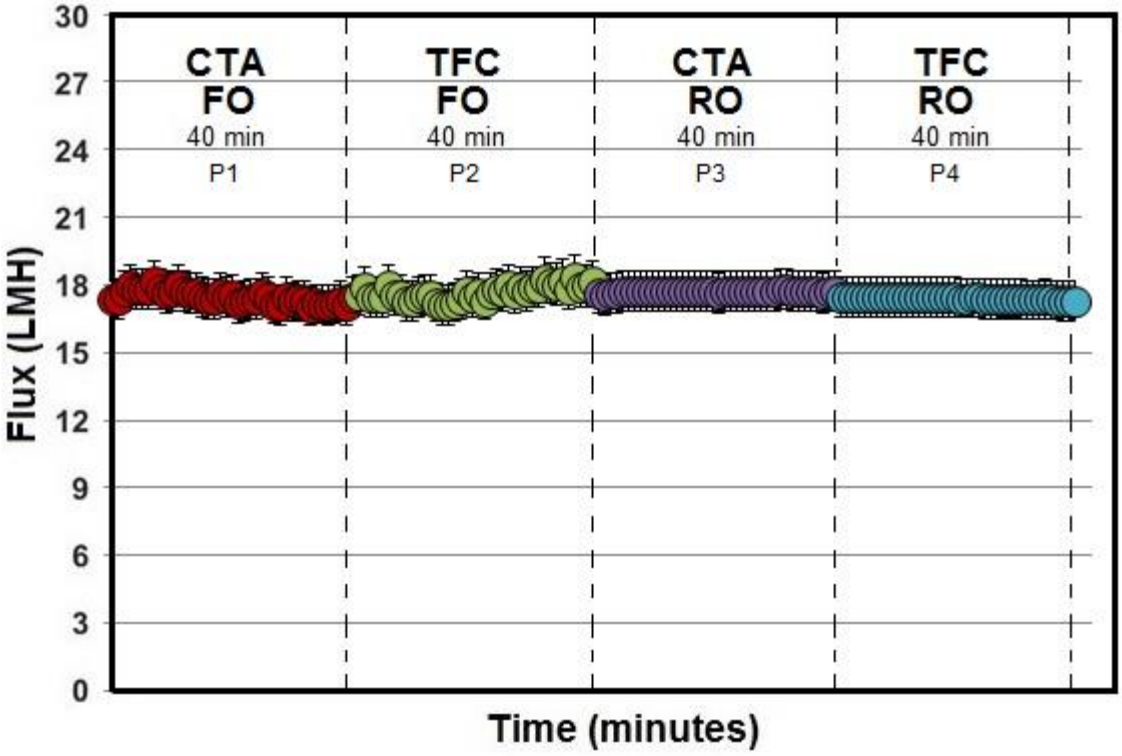

Figure 5.20: Flux variation with time for baseline experiments for forward osmosis and reverse osmosis experiments (ALFS orientation) with CTA and TFC pre–compacted membranes with feed solution (45 mM NaCl + 5 mM $CaCl_2$). Crossflow velocity of feed solution 7.4 cm/s (in FO and RO). Draw solution for CTA and TFC membranes in FO set ups was NaCl solution with concentrations of 2 M and 3 M respectively with crossflow velocity in each setup as 11.1 cm/s. For RO set ups, the applied hydraulic pressure on feed side of CTA and TFC membranes was 15.5 bar and 12.2 bar respectively

5.3.2.9.2 Fouling experiments with pre-compacted membranes

Experimental results for forward and reverse osmosis fouling experiments for both CTA and TFC membrane are graphically illustrated in Figures 5.21 (a)–(h) for un-compacted and pre-compacted membranes respectively. The findings for reverse osmosis reveal that compressing the membranes for 24 hours did not bring any substantial change in permeation efficiency. However for forward osmosis, the foulant resistance for the TFC membrane is increased (Figure 5.21 (d)) and this is probably due to fairly even compaction of the support layer. A compacted layer would have a reduced free volume and an increased ‘S’ value. This would cause increased internal concentration polarisation and an

additional resistance that has been calculated as increased fouling. The FO data for the CTA membrane shows for the pre-compacted membrane an abrupt decrease in flux at the beginning. This could be attributed to a partially compacted support layer reducing flux relatively in certain areas and leading to intensified fouling in the unaffected areas (the overall average flux was kept the same). There was rapid flux decline due to the effect of internal concentration polarisation (ICP) in the beginning but later on the flux was settled probably due to ICP-self compensation effect. Overall, there was probably no significant change in fouling behaviour itself due to pre-compaction but pre-compaction at 28 bar probably damages the support layer. However, there is no evidence to support the hypothesis that the outcome of reverse osmosis experiments is affected by hydraulic pressure.

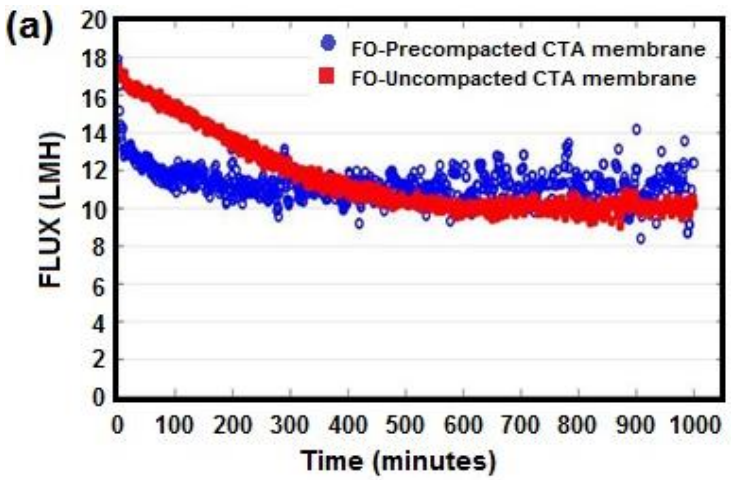

Figure 5.21: (a) Behaviour of flux decline in forward osmosis (ALFS orientation) after pre compaction of CTA membrane (P1)

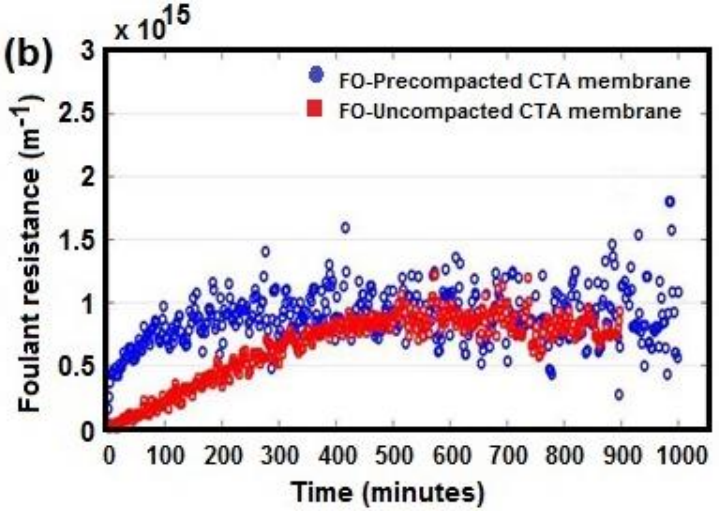

Figure 5.21: (b) Behaviour of increase in foulant resistance in FO (ALFS orientation) after pre-compaction of CTA membrane

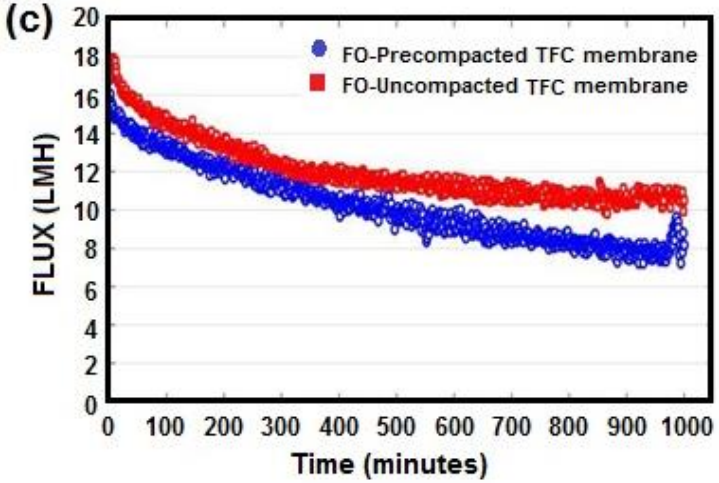

Figure 5.21: (c) Behaviour of flux decline in forward osmosis (ALFS orientation) after pre compaction of TFC membrane (P2)

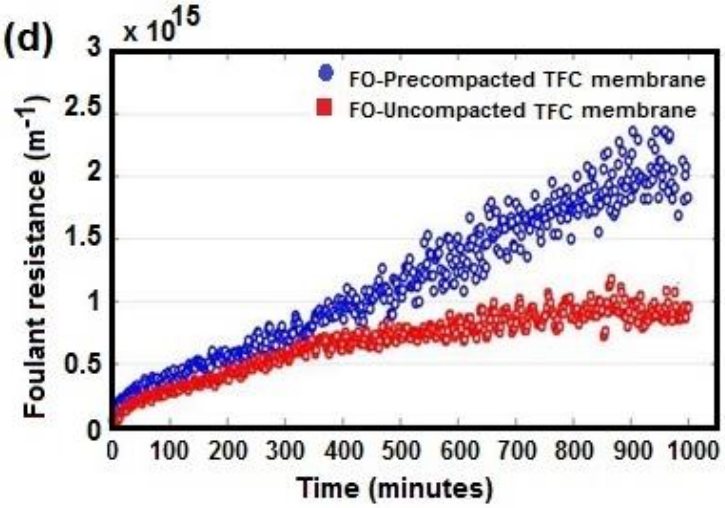

Figure 5.21: (d) Behaviour of increase in foulant resistance in FO (ALFS orientation) after pre-compaction of TFC membrane

Figure 5.21 continued…

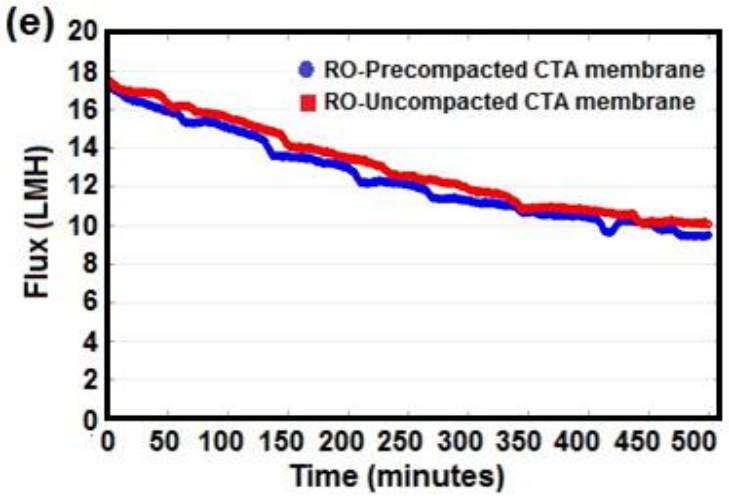

Figure 5.21: (e) Behaviour of flux decline in reverse osmosis (ALFS orientation) after pre compaction of CTA membrane (P3)

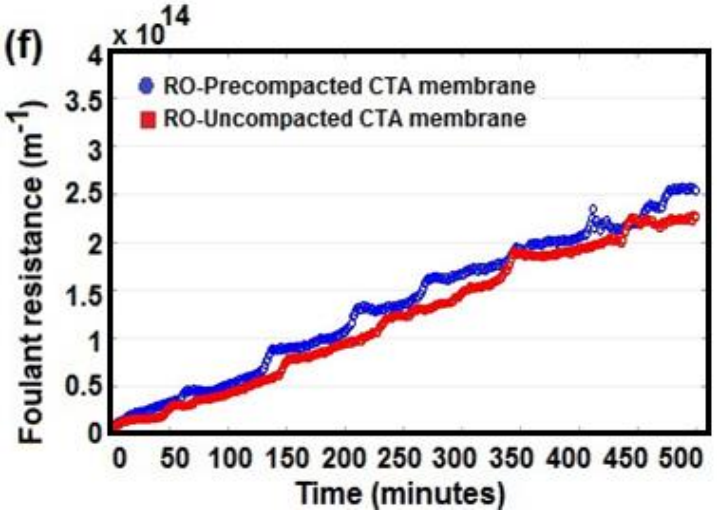

Figure 5.21: (f) Behaviour of increase in foulant resistance in RO (ALFS orientation) after pre-compaction of CTA membrane

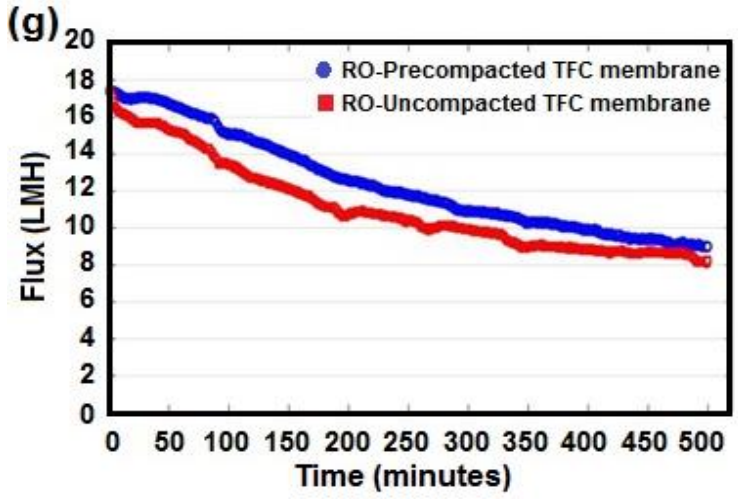

Figure 5.21: (g) Behaviour of flux decline in reverse osmosis (ALFS orientation) after pre-compaction of TFC membrane **(**P4)

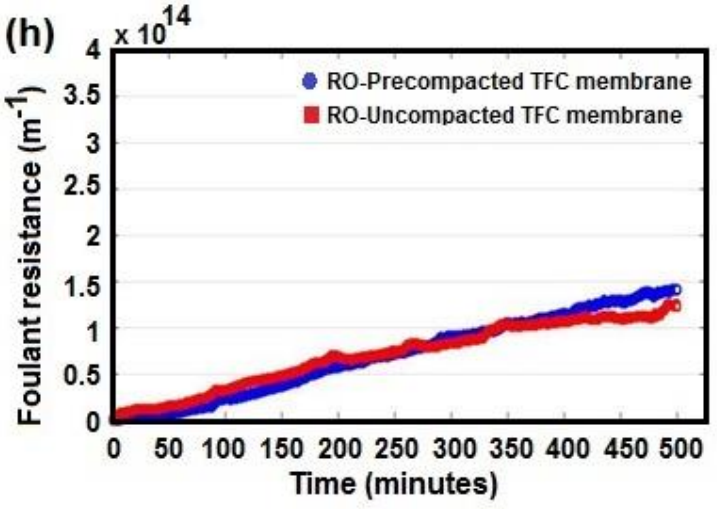

Figure 5.21: (h) Behaviour of increase in foulant resistance in RO (ALFS orientation) after pre-compaction of TFC membrane

5.3.3 Applied and effective driving force in osmotically driven membranes

Whilst the importance of concentration polarisation in fouling mechanism in osmotically driven membranes is explored in the previous sections, the importance of the phenomenon is best explained graphically in Figure 5.22 which depicts the ratio of effective to applied osmotic pressure difference as a function of the inverse water flux. Applied osmotic pressure difference between draw and feed side is the imposed driving force i.e. the difference between osmotic pressure on draw side (π_{ds}) and the osmotic pressure on the feed side (π_{fs}) at the start of the experiment. The applied osmotic pressure difference ($\Delta\pi_{app}$) is the difference in osmotic pressure across the skin layer between the feed and draw sides.

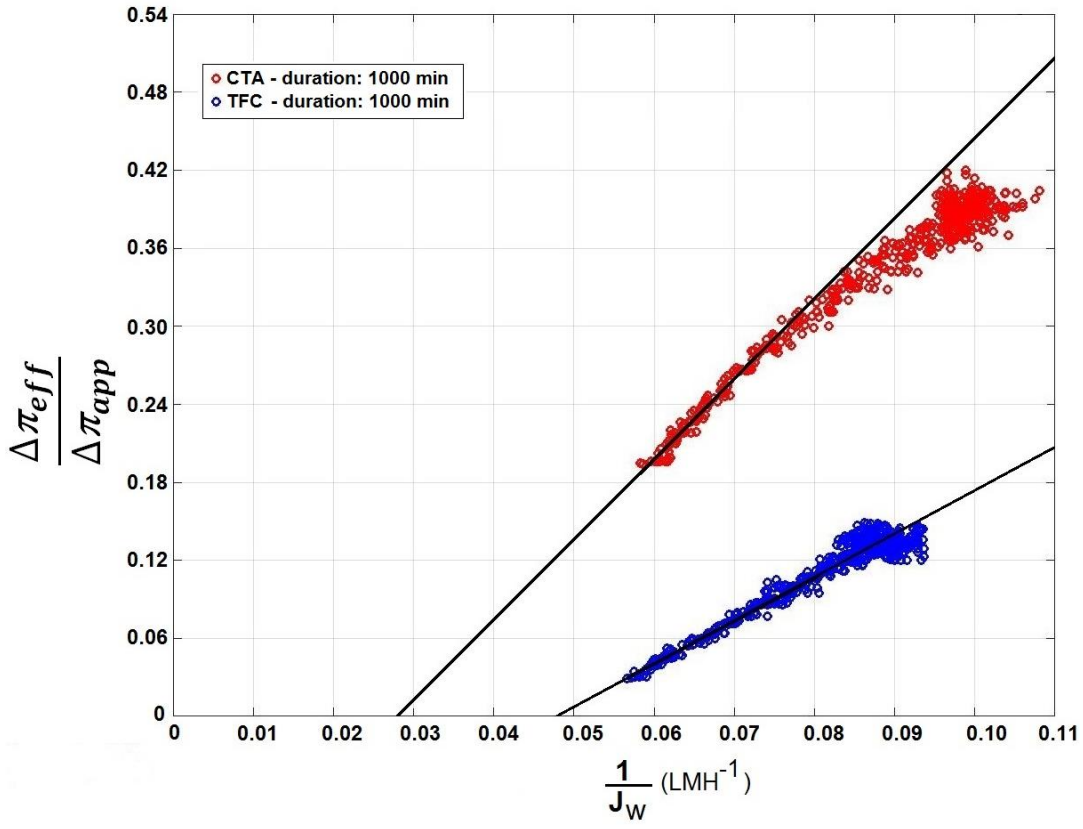

Jw: water flux

$\Delta\pi_{eff}$**:** osmotic pressure difference between draw and feed side considering concentration polarisation and reverse solute diffusion in account

$\Delta\pi_{app}$**:** osmotic pressure difference between draw and feed side **without** considering concentration polarisation and reverse solute diffusion in account

Figure 5.22: Graph between Flux (J_w) and ratio of effective & applied osmotic pressure ($\frac{\Delta\pi_{eff}}{\Delta\pi_{app}}$)

It can be seen from Figure 5.22 that for both the cellulose tri acetate (CTA) and the thin film composite (TFC) membranes, the ratio of effective to applied force is increasing gradually with the decrease in flux. The reason can be attributed to the self-adjusting process in FO which has been explained in detail in section 2.2.3. Not only is the self-increase in effective driving force with decrease in flux demonstrated in Figure 5.22 but it clearly demonstrates the severity of ICP, particularly for the TFC membrane. At the end of the fouling tests, the ratio for the CTA membrane stabilises around 0.39 but for the TFC it stabilised around just 0.13.

5.3.4 Determination of mass of foulant deposition on membrane surface

In order to analyse the amount of foulant deposited on the membrane surface, membrane samples were cut from the fouled membrane coupons and the mass of foulant deposition on the membrane was measured based on total organic carbon (TOC). The following steps were followed in the foulant extraction from the fouled membrane.

1. Fouled membrane coupon was carefully taken out from the FO membrane cell.

2. Coupon was rinsed with Milli-Q deionised water (from draw side) in order to remove any leftover deposition of the salt on the membrane surface.

3. Three small fouled membrane samples (each of an area of 4 cm^2) were cut from multiple locations of the fouled membrane coupon.

4. The samples were transferred into three sample tubes containing 40 ml basic solution with pH 11 as shown in Figure 5.23.

5. In order to avoid the error of interference from the membrane dissolution during foulant extraction, a blank solution was also prepared by extracting three clean membrane samples (with the same area of 4 cm^2) at the same time.

6. Sample tubes were put on a shaking table overnight to extract the deposited foulant on the membrane.
7. The TOC of the extracted foulant solutions and the blank solution was measured subsequently by a TOC analyser.
8. The actual TOC of the deposited foulant was determined by the difference of the TOC in the extracted foulant solution and in the blank solution.
9. Concentration of the deposited foulant in each of the extracted solutions was determined by comparing its TOC with a calibration curve constructed from the TOC of standard solutions with concentrations of 0–50 mg of foulant per litre.

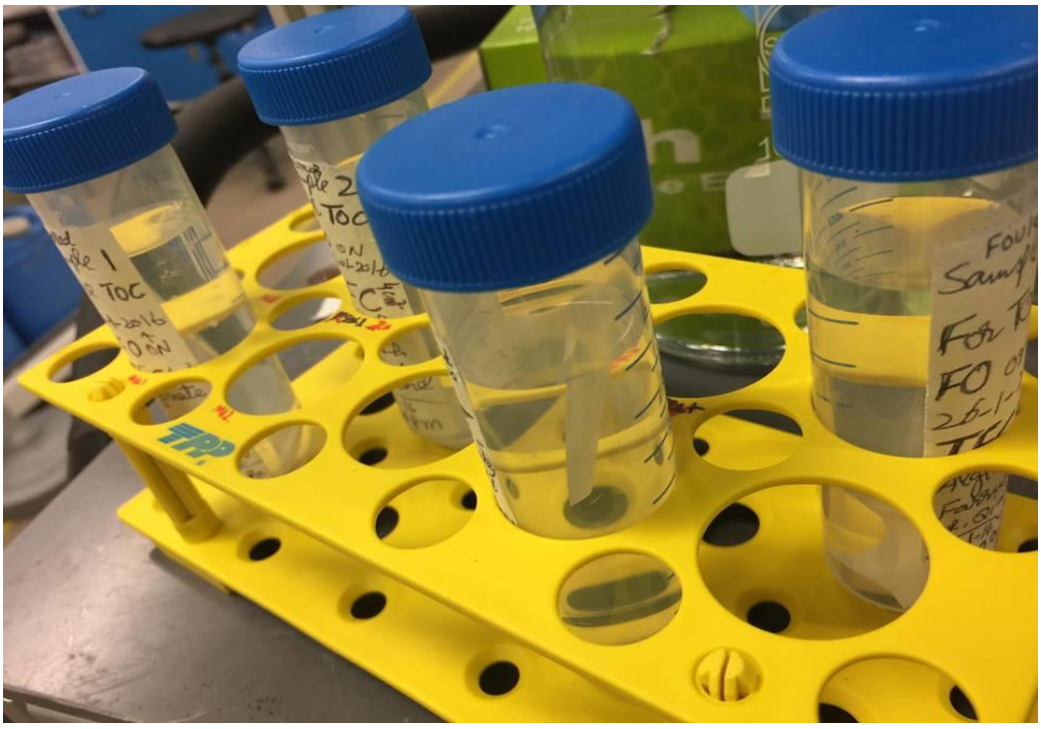

Figure 5.23: Membrane samples saved in basic solution of pH 11 for mass determination of the level of fouling

Following the procedure stated above, the density of deposited foulant on the surface of each of the samples of CTA and TFC membrane was determined for both FO and RO. The results are demonstrated in **Table 5.4**.

Table 5.4: Foulant deposition densities on membrane samples in FO and RO tests of 1000 minutes duration

Sample No.	Type of sample	Process	TOC (mg/L)	Amount of Alginate in solution (mg)	Density of alginate (mg/cm^2)	Average alginate density (mg/cm^2)	Ratio of alginate densities of FO & RO
1	Clean CTA	--	14.56	-	-	-	-
2	Clean TFC	--	02.12	-	-	-	-
3	**Fouled CTA Membrane sample**	FO	63.33	7.36	1.84	1.70	1.51
4		//	62.40	7.22	1.81		
5		//	53.27	5.84	1.46		
6		RO	35.19	3.11	0.8	1.13	
7		//	56.69	6.36	1.6		
8		//	41.01	3.99	1.0		
9	**Fouled TFC Membrane sample**	FO	27.72	3.86	0.97	0.73	1.66
10		//	08.93	1.03	0.26		
11		//	15.08	1.96	0.49		
12		RO	07.75	0.85	0.21	0.44	
13		//	18.03	2.40	0. 6		
14		//	15.38	2.01	0. 5		

The data in **Table 5.4** reveals that the foulant deposition density for forward osmosis process is greater than that in reverse osmosis. For CTA membrane, the difference was 15 times. However, for TFC membranes, it was found to be 5.41. This could be related to the difference in intrinsic properties of both membranes. Nevertheless, in each case, the fouling in FO is reported to be more than that in RO. This confirms the hypothesis that FO is more prone to fouling than RO and merely relying on flux decline may not demonstrate the fouling trend.

5.3.4.1 Thickness of the foulant cake

The thickness of the cake layer is determined by assuming the density of the foulant cake is comparable to that of water. The calculated thickness of the foulant cake for CTA and TFC membranes for both FO and RO processes are given in Table 5.5. The method for calculating foulant accumulation is mentioned in section 5.3.4. Tow and Lienhard V (2016) developed a method to quantify membrane fouling by employing two parameters – cake structural parameter (that is related to cake-enhanced concentration polarization) and

pore hydraulic diameter (that is related to hydraulic resistance of foulant layer), it appears that their study only focused on the analysis of the former under conditions where cake hydraulic resistance is negligible. Their findings also reveal that greater foulant accumulation occurred over time in FO than RO, which suggests fouling in FO might be more severe than RO despite lower flux decline in FO. In addition, their study did not find any evidence that the thinner cake layer (less foulant accumulation) in RO could be attributed to the hydraulic pressure compaction. In addition, the controversy over FO and RO fouling in prior studies as well provided an impetus for to perform an insightful comparison of fouling accumulation between FO and RO processes. The calculated thickness of the foulant cake through quantification of the mass of foulant accumulation is illustrated in Table 5.5.

Table 5.5: Thickness of the foulant cake

Membrane	**Process**	**Average alginate density per unit area of membrane**	**Density**	**Average thickness of the foulant cake**
		mg/cm^2	**mg/cm^3**	**cm**
CTA	FO	1.7	1000	0.0017
	RO	1.13		0.00113
TFC	FO	0.73	1000	0.00073
	RO	0.44		0.00044

5.3.5 Images of membrane samples using scanning-electron microscopy and atomic-force microscopy

The images of both of the CTA and TFC membranes, obtained from HTI (Hydrowell Filter System), were taken using Scanning electron microscopy (SEM) and atomic-force microscopy (AFM) techniques. The images of clean and fouled membranes are shown in Figures (5.24) – (5.30).

The selected samples of the HTI membrane (sizes mentioned in figures' captions) were scanned by a Zeiss Evo® scanning electron microscope (SEM) at 2.00 kV accelerating voltage. Membrane samples were coated in a sputter coating chamber with uniform gold layer after freezing dried. An atomic force microscope (AFM) was used for determining the roughness and morphology of the membranes. For AFM, micrographs in sizes of 5μm x 5 μm were attained in tapping mode with a multimode piezoelectric scanner using single-crystal-etched silicon probes. It has been reported that during HTI CTA membranes manufacture, cellulose tri-acetate is coated on embedded polyester mesh material which acts as the mechanical support (Cath et al., 2006). In thin film composite (TFC) membranes, the active layer has a ridge and valley (uniform) morphology (a usual feature of polyamide layer). The support side constitutes polyester fibres in embedded mesh providing a good mechanical support. Figure 5.24 (a) and Figure 5.24 (b) show morphological images with 200 magnifications of clean cellulose triacetate membranes samples (each of the size 100 μm x 8 mm) for active and support layers respectively.

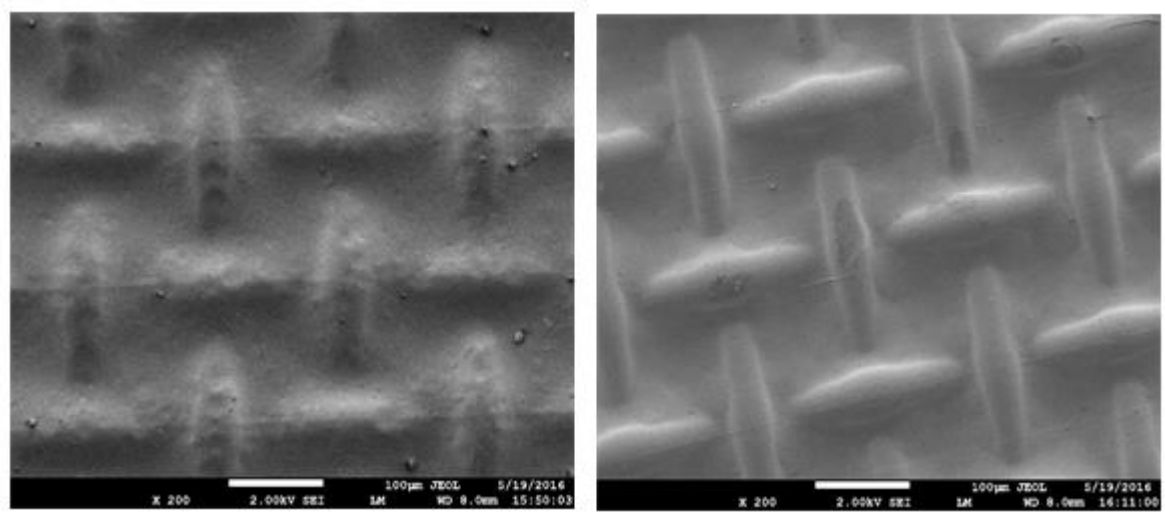

(a) Clean CTA active layer (b) Clean CTA support layer

Figure 5.24: SEM images for CTA membrane (with 200 magnification)

The impact of the embedded polyester mesh in the coating is to reduce the overall thickness of the membrane along with provision of mechanical strength.

Figures 5.25 (a) and 5.25 (b) SEM images (of 200 magnification) with top (active) and bottom (support) surfaces ofTFC membrane of size 100 μ m x 8 mm for each sample.

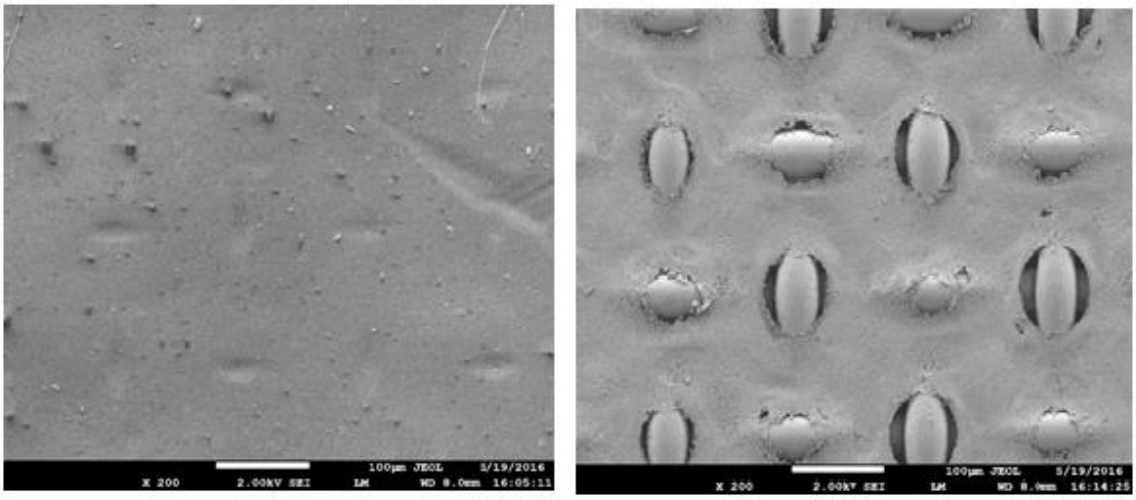

(a) Clean TFC active layer (b) Clean TFC support layer

Figure 5.25: SEM images for TFC membrane (with 200 magnification)

The magnification of SEM images was further increased up to 5000 for clean samples of CTA and TFC membranes. Figure 5.26 (a) and 5.26 (b) demonstrate active layers of CTA and TFC membrane samples respectively (each of the samples with size of 1μm x 8.9mm). SEM micrographs of the CTA and TFC membranes' active layers in Figure 5.26, in general, suggest that the surface of the active layer is fairly smooth. However, the AFM images in Figure 5.30 reveal the details of the roughness.

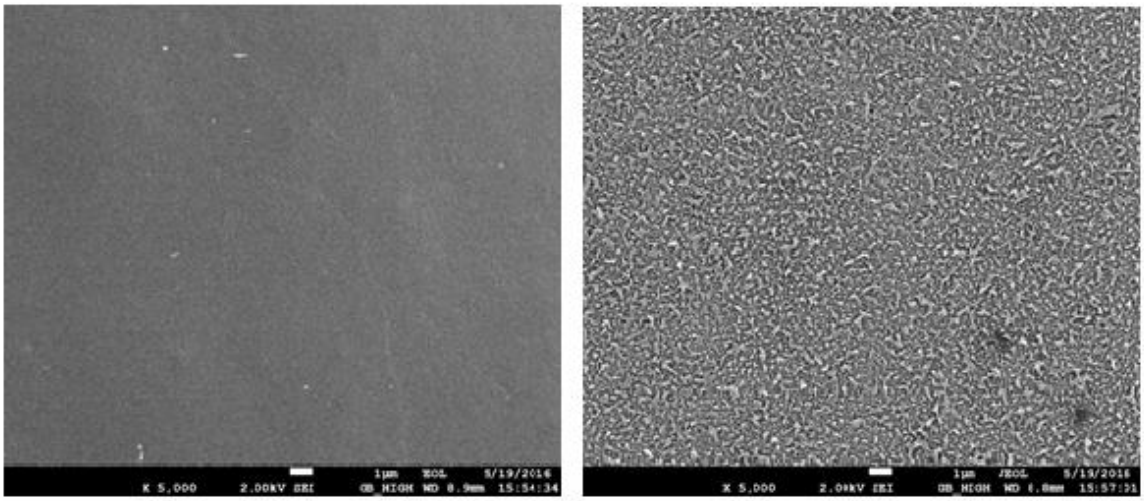

(a) Clean CTA active layer (b) Clean TFC active layer

Figure 5.26: SEM images for CTA and TFC membrane active layers (with 5000 magnification)

With extra increased magnification up to 20, 000 for active layer SEM images of CTA and TFC membranes' clean samples are shown in Figure 5.27 (a) and Figures 5.27 (b) respectively. Each sample has a size of 1μm x 8.9mm.

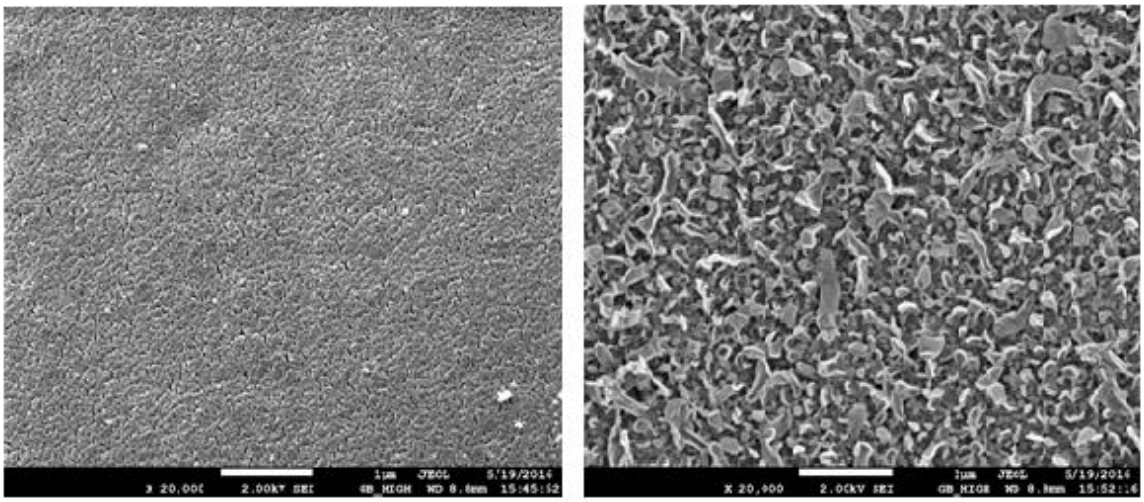

(a) Clean CTA active layer (b) Clean TFC active layer

Figure 5.27: SEM images for CTA and TFC membrane active layers (with 20,000 magnification)

Fouled samples were selected for both membranes after FO experiments. Figure 5.28 (a) and Figure 5.28 (b) show SEM images (5000 magnification) of fouled active layers of CTA and TFC membrane respectively. Each of the samples has size of 1μm x 8.8 mm.

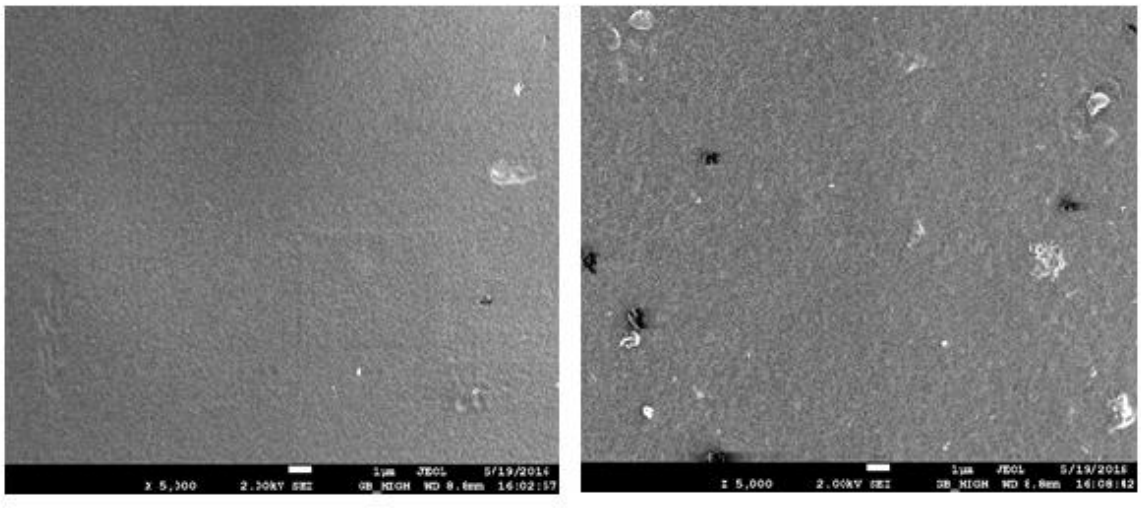

(a) Fouled CTA active layer (b) Fouled TFC active layer

Figure 5.28: SEM images for CTA and TFC membrane active layers (with 5000 magnification)

The magnification of the fouled membrane samples was increased up to 20,000 during SEM analysis. The images in Figure 2.29 (a) and 5.29(b) reveal the respective SEM images of CTA and TFC membrane samples.

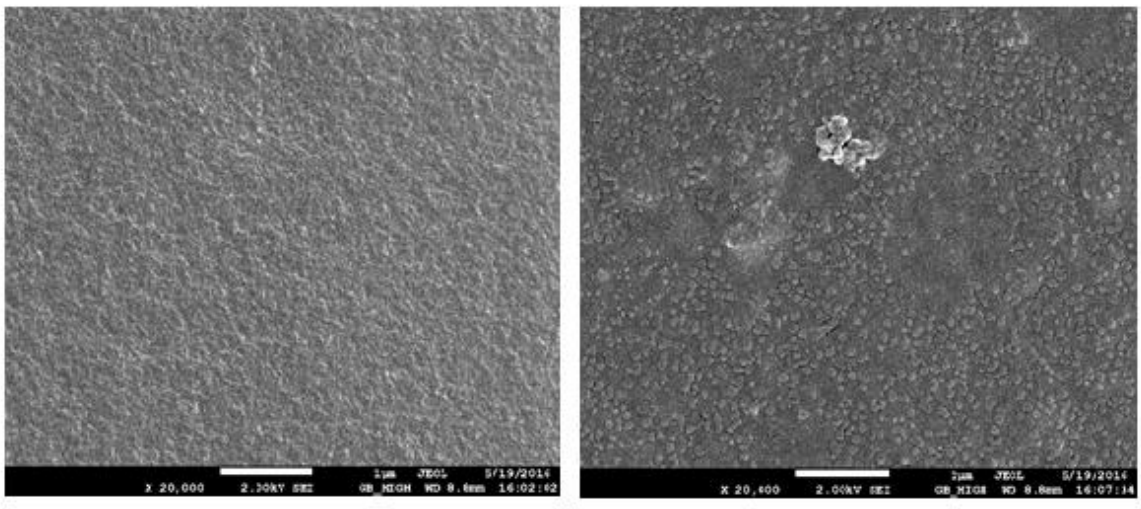

(b) Fouled CTA active layer (b) Fouled TFC active layer

Figure 5.29: SEM images for CTA and TFC membrane active layers (with 20,000 magnification)

For measuring the roughness, atomic force microscopic (AFM) images were taken for the CTA and TFC active layers square samples (each of them with scale of 5 μm).

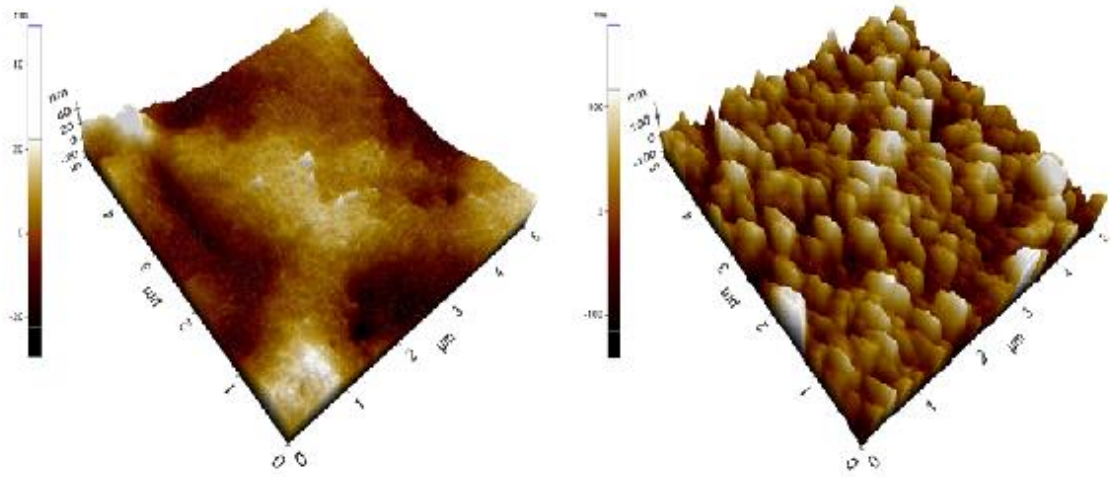

(a) CTA membrane (Roughness: 6.727 nm) (b) TFC membrane (Roughness: 37.954 nm)

Figure 5.30: AFM images for CTA and TFC membrane

It was noted through AFM imaging that the mean roughness of the HTI CTA and TFC membranes was ~6.73mm and 37.95 mm respectively which is considerably smoother compared to usual aromatic polyamide membranes (Tang et al., 2007).

5.4 Conclusions

- By using NaCl as draw solute with dosing mechanism and colloidal silica as the foulant, fouling was not attained. The reason could be attributed to not achieving critical flux value.

- Most of the previous researches on fouling in FO are based mainly on flux analysis. In the current research, even with constant driving force in both FO and RO, water flux decline during both FO and RO were comparable and water flux recovery after

membrane cleaning for both FO and RO reached nearly a similar level. However, an analysis of the hydraulic resistance of foulant layers accumulated on the membranes showed that the increase in foulant resistance for FO was increasingly greater than that for RO. Once allowance has been made for concentration polarization the calculated final R_f for FO was multiple times of that for RO for both CTA and TFC membranes. However the changing level of ICP under fouling conditions has an upside in that it helps to maintain water flux stability.

- Membrane autopsy after the fouling tests showed that more foulant had been deposited on the FO fouled membrane than that in reverse osmosis with both membranes with the load being more than 1.5 times of the RO fouled membrane in both cases. Also the specific foulant resistance was greater with FO than RO.

- Whilst the increase in specific foulant resistance is probably case specific, the reasons for the higher fouling propensity in forward osmosis was explained by a thorough examination of the background theory. This result is a general one that is true for all systems which manifest ICP.

- Cake enhanced osmotic pressure has more effect in osmotically driven membranes than in pressure driven membranes in terms of affecting the fouling resistance. Compared with ICP its role is minor but nevertheless noticeable.

- Overall and not withstanding its higher fouling propensity, FO was found to exhibit higher flux stability against membrane fouling. Excluding those applications where the

reverse salt flux generates additional fouling it may be concluded that for other practical applications FO is potentially a more resilient process than RO.

- Water flushing after fouling successfully removed most of the foulants, indicating that the fouling was mostly reversible. The reversibility of the fouling formed in this study was greater than that found in chapter 4; indeed the extent of reversibility was large.

6

Performance of an osmotically driven module at pilot and bench scale

6.1 Introduction

This chapter is concerned with a performance evaluation and analysis of a pilot scale spiral wound membrane module and a bench scale flat sheet membrane module used in forward osmosis experiments to treat waste water obtained from Bedok NEWater factory, Singapore. The NEWater brine solution, which was used as a feed solution during the experiments, was the retentate of treated sewage waste water from the RO stage that is intermediate between the MBRs and the ultraviolet (UV) treatment. Firstly, the flux decline trend was observed at the pilot scale using a commercial spiral wound (S-W) Cellulose tri acetate (CTA) membrane from Hydration Technologies Innovations. The impact of membrane orientation and its role in the removal of reversible fouling by changing the membrane orientation after specified intervals was undertaken. This first-of-its-kind performance comparison utilised coupons of the membrane and spacers taken from the module. Finally, the potential of the respective modules to recover water from NEWater brine was assessed by taking an innovative approach to obtaining the mass transfer coefficients along with an insightful analysis of the role of windings involved in S-W construction. The findings of this study with a S-W module suggest potential for this niche application; nevertheless the level of the water flux through the S-W module clearly indicates that industrial applications of S-W FO will be constrained to special cases.

6.2 Experimental set up

The bench scale setup used in this study was essentially the same as that described in section 3.2.2.1 (Chapter 3). The pilot scale spiral module setup is schematically shown in Figure 6.1. Draw solution from the draw tank was pumped into the membrane element through a booster pump (BP) as the setup was initially used for PRO tests, whilst a low pressure pump (LP) was used for the feed. Both pumps were operated via the computer.

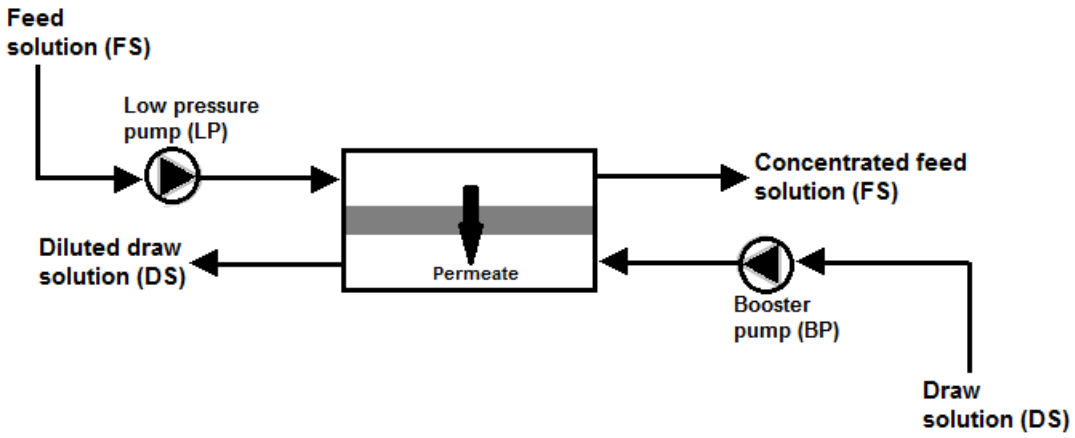

Figure 6.1: Pilot scale forward osmosis setup with an effective membrane area of approximately 1.06 m^2. The feed solution and the draw solution were re-circulated, without concentration correction.

The pressure on both feed and draw sides were kept essentially at zero in order to ensure osmotic pressure difference was the only driving force. The frequency of both of the booster pump and low pressure pump were adjusted in such a way as to obtain the desired flow rates of feed and draw solution i.e. 3 litres per minute. The crossflow velocity for feed and draw solution was calculated to be 18.2 cm/s and 6.7 cm/s respectively.

6.2.1 Experimental procedure

Baseline tests for bench scale were performed using 5 L of the draw solution of 1 M NaCl solution with the same volume of tap water, deionised water, 10 mM NaCl and 25 mM NaCl solution respectively at the feed side. Each of the baseline experiments had two

phases, based on the membrane orientation. At first, the experiment was run by keeping the active layer at the draw side (AL-DS); and for the second phase, the orientation of the membrane was reversed i.e. active layer at feed side (AL-FS). Before reversing the membrane orientation, feed and draw tanks were recalibrated to set values. For the fouling tests, 5 L of NEWater brine solution was used at the feed side while the draw side remained 1 M NaCl solution. During the first phase, the experiment was run with AL-DS orientation for 200 minutes. For the second phase, the orientation of the membrane was reversed by interchanging the feed and draw tubings into the module. Before switching to the second phase, the draw side was flushed thoroughly with tap water to remove any remaining salt.

During the first phase, the feed solution was gradually concentrated as a result of permeation of water from feed side to the draw side, resulting in dilution of the draw solution. By noting the conductivity values of solutions on both sides at the start and end of each test, the change in osmotic pressure difference could be estimated. Before moving to the second phase, both solutions were adjusted to approximate levels. For the feed solution, tap water was added to the feed solution up to the level of the previous test. For counter checking, the conductivity was also checked. A very small increase in conductivity was noted each time but was ignored being negligible. For the draw solution, 5 M NaCl was added until the conductivity of the draw solution matched that of 1 M NaCl solution.

6.2.2 Membrane Module

A commercial FO membrane was used as supplied by Hydration Technologies Innovations (HTI, Albany, OR). It was a spiral wound membrane set up with standard spacer (Spiral Elements Sepra. Mem. 4040). The membrane was made up of Cellulose tri acetate (CTA)

supported by an embedded polyester mesh and had an asymmetric structure. The membrane sheet was sandwiched tightly between mesh spacers and wrapped in a diameter tube and module housing as according to details depicted in Figures 6.2 – 6.3.

Figure 6.2: Spiral wound CTA membrane element (a) inside the module (b) out of the module

Figure 6.3: Cross-sectional view of the spiral wound CTA membrane taken out of its module casing (left) and unwound (right).

The spacer on the draw side was 0.87 mm thick. The one on the feed side was 0.64 mm thick and was in two pieces reflecting the fact that there is a central seal over 70 cm of the element – see Figure 6.3 (right) and Figure 6.5. The mesh sizes are also different as shown in Figure 6.4.

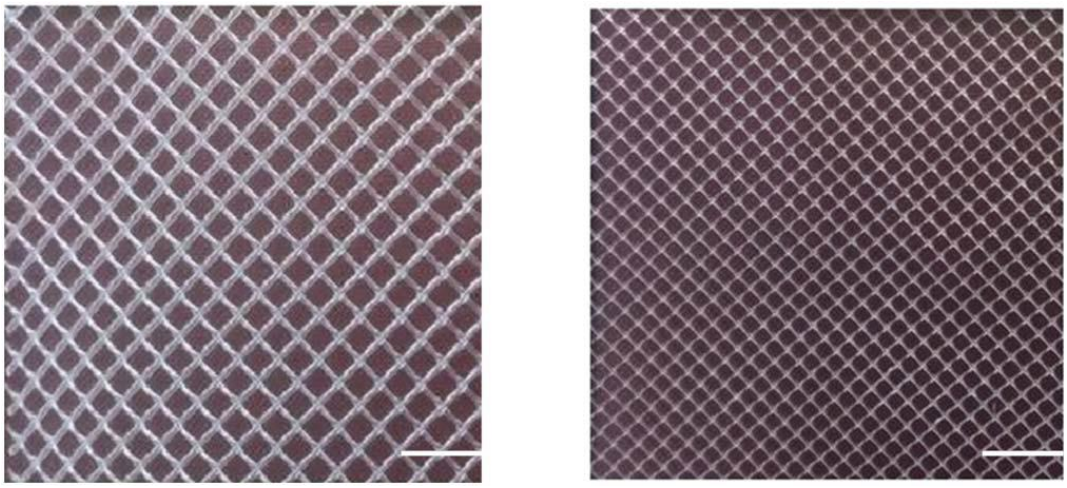

Figure 6.4: Photographs of the draw side (left) and feed side (right) spacers used within the spiral wound module. The scale bar is 10 mm.

The parameters with the defined values for the spiral wound CTA membrane module are revealed in **Table 6.1.** The dimensions of the module element are given in Figure 6.5. This membrane has an asymmetric structure and is prepared by coating cellulose triacetate (CTA) into a polyester mesh (Cath et al., 2006). It has been reported that the membrane itself has a thickness of less than 50 μm (Tang et al., 2010).

Table 6.1: Pilot scale module parameters

Module Parameter	Specifications
Effective membrane area, A_m (m^2)	1.5784
Water permeability, A (m/s Pa)	$2.87 \pm 0.07 \times 10^{-12}$
Feed inlet flow, $Q_{f,in}$ (L/min)	3
Draw inlet flow, $Q_{d,in}$ (L/min)	3
Inner diameter of feed inlet in module, d_{in} (cm)	1.4
Outer diameter of feed inlet in module , d_{out} (cm)	1.8
Thickness of spacer, Ts (cm)	0.0864
Porosity of spacer, Ps	0.84

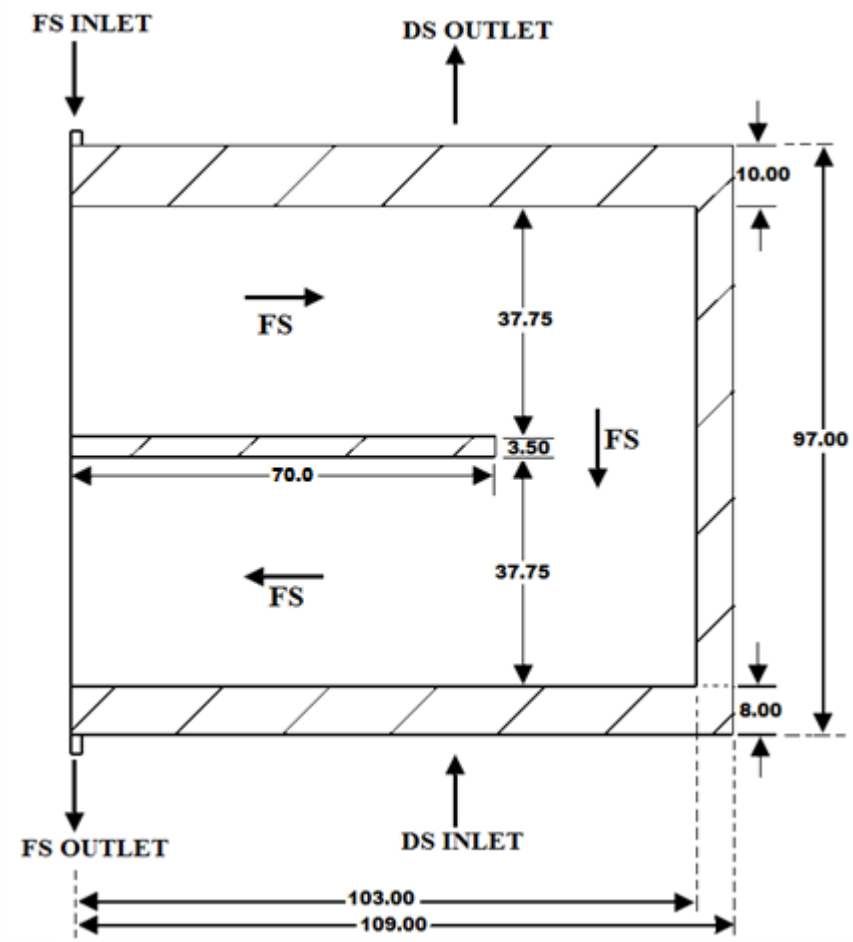

Figure 6.5: Dimensions (in cm) of pilot scale, spiral wound CTA membrane element. The draw flows axially through the module whilst the feed is within the envelope and spirals out and then spirals inwards

6.2.3 Test conditions for experiments

The experimental conditions along with information for the feed and draw solutions for spiral wound (S-W) pilot scale membrane set-up are shown in **Table 6.2** and **Table 6.3**.

Table 6.2: Test conditions for baseline experiments with 25 mM NaCl feed solution using the pilot scale spiral wound CTA membrane module (experimental duration of 4 hours)

		Draw solution (NaCl solution)			**Feed solution (NaCl solution)**		
Test No.	Orientation	Conc. (M)	Flow rate (LPM)	Crossflow velocity (cm/s)	Concentration (mM)	Flow rate (LPM)	Crossflow velocity (cm/s)
1	AL-DS	1	3	6.7	25	3	18. 2
2	AL-FS	1	3	18.2	25	3	6.7

Table 6.3: Test conditions for fouling experiments with NEWater brine using the pilot scale spiral wound CTA membrane module (experimental duration of 4 hours)

		Draw solution (NaCl solution)			Feed solution (NEWater Brine)		
Test No.	Orientation	Conc. (M)	Flow rate (LPM)	Crossflow velocity (cm/s)	Concentration (mM)	Flow rate (LPM)	Crossflow velocity (cm/s)
1	AL-DS	1	3	6.7	As received	3	18. 2
2	AL-FS	1	3	18.2	As received	3	6.7
3	AL-DS	1	3	6.7	As received	3	18. 2
4	AL-FS	1	3	18.2	As received	3	6.7
5	AL-DS	1	3	6.7	As received	3	18. 2
6	AL-FS	1	3	18.2	As received	3	6.7

For the series of tests as listed in **Table 6.3**, after each test, the tank containing draw solution was recalibrated to 100 L of 1M NaCl solution whereas for the tank containing the feed solution (NEWater Brine), tap water was added to refill the tank up to 100 L. As there was no provision of maintaining the concentration (i.e. dosing mechanism), the feed solution became concentrated with the passage of time. This is illustrated by the record of conductivity values in **Table 6.6** noted at the start and end of each fouling test. A Thermo Scientific Orion Star Conductivity meter was used. Although, there were identical flow rates on both sides, the crossflow velocity on the active layer side (axial flow) was lower than that on the support layer (spiral flow), as on the spiral flow side the cross-sectional area was 2.71 times smaller than that of the axial flow.

6.3 Pilot Scale experiments

6.3.1 Baseline experiments

In the initial stage, baseline experiments were performed using a solution of 25 mM of the NaCl solution. The reason for selecting 25 mM NaCl as feed solution was that it has similar osmotic pressure to that of the NEWater Brine solution.

During the tests, there was no provision for maintaining the concentration of feed and draw solutions during the experiments, as normally done in the pilot scale tests. For AL-DS orientation, the osmotic pressure difference was initially 48.3 bar but it declined to 34.2 bar, while for AL-FS orientation, it changed from 48.3 bar to 38.7 bar. The results of the base line experiments with both orientations for duration of around 4 hours are depicted graphically in Figure 6.6.

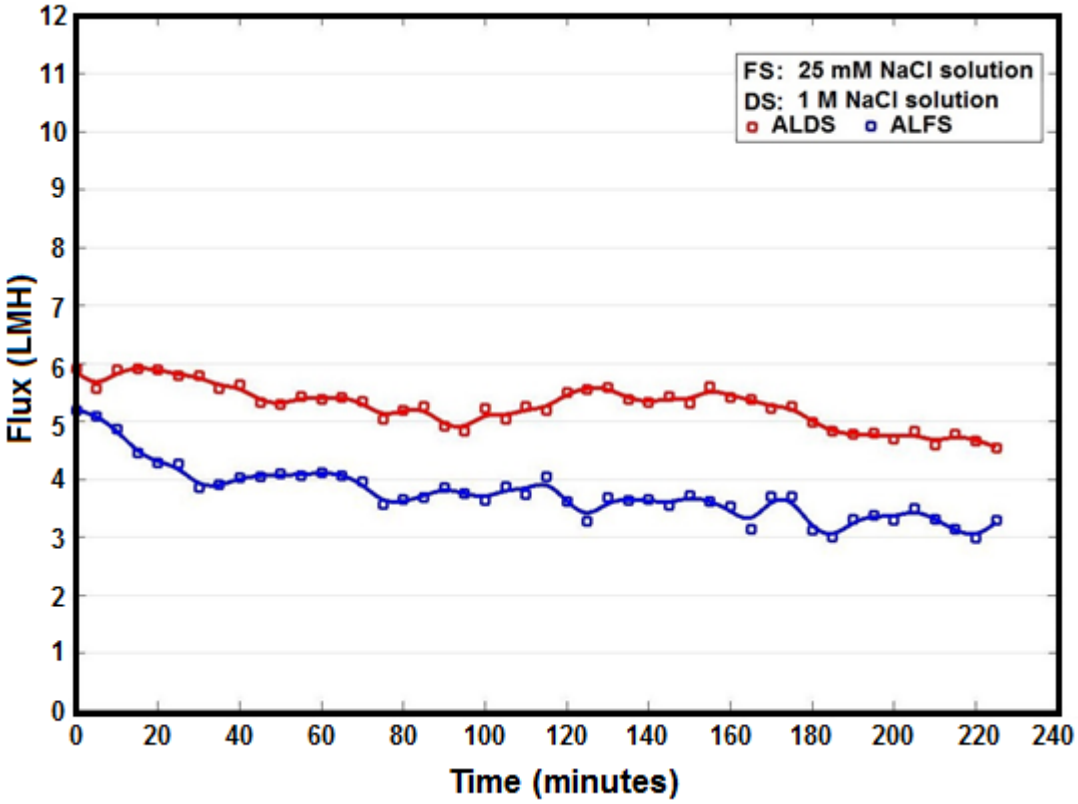

Figure 6.6: Baseline test with 1 M NaCl solution at draw side and 25 m M NaCl solution at feed side with spiral wound CTA membrane at pilot scale (with AL-DS and AL-FS orientation). The osmotic flow caused the feed solution to increase in salinity and the draw solution to decrease in salinity

The results reveal that when the active layer faced the draw side a higher flux was obtained than when the active layer was oriented towards the feed solution. The reason is discussed in detail in next section. In addition to that, a sharp flux decline can be seen during the first 30 minutes in AL-FS orientation when the flux was declined from 5.2 LMH to 3.85 LMH. This could be attributed to the reason that as the water permeated from feed side to the

draw side (support layer), the salt within the support layer was pushed away and the concentration of the draw solution within the support layer decreased giving rise to ICP. This resulted in abrupt decrease in driving force and the flux is decreased consequently. After a while, the rate of flux decline slowed down. Subsequent gentle decline is attributed to the osmotic flow, and reverse salt flux, which decreased the salinity of the draw and increased the salinity of the feed. However, there was a continuous decline in flux in both cases due to a constant decrease in the osmotic pressure difference (driving force) across the membrane.

6.3.2 Fouling experiments and flux analysis

For the fouling experiments, NEWater Brine collected from Bedok NEWater factory, Singapore was used as the feed solution while at the draw side, 1 M NaCl solution was used. At first, the membrane was oriented in AL-DS mode and was followed by AL-FS mode in the second stage. The flux decline with time for both cases is illustrated in Figure 6.7. The pairs of experiments (AL-DS then AL-FS mode) were repeated twice. Before switching the orientation after each run, the draw side was flushed with deionised water in order to remove traces of salt. The flux trends obtained were the same.

For the FO S-W module CTA membrane at pilot scale, a comparison (Figure 6.7) clearly showed that the AL-DS orientation out-performed that of AL-FS. This is counter intuitive because once allowance is made for the fact that there was no control of either the feed or the draw concentration, and that flux decline would occur due to a weakened driving force, the fouling in AL-DS mode was very modest or non-existent, but fouling was very apparent in AL-FS mode. This is seemingly in contrast to the result for the flat sheet unit (explained later in section 6.4.2.1) where the flux declined from 20 LMH to a plateau of

around 8 LMH when the membrane was in AL-DS orientation. A word ‘seemingly’ is used because one should distinguish between flux decline and the steady-state flux reached once any decline has occurred. It has been concluded that the NEWater brine does not foul the support structure of the membrane when the fluxes are sufficiently low. There remains the question as to why, for the S-W module there is flux decline in AL-FS mode. An initial thought was, “Has the data been inadvertently swapped?”; however examination of the fluxes at the beginning of the runs shows that the fluxes for AL-FS orientation are lower than for AL-DS as one would expect; when the draw is on the same side as the support layer there is stronger internal concentration polarisation and fluxes are lower. Whilst this is expected, the fact that the fouling rates were higher for the AL-FS orientation was unexpected. The data shown is the mean for three runs but all of the individual flux declines in AL-FS orientation were over 40%. In section 6.6, an explanation is considered.

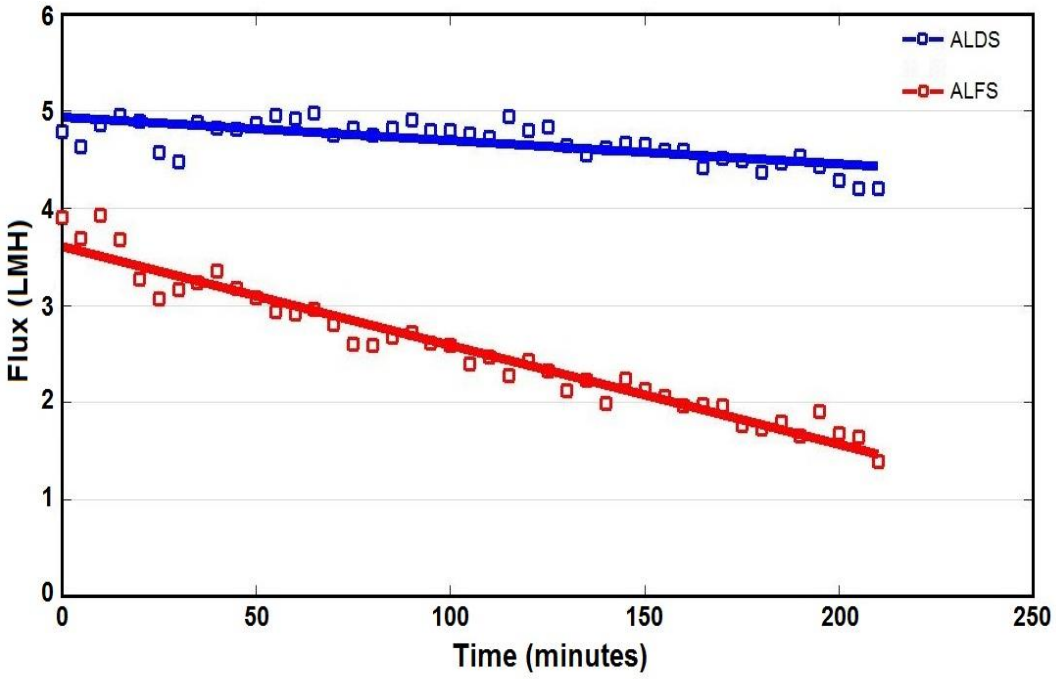

Figure 6.7: Spiral-wound CTA membrane at pilot scale - comparison AL-FS and AL-DS orientations. The flux-time profiles are for a feed of NEWater brine with a 1 M NaCl draw. There was no control of either the feed or the draw concentration and thus the driving force decreased with time; this is the reason for the slight decline in AL-DS orientation. The data shown are the average of three runs. The initial increase in flux in AL-DS orientation is due to the fact that as the orientation is changed from AL-FS to AL-DS, reversible fouling due to NEWater brine on active layer was removed.

For the S-W module, the fact that the NEWater feed was in the channel adjacent to the support side did not lead to significant fouling when the flux was just 5 LMH. There are two key differences between the flat sheet unit and S-W module, namely the volumetric flux and the tightness of the spacers. These factors are discussed further in section 6.6.

6.3.3 Comparative analysis of pilot scale tests of AL-DS and AL-FS orientation

In Figure 6.7, a notable difference in flux trend is noted for both orientations. The reason for this difference can be attributed to effective osmotic pressure difference due to the different effects of internal concentration polarization (ICP) with each orientation. In the case of active layer facing the feed side (AL-FS), dilutive ICP takes place in the support layer, and concentrative ICP occurs in the support layer when active layer faces the draw side (AL-DS). It has previously been noted by other researchers that the effects of dilutive ICP are more severe than concentrative ICP effects and flux values with the AL-FS orientation of the membrane are comparatively low (Gray et al., 2006, Cornelissen et al., 2008, Tang et al., 2010).

In addition to that, with NEWater Brine as feed solution, a severe flux decline for AL-FS was observed during the first 30 minutes during baseline as well as in fouling tests. The reason for this sharp flux decline could be related to ICP effect as explained before (Section 6.3.1). In the present case, the flux continues to decline due to a gradual decrease in driving force as the draw solution is continuously diluted and in the same way, the concentration of the feed solution is continuously increasing.

6.4 Bench Scale experiments

6.4.1 FO baseline experiments

For the bench scale experiments, the setup used is that given in section 3.2.2.1. The crossflow velocity at feed and draw side was 7.4 cm/s. The standard spacers (Spiral Elements Sepra. Mem. 4040) were used on both sides i.e. the same which were used in pilot scale setup (see Figure 6.4). Initially, baseline experiments were performed using a series of feed solutions i.e. tap water, deionized water, 10 mM of the NaCl solution and 25 mM of the NaCl solution. At the draw side, 1 M of NaCl solution was used for each test. The tests were repeated for both membrane orientations, namely active layer on draw side (AL-DS) and active layer on feed side (AL-FS).

6.4.1.1 Tests with AL-DS orientation

The results of baseline tests for AL-DS orientation are shown in Figure 6.8. The results reveal that the feed solution comprising of deionised water and tap water had an average

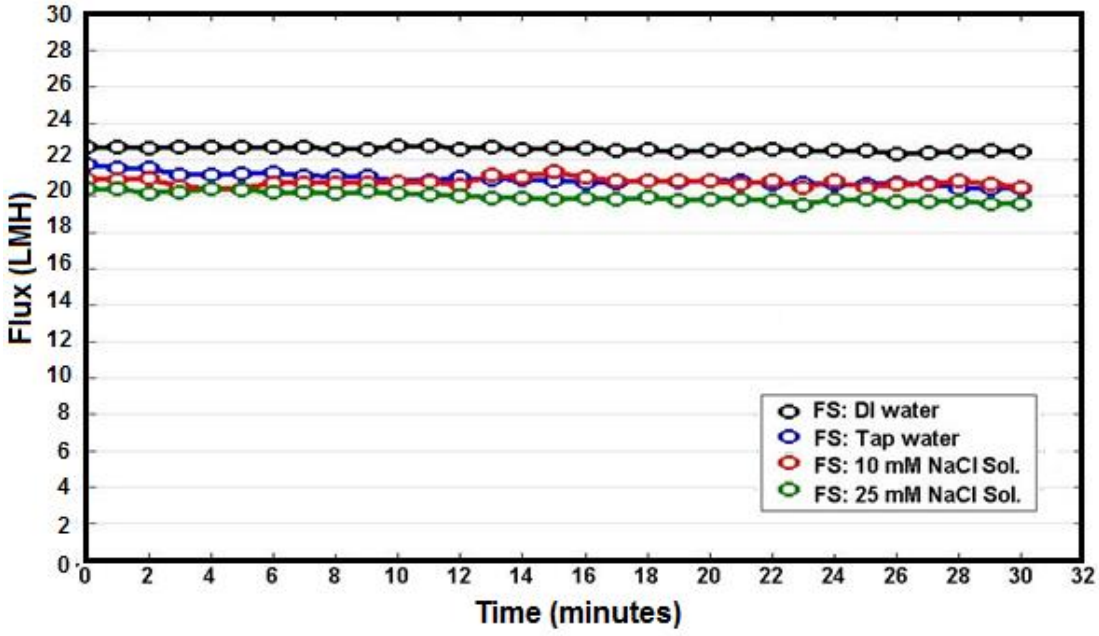

Figure 6.8: Baseline experiments with 1 M NaCl solution at draw side and tap water, DI water, 10 mM NaCl solution, and 25 mM NaCl solution at feed side with flat sheet CTA membrane at bench scale (AL-DS orientation). Lines added have no significance and have been added to distinguish data sets from each other.

flux of 22.6 LMH and 20.9 LMH respectively. However, for the feed solution of 10 mM NaCl solution and 25 mM NaCl solution, the average flux was 20.4 LMH and 19.9 LMH respectively. There is a gradual but mild decrease in flux in all cases.

6.4.1.2 Tests with AL-FS orientation

The results for AL-FS are depicted in Figure 6.9. Unlike AL-DS orientation, upon changing the concentration of feed solution from deionised water to tap water, 10 mM NaCl solution and 25 mM NaCl solution, the flux change is minor; the average flux values (in LMH) for the mentioned feed solutions in sequence are 13.7, 13.4, 12.4, 11.9 respectively. The stability in flux in AL-FS orientation has been observed by other researchers as well (Lay et al., 2011, Parida and Ng, 2013, Zou et al., 2013). Tang et al. (2010) attributed this to the ICP self-compensation effect, which was further endorsed by She et al. (2016) in a recent paper. By this effect, any attempt to change flux is mitigated by a corresponding change in internal concentration polarization and hence the average flux value is altered modestly.

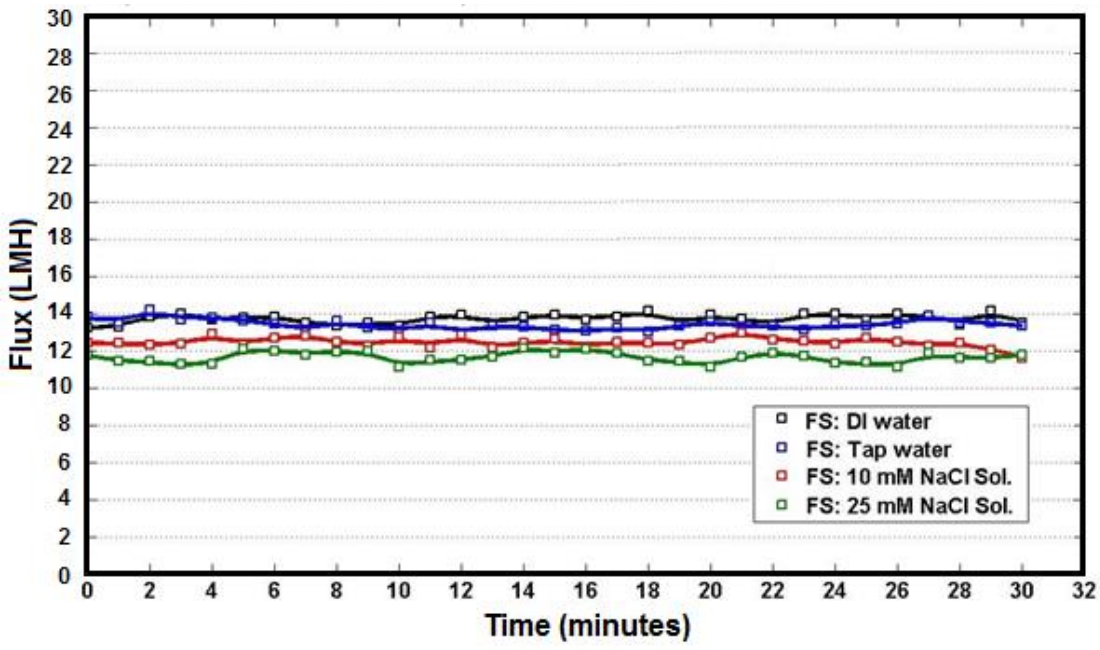

Figure 6.9: Baseline experiments with 1 M NaCl solution at draw side and tap water, DI water, 10 mM NaCl solution, and 25 mM NaCl solution at feed side with flat sheet CTA membrane at bench scale (AL-FS orientation). Lines added have no significance and have been added to distinguish data sets from each other.

6.4.2 FO Fouling experiments and flux analysis

The flux was analysed in fouling experiments using NEWater Brine solution as feed and 1 M NaCl solution as the draw solution.

6.4.2.1 Tests with AL-DS orientation

It was observed that the starting flux was the same as it was with 25 mM NaCl baseline feed solution with the same orientation. A steep gradient could be seen in the first hour for the flux curve; however, there is steady decline of flux afterwards. Change in flux with time for NEWater Brine feed solution and 25 mM NaCl solution is shown in Figure 6.10 indicating a comparison with 25 mM NaCl, which is of similar salinity. This is for the flat sheet unit operated in AL-DS orientation and both feeds, but particularly the NEWater brine, foul the support structure at the fluxes generated. This was done in order to have a fair comparison with the pilot scale experiments, as explained earlier in section 6.3.

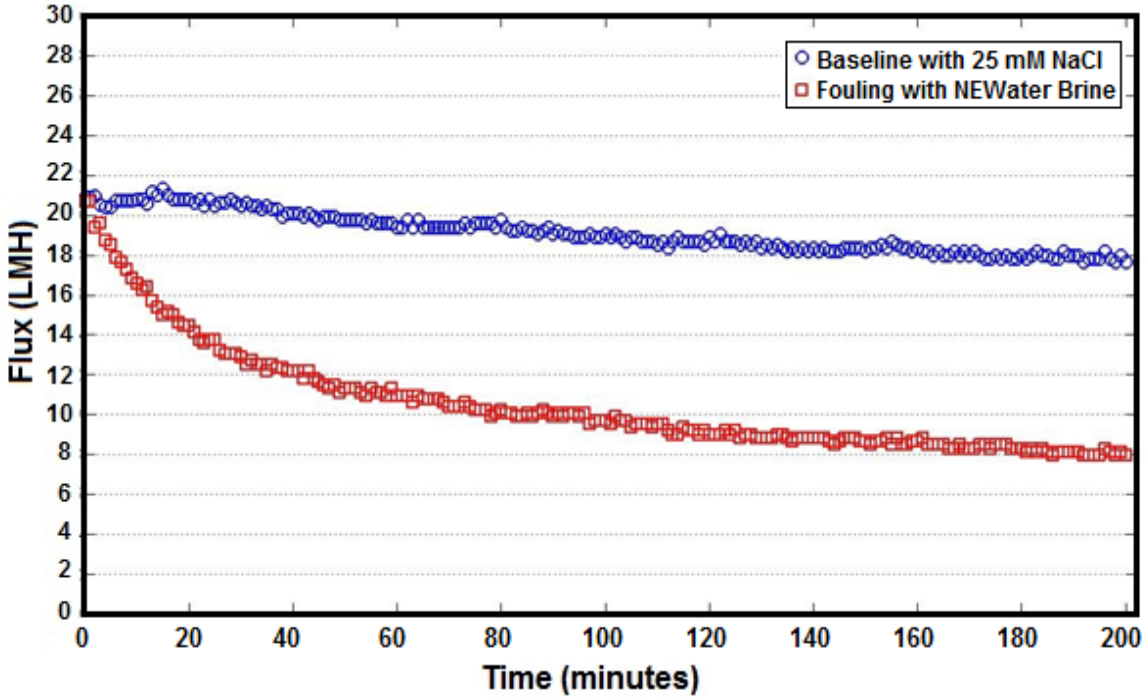

Figure 6.10: Flux Vs Time for FO for fouling and base line tests with NEWater Brine and 25 mM NaCl solution at feed side respectively and 1 M NaCl solution at the draw side with flat sheet CTA membrane at bench scale (AL-DS orientation)

In AL-DS orientation, concentrative internal (and external) concentration polarization takes place at the feed side. However, dilutive external concentration polarization takes place at the draw side.

6.4.2.2 Tests with AL-FS orientation

After the fouling test with active layer on draw side (AL-DS), the orientation of the membrane was reversed to active layer on the feed side (AL-FS). Initially, the flux was only 7.65 LMH due to the foulant deposits within the support layer from the previous fouling experiment (with AL-DS orientation). The fouling layer was gradually removed and the flux increased to that of the baseline experiment after about 25 minutes.

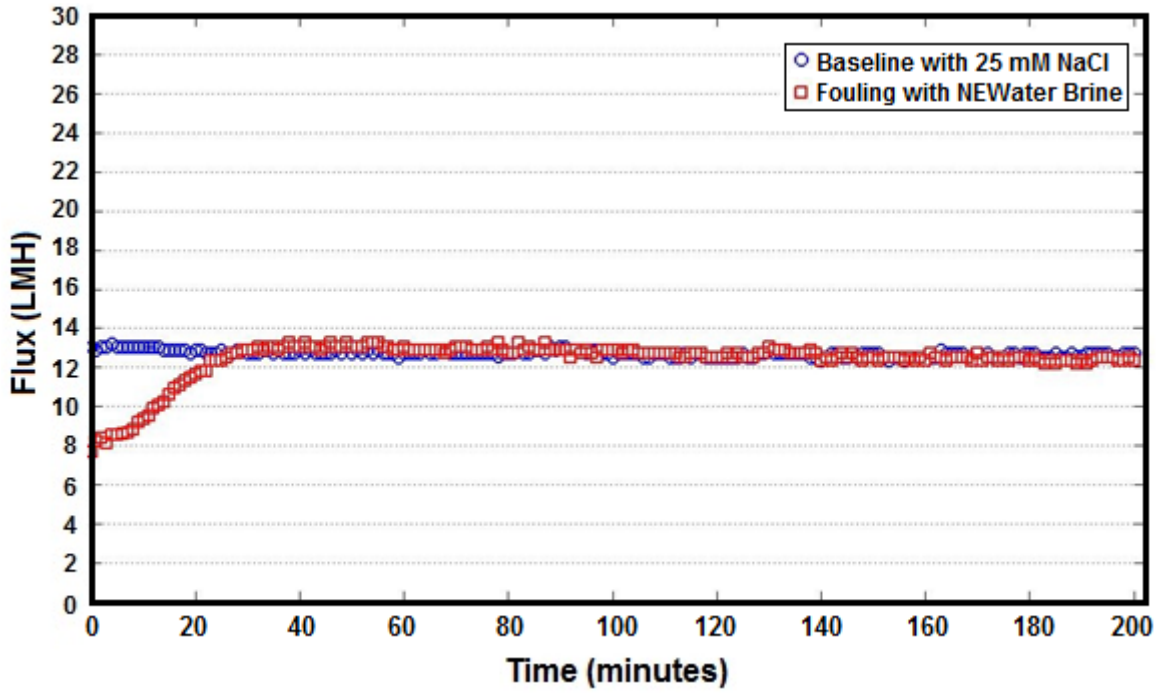

Figure 6.11: Flat sheet CTA membrane at bench scale run in AL-FS orientation, operated under standard conditions, after having been run in AL-DS orientation. Comparison of Flux vs Time curves for (a) NEWater Brine and (b) 25 mM NaCl solution. For (a) there is an increase in flux over the first 30 min as the fouling accumulated during the AL-DS run is cleared.

Unlike the results in Figure 6.10 for AL-DS, those in Figure 6.11 for AL-FS with the same feed solution and draw solution show no divergence between the baseline and the fouling experiments with AL-FS orientation. This is notable. There are minor declines in flux, but

that due to the foulants in NEWater brine is matched by the decline in baseline test. The decline due to the presence of the fouling is partially compensated by the ICP self-compensating effect, which is important for this orientation.

6.4.2.3 Comparative analysis of bench scale tests of AL-DS and AL-FS orientation

There is a notable flux decline with NEWater brine as feed solution in AL-DS orientation which was more abrupt in the beginning, though the steepness of the flux graph is lowered in the later stage. The main reason is that in AL-DS orientation, the support layer faces the feed solution allowing foulant particles to pass easily into the support layer and this results in internal clogging within the support layer structure (Tang et al., 2010). This likely reduces the porosity of the membrane and possibly blocks the membrane pores. This reduction in porosity results in an increase in the value of the structural parameter, which is defined as the product of the support layer thickness and tortuosity over its porosity (Loeb et al., 1997):

$$S = \frac{\tau l}{\varepsilon} \tag{6.1}$$

where, τ is the tortuosity of the membrane; l represents support layer's actual thickness and ε is the porosity. The greater the value of the structural parameter, the lower the mass transfer coefficient for the support side (She et al., 2016).

Moreover, the back salt diffusion from the draw side to the feed side contributes in cake enhanced osmotic pressure (Hoek and Elimelech, 2003, Chong et al., 2007). Another

important reason for the stability of flux in AL-FS orientation with relatively less fouling propensity in comparison to that in AL-DS orientation due to the lower effective driving force, as explained earlier. Owing to this effect, the flux in AL-FS orientation is controlled and more stable but fouling still not ignorable. Longer term tests would be desirable.

6.4.3 RO baseline experiments

In order to calculate the values of physical parameters of the CTA membrane used in the experiments under discussion in this chapter, a limited number of reverse osmosis baseline experiments were conducted using the same membrane. The membrane was oriented in AL-FS direction and a feed solution of 10 mM NaCl solution was used. Initially, the applied hydraulic pressure was 3.5 bar, which was further elevated to 6.9, 10.3 and 13.8 bar in a sequential manner. The flux was noted for each test, as depicted in Figure 6.12.

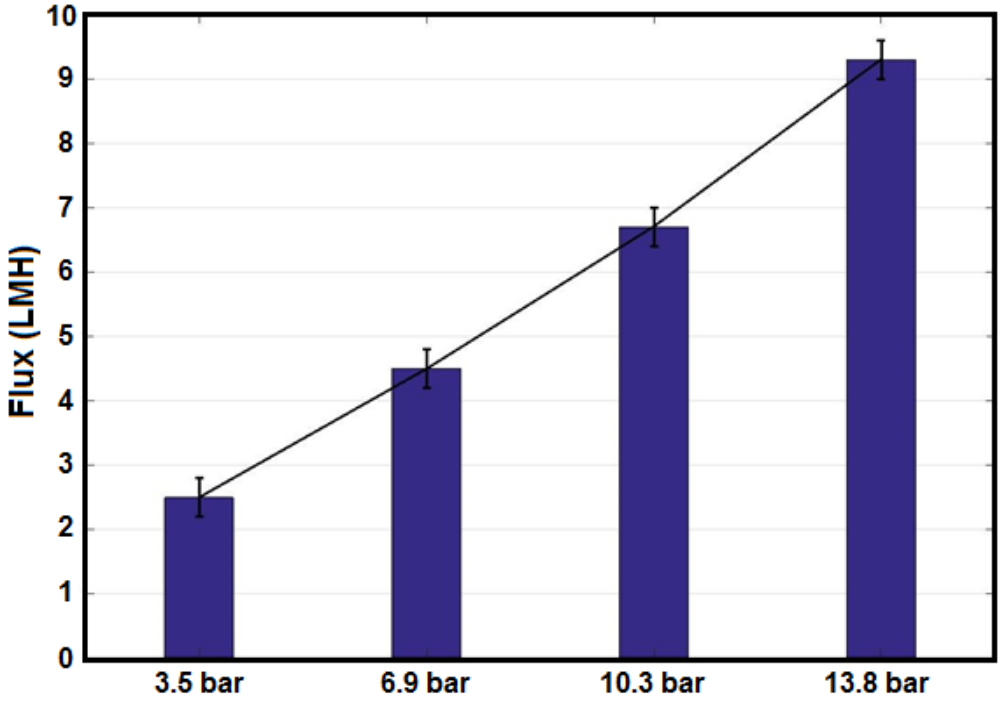

Figure 6.12: Flux values for RO base line tests with gradual increase in hydraulic pressure with 10 mM NaCl feed solution with flat sheet CTA membrane at bench scale (AL-FS orientation)

6.5 Physical properties of feed solutions

6.5.1 Determination of water permeability and salt permeability coefficient

In the RO tests, water flux increased linearly as the hydraulic pressure increased. The permeability was determined in the flat sheet bench scale unit to be 0.75 LMH per bar which gives an 'A' parameter of 2.08×10^{-12} m/s per Pa. This is close to the value of 1.87×10^{-12} m/s per Pa determined elsewhere (Achilli et al., 2009) and comparable with the value of 3.3×10^{-12} m/s per Pa (Wei et al., 2011). The value determined experimentally was used in all subsequent calculations.

From measurements of the conductivity before and after tests with the S-W module, and from knowledge of the starting and finishing volumes, the reverse salt flux was calculated for the sets of data available. This was then used to calculated values of 'B' parameter. The data for AL-DS and AL-FS were divided into two groups and Equation (6.2) used to calculate 'B', given the 'A' value of 2.08×10^{-12} m/s per Pa.

$$\frac{B}{A} = \frac{J_s}{J_w}\beta RT \tag{6.2}$$

For AL-DS, the 'B' value was 2.44×10^{-7} m/s but for AL-FS it was 1.88×10^{-7} m/s. These values are comparable with the value obtained using an RO set-up for the same membrane, namely 2.56×10^{-7} m/s (see entry CTA-HW in Table 3 of (Wei et al., 2011)).

6.5.2 Determination of mass transfer coefficients

The flux data obtained with the flat sheet bench scale unit for various saline solutions was used to determine the mass transfer coefficients. As the channel dimensions and crossflow

velocities in bench scale rig on either side were identical, and the variations of density and viscosity with salt concentration are minor, the Reynolds numbers for the two flows could be taken to be the same. The diffusivity of salt in water, D, has a moderate dependency upon concentration and so allowance was made for this (Vitagliano and Lyons, 1956). Following some early work on spacer characterisation in spacer-filled channels, the Sherwood number was taken to be proportional to the Schmidt number raised to the power 0.33, thus, the mass transfer coefficient in the channel was taken to vary with $D^{0.67}$ (Da Costa et al., 1994). If the correlation in were to have been used, the variation would have been taken to be $D^{0.60}$ (Achilli et al., 2009).

For the channel adjacent to the active layer the mass transfer coefficient is designated as k_c where subscript 'c' indicates channel. For the channel adjacent to the support layer, the mass transfer coefficient is designated as k_{sup} where subscript 'sup' indicates the combined mass transfer coefficient for the support layer itself and the adjacent external mass transfer layer. The former can be written as D/S where D is the diffusivity of salt in water (it has a moderate dependency upon concentration (Vitagliano and Lyons, 1956)) and *S* is the structural parameter, defined as the product of the support layer thickness and tortuosity over its porosity coefficient is designated as k_c where subscript 'c' indicates channel. For the channel adjacent to the support layer the mass transfer coefficient is designated as k_{sup} where subscript '*sup*' indicates the combined mass transfer coefficient for the support layer itself and the adjacent external mass transfer layer. The former can be written as D/S where D is the diffusivity of salt in water (it has a moderate dependency upon concentration (Vitagliano and Lyons, 1956) and S is the structural parameter (see equation 6.1). Thus,

$$\frac{1}{k_{sup}} = \frac{1}{k_c} + \frac{S}{D} \tag{6.3}$$

For the AL-FS orientation, the equation relating flux, ‘A’, ‘B’ and the mass transfer coefficients k_c and k_{sup} can be written as:

$$J_w = A\left[\pi_{ds}\, exp\left(-\frac{J_w}{k_{sup}}\right) - \pi_{fs}\, exp\left(\frac{J_w}{k_c}\right)\right] + B\left[exp\left(-\frac{J_w}{k_{sup}}\right) - exp\left(\frac{J_w}{k_c}\right)\right] \quad (6.4)$$

For the AL-DS orientation, the equation relating flux, ‘A’, ‘B’ and the mass transfer coefficients k_c and k_{sup} can be written as:

$$J_w = A\left[\pi_{ds}\, exp\left(-\frac{J_w}{k_c}\right) - \pi_{fs}\, exp\left(\frac{J_w}{k_{sup}}\right)\right] + B\left[exp\left(-\frac{J_w}{k_c}\right) - exp\left(\frac{J_w}{k_{sup}}\right)\right] \quad (6.5)$$

These equations are fully consistent for those for FO found elsewhere e.g. (She et al., 2016) but are presented in a manner which avoids the use of an overall mass transfer coefficient. Furthermore, it is readily seen that given (i) knowledge of fluxes and concentrations (and hence values of π_{ds} and π_{fs}); (ii) estimates of the mass transfer coefficients k_c and k_{sup}, and (iii) an estimate of the ‘B’ parameter then the ‘A’ parameter can be checked. The estimate of the ‘B’ parameter was constrained to be within 10 % of the literature value cited above.

As is clear from Equation (6.5), and the earlier work of Sagiv et al. (2015), estimation of the mass transfer coefficients depends on the permeability coefficients. For a given flux, over-estimation of the RO derived coefficients ‘A’ and ‘B’ yields lower mass transfer coefficients and vice versa. Now, it might be supposed that with sufficient data sets at various values of draw and feed salinities one could avoid the use of any RO derived coefficients and use just FO data to obtain estimates of coefficients ‘A’ and ‘B’ and the two mass transfer coefficients k_c and k_{sup}. In principle, the number of data sets to hand was

sufficient but given the uncertainties in the experimental data and the form of the equations, the variation in salinity was insufficient. Thus, in common with others, the RO derived coefficients were used to inform the FO analysis.

For the flat sheet bench scale unit, there were six data sets and the fluxes were invariant with time when saline solutions were used as feed. The methodology for obtaining the best estimates of the two mass transfer coefficients was to change the values of k_c and k_{sup} (and 'B' within its constraint) until the six calculated values of 'A' found from Equations (6.4) and (6.5) gave values of 'A'; as close as possible to the set value of 2.08×10^{-12} m/s per Pa (i.e. 0.208 μm/s per bar). The outcome is summarised in **Table 6.4**. "The two values of mass transfer coefficient" are referred since there are two basic values and all other values could be linked to the base values by Equation (6.6).

$$\frac{k}{k_0} = \left(\frac{D}{D_0}\right)^{2/3} \tag{6.6}$$

The values of mass transfer coefficients were independent of Reynolds number as it was invariant across these data sets. The $D^{0.67}$ allowance for the variation in diffusivity gave a maximum 5.4 % correction in mass transfer coefficient.

The value of 321 μm for the structural parameter is similar to that obtained by (Tang et al., 2010) who gave a value of ~400 μm but they made no allowance for external concentration polarisation (ECP) in their calculations. Their value was determined from RO experiments so the effect of ECP would have been only on one side.

The procedure for calculating the FO S-W module mass transfer coefficients k_c and k_{sup} was similar except that for the 'B' parameter the experimental values 2.44×10^{-7} m/s (AL-

DS) and 1.88×10^{-7} m/s (AL-FS) were used. The results are summarised in **Table 6.5**. The estimated values are based upon an assumption that the structural parameter would be unchanged and that the mass transfer coefficients would scale with Reynolds number (based upon an empty channel) raised to the power of 0.33. The respective Reynolds numbers are 360 for the FS unit (both sides), 296 for the feed side of the S-W module and 108 for the draw side of the S-W module. Given that the spacers are a tight fit in the S-W unit, but unduly loose in the FS unit, the scaling is very approximate. At this stage, it is noted the main significance lies with the experimental finding that the mass transfer coefficients in the S-W module are roughly half those found in the flat sheet unit. This is discussed further in Section 6.6.

Table 6.4
Data from flat sheet bench scale rig and resultant mass transfers and structural parameter, S.

Orientation	Feed salinity (mM)	Flux J_w μm/s	Estimated 'A' μm/s per bar	k_c μm/s	k_{sup} μm/s	S μm
AL-DS	0	6.28	0.228	14.1	3.5	321
AL-DS	10	5.53	0.205			
AL-DS	25	4.89	0.186			
AL-FS	0	3.81	0.229			
AL-FS	10	3.44	0.199			
AL-FS	25	3.31	0.195			

Table 6.5
Analysis of results from Spiral-Wound module.

Orientation	k_c μm/s	k_{sup} μm/s	S μm
Measured	6.66	1.71	645
Estimate for AL-FS based on FS unit using $Re^{0.33}$	13.2	3.11	321
Percentage of expected	50	55	200

6.6 Analysis of spiral wound pilot scale and flat sheet bench scale setups

During the analysis, the results from the mass transfer analysis have been addressed prior to the fouling results. For the S-W module, the value of 6.66 μm/s for the channel adjacent to the active layer superficially compares well with those obtained by Da Costa et al. (1994) who evaluated a large range of spacers. Figure 10 in (Da Costa et al., 1994) gives values of 4–8 μm/s depending on the angle of the spacer but in that study dextran, which has a significantly lower diffusivity than salt, was used. Thus, the magnitude of the mass transfer coefficients found for the S-W module herein might be considered to be surprisingly small.

One of the main results in the current study is that the calculated mass transfer coefficients in the S-W module are only about 50% of the corresponding values in the flat sheet unit. This experimental comparison was not made at the same crossflow velocity. Given that the spacers are turbulence promoters one might have expected increases in mass transfer coefficients as the Reynolds numbers were similar. However, this was not the case. Now the local fluxes in the S-W module will be higher than those based on the superficial area because part of the membrane surface will be obscured at the points of contact between the spacer and the membrane. In FO units, this affects the mass transfer on both sides of the membrane and increases the degree of concentration polarisation on both sides. The tightness of the winding will also influence the degree of "blinding" and the estimated value of 'S' at 645 μm (Table 6.5) may reflect the fact that the effective porosity has been reduced through blockage of some pores. As shown by Equation (6.1), 'S' is inversely proportional to porosity so a decrease in the latter increases the former.

Not having had a close duplication of the hydrodynamic conditions between flat sheet and S-W modules has generated results suggesting that the tightness of the binding in S-W modules is important. This is probably a particular strong effect for FO because of the importance of mass transfer on both sides of the membrane, and is worthy of further investigation.

The approach outlined in Section 6.5.2, for the calculation of mass transfer coefficients, will permit the mining of a wide range of data sets. Where, the Reynolds numbers are different on each side, the procedure will need to be generalised but this is straightforward. An analysis of the equations indicates that a wide range of feed solutions of different salinities should be used in order for accurate estimates of all parameters and coefficients to be obtained.

These are the first results for a S-W module to suggest that the potential application of recovering water from NEWater brine could be low fouling. In AL-DS orientation, the NEWater brine was found to hardly foul the support structure of the membrane albeit at the low flux of 5 LMH. Whilst with the bench scale flat sheet rig, there was fouling at an initial flux of 20 LMH (with flux declining to a steady-state value of 8 LMH), this fouling was readily reversible. It was established that reversal of the flow cleared the fouling within the support structure; see Figure 6.11 and comment in the caption. Thus at the low fluxes achieved in the S-W module the fouling potential of the NEWater brine is per se low. Whether these fluxes can lead to an economic process has yet to be established.

A key advantage of this potential application is that the draw solution would be brine from a seawater desalination plant which would be returned to that plant for recovery of the

water extracted from the NEWater brine. Thus there would be no need to regenerate a draw solution and this is one of the few FO applications that might come to fruition. Much of the FO literature mistakenly equates the absence of high pressure pumps (as required by RO) with great potential for reducing energy requirements seemingly oblivious to the energy requirements of draw regeneration, which is generally required. Agreeing with an anonymous review of this work that the type of application is critical and that over-generalisation of the potential of FO should be avoided. FO has a place in the treatment of challenging waters, and potentially for special cases such as the present example, but realistic applications are not numerous.

Regarding the flux decline exhibited by NEWater brine, there are four results overall, there being two orientations for both the flat sheet unit and the S-W module. The AL-FS result for the flat sheet unit indicates that the fouling potential of NEWater brine per se is very low indeed. In an essentially open channel, in AL-FS orientation, the critical flux (Field et al., 1995) was not exceeded. With the S-W module, there is essentially no fouling in AL-DS orientation. Here, the draw flows across the more open, less dense spacer (see Figure 6.4). Due to the mass transfer limitations only a low flux of circa 4.5 LMH was achieved but at this flux there was little fouling even though the NEWater brine was in the channel adjacent to the support structure.

However, with the S-W module there is fouling in AL-FS orientation but this is probably due to the fouling of the tight spacer (see Figure 6.4) by the draw solution. The spacer in the tightly wound spiral module probably increases the ‘S’ parameter, whereas in the bench-scale rig it does not. One might suppose that the NEWater brine would be more fouling than the draw solution but the results suggest that this was not the case. The

NEWater brine that had passed through a microfiltration membrane during the NEWater process, and which arrived in carboys, was not diluted whereas the draw solution was prepared with tap water. It is suggested that in future pilot plant work, the draw solution needs to be filtered to avoid the draw solution fouling the support layer and/or clogging the fine mesh. The unexpected fouling in the present work was readily reversible because the tests were run in alternate fashion and there was no discernible influence of an AL-FS run upon the next AL-DS run. Taken together the results suggest that with an appropriate spacer, NEWater brine should be essentially non-fouling of a CTA membrane operated at an appropriate flux.

Table 6.6: Summary of baseline and fouling FO tests at pilot and bench scales at AL-DS and AL-FS orientations. The draw solution used was 1.0 M NaCl.

		Test No.	Orientation	Feed solution	Test duration	Applied Osmotic pressure difference (bar)[1]	Initial flux (LMH)	Flux at the end of the test (LMH)	Conductivity of feed at start (mS/cm)	Conductivity of feed at end (mS/cm)	Conductivity of DS at start (mS/cm)	Conductivity of DS at end (mS/cm)
Pilot scale experiments	Baseline experiments	1	AL-DS	25 mM NaCl sol.	4 hours	49.1	5.9	4.5	2.98	5.44	83.82	62.76
		2	AL-FS	25 mM NaCl sol.	4 hours	48.3	5.1	3.3	2.97	4.25	83.44	67.01
	Fouling experiments	3	AL-DS	NEWater	4 hours	49.1	4.2	4.5	2.61	4.77	83.92	64.00
		4	AL-FS	NEWater	4 hours	48.9	4.9	1.0	2.92	4.18	83.95	68.45
		5	AL-DS	NEWater	4 hours	48.5	4.8	3.9	3.82	6.88	84.1	62.97
		6	AL-FS	NEWater	4 hours	48.3	4.4	1.5	3.72	5.48	83.75	66.59
		7	AL-DS	NEWater	4 hours	48.4	5.3	4.2	3.65	6.95	83.80	62.08
		8	AL-FS	NEWater	4 hours	48.3	5.4	2.1	4.03	5.67	83.95	67.42
Bench scale experiments	Baseline experiments	9	AL-DS	DI water	30 min.	49.5	23.4	22.5	0.0028	0.0098	83.65	83.61
		10	AL-DS	Tap water	40 min.	49.5	20.6	19.5	0.292	0.301	83.75	83.48
		11	AL-DS	10 mM NaCl	35 min.	49.1	20.4	20.1	1.21	1.22	83.60	83.59
		12	AL-DS	25 mM NaCl	40 min.	48.3	17.9	17.5	2.89	2.90	83.35	83.13
		13	AL-FS	DI water	50	49.5	13.8	13.5	0.00198	0.00608	84.3	83.95
		14	AL-FS	Tap water	40	49.5	13.8	13.3	0.296	0.301	84.75	84.13
		15	AL-FS	10 mM NaCl	40	49.1	12.4	12.1	1.22	1.23	84.3	84.08
		16	AL-FS	25 mM NaCl	40	48.3	11.8	11.7	2.81	2.82	83.85	83.63
	Fouling experiments	17	AL-DS	NEWater	4 hours	49.1	20.7	7.9	2.49	2.57	83.8	82.76
		18	AL-FS	NEWater	4 hours	48.8	9.3	12.3	2.52	2.61	83.35	81.58

[1] The applied osmotic pressure difference was estimated from knowledge of the draw solution concentration and the measured conductivity of NEWater feed

6.7 Conclusions

It was observed that for the bench scale rig, switching the orientation resulted in removal of the reversible fouling and improvement in flux. In AL-FS orientation, the flux was comparatively stable with low propensity to fouling, as noted previously by Tang et al. (2010). The two observations that (i) the foulants are removed upon a change of orientation from AL-DS to AL-FS and (ii) that the flux in AL-FS follows (after the initial transition) the flux for baseline solution suggest that the foulants are not bound to any surface. Thus, the decline in AL-DS orientation is probably due to pore filling and a change in 'S' parameter.

Comparatively, bench scale experiments with flat sheet membrane setup showed significantly higher flux values than those in spiral wound pilot scale setup. The low values of flux with the commercial spiral wound module are probably related to much more intense ICP within this module compared with the flat sheet bench scale set-up. If osmotically driven processes are to play an increasing role, attention needs to be given to the necessity of improved channel hydrodynamics. The mass transfer coefficients in the Spiral-Wound module were around 50% lower than the corresponding values in the Flat Sheet unit and this severely limited the fluxes.

At pilot scale, like in bench scale, higher flux was observed in AL-DS orientation (during baseline and fouling experiments) as compared to AL-FS orientation, indicating that overall mass transfer was poor in AL-FS orientation. With the bench scale experiments, switching of the orientation resulted in improvement of the flux indicating reversible fouling.

The fouling potential of NEWater brine per se is low but orientation and choice of spacer is crucial to performance. In an open channel in AL-FS orientation the critical flux was not exceeded.

Owing to the availability of a readily available saline stream, which does not require regeneration, recovering water from NEWater brine by FO may be economically feasible even though the fluxes are very modest.

7

Concluding remarks and recommendation for future work

7.1 Summary and concluding remarks

Although it has already attracted a lot of attention by researchers, there is still room available for investigation on membrane fouling. The common problem in the application of osmotically driven and pressure driven membrane filtration is fouling. This not only results in permeation flux decline but also necessitates periodic cleaning. The current research work reveals some important findings which could significantly contribute to improving the efficiency of membrane filtration through FO and RO.

With regard to the ceramic membrane study, the application of a combination of strong alkaline solutions along with oxidizing agent (sodium hypochlorite in the current case) followed by the acid was found to be suitable for cleaning. The combination of these chemicals is widely accepted to be appropriate by other researchers for cleaning the ceramic membranes. For the foulants used, namely dextran and carboxymethyl cellulose (CMC), it was found that intermittent rinsing can play a significant role in removing the reversible fouling and this rate of removal increases if the temperature of the rinsing water is increased. It was noted that the rate of change of foulant resistance with the transmembrane pressure was significantly greater for the dextran solutions than for the CMC solutions.

The main study compared the membrane fouling of FO and RO for two types of membrane, cellulose tri acetate (CTA) and a thin film composite (TFC) membrane. Silica and alginate were selected as model organic foulants. For the former, the critical flux concept was relevant in that no fouling was obtained at fluxes of 17.8 LMH and 25.3 LMH for TFC membrane and CTA membrane respectively. Higher fluxes could not be obtained with the draw solutions available.

With regard to alginate, fouling was found that resulted in the water flux decline for both FO and RO when starting from a flux of 17.5 LMH. The flux trend was similar for both FO and RO but as the influence of ICP is abated with decreasing flux the calculated foulant resistance for FO was increasingly greater than that for RO. It was found that the calculated foulant resistance in FO membranes is increasingly greater and more severe than that in RO when operated on identical experimental conditions, and that greater flux decline in RO does not reflect greater fouling accumulation. The reversibility of fouling on rinsing was greater with FO; with FO 100% flux recovery can be obtained. This was further confirmed by the measurement of fouling accumulation on the membrane surface, which showed that the foulant accumulation on the membrane surface during FO test was greater than that during RO fouling test. Whilst FO fouling may be quantitatively greater in amount, it is gentler. For FO, internal concentration polarization continues to play a vital role in flux decline even in the presence of severe fouling.

In Chapter 5, it was shown that the effective driving force can be as low as a 3% of the applied driving force for a TFC membrane and around 19% for a CTA membrane. It clearly demonstrates the severity of ICP, particularly for the TFC membrane. In addition to that, for both membranes, the ratio of effective to applied driving force was found to be increasing

gradually with the decrease in flux. The reason can be attributed to the self-adjusting process in FO which has been explained in detail in Chapter 2.

Along with experimental demonstration, a simulated analysis during the current research endorses the ICP's upside role to help to maintain water flux stability in forward osmosis apart from having a detrimental effect in decreasing the effective driving force.

Whilst the role of specific cake resistance may vary from one case to another, through a thorough investigation, the reasons for the higher fouling propensity in FO was demonstrated after incorporating the background theory. The general findings are applicable for all systems with apparent ICP.

The effect of cake enhanced osmotic pressure was also studied, and it was noted that it plays a modest role in FO in reducing the effective osmotic pressure difference across the membrane ($\Delta\pi_{eff}$) and calculated foulant resistance (R_f).

As demonstrated in section 5.3.2.4, the effect of hydraulic pressure has a negligible effect in compressing the foulant layer. By keeping the flux at zero and applying the hydraulic pressure only for 4 hours, it was observed that there was no increase in foulant resistance (R_f). Instead, the flux was improved, indicating the removal of part of the reversible fouling from the surface of the membrane.

Chapter 6 of the thesis focussed on a study of fouling by real waters at bench and pilot scale using treated waste water obtained from Bedok NEWater factory, Singapore. It was found that flux remains comparatively stable in AL-FS orientation than in AL-DS orientation,

probably due to a lower propensity to fouling and greater ICP-self compensation. For the bench scale set up, it was observed that switching of the orientation from AL-DS to AL-FS mode resulted not only in removal of reversible fouling and improvement in flux but it was also noted that the flux in AL-FS followed the flux for baseline water suggesting that foulants do not bind to any surface in this mode at the imposed flux. Change in structural parameter and severe pore clogging in AL-DS orientation could be the potential reason for intensive flux decline.

It was also observed that the windings of the spiral wound membranes affect the mass transfer coefficient up to a notable effect. Its values in the Spiral-Wound module were around 50% lower than the corresponding values in the flat sheet unit which has a severe effect on flux values as well. This reveals that orientation of the membrane and the choice of the spacers play a crucial role in membrane's performance.

Higher flux values were observed in flat sheet bench scale setup than those in spiral wound commercial setup at identical test conditions. The reason could be attributed to intense ICP in the latter, in which tightly wound spacers act to increase the structural parameter due to which the mass transfer coefficients in spiral wound setup were only around 43% of those in bench scale setup. Unlike in bench scale set up, in overall, the poor mass transfer in both orientations of pilot scale setup resulted in comparatively lower flux values in AL-DS and AL-FS orientations.

7.2 Research hypothesis and implications of the research work

During all phases of the research, cleaning of the membranes has remained an essential part of the studies particularly when it comes to removal of reversible fouling by rinsing.

However, the robustness of the ceramic ultrafiltration membrane meant that different chemicals were used. The reversibility of the fouling formed in studying FO and RO fouling was greater than that found in Chapter 4. Indeed the extent of reversibility was large albeit any variation in temperature was avoided. This reveals that ceramic ultrafiltration membranes exhibit greater irreversibility for fouling than that in polymeric membranes for forward and reverse osmosis processes. In comparison of FO and RO fouling behaviour, forward osmosis is noted to be more prone to fouling than reverse osmosis which agrees with the research hypothesis.

Keeping in account these factors in connection with ceramic and polymeric membrane comparisons may enable a membrane user to have an appropriate choice of membrane, foulants and other conditions as to meet the required targets. Greater fouling in FO and its difference for fouling reversibility than other processes is mainly due to ICP effect. Taking measures to affect ICP in FO may increase the filtration efficiency in FO. Similarly, dealing with the relative factors for other discussed processes will affect likewise. Lastly, the appropriate selection of cleaning method and chemicals for all methods may ensure the effectiveness of respective application and would help to reduce costs as well.

7.3 Recommendations for future work

A number of exciting possibilities could be connected to the work of this thesis.

- *Experiments with incompressible foulants like silica*. In the current research connected to FO experiments with silica as foulant, the critical flux could not be achieved due to limitations with concentration of the draw solution (NaCl brine). For possible future research, the same experiments could be conducted with other suitable options of the

draw solution which may help in increasing the effective driving force (osmotic pressure difference) for achieving the targeted flux values.

- *Extension to other membrane modules*. Although the experimental results on the comparison of FO and RO fouling with current bench scale flat sheet membrane set-up using alginate as model foulant ensured promising findings, a possibility for future work stemming from this could involve other module types like spiral wound, tubular or hollow fibre membranes. A comparison with current results would then be a possible option.

- *Extension to DOTM technique*. Current analysis of fouling in FO and RO was based on mass accumulation and calculated foulant resistance. Another possible option could be the microscopic analysis of fouling in both processes using the method of direct observation through the membrane with suitable transparent membranes. The current results may give a possible option of comparative analysis with the results obtained through DOTM technique.

- *Improved analysis of fouling with NEWater brine*. Current analysis of fouling with NEWater brine as the feed solution was based on flux analysis. The experiments could be further extended to the analysis of foulant accumulation and foulant resistance. Moreover, during these tests, feed and draw solutions were not topped up during the tests due to which the driving force gradually decreased during the test. It is understandable that at pilot scale, it is nearly impossible to keep the driving force constant at accurate level but possible at bench scale.

- *Possible options and design of draw solutions and support layer*. In the current study of NEWater test, 1 M NaCl solution was used as draw solution. While working with AL-FS orientation, the effective driving force was reduced to a large extent due to dilutive ICP. This effect could be reduced by testing other possible options of draw solutions. Structural parameter plays a significant role in designing the support layer. The greater the structural parameter, the lower the mass transfer coefficient.

- *Comparison of forword –flushing with back-flushing.* As tubular ceramic ultrafiltration systems are robust and amenable to hydraulic stresses, it is straight forward to carry out back-flushing with such systems. Therefore, it is recommended that future studies should compare forward-flushing with back-flushing.

APPENDIX – I

Mass transfer coefficients and concentration polarization factors

The water flux (J_w) in membrane filtration can be described (Lee et al., 1981) by the equation:

$$J_w = A\,(\Delta\pi_{eff} - \Delta P) \qquad \text{(i)}$$

where, A is the membrane water permeability coefficient, $\Delta\pi_{eff}$ is the effective osmotic pressure difference across the membrane while ΔP represents the overall applied to reverse hydraulic pressure. The reverse solute flux across the membrane can be described as:

$$J_s = B\,\Delta C_{eff} \qquad \text{(ii)}$$

where, B represents the solute permeability coefficient of the membrane and ΔC_{eff} is the effective solute concentration difference across the membrane. Combining Eq. (i) and (ii) with the van't Hoff Equation to link ΔC_{eff} with $\Delta\pi_{eff}$ one obtains:

$$\frac{J_s}{J_w} = \frac{B}{A\beta R_g T}\left(1 + \frac{A\,\Delta P}{J_w}\right) \qquad \text{(iii)}$$

By Equation (i) and (iii) and via calculations given elsewhere (She et al., 2016), one can take the external and internal concentration polarization in to account and obtain an implicit equation for the water flux. The equation for J_w for AL-FS orientation is:

$$J_w = K \ ln \left[\frac{\pi_{ds} + \frac{B}{A}\left(1 + \frac{A\Delta P}{J_w}\right)}{\pi_{fs} + \frac{B}{A}\left(1 + \frac{A\Delta P}{J_w}\right) + \frac{J_w}{A}\left(1 + \frac{A\Delta P}{J_w}\right) exp\left(\frac{J_w}{k_F}\right)} \right] \quad \text{(iv)}$$

Similarly, for AL-DS orientation,

$$J_w = K \ ln \left[\frac{\pi_{ds} + \frac{B}{A}\left(1 + \frac{A\Delta P}{J_w}\right) - \frac{J_w}{A}\left(1 + \frac{A\Delta P}{J_w}\right) exp\left(\frac{J_w}{k_F}\right)}{\pi_{fs} + \frac{B}{A}\left(1 + \frac{A\Delta P}{J_w}\right)} \right] \quad \text{(v)}$$

K is the overall mass transfer coefficient:

For AL-FS orientation: $$\frac{1}{K} = \frac{1}{K_D} + \frac{1}{k_D} + \frac{1}{k_F} \quad \text{(vi)}$$

For AL-DS orientation: $$\frac{1}{K} = \frac{1}{K_F} + \frac{1}{k_D} + \frac{1}{k_F} \quad \text{(vii)}$$

where, K_F *and* K_D represents the mass transfer coefficients within the support layer for AL-DS and AL-FS orientation respectively. While, k_F and k_D are the mass transfer coefficients near the surfaces of support layer and active layer (depending upon the orientation). Equations (vi)-(vii) indicate that the overall mass transfer coefficient (*K*) is dependent on the coefficients within the support layer (for ICP effect), near the structure of support layer and near the surface of the active layer. The value of '*K*' is significant in demonstrating the extent of concentration polarisation (external and internal).

It is useful to define the following terms. The concentration polarization factors (concentrative and dilutive) are given as:

ALFS orientation

$$\begin{cases} F_{F-ALFS} = \exp\left(\frac{J_w}{k_F}\right) - 1 & \text{(viii)} \\ F_{D-ALFS} = 1 - \exp\left(-\frac{J_w}{K_D}\right) & \text{(ix)} \end{cases}$$

ALDS orientation

$$\begin{cases} F_{F-ALDS} = \exp\left(\frac{J_w}{K_F}\right) - 1 & \text{(x)} \\ F_{D-ALDS} = 1 - \exp\left(-\frac{J_w}{k_D}\right) & \text{(xi)} \end{cases}$$

where, F_F and F_D are concentration polarization factors at feed and draw side respectively as according to orientation. The detailed derivation of Equations (viii)–(xi) can be found elsewhere (She et al., 2016). Re-arranging Equation-(iv) and Equation-(v) and incorporating Equation-(iii), the mathematical equation for the osmotic resistance filtration model is obtained as:

$$J_w = \frac{(\pi_{ds} - \pi_{fs}) - \Delta P - F_D\left(\pi_{ds} + \frac{J_s}{J_w}\beta R_g T\right) - F_F\left(\pi_{fs} + \frac{J_s}{J_w}\beta R_g T\right)}{\mu R_m} \quad \text{(AL-FS orientation)} \quad \text{(xii)}$$

$$J_w = \frac{(\pi_{ds} - \pi_{fs}) - \Delta P - F_F\left(\pi_{fs} + \frac{J_s}{J_w}\beta R_g T\right) - F_D\left(\pi_{ds} + \frac{J_s}{J_w}\beta R_g T\right)}{\mu R_m} \quad \text{(AL-DS orientation)} \quad \text{(xiii)}$$

As the fouling occurs, the accumulated foulants increase the overall membrane resistance and is termed as foulant resistance. The overall membrane resistance is the sum of membrane resistance (R_m) and the foulant resistance (R_f). The water flux of the fouled membrane ($J_{w,f}$)[1] is given as:

$$J_{w,f} = \frac{(\pi_{ds} - \pi_{fs}) - \Delta P - F_{D,f}\left(\pi_{ds} + \frac{J_{s,f}}{J_{w,f}}\beta R_g T\right) - F_{F,f}\left(\pi_{fs} + \frac{J_{s,f}}{J_{w,f}}\beta R_g T\right)}{\mu (R_f + R_{,f})} \quad \text{(AL-FS orientation)} \quad \text{(xiv)}$$

$$J_{w,f} = \frac{(\pi_{ds} - \pi_{fs}) - \Delta P - F_{F,f}\left(\pi_{fs} + \frac{J_{s,f}}{J_{w,f}}\beta R_g T\right) - F_{D,f}\left(\pi_{ds} + \frac{J_{s,f}}{J_{w,f}}\beta R_g T\right)}{\mu (R_f + R_{,f})} \quad \text{(AL-DS orientation)} \quad \text{(xv)}$$

[1] The subscript '*f*' in each case represents the fouled situation

APPENDIX–II:

Fouling data for CTA & TFC membranes

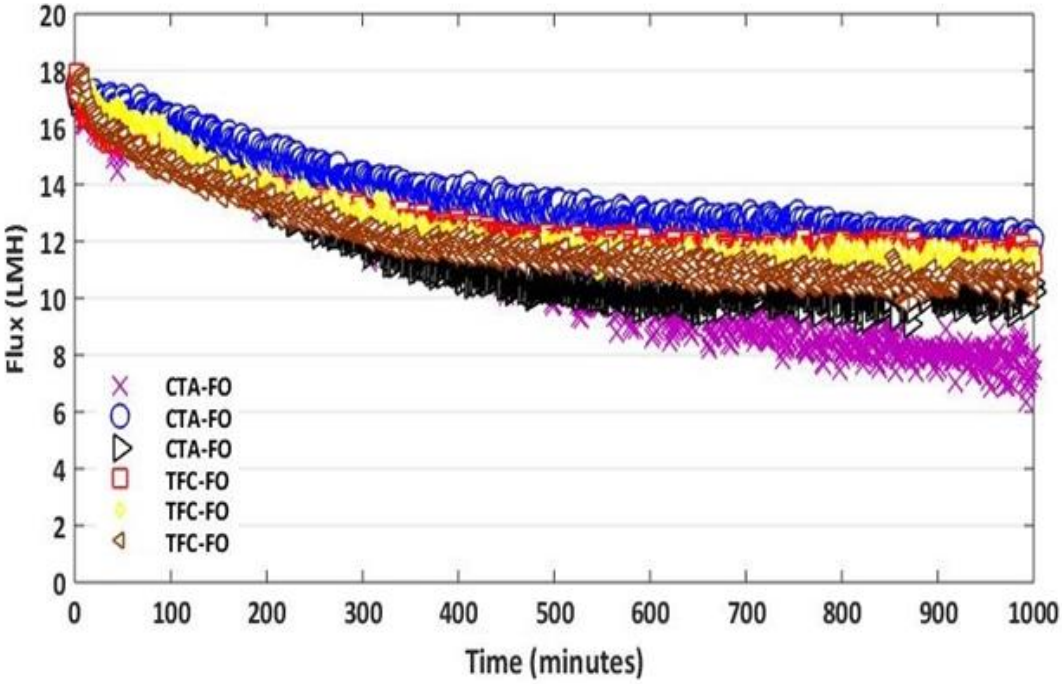

Figure A1: Flux variation with time for fouling experiments for forward osmosis for CTA and TFC membranes with feed solution (45 mM NaCl + 5 mM $CaCl_2$) with alginate (200 mg/L) as foulant. Crossflow velocity of feed solution 7.4 cm/s of draw solution 11.1 cm/s. Draw solution for CTA and TFC membranes was NaCl solution with concentration of 2 M and 3 M respectively.

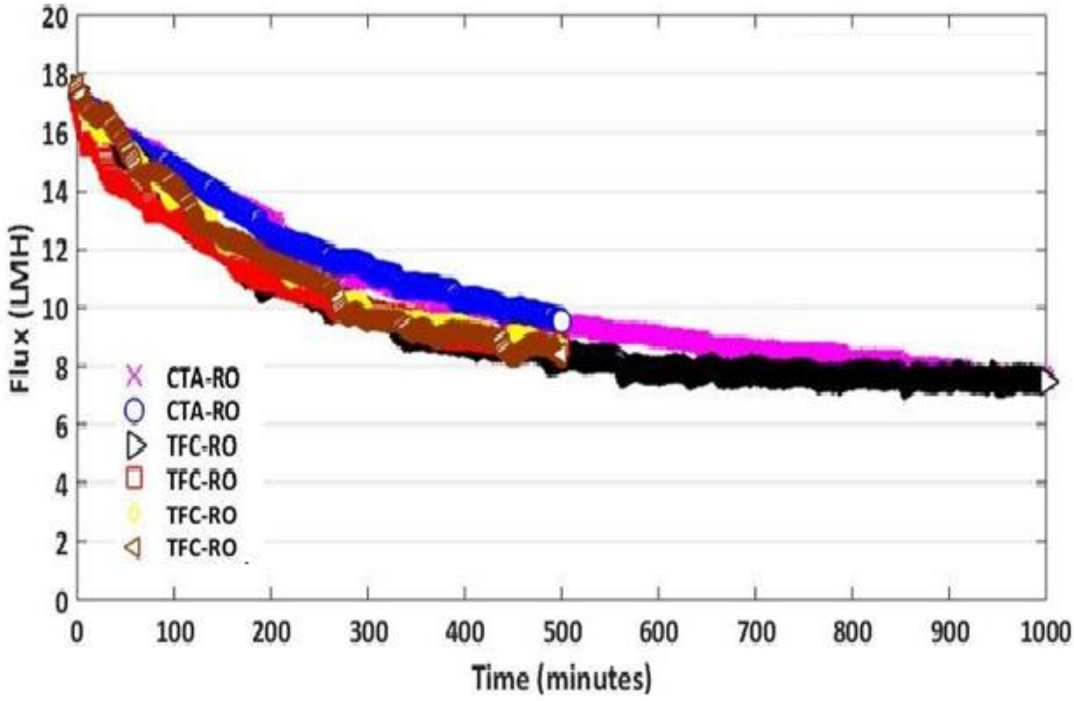

Figure A2: Flux variation with time for fouling experiments for reverse osmosis for CTA and TFC membranes with feed solution (45 mM NaCl + 5 mM $CaCl_2$) with alginate (200 mg/L) as foulant. Crossflow velocity of feed solution 7.4 cm/s with hydraulic pressure of 19.8 bar for CTA and 7.6 bar for TFC membrane.

APPENDIX III

Analysis of effect of cake-enhanced concentration polarisation on the calculated values of foulant resistance

This section shows the results of a sensitive analysis in which the influence of assumed levels of cake-enhanced concentration polarisation (CECP) on the calculated R_f for FO and RO were explored. R_f was calculated for the following four scenarios using the experimentally measured data (i.e., J_w, J_s/J_w, R_f, S, π_{ds} and π_{fs}):

(1) ECP at the feed side is neglected (i.e., assuming $\overline{S_f} = 0$ in Equation (5.4));

(2) ECP at the feed side is considered but CECP is neglected (i.e., assuming $S_f = 0$ and $\overline{S_f} = \delta$ in Equation (5.4); using $\overline{S_f}$ of 125 μm that is estimated for empty flow channel following the method reported elsewhere (Hoek et al., 2002a)),

(3) CECP is considered and S_f is the same for both FO and RO (i.e., assuming that $\overline{S_f}$ for both FO and RO increases at the same rate with the progress of fouling test from 125 μm at the beginning of fouling test to 422 μm at the end of fouling test), and

(4) CECP is considered and S_f for FO becomes increasingly greater than that for RO based on the analysis of Tow et al. (Tow and Lienhard V, 2016) (i.e., $\overline{S_f}$ for FO increases faster with the progress of fouling than that for RO; specifically it was assumed that $\overline{S_f}$ for FO increases from 125 μm to 719 μm whilst that for RO increases from 125 μm to 422 μm during the fouling tests).

As shown in Figure A3 (a), for all the scenarios R_f for both FO and RO increased with the progress of fouling test. Moreover, although the increase of concentration polarisation from scenario (1) to (4) at a fixed time could decrease the calculated R_f for both FO and RO, R_f for FO would become increasingly greater than that for RO for each scenario.

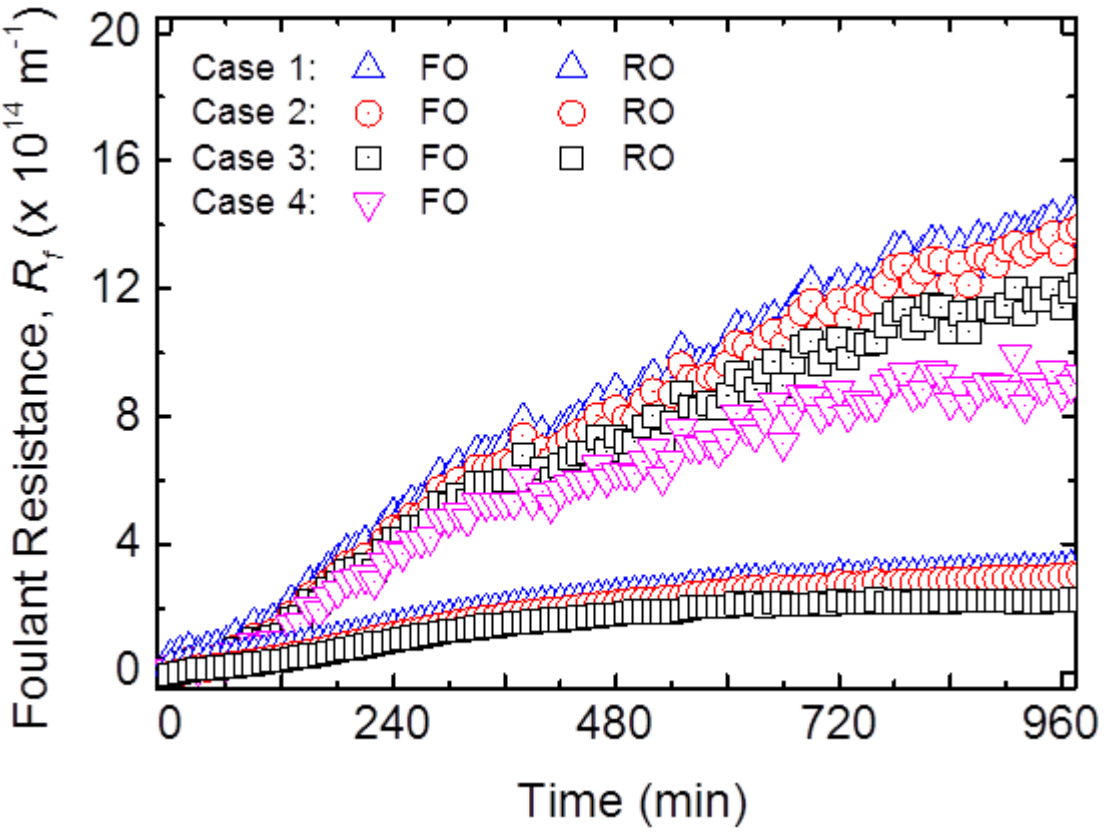

Figure A3: **(a) Calculated foulant resistance (R_f)** for FO and RO based on the osmotic-resistance filtration model in different scenarios: (1) CECP is neglected (i.e., assuming that the ECP boundary layer thickness (δ) is zero), (2) CECP is considered but cake-enhanced concentration polarisation is neglected (i.e., using δ of 125 µm that is estimated for empty flow channel following the method reported elsewhere (Hoek et al., 2002b)), (3) cake-enhanced concentration polarisation is considered and the foulant layer structural parameter (S_f) is the same for both FO and RO (i.e., $(\delta + S_f)$ for both FO and RO increases at the same rate with the progress of fouling test from 125 µm at the beginning to 422 µm at the end of fouling test), and (4) cake-enhanced concentration polarisation is considered and the foulant layer structural parameter (S_f) for FO becomes increasingly more greater than that for RO (i.e., $(\delta + S_f)$ for FO increases faster with the progress of fouling than that for RO; $(\delta + S_f)$ for FO increases from 125 µm to 719 µm, while that for RO increases from 125 µm to 422 µm).

Figure A3 (b) below shows the effective driving force for FO and RO. For all the scenarios the effective driving force for FO increased with the progress of fouling test and became increasingly greater than that for RO. In contrast to FO, the effective driving force for RO behaved differently for different scenarios: it maintained constant for scenario (1), increased gradually with fouling test for scenario (2), and decreased gradually with fouling test for scenario (3). Although the increase of concentration polarisation from scenario (1) to scenario

(4) led to the decrease of effective driving force for both FO and RO at a fixed time of fouling test, the effective driving force for FO was always increasing with the fouling test and becoming increasingly greater than that for RO. This suggests that (1) the different response of the effective driving force to fouling test between FO and RO should be the major reason for their different fouling behaviours, and (2) CECP for FO plays a much less important role in flux decline than that for RO.

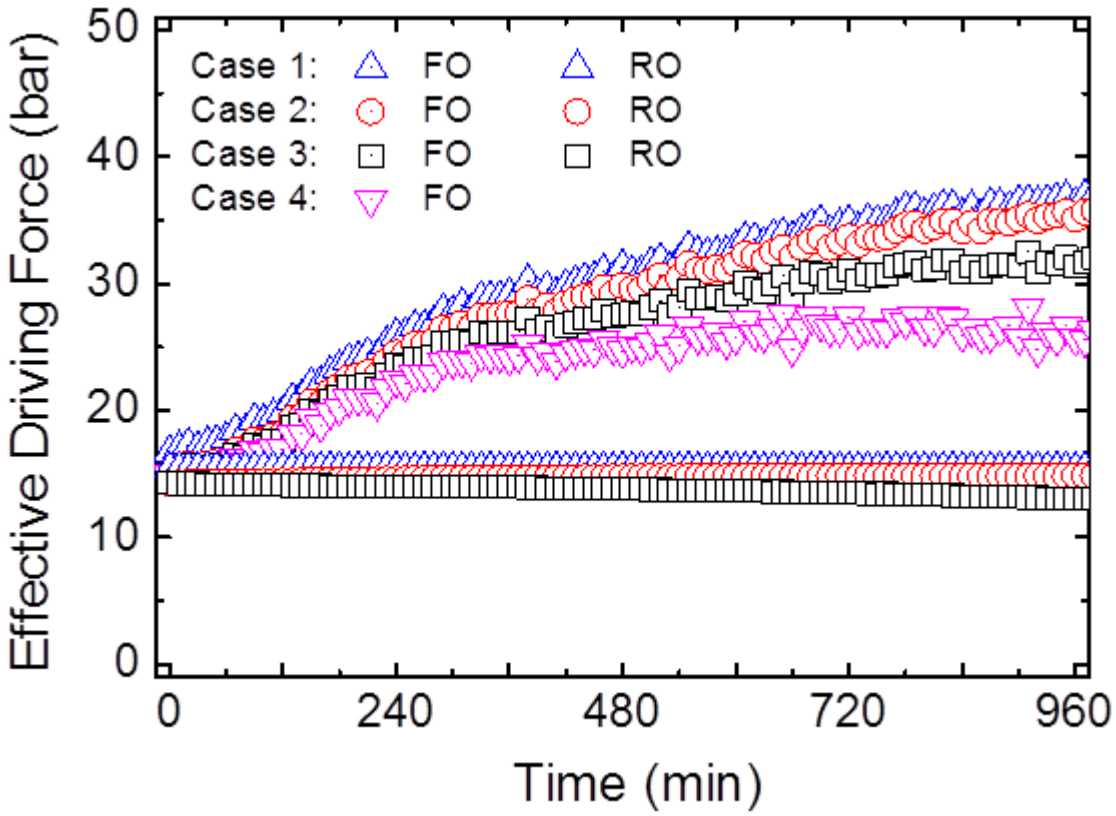

Figure A3: **(b) Calculated effective driving force** for FO and RO based on the osmotic-resistance filtration model in different scenarios: (1) CECP is neglected (i.e., assuming that the ECP boundary layer thickness (δ) is zero), (2) CECP is considered but cake-enhanced concentration polarisation is neglected (i.e., using δ of 125 μm that is estimated for empty flow channel following the method reported elsewhere (Hoek et al., 2002b)), (3) cake-enhanced concentration polarisation is considered and the foulant layer structural parameter (S_f) is the same for both FO and RO (i.e., $(\delta + S_f)$ for both FO and RO increases at the same rate with the progress of fouling test from 125 μm at the beginning to 422 μm at the end of fouling test), and (4) cake-enhanced concentration polarisation is considered and the foulant layer structural parameter (S_f) for FO becomes increasingly more greater than that for RO (i.e., $(\delta + S_f)$ for FO increases faster with the progress of fouling than that for RO; $(\delta + S_f)$ for FO increases from 125 μm to 719 μm, while that for RO increases from 125 μm to 422 μm).

BIBLIOGRAPHY

ABDEL-KARIM, A., GAD-ALLAH, T. A., BADAWY, M. I., KHALIL, A. S. & ULBRICHT, M. 2017. Removal of humic acid and chloroform from drinking water by using commercial nanofiltration and reverse osmosis membranes. *DESALINATION AND WATER TREATMENT,* 59**,** 48-54.

ACHILLI, A., CATH, T. Y. & CHILDRESS, A. E. 2009. Power generation with pressure retarded osmosis: An experimental and theoretical investigation. *Journal of membrane science,* 343**,** 42-52.

AKTHER, N., SODIQ, A., GIWA, A., DAER, S., ARAFAT, H. & HASAN, S. 2015. Recent advancements in forward osmosis desalintion: a review. *Chemical Engineering Journal,* 281**,** 502-522.

AL-OBAIDI, M., KARA-ZAITRI, C. & MUJTABA, I. M. 2017. Development of a mathematical model for apple juice compounds rejection in a spiral-wound reverse osmosis process. *Journal of Food Engineering,* 192**,** 111-121.

ALTAEE, A., ZARAGOZA, G. & VAN TONNINGEN, H. R. 2014. Comparison between forward osmosis-reverse osmosis and reverse osmosis processes for seawater desalination. *Desalination,* 336**,** 50-57.

ANDERSON, D. K. 1977. *Concentration of dilute industrial wastes by Direct osmosis*, University of Rhode Island.

ARGÜELLO, M. A., ÁLVAREZ, S., RIERA, F. A. & ÁLVAREZ, R. 2002. Enzymatic cleaning of inorganic ultrafiltration membranes fouled by whey proteins. *Journal of agricultural and food chemistry,* 50**,** 1951-1958.

ARKHANGELSKY, E., KUZMENKO, D. & GITIS, V. 2007. Impact of chemical cleaning on properties and functioning of polyethersulfone membranes. *Journal of Membrane Science,* 305**,** 176-184.

ARNAL, J. M., GARCÍA-FAYOS, B. & SANCHO, M. 2011. *Membrane cleaning,* INTECH Open Access Publisher.

AYDINER, C. 2015. A model-based analysis of water transport dynamics and fouling behaviors of osmotic membrane. *Chemical Engineering Journal,* 266**,** 289-298.

BACCHIN, P., AIMAR, P. & FIELD, R. W. 2006. Critical and sustainable fluxes: theory, experiments and applications. *Journal of Membrane Science,* 281**,** 42-69.

BAKER, R. W. 2004. Membrane technology and applications. *John Wiley & Sons, Ltd***,** 96-103.

BEAUDRY, E. G. & HERRON, J. R. 1997. Direct osmosis for concentrating wastewater. SAE Technical Paper.

BELFORT, G., DAVIS, R. H. & ZYDNEY, A. L. 1994. The behavior of suspensions and macromolecular solutions in crossflow microfiltration. *Journal of Membrane Science,* 96**,** 1-58.

BELL, E. A., HOLLOWAY, R. W. & CATH, T. Y. 2016. Evaluation of forward osmosis membrane performance and fouling during long-term osmotic membrane bioreactor study. *Journal of Membrane Science,* 517**,** 1-13.

BOO, C., LEE, S., ELIMELECH, M., MENG, Z. & HONG, S. 2012. Colloidal fouling in forward osmosis: role of reverse salt diffusion. *Journal of membrane science,* 390**,** 277-284.

CABERO, M., RIERA, F. & ALVAREZ, R. 1999. Rinsing of ultrafiltration ceramic membranes fouled with whey proteins: effects on cleaning procedures. *Journal of Membrane Science,* 154**,** 239-250.

CAKL, J., BAUER, I., DOLEČEK, P. & MIKULÁŠEK, P. 2000. Effects of backflushing conditions on permeate flux in membrane crossflow microfiltration of oil emulsion. *Desalination,* 127**,** 189-198.

CARRIER III, W. D. 2003. Goodbye, hazen; hello, kozeny-carman. *Journal of geotechnical and geoenvironmental engineering,* 129**,** 1054-1056.

CATH, T. Y., CHILDRESS, A. E. & ELIMELECH, M. 2006. Forward osmosis: principles, applications, and recent developments. *Journal of membrane science,* 281**,** 70-87.

CAY-DURGUN, P., MCCLOSKEY, C., KONECNY, J., KHOSRAVI, A. & LIND, M. L. 2017. Evaluation of thin film nanocomposite reverse osmosis membranes for long-term brackish water desalination performance. *Desalination,* 404**,** 304-312.

CHANG, H., LIANG, H., QU, F., LIU, B., YU, H., DU, X., LI, G. & SNYDER, S. A. 2017. Hydraulic backwashing for low-pressure membranes in drinking water treatment: a review. *Journal of Membrane Science,* 540**,** 362-380.

CHERYAN, M. & KUO, K. 1984. Hollow fibers and spiral wound modules for ultrafiltration of whey: energy consumption and performance. *Journal of Dairy Science,* 67**,** 1406-1413**.**

CHERYAN, M. 1998. *Ultrafiltration and microfiltration handbook*, CRC press.

CHOI, H., ZHANG, K., DIONYSIOU, D. D., OERTHER, D. B. & SORIAL, G. A. 2005. Influence of cross-flow velocity on membrane performance during filtration of biological suspension. *Journal of membrane science,* 248**,** 189-199.

CHOI, Y.-J., CHOI, J.-S., OH, H.-J., LEE, S., YANG, D. R. & KIM, J. H. 2009. Toward a combined system of forward osmosis and reverse osmosis for seawater desalination. *Desalination,* 247**,** 239-246.

CHONG, T., WONG, F. & FANE, A. 2007. Enhanced concentration polarization by unstirred fouling layers in reverse osmosis: detection by sodium chloride tracer response technique. *Journal of Membrane Science,* 287**,** 198-210.

CHONG, T., WONG, F. & FANE, A. 2008a. The effect of imposed flux on biofouling in reverse osmosis: role of concentration polarisation and biofilm enhanced osmotic pressure phenomena. *Journal of Membrane Science,* 325**,** 840-850.

CHONG, T., WONG, F. & FANE, A. 2008b. Implications of critical flux and cake enhanced osmotic pressure (CEOP) on colloidal fouling in reverse osmosis: experimental observations. *Journal of Membrane Science,* 314**,** 101-111.

CHUNG, T.-S., ZHANG, S., WANG, K. Y., SU, J. & LING, M. M. 2012. Forward osmosis processes: yesterday, today and tomorrow. *Desalination,* 287**,** 78-81.

CORNELISSEN, E., HARMSEN, D., DE KORTE, K., RUIKEN, C., QIN, J.-J., OO, H. & WESSELS, L. 2008. Membrane fouling and process performance of forward osmosis membranes on activated sludge. *Journal of Membrane Science,* 319**,** 158-168.

CORTALEZZI, M. M., ROSE, J., BARRON, A. R. & WIESNER, M. R. 2002. Characteristics of ultrafiltration ceramic membranes derived from alumoxane nanoparticles. *Journal of Membrane Science,* 205**,** 33-43.

DA COSTA, A., FANE, A. & WILEY, D. 1994. Spacer characterization and pressure drop modelling in spacer-filled channels for ultrafiltration. *Journal of membrane science,* 87**,** 79-98.

DARWISH, M., AL-NAJEM, N. & LIOR, N. 2009. Towards sustainable seawater desalting in the Gulf area. *Desalination,* 235**,** 58-87.

DEN, W. & WANG, C.-J. 2008. Removal of silica from brackish water by electrocoagulation pretreatment to prevent fouling of reverse osmosis membranes. *Separation and Purification Technology,* 59**,** 318-325.

DREIZIN, Y., TENNE, A. & HOFFMAN, D. 2008. Integrating large scale seawater desalination plants within Israel's water supply system. *Desalination,* 220**,** 132-149.

D'SOUZA, N. & MAWSON, A. 2005. Membrane cleaning in the dairy industry: a review. *Critical reviews in food science and nutrition,* 45**,** 125-134.

EISENBERG, T. N. & MIDDLEBROOKS, E. J. 2013. *Reverse osmosis treatment of drinking water*, Elsevier.

ELIMELECH, M. & BHATTACHARJEE, S. 1998. A novel approach for modeling concentration polarization in crossflow membrane filtration based on the equivalence of osmotic pressure model and filtration theory. *Journal of Membrane Science,* 145**,** 223-241.

ELIMELECH, M. & PHILLIP, W. A. 2011. The future of seawater desalination: energy, technology, and the environment. *science,* 333**,** 712-717.

EL-RAMLY, N. & CONGDON, C. 1981. Desalting Plants Inventory No. 7. *Water Supply Improvement Association*.

FANE, A. G., CHONG, T. H., ZHANG, J. & LAY, W. C. L. 2009. The Effect of Flux and Pressure on Fouling in Reverse Osmosis Desalination. *Proceedings IDA World Congress*.

FIELD, R. W. & PEARCE, G. K. 2011. Critical, sustainable and threshold fluxes for membrane filtration with water industry applications. *Advances in Colloid and Interface Science,* 164**,** 38-44.

FIELD, R. W. & WU, J. J. 2013. Mass transfer limitations in forward osmosis: Are some potential applications overhyped? *Desalination,* 318**,** 118-124.

FIELD, R., HUGHES, D., CUI, Z. & TIRLAPUR, U. 2008. Some observations on the chemical cleaning of fouled membranes. *Desalination,* 227**,** 132-138.

FIELD, R., WU, D., HOWELL, J. & GUPTA, B. 1995. Critical flux concept for microfiltration fouling. *Journal of Membrane Science,* 100**,** 259-272.

FRANK, M., BARGEMAN, G., ZWIJNENBURG, A. & WESSLING, M. 2001. Capillary hollow fiber nanofiltration membranes. *Separation and purification technology,* 22**,** 499-506.

FRITZMANN, C., LÖWENBERG, J., WINTGENS, T. & MELIN, T. 2007. State-of-the-art of reverse osmosis desalination. *Desalination,* 216**,** 1-76.

GABRUS, E. & SZANIAWSKA, D. 2009. Application of backflushing for fouling reduction during microfiltration of yeast suspensions. *Desalination,* 240**,** 46-53.

GANDER, M., JEFFERSON, B. & JUDD, S. 2000. Aerobic MBRs for domestic wastewater treatment: a review with cost considerations. *Separation and purification Technology,* 18**,** 119-130.

GARCIA-CASTELLO, E. M., MCCUTCHEON, J. R. & ELIMELECH, M. 2009. Performance evaluation of sucrose concentration using forward osmosis. *Journal of membrane science,* 338**,** 61-66.

GARCIA-CASTELLO, E., MAYOR, L., CHORQUES, S., ARGÜELLES, A., VIDAL-BROTONS, D. & GRAS, M. 2011. Reverse osmosis concentration of press liquid

from orange juice solid wastes: Flux decline mechanisms. *Journal of food engineering,* 106**,** 199-205.

GRAY, G. T., MCCUTCHEON, J. R. & ELIMELECH, M. 2006. Internal concentration polarization in forward osmosis: role of membrane orientation. *Desalination,* 197**,** 1-8.

GREENLEE, L. F., LAWLER, D. F., FREEMAN, B. D., MARROT, B. & MOULIN, P. 2009. Reverse osmosis desalination: water sources, technology, and today's challenges. *Water research,* 43**,** 2317-2348.

GU, Y., WANG, Y.-N., WEI, J. & TANG, C. Y. 2013. Organic fouling of thin-film composite polyamide and cellulose triacetate forward osmosis membranes by oppositely charged macromolecules. *Water research,* 47**,** 1867-1874.

GURAK, P. D., CABRAL, L. M., ROCHA-LEÃO, M. H. M., MATTA, V. M. & FREITAS, S. P. 2010. Quality evaluation of grape juice concentrated by reverse osmosis. *Journal of food engineering,* 96**,** 421-426.

HISHIKAWA, Y., INOUE, S.-I., MAGOSHI, J. & KONDO, T. 2005. Novel tool for characterization of noncrystalline regions in cellulose: a FTIR deuteration monitoring and generalized two-dimensional correlation spectroscopy. *Biomacromolecules,* 6**,** 2468-2473.

HOEK, E. M. & ELIMELECH, M. 2003. Cake-enhanced concentration polarization: a new fouling mechanism for salt-rejecting membranes. *Environmental science & technology,* 37**,** 5581-5588.

HOEK, E. M., KIM, A. S. & ELIMELECH, M. 2002. Influence of crossflow membrane filter geometry and shear rate on colloidal fouling in reverse osmosis and nanofiltration separations. *Environmental Engineering Science,* 19**,** 357-372.

HOLLOWAY, R. W., CHILDRESS, A. E., DENNETT, K. E. & CATH, T. Y. 2007. Forward osmosis for concentration of anaerobic digester centrate. *Water research,* 41**,** 4005-4014.

HOOVER, L. A., PHILLIP, W. A., TIRAFERRI, A., YIP, N. Y. & ELIMELECH, M. 2011. Forward with osmosis: emerging applications for greater sustainability. *Environmental science & technology,* 45**,** 9824-9830.

HUGHES, D. & FIELD, R. 2006. Crossflow filtration of washed and unwashed yeast suspensions at constant shear under nominally sub-critical conditions. *Journal of membrane science,* 280**,** 89-98.

JIAO, B., CASSANO, A. & DRIOLI, E. 2004. Recent advances on membrane processes for the concentration of fruit juices: a review. *Journal of food engineering,* 63**,** 303-324.

JOHN, D. M. & WEEKS, K. M. 2000. van't Hoff enthalpies without baselines. *Protein Science,* 9**,** 1416-1419.

KESSLER, J. & MOODY, C. 1976. Drinking water from sea water by forward osmosis. *Desalination,* 18**,** 297-306.

KIM, Y., ELIMELECH, M., SHON, H. K. & HONG, S. 2014. Combined organic and colloidal fouling in forward osmosis: Fouling reversibility and the role of applied pressure. *Journal of Membrane Science,* 460**,** 206-212.

KISHINO, H., ISHIDA, H., IWABU, H. & NAKANO, I. 1996. Domestic wastewater reuse using a submerged membrane bioreactor. *Desalination,* 106**,** 115-119.

KNOERZER, K., JULIANO, P. & SMITHERS, G. W. 2016. *Innovative Food Processing Technologies: Extraction, Separation, Component Modification and Process Intensification*, Woodhead Publishing.

KOKUGAN, T., FUJIWARA, S. & SHIMIZU, M. 1995. Ultrasonic effect on ultrafiltration properties of ceramic membrane. *Membrane,* 20**,** 213-223.

KOROS, W., MA, Y. & SHIMIDZU, T. 1996. Terminology for membranes and membrane processes (IUPAC Recommendations 1996). *Pure and Applied Chemistry,* 68**,** 1479-1489.

KRAVATH, R. E. & DAVIS, J. A. 1975. Desalination of sea water by direct osmosis. *Desalination,* 16**,** 151-155.

KURTH, C. J., KOEHLER, J. A., ZHOU, M., HOLMBERG, B. A. & BURK, R. L. 2012. Reverse osmosis membranes. Google Patents.

KWAN, S. E., BAR-ZEEV, E. & ELIMELECH, M. 2015. Biofouling in forward osmosis and reverse osmosis: Measurements and mechanisms. *Journal of Membrane Science,* 493**,** 703-708.

LAITINEN, N., LUONSI, A., LEVÄNEN, E. & NYSTRÖM, M. 2001. Effect of backflushing conditions on ultrafiltration of board industry wastewaters with ceramic membranes. *Separation and Purification Technology,* 25**,** 323-331.

LAY, W. C., ZHANG, Q., ZHANG, J., MCDOUGALD, D., TANG, C., WANG, R., LIU, Y. & FANE, A. G. 2011. Study of integration of forward osmosis and biological process: membrane performance under elevated salt environment. *Desalination,* 283**,** 123-130.

LE CLECH, P., JEFFERSON, B., CHANG, I. S. & JUDD, S. J. 2003. Critical flux determination by the flux-step method in a submerged membrane bioreactor. *Journal of membrane science,* 227**,** 81-93.

LEE, H., AMY, G., CHO, J., YOON, Y., MOON, S.-H. & KIM, I. S. 2001. Cleaning strategies for flux recovery of an ultrafiltration membrane fouled by natural organic matter. *Water research,* 35**,** 3301-3308.

LEE, J., KOOK, S., LEE, C. & KIM, I. S. 2017. Effect of intermittent pressure-assisted forward osmosis (I-PAFO) on organic fouling. *Desalination,* 419**,** 60-69.

LEE, K. P., ARNOT, T. C. & MATTIA, D. 2011. A review of reverse osmosis membrane materials for desalination—development to date and future potential. *Journal of Membrane Science,* 370**,** 1-22.

LEE, K., BAKER, R. & LONSDALE, H. 1981. Membranes for power generation by pressure-retarded osmosis. *Journal of Membrane Science,* 8**,** 141-171.

LEE, S., BOO, C., ELIMELECH, M. & HONG, S. 2010. Comparison of fouling behavior in forward osmosis (FO) and reverse osmosis (RO). *Journal of Membrane Science,* 365**,** 34-39.

LEVENSPIEL, O. & DE NEVERS, N. 1974. The osmotic pump. *Science,* 183**,** 157-160.

LI, H., FANE, A., COSTER, H. & VIGNESWARAN, S. 2000. An assessment of depolarisation models of crossflow microfiltration by direct observation through the membrane. *Journal of Membrane Science,* 172**,** 135-147.

LI, Q. & ELIMELECH, M. 2004. Organic fouling and chemical cleaning of nanofiltration membranes: measurements and mechanisms. *Environmental Science & Technology,* 38**,** 4683-4693.

LI, Z.-Y., YANGALI-QUINTANILLA, V., VALLADARES-LINARES, R., LI, Q., ZHAN, T. & AMY, G. 2012. Flux patterns and membrane fouling propensity during desalination of seawater by forward osmosis. *Water research,* 46**,** 195-204.

LIANG, H., GONG, W., CHEN, J. & LI, G. 2008. Cleaning of fouled ultrafiltration (UF) membrane by algae during reservoir water treatment. *Desalination,* 220**,** 267-272.

LIM, A. & BAI, R. 2003. Membrane fouling and cleaning in microfiltration of activated sludge wastewater. *Journal of membrane science,* 216**,** 279-290.

LIN, J. C.-T., LEE, D.-J. & HUANG, C. 2010. Membrane fouling mitigation: membrane cleaning. *Separation Science and Technology,* 45**,** 858-872.

LIU, C., CAOTHIEN, S., HAYES, J., CAOTHUY, T., OTOYO, T. & OGAWA, T. 2001. Membrane chemical cleaning: from art to science. *Pall Corporation, Port Washington, NY,* 11050.

LOEB, S. & SOURIRAJAN, S. 1962. High-flow semipermeable membranes for separation of water from saline solutions. *Adv Chem Ser,* 38**,** 117-132.

LOEB, S. 1976. Production of energy from concentrated brines by pressure-retarded osmosis: I. Preliminary technical and economic correlations. *Journal of Membrane Science,* 1**,** 49-63.

LOEB, S. The Loeb-Sourirajan membrane: How it came about [Desalination]. ACS symposium series (USA). no. 153-154., 1981.

LOEB, S., TITELMAN, L., KORNGOLD, E. & FREIMAN, J. 1997. Effect of porous support fabric on osmosis through a Loeb-Sourirajan type asymmetric membrane. *Journal of Membrane Science,* 129**,** 243-249.

LOEB, S., VAN HESSEN, F., LEVI, J. & VENTURA, M. The osmotic power plant. 11th Intersociety Energy Conversion Engineering Conference, 1976. 51-57.

LOTFI, F., CHEKLI, L., PHUNTSHO, S., HONG, S., CHOI, J. Y. & SHON, H. K. 2017. Understanding the possible underlying mechanisms for low fouling tendency of the forward osmosis and pressure assisted osmosis processes. *Desalination*.

LOZIER, J. & FERNANDEZ, A. 2001. Using a membrane bioreactor/reverse osmosis system for indirect potable reuse. *Water Science and Technology: Water Supply,* 1**,** 303-313.

LU, X., ARIAS CHAVEZ, L. H., ROMERO-VARGAS CASTRILLÓN, S., MA, J. & ELIMELECH, M. 2015. Influence of active layer and support layer surface structures on organic fouling propensity of thin-film composite forward osmosis membranes. *Environmental science & technology,* 49**,** 1436-1444.

LUO, W., HAI, F. I., PRICE, W. E. & NGHIEM, L. D. 2015. Water extraction from mixed liquor of an aerobic bioreactor by forward osmosis: membrane fouling and biomass characteristics assessment. *Separation and Purification Technology,* 145**,** 56-62.

LUTCHMIAH, K., CORNELISSEN, E. R., HARMSEN, D. J., POST, J. W., LAMPI, K., RAMAEKERS, H., RIETVELD, L. C. & ROEST, K. 2011. Water recovery from sewage using forward osmosis. *Water Science and Technology,* 64**,** 1443-1449.

LUTCHMIAH, K., VERLIEFDE, A., ROEST, K., RIETVELD, L. C. & CORNELISSEN, E. R. 2014. Forward osmosis for application in wastewater treatment: a review. *Water research,* 58**,** 179-197.

MALAEB, L. & AYOUB, G. M. 2011. Reverse osmosis technology for water treatment: state of the art review. *Desalination,* 267**,** 1-8.

MARRIOTT, N. & GRAVANI, R. B. 2006. *Principles of food sanitation,* Springer Science & Business Media.

MATSUMOTO, K., KAWAHARA, M. & OHYA, H. 1988. Cross-flow filtration of yeast by microporous ceramic membrane with backwashing. *Journal of fermentation technology,* 66**,** 199-205.

MCCUTCHEON, J. R. & ELIMELECH, M. 2006. Influence of concentrative and dilutive internal concentration polarization on flux behavior in forward osmosis. *Journal of Membrane Science,* 284**,** 237-247.

MCGINNIS, R. & MCGURGAN, G. 2012. Forward osmosis membranes. Google Patents.

MCGINNIS, R. L., ELIMELECH, M. & MCCUTCHEON, J. 2015. Osmotic heat engine. Google Patents.

MI, B. & ELIMELECH, M. 2008. Chemical and physical aspects of organic fouling of forward osmosis membranes. *Journal of Membrane Science,* 320**,** 292-302.

MI, B. & ELIMELECH, M. 2010a. Gypsum scaling and cleaning in forward osmosis: measurements and mechanisms. *Environmental science & technology,* 44**,** 2022-2028.

MI, B. & ELIMELECH, M. 2010c. Organic fouling of forward osmosis membranes: Fouling reversibility and cleaning without chemical reagents. *Journal of Membrane Science,* 348**,** 337-345.

MI, B. & ELIMELECH, M. 2013. Silica scaling and scaling reversibility in forward osmosis. *Desalination,* 312**,** 75-81.

MINIER-MATAR, J., HUSSAIN, A., JANSON, A., WANG, R., FANE, A. G. & ADHAM, S. 2015. Application of forward osmosis for reducing volume of produced/Process water from oil and gas operations. *Desalination,* 376**,** 1-8.

MOHAMMADI, T., MADAENI, S. & MOGHADAM, M. 2003. Investigation of membrane fouling. *Desalination,* 153**,** 155-160.

MONNOT, M., NGUYÊN, H. T. K., LABORIE, S. & CABASSUD, C. 2017. Seawater reverse osmosis desalination plant at community-scale: Role of an innovative pretreatment on process performances and intensification. *Chemical Engineering and Processing: Process Intensification,* 113**,** 42-55.

MOTSA, M. M., MAMBA, B. B., D'HAESE, A., HOEK, E. M. & VERLIEFDE, A. R. 2014. Organic fouling in forward osmosis membranes: The role of feed solution chemistry and membrane structural properties. *Journal of Membrane Science,* 460**,** 99-109.

NAYAR, K. G., SHARQAWY, M. H. & BANCHIK, L. D. 2016. Thermophysical properties of seawater: a review and new correlations that include pressure dependence. *Desalination,* 390**,** 1-24.

NGUYEN, T. P. N., JUN, B.-M., PARK, H. G., HAN, S.-W., KIM, Y.-K., LEE, H. K. & KWON, Y.-N. 2016. Concentration polarization effect and preferable membrane configuration at pressure-retarded osmosis operation. *Desalination,* 389**,** 58-67.

NING, R. Y. 2002. Arsenic removal by reverse osmosis. *Desalination,* 143**,** 237-241.

NOBEL, P. S. 1969. The Boyle-van't Hoff relation. *Journal of theoretical biology,* 23**,** 375-379.

NORMAN, R. S. 1974. Water salination: a source of energy. *Science,* 186**,** 350-352.

OCHANDO-PULIDO, J. & MARTINEZ-FEREZ, A. 2017. Experimental design optimization of reverse osmosis purification of pretreatedolive mill wastewater. *Science of The Total Environment,* 587**,** 414-422.

OGUNBIYI, O. O., MILES, N. J. & HILAL, N. 2008. The effects of performance and cleaning cycles of new tubular ceramic microfiltration membrane fouled with a model yeast suspension. *Desalination,* 220**,** 273-289.

PARIDA, V. & NG, H. Y. 2013. Forward osmosis organic fouling: Effects of organic loading, calcium and membrane orientation. *Desalination,* 312**,** 88-98.

PATTLE, R. 1954. Production of electric power by mixing fresh and salt water in the hydroelectric pile.

PEARCE, G. K. 2011. *UF/MF Membrane Water Treatment: Principles and Design*, Water Treatment Academy Bangkok.

PETRINIC, I., KORENAK, J., POVODNIK, D. & HÉLIX-NIELSEN, C. 2015. A feasibility study of ultrafiltration/reverse osmosis (UF/RO)-based wastewater treatment and reuse in the metal finishing industry. *Journal of Cleaner Production,* 101**,** 292-300.

PHILLIP, W. A., YONG, J. S. & ELIMELECH, M. 2010. Reverse draw solute permeation in forward osmosis: modeling and experiments. *Environmental science & technology,* 44**,** 5170-5176.

PONGPAIROJ, P., FIELD, R., CUI, Z., WICAKSANA, F. & FANE, A. G. 2011. Transmission of and fouling by long chain molecules during crossflow microfiltration of algal suspensions: influence of shear. *Desalination and Water Treatment,* 35**,** 138-149.

PORCELLI, N. & JUDD, S. 2010. Chemical cleaning of potable water membranes: a review. *Separation and Purification Technology,* 71**,** 137-143.

PORTER, M. C. 1972. Concentration polarization with membrane ultrafiltration. *Industrial & Engineering Chemistry Product Research and Development,* 11**,** 234-248.

QAISRANI, T. & SAMHABER, W. 2011. Impact of gas bubbling and backflushing on fouling control and membrane cleaning. *Desalination,* 266**,** 154-161.

QIN, J.-J., KEKRE, K. A., TAO, G., OO, M. H., WAI, M. N., LEE, T. C., VISWANATH, B. & SEAH, H. 2006. New option of MBR-RO process for production of NEWater from domestic sewage. *Journal of Membrane Science,* 272**,** 70-77.

QURESHI, B. A. & ZUBAIR, S. M. 2015. Exergetic analysis of a brackish water reverse osmosis desalination unit with various energy recovery systems. *Energy,* 93**,** 256-265.

RADJENOVIĆ, J., PETROVIĆ, M., VENTURA, F. & BARCELÓ, D. 2008. Rejection of pharmaceuticals in nanofiltration and reverse osmosis membrane drinking water treatment. *Water Research,* 42**,** 3601-3610.

RILEY, R. L., MERTEN, U. & GARDNER, J. 1966. Replication electron microscopy of cellulose acetate osmotic membranes. *Desalination,* 1**,** 30-34.

SABLANI, S., GOOSEN, M., AL-BELUSHI, R. & WILF, M. 2001. Concentration polarization in ultrafiltration and reverse osmosis: a critical review. *Desalination,* 141**,** 269-289.

SAGIV, A., CHRISTOFIDES, P. D., COHEN, Y. & SEMIAT, R. 2015. On the analysis of FO mass transfer resistances via CFD analysis and film theory. *Journal of Membrane Science,* 495**,** 198-205.

SALLADINI, A., PRISCIANDARO, M. & BARBA, D. 2007. Ultrafiltration of biologically treated wastewater by using backflushing. *Desalination,* 207**,** 24-34.

SCHÄFER, A., FANE, A. G. & WAITE, T. 2001. Cost factors and chemical pretreatment effects in the membrane filtration of waters containing natural organic matter. *Water Research,* 35**,** 1509-1517.

SHAFFER, D. L., WERBER, J. R., JARAMILLO, H., LIN, S. & ELIMELECH, M. 2015. Forward osmosis: where are we now? *Desalination,* 356**,** 271-284.

SHANNON, M. A., BOHN, P. W., ELIMELECH, M., GEORGIADIS, J. G., MARINAS, B. J. & MAYES, A. M. 2008. Science and technology for water purification in the coming decades. *Nature,* 452**,** 301-310.

SHE, Q., HOU, D., LIU, J., TAN, K. H. & TANG, C. Y. 2013. Effect of feed spacer induced membrane deformation on the performance of pressure retarded osmosis (PRO): Implications for PRO process operation. *Journal of membrane science,* 445**,** 170-182.

SHE, Q., JIN, X., LI, Q. & TANG, C. Y. 2012. Relating reverse and forward solute diffusion to membrane fouling in osmotically driven membrane processes. *Water research,* 46**,** 2478-2486.

SHE, Q., WANG, R., FANE, A. G. & TANG, C. Y. 2016. Membrane fouling in osmotically driven membrane processes: a review. *Journal of Membrane Science,* 499**,** 201-233.

SHI, X., TAL, G., HANKINS, N. P. & GITIS, V. 2014. Fouling and cleaning of ultrafiltration membranes: a review. *Journal of Water Process Engineering,* 1**,** 121-138.

SHINJOU, I. & SHOJI, R. 1988. Semipermeable membrane support and process for preparation thereof. Google Patents.

SHORROCK, C. & BIRD, M. 1998. Membrane cleaning: chemically enhanced removal of deposits formed during yeast cell harvesting. *Food and bioproducts processing,* 76**,** 30-38.

SIDDIQUI, F. A. & FIELD, R. W. 2016. Fouling and cleaning of a tubular ultrafiltration ceramic membrane. *MEMBRANE WATER TREATMENT,* 7**,** 433-449.

SIM, L. N., YE, Y., CHEN, V. & FANE, A. G. 2011. Investigations of the coupled effect of cake-enhanced osmotic pressure and colloidal fouling in RO using crossflow sampler-modified fouling index ultrafiltration. *Desalination,* 273**,** 184-196.

SONDHI, R. & BHAVE, R. 2001. Role of backpulsing in fouling minimization in crossflow filtration with ceramic membranes. *Journal of Membrane Science,* 186**,** 41-52.

STRATHMANN, H., SCHEIBLE, P. & BAKER, R. 1971. A rationale for the preparation of Loeb-Sourirajan-type cellulose acetate membranes. *Journal of Applied Polymer Science,* 15**,** 811-828.

SUÁREZ, A. & RIERA, F. A. 2015. Production of high-quality water by reverse osmosis of milk dairy condensates. *Journal of Industrial and Engineering Chemistry,* 21**,** 1340-1349.

SUÁREZ, A., FIDALGO, T. & RIERA, F. A. 2014. Recovery of dairy industry wastewaters by reverse osmosis. Production of boiler water. *Separation and Purification Technology,* 133**,** 204-211.

TANG, C. Y., CHONG, T. & FANE, A. G. 2011. Colloidal interactions and fouling of NF and RO membranes: a review. *Advances in colloid and interface science,* 164**,** 126-143.

TANG, C. Y., KWON, Y.-N. & LECKIE, J. O. 2007. Probing the nano-and micro-scales of reverse osmosis membranes—a comprehensive characterization of physiochemical properties of uncoated and coated membranes by XPS, TEM, ATR-FTIR, and streaming potential measurements. *Journal of Membrane Science,* 287**,** 146-156.

TANG, C. Y., SHE, Q., LAY, W. C., WANG, R. & FANE, A. G. 2010. Coupled effects of internal concentration polarization and fouling on flux behavior of forward osmosis membranes during humic acid filtration. *Journal of Membrane Science,* 354**,** 123-133.

TARDIEU, E., GRASMICK, A., GEAUGEY, V. & MANEM, J. 1999. Influence of hydrodynamics on fouling velocity in a recirculated MBR for wastewater treatment. *Journal of Membrane Science,* 156**,** 131-140.

THOMPSON, N. A. & NICOLL, P. G. Forward osmosis desalination: a commercial reality. IDA World Congress–Perth Convention and Exhibition Centre (PCEC), Perth, Western Australia September, 2011. 4-9.

TOMASZEWSKA, M. & BIAŁOŃCZYK, L. 2012. The chemical cleaning of ceramic membrane used in UF. *Polish Journal of Chemical Technology,* 14**,** 105-109.

TOW, E. W. & LIENHARD V, J. H. 2016. Quantifying osmotic membrane fouling to enable comparisons across diverse processes. *Journal of Membrane Science,* 511**,** 92-107.

TOW, E. W. & LIENHARD V, J. H. 2017. Unpacking compaction: Effect of hydraulic pressure on alginate fouling. *Journal of Membrane Science, 544,* pp.221-233.

TRÄGÅRDH, G. 1989. Membrane cleaning. *Desalination,* 71**,** 325-335.

VAN DER MAREL, P., ZWIJNENBURG, A., KEMPERMAN, A., WESSLING, M., TEMMINK, H. & VAN DER MEER, W. 2009. An improved flux-step method to determine the critical flux and the critical flux for irreversibility in a membrane bioreactor. *Journal of Membrane Science,* 332**,** 24-29.

VANYSACKER, L., BERNSHTEIN, R. & VANKELECOM, I. F. 2014. Effect of chemical cleaning and membrane aging on membrane biofouling using model organisms with increasing complexity. *Journal of Membrane Science,* 457**,** 19-28.

VERBERK, J. & VAN DIJK, H. 2003. Research on AirFlush®: distribution of water and air in tubular and capillary membrane modules. *Water Science and Technology: Water Supply,* 3**,** 409-414.

VETTER, T., PERDUE, E., INGALL, E., KOPRIVNJAK, J.-F. & PFROMM, P. 2007. Combining reverse osmosis and electrodialysis for more complete recovery of

dissolved organic matter from seawater. *Separation and purification Technology,* 56**,** 383-387.

VITAGLIANO, V. & LYONS, P. 1956. Diffusion coefficients for aqueous solutions of sodium chloride and barium chloride. *Journal of the American Chemical Society,* 78**,** 1549-1552.

VON MEDEAZZA, G. M. 2005. "Direct" and socially-induced environmental impacts of desalination. *Desalination,* 185**,** 57-70.

VOTTA, F. 1974. Concentration of Industial Waste by Direct Osmosis.

VRIJENHOEK, E. M., HONG, S. & ELIMELECH, M. 2001. Influence of membrane surface properties on initial rate of colloidal fouling of reverse osmosis and nanofiltration membranes. *Journal of membrane science,* 188**,** 115-128.

WANG, R., SHI, L., TANG, C. Y., CHOU, S., QIU, C. & FANE, A. G. 2010a. Characterization of novel forward osmosis hollow fiber membranes. *Journal of membrane science,* 355**,** 158-167.

WANG, Y., WICAKSANA, F., TANG, C. Y. & FANE, A. G. 2010b. Direct microscopic observation of forward osmosis membrane fouling. *Environmental science & technology,* 44**,** 7102-7109.

WANG, Z., MA, J., TANG, C. Y., KIMURA, K., WANG, Q. & HAN, X. 2014. Membrane cleaning in membrane bioreactors: a review. *Journal of Membrane Science,* 468**,** 276-307.

WEI, J., QIU, C., TANG, C. Y., WANG, R. & FANE, A. G. 2011. Synthesis and characterization of flat-sheet thin film composite forward osmosis membranes. *Journal of Membrane Science,* 372**,** 292-302.

WU, J., LE-CLECH, P., STUETZ, R. M., FANE, A. G. & CHEN, V. 2008a. Novel filtration mode for fouling limitation in membrane bioreactors. *Water research,* 42**,** 3677-3684.

WU, J., LE-CLECH, P., STUETZ, R. M., FANE, A. G. & CHEN, V. 2008b. Effects of relaxation and backwashing conditions on fouling in membrane bioreactor. *Journal of Membrane Science,* 324**,** 26-32.

XIAO-JUN, F., URBAIN, V., QIAN, Y. & MANEM, J. 1996. Nitrification and mass balance with a membrane bioreactor for municipal wastewater treatment. *Water Science and Technology,* 34**,** 129-136.

XIE, M., LEE, J., NGHIEM, L. D. & ELIMELECH, M. 2015. Role of pressure in organic fouling in forward osmosis and reverse osmosis. *Journal of Membrane Science,* 493**,** 748-754.

XIE, M., NGHIEM, L. D., PRICE, W. E. & ELIMELECH, M. 2012. Comparison of the removal of hydrophobic trace organic contaminants by forward osmosis and reverse osmosis. *Water research,* 46**,** 2683-2692.

XU, J., TANG, Y., WANG, Y., SHAN, B., YU, L. & GAO, C. 2014. Effect of coagulation bath conditions on the morphology and performance of PSf membrane blended with a capsaicin-mimic copolymer. *Journal of Membrane Science,* 455**,** 121-130.

YIP, N. Y. & ELIMELECH, M. 2013. Influence of natural organic matter fouling and osmotic backwash on pressure retarded osmosis energy production from natural salinity gradients. *Environmental science & technology,* 47**,** 12607-12616.

YORK, R., THIEL, R. & BEAUDRY, E. Full-scale experience of direct osmosis concentration applied to leachate management. Proceedings of the Seventh International Waste Management and Landfill Symposium (Sardinia'99), S. Margherita di Pula, Cagliari, Sardinia, Italy, 1999.

YUSTER, S. T., SOURIRAJAN, S. & BERNSTEIN, K. 1958. *Sea Water Demineralization by the" surface Skimming" Process*, University of California, Department of Engineering.

ZHANG, M., HOU, D., SHE, Q. & TANG, C. Y. 2014. Gypsum scaling in pressure retarded osmosis: Experiments, mechanisms and implications. *Water Research,* 48**,** 387-395.

ZHANG, M., SHE, Q., YAN, X. & TANG, C. Y. 2017. Effect of reverse solute diffusion on scaling in forward osmosis: A new control strategy by tailoring draw solution chemistry. *Desalination,* 401**,** 230-237.

ZHAO, S., ZOU, L. & MULCAHY, D. 2011. Effects of membrane orientation on process performance in forward osmosis applications. *Journal of Membrane Science,* 382**,** 308-315.

ZHAO, S., ZOU, L., TANG, C. Y. & MULCAHY, D. 2012. Recent developments in forward osmosis: opportunities and challenges. *Journal of Membrane Science,* 396**,** 1-21.

ZOU, S., WANG, Y.-N., WICAKSANA, F., AUNG, T., WONG, P. C. Y., FANE, A. G. & TANG, C. Y. 2013. Direct microscopic observation of forward osmosis membrane fouling by microalgae: critical flux and the role of operational conditions. *Journal of membrane science,* 436**,** 174-185.

ZURIAGA-AGUSTÍ, E., ALVENTOSA-DELARA, E., BARREDO-DAMAS, S., ALCAINA-MIRANDA, M., IBORRA-CLAR, M. & MENDOZA-ROCA, J. 2014. Performance of ceramic ultrafiltration membranes and fouling behavior of a dye-polysaccharide binary system. *Water research,* 54**,** 199-210.

ZYDNEY, A. L. & COLTON, C. K. 1986. A concentration polarization model for the filtrate flux in cross-flow microfiltration of particulate suspensions. *Chemical Engineering Communications,* 47**,** 1-21.

PUBLICATIONS, PRESENTATIONS, AND AWARDS

Journal publications:

- Siddiqui, F. A. & Field, R. W., 2016, Fouling and cleaning of a tubular ultrafiltration ceramic membrane. *Membrane Water Treatment*, 7, 433-449.
- Field, R.W., Siddiqui, F.A., Ang, P. and Wu, J.J., 2017. Analysis of the influence of module construction upon forward osmosis performance. *Desalination*.
- Siddiqui, F. A., She, Q. H., Field, R. W., Fane, A. G., 2017, Exploring the Differences between Forward Osmosis and Reverse Osmosis Fouling, *Water research*.

Conferences/meetings:

- Siddiqui, F. A. & Field, R. W. 2014, Criticality Concepts in Membrane Filtration: A brief review. 10th International Congress on Membranes and Membrane Processes (ICOM), 20–25 July 2014, Suzhou, China.
- Siddiqui, F. A. & Field, R. W. 2014, Comparative analysis of filtration mechanism of solutions of Dextran and Carboxymethyl Cellulose and cleaning agents' impact in tubular ultrafiltration ceramic membrane. MSA Early Career Researchers Membrane Symposium, 19–21 Nov. 2014, Deakin University, Australia.
- Siddiqui, F. A., 3rd Membrane Society of Australasia (MSA) membrane Workshop Integration of Oxidation and Membrane Technologies, 18th Nov. 2014, Victoria University, Melbourne, Australia.
- Siddiqui, F. A. & Field, R. W., 2015, Membrane Filtration: Fouling Mechanism and Cleaning, 2nd Year DPhils-Poster presentation (Chem. Eng. Day), 2nd October, 2015, Department of Engineering Science, University of Oxford, United Kingdom.
- Siddiqui, F. A. & Field, R. W. 2017, Comparative fouling performance of CA and TFC membrane under FO and under RO conditions of operation, 11th International Congress on Membranes and Membrane Processes (ICOM), 29 July–4 August 2017, San Francisco, U.S.A.
- Siddiqui, F. A. & Field, R. W. 2017, Performance of an osmotically driven module at pilot and bench scale, 11th International Congress on Membranes and Membrane Processes (ICOM), 29 July–4 August 2017, San Francisco, U.S.A.

Awards:

- Professor Tony Fane Travel Award – (2014), Membrane Society of Australasia – Early Career Researcher Symposium, Melbourne, Australia.
- Student Research Attachment Project [12 months] – (2015), Singapore Membrane Technology Centre (SMTC) at Nanyang technological University, Singapore.